ON THE CHARACTERIZATION OF MOTOR IMAGERY FUNCTIONS BASED ON SYSTEMATIC TIMING ORGANIZATION OF THE HUMAN BRAIN

A Thesis Submitted to
the Graduate School of
İzmir Institute of Technology
in Partial Fulfillment of the Requirements for the Degree of

DOCTOR OF PHILOSOPHY

in Electronics and Communication Engineering

by
Bilal Orkan OLCAY

July 2021
İZMİR

ACKNOWLEDGEMENTS

At the end of my Ph.D. research, I would like to start by thanking my supervisor, Prof. Dr. Bilge Karaçalı, for his encouraging and inspiring style that made me possible the completion of this work. Without his guidance, imagination, and enthusiasm, which I admire, this dissertation would not have been possible.

I also thank the members of my committee, Assoc. Prof. Dr. Şevket Gümüştekin, Assoc. Prof. Dr. Devrim Ünay, Prof. Dr. Aydın Akan, and Assoc. Prof. Dr. Mustafa Özuysal for their valuable time and interest in serving on my supervisory committee, as well as their comments, which helped to improve the quality of this dissertation.

Throughout my Ph.D. adventure, I had chances to work with several good people such as, Fatih Onay, Çağın Ekici, Hasan Önder Yılmaz, and Esra Tunçer that I want to express my gratitude. Also, I would like to thank Prof. Dr. Murat Özgören, Prof. Dr. Gürcan Eskitaşçıoğlu, Prof. Dr. Enver Tatlıcıoğlu, Dr. Oktay Karakuş, Dr. İlhan Baştürk, Dr. Alper Bayrak, Dr. Çağdaş Güdücü, and Dr. Tuğçe Demirdelen for both their vital suggestions and support.

I also want to serve my positive feelings and gratefulness to Bahri Yavaş, Onur Örgün, Meryem Deniz, Göksel Bayamlıoğlu, Oğuz Han, Mustafa Melih Doğan, Başak and Erdem Karayaka, Erkan Keleş, Cemil Yorğun, and Erhan Bölük for their endless friendship.

I would like to express my gratitude to my mother Betigül Olcay for her endless support which has been my main thrust to continue working. I think that nothing would be done without her. And, also, I would like to thank my aunts Türkan and Nalan Olcay deserves my thanks for their moral and motivational support.

Finally, I would like to thank to The Scientific and Research Council of Turkey (TUBITAK) for accepting and financial support to our project with the grant number 117E784.

ABSTRACT

ON THE CHARACTERIZATION OF MOTOR IMAGERY FUNCTIONS BASED ON SYSTEMATIC TIMING ORGANIZATION OF THE HUMAN BRAIN

The main objective of this thesis is to analyze the timing organization of the brain. The human brain is known to adjust its localized and also the reciprocal operations for each different cognitive task adaptively. This flexibility of the brain has attracted considerable interest in neuroscience. Elucidation of timing adaptation property of brain, however, remains as unresolved due to dynamically changing and nonlinear nature of the brain. In this thesis, we characterize the timing organization of the brain during motor imagery activity using electroencephalography signals. First, we propose a novel motor imagery activity recognition method that relies on the activity-specific time-lag between electroencephalography signals obtained from different brain regions. Next, we generalize this approach into three-parameter formulation to determine the timing profiles of activity-specific short-lived synchronization. The identification of activity-specific timing parameters was carried out using a heuristic approach that maximizes the average pairwise channel synchronizations during associated activity periods. Thereafter, we propose a novel BCI framework that find and use the timings of electroencephalography signals of localized brain regions that elicit localized activity-specific complexity features. We identify the timings for each different brain regions by adopting a heuristic-probabilistic method. Finally, we propose a novel autoregressive modeling framework that finds a representative model for each different cognitive activity. We demonstrated the efficacy of the proposed methods on publicly available brain-computer interfacing datasets on motor imagery. The performance results indicate that considering the timing organization of the brain is crucial for accurate characterization of cognitive activity. In addition, it may also account for the inconsistency of brain computer interfacing performance obtained from different subjects.

ÖZET

İNSAN BEYNİNİN SİSTEMATİK ZAMANLAMA ORGANİZASYONUNA DAYALI HAYALİ MOTOR FONKSİYONLARININ KARAKTERİZASYONU ÜZERİNE

Bu tezin temel amacı beynin zamanlama organizasyonunu analiz etmektir. İnsan beyninin, her farklı bilişsel aktivite için bölgesel ve farklı beyin bölgeleri arasında meydana gelen işlemlerin uyarlanabilir bir şekilde düzenlendiği bilinmektedir. Beynin bu esnekliği, sinirbilim alanında büyük ilgi görmüştür. Bununla birlikte, beynin zamanlama organizasyonu özelliğinin aydınlatılması, beynin dinamik ve doğrusal olmayan doğası nedeniyle çözümsüz kalmaktadır. Bu tezde, elektroansefalografi sinyallerini kullanarak hayali motor fonksiyonlar esnasında beynin zamanlama organizasyonu karakterize edilmiştir. İlk olarak, farklı beyin bölgelerinden elde edilen elektroansefalografi sinyalleri arasındaki aktiviteye-özgü zaman gecikmesine dayanan yeni bir hayali motor fonksiyonları tanıma yaklaşımı önerilmiştir. Daha sonra, aktiviteye-özgü kısa-süreli senkronizasyonların zamanlama profilini genelleştirmek için üç-parametreli bir tanıma yaklaşımı önerdik. Aktiviteye-özgü zamanlama parametreleri, ilgili görev aktivite periyodları esnasında en yüksek seviyede ortalama senkronizasyonu dikkate alan sezgisel bir yöntemle elde edilmiştir. Tezin sonraki aşamasında, beynin bölgesel olarak aktiviteye-özgü özniteliklerinin bulunduğu elektroansefalografi sinyallerinin zamanlamasını bulan ve kullanan yeni bir beyin-bilgisayar ara yüzü yaklaşımı önerilmiştir. Her bir aktivite ve beyin bölgesi için bu parametreleri sezgisel-olasılıksal bir yöntem ile belirlenmiştir. Tezin son bölümünde, her farklı bilişsel aktivite için temsili bir model bulan yeni bir öz-bağlanımlı modelleme yaklaşımı önerilmiştir. Önerilen bu yöntemlerin başarımları, halka açık olarak paylaşılan beyin-bilgisayar ara yüzü veri setlerindeki tanıma başarımları ile gösterilmiştir. Performans sonuçları, bilişsel aktivitelerin karakterizasyonu için beynin sistematik zamanlama organizasyonunun dikkate alınmasının önemini vurgulamaktadır. Buna ek olarak, bu yöntemler farklı katılımcılardan elde edilen beyin-bilgisayar ara yüzü kullanım performansının tutarsızlığını da açıklayabilmektedir.

ad augusta per angusta…

TABLE OF CONTENTS

LIST OF FIGURES

LIST OF TABLES

CHAPTER 1

INTRODUCTION

If the brain were simple enough for us to understand it,
we would be too simple to understand.
-Ken Hill-

The human brain is known as the most complex structure of the central nervous system (CNS) of the human body that is located inside the skull. It contains more than 100 billion neurons and each of them has more than ten thousand structural connections with other neurons (Eagleman 2019). It controls and also regulates our behaviors, motions, emotions, and thoughts. Besides, it conducts continuous interactions with the other mechanisms/subsystems of our body that undertake substantial roles for our living (Sanei and Chambers 2013; Bilal Orkan Olcay 2014).

The question "how the brain works" is the oldest as well as the most difficult problem (Fadlallah 2015). Understanding and characterization of the operational dynamics of such a complex system during various types of sensory, perceptual, cognitive events as well as in the case of neurological impairments have been the subject of intense research of neuroscience discipline for many years (Güdücü et al. 2019; Koley and Dey 2012; Asif, Majid, and Anwar 2019; Hipólito et al. 2021). The experimental and clinical studies for understanding the principles of brain machinery were accelerated shortly after noticing that the collected electrical activity from the brain is far from a simple noise. This finding, which is discovered by Hans Berger, told that the brain generates measurable as well as meaningful electrical oscillations that were considered as the renaissance for brain researches. This renaissance opened new avenues for the discovery of mysteries of the brain (Berger 1929; Başar 2006).

Advanced mathematical methods, biophysical models, and visualization techniques have been developed for different brain scales to extinguish the debates faced in the cognitive and systems neuroscience field (Jensen and Mazaheri 2010; Makeig et al. 2004). These methodological and technological advancements in the neuroscience area were used together to provide new insights to the researchers and advance their

understanding of how brain circuits distributed across many areas orchestrate motor and cognitive functions (Shenoy and Kao 2021). Also, these advancements enabled the researchers to put several basic principles related to the operation/coordination dynamics of the brain (F. He and Yang 2021). The four basic principles are (Başar 2006):

- Brain functions are manifested themselves as oscillations at specialized frequency tones (Özgören, Başar-Eroğlu, and Başar 2005; Başar et al. 2008). Multiple oscillations occurred in the distributed regions of the brain provides the basis of integrative brain functions (Başar et al. 2001).
- There is a super-synergy mechanism in the brain that emerged in all memory, cognitive, and perceptual processes. This mechanism manifests itself as synchronization between the oscillatory activities generate from distinct brain regions (Fingelkurts, Fingelkurts, and Kähkönen 2005; Hutchison et al. 2013; Tognoli and Kelso 2009).
- The super-synergy between distinct brain regions is selective. The selectivity of this inter-regional cooperation demonstrates itself by the magnitude of the synchronization (B. Orkan Olcay and Karaçalı 2019; Cornelis J. Stam et al. 2003; Bilal Orkan Olcay et al. 2017; B. M. Adhikari, Epstein, and Dhamala 2018).
- The super-synergy machinery is comprised of many cortical sub-mechanisms. These sub-mechanisms act in a coherent way during the cognitive, motor, or perceptual tasks (C. J. Stam and van Straaten 2012; Fries 2005).

In addition to the principles given above, several theoretical/experimental models have pointed that the coordination dynamics (i.e., self-organization, multi-functionality, switching, stability,…) and complexity are of great importance that governs the dynamics of the brain (Tognoli and Kelso 2009; Kelso, Dumas, and Tognoli 2013; D. J. J. Wang et al. 2018a). The complexity of the brain viewed as information processing capacity and shows a strong correlation with the transiently organized neural interactions which may alter depending on the analyzed temporal and spatial scale (D. J. J. Wang et al. 2018a; Nobukawa et al. 2020; 2019). The flexibility of transient organization implies that there is a low energy barrier among the quasi stable brain states in which the brain adjusts its operational dynamics rapidly. In addition to these, it was demonstrated that neural interactions represent a “small-world” topological structure which has been observed from micro- to large-scale networks (Danielle Smith Bassett and Bullmore 2006). Besides

these, two important models have been proposed to describe the collective dynamics of neuronal populations during executive functioning. These are (O'Neill et al. 2018; Breakspear 2017):

- Fokker-Planck equations (FPE) that assumes uncorrelatedness of distinct activities of ensembles (Bahraminasab et al. 2009).
- Neural Mass Models (NMM) that assumes existence of statistical correlation among neuronal activities which is biologically more meaningful (Shine et al. 2021).

These models can unveil how brain execute, inhibit, and delay the inherent processes which are important features of executive brain functioning (D. Huang et al. 2016). The above mentioned models and principles have opened new avenues that enable understanding not only the underlying neural mechanism of cognition but also the reasons/consequences of impairments of the functional organization of the brain during neurological disorders (Dawson 2004; Mammone et al. 2018).

Neurological disorders significantly affects the quality of human life by disrupting the communication among neural structures or the communication pathway between the brain and some parts of the muscular system (i.e., failure of organic neuromuscular communication) (C. J. Stam and Van Dijk 2002). In such a case, several capabilities/flexibilities of the human body may be lost or restricted, which imposes challenges to individuals during interacting with their surroundings (Ramadan and Vasilakos 2017). Among a wide variety of neurological disorders, amyotrophic lateral sclerosis (ALS), locked-in syndrome, brainstem stroke, cerebral palsy, multiple sclerosis (MS), Alzheimer and epilepsy are some of the widely encountered disorders that significantly limits the control ability of the brain on muscles (Wolpaw et al. 2002; Afshari and Jalili 2017; Sharma, Pachori, and Acharya 2015). Fortunately, with the recent advancements in the medical/health sciences, it is now possible that neurological disorders can be repaired with surgical operations (via tissue resection) and/or rehabilitation. In rare cases, these damages cannot be repaired. In such circumstances, three different ways were stressed in the literature for regaining the brain-muscle communication ability (Wolpaw et al. 2002). The adopted ways are as follows:

- Enforce using different neural pathways.
- Enhance the capabilities of the remaining intact neural communication channels.

- Use brain-computer interface (BCI) technology as an alternative means to the organic brain-muscle or brain-environment communication.

Please note that we will mainly be concentrated on the brain-computer interface systems and related mental activity decoding algorithms in this thesis.

1.1. BCI Systems

Basically, the BCI system aims to provide an external communication pathway via computers between the brain and the real world that helps to retrieve, among other things, the movement ability of subjects who suffer from movement disabilities (Wolpaw et al. 2002; Nicolas-Alonso and Gomez-Gil 2012). It basically translates neural signals from nervous system into commands for assistive technology (Chestek et al. 2013). In line with technological advancements, BCI systems have become a crucial alternative in many areas, especially in rehabilitation technologies (U. Chaudhary, Birbaumer, and Ramos-Murguialday 2016). Some well-known applications of the BCI system can be wheelchair control that retrieves the movement ability for paralyzed individuals (Yuan and He 2014), computer control (Bai, Yu, and Li 2015), internet surfing (Yu et al. 2012), deceit identification (Dodia et al. 2019), and implicit intent recognition (J. S. Kang et al. 2015).

There are different types of BCI systems that use different neural signals to provide communication between the brain and computer. Among several alternatives, researchers have put their efforts to improve the usage capability of the motor imagery type BCI technology for several years. This is due to the fact that the previous studies showed that people can learn to modulate their brain activities for a better BCI control performance to a certain extent. As the result of these modulations, it was observed that the damaged functions of the brain were restored and the movement talent of healthy individuals was enhanced (B. He et al. 2015).

In a generic BCI system, the feature extraction block extracts salient features from the electrophysiological/hemodynamical brain activity via mathematical methods, and a classification algorithm decides the category of the user intent by classifying the features extracted from the brain activity (Sitaram, Caria, and Birbaumer 2009; Blankertz et al.

2006). In Figure 1, we illustrated a generic block diagram that represents the operational steps of a generic BCI system. The blocks of the BCI system are as follows:

- Recording the brain activity.
- Preprocessing the recorded brain activity to make the raw data suitable for the feature extraction procedure.
- Extracting salient features for characterizing the cognitive task.
- Classification of the features for deciding the category of performed cognitive task.
- Translation of the estimated category of the brain activity into a real world action.

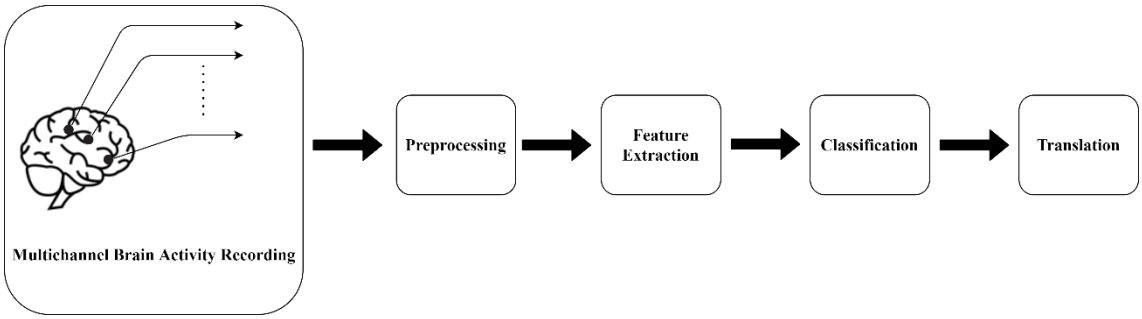

Figure 1. The graphical illustration of the generic framework of a BCI system.

In order to convert human intentions into a real world actions via a computerized system (i.e., BCI system), various types of brain imaging modalities have been used in many studies (Lenartowicz and Poldrack 2010). Some of the well-known electrical/magnetic as well as the hemodynamic neuroimaging modalities are as follows:

- Electroencephalography (EEG) (Berger 1929)
- Magnetoencephalography (MEG) (D. Cohen 1968)
- Electrocorticography (ECoG) (Palmini 2006; Chestek et al. 2013)
- Intracortical single neuron recordings,
- Functional magnetic resonance imaging (fMRI) (Mizuhara and Yamaguchi 2007),
- Positron emission tomography (PET),
- Functional near infrared spectroscopy (fNIRS) (Batula et al. 2017),
- Single-photon emission computerized tomography (SPECT).

The advantages/disadvantages of each different recording modality were provided in detail in (Ramadan and Vasilakos 2017). Note that the recording modalities such as fMRI, fNIRS, PET, and SPECT are known to collect slow metabolic (i.e., hemodynamical - blood oxygen level dependent (BOLD)-) activity which means they are not good at collecting fast transient oscillatory dynamics of the brain (Milton et al. 2007). This incapability states that they are not suitable for providing the rapid communication required for BCI systems. However, few studies in the literature make use of hemodynamical measurement modalities in BCI frameworks in rehabilitation and communication manner (Sitaram, Caria, and Birbaumer 2009; Porro et al. 1996). Since they cannot provide fast and effective communication as an electrophysiological modality, their main usage purpose is to understand the metabolic behavior of the brain by analyzing task-related BOLD responses during motor imagery activity.

The majority of the current BCI settings are designed for M/EEG signals due to their high temporal resolution which enables recording time-resolved brain dynamics (Lenartowicz and Poldrack 2010; Ramadan and Vasilakos 2017; Guger 2018). Another advantage of using EEG is that its ease of use, high portability, noninvasiveness, and harmlessness to man's health (Morash et al. 2008; Yuan and He 2014). Despite its numerous advantages, however, the main disadvantage of using M/EEG is it has very low spatial resolution due to the volume (tissue) conduction which may cause emergence of spurious or ghost interactions/activation patterns (Palva et al. 2018). Technically speaking, the volume conduction problem is defined as the smearing of the electrical activity, which is generated by the underlying neuronal networks, during traveling towards the scalp. The scalp, skull, and the other intracortical layers of the head act as a low-pass filter to these electrical signals which means that the EEG sensors collect the spatially weighted combination of the underlying neuronal activities. This problem markedly complicates the recording of localized brain signals from a particular cortical region (Babiloni et al. 2005). In Figure **2**, we provided the temporal as well as the spatial resolutions of different neuroimaging modalities.

In order to recover the spatially-resolved cortical oscillations different kinds of spatial filtering methods, inverse solutions, and head conductivity/shape modeling approaches have been developed (Rathee et al. 2017; Nyhof 2014; Tsuchimoto et al. 2021). Some of the popular referencing/spatial filtering approaches can be listed as:

- Common average reference (CAR) (McFarland et al. 1997)

- Surface (small/large) Laplacian filtering (Hjorth Derivation) (McFarland et al. 1997; Oostendorp and Van Oosterom 1996; Carvalhaes and De Barros 2015)
- Spline Laplacian filtering (Deng et al. 2012)
- Common spatial subspace decomposition (CSSD) (Yunhua Wang, Berg, and Scherg 1999)
- Common spatial patterns (CSP) (Ramoser, Müller-Gerking, and Pfurtscheller 2000; Blankertz et al. 2008)
- ICA/PCA (Hyvärinen and Oja 2000; Jolliffe 1986)

These approaches, in general, tries to minimize the effects of the volume conduction by incorporating some mathematical/biophysical assumptions and provides an estimate of localized brain oscillations (McFarland et al. 1997). Several studies conducted comparative performance analyses on these methods to see which method perform better. The outcome of these analyses highlights that none of the proposed methods are better than another and importantly, the performance of these methods heavily depends on the preferred signal processing method for brain activity characterization and adopted a priori model of choice (i.e., inverse lead field model) (Van de Steen et al. 2019; Rathee et al. 2017).

The performance of the inverse models and current source density estimation methods for obtaining the electrical activities of current dipole sources achieved slightly better estimates than the other methods (Rathee et al. 2017). However, these models assume that each participant has a nearly similar head conductivity model, which may not be a realistic case. In such circumstances, the spatial filtering methods, which does not consider *a priori* model, are appeared to be the simplest and most applicable methods (Tsuchimoto et al. 2021). In this thesis, we proposed novel brain activity characterization methods for BCI frameworks. We evaluated the performance of these methods on the publicly available EEG signals collected from individuals during several imagery hand/foot movement experiments. We adopted the CAR method to reduce the effects of volume conduction, referencing problems, and voltage level shifts in EEG signals throughout this thesis (Fabien Lotte 2008; McFarland et al. 1997). The mathematical expression of CAR method will be provided in the next chapter.

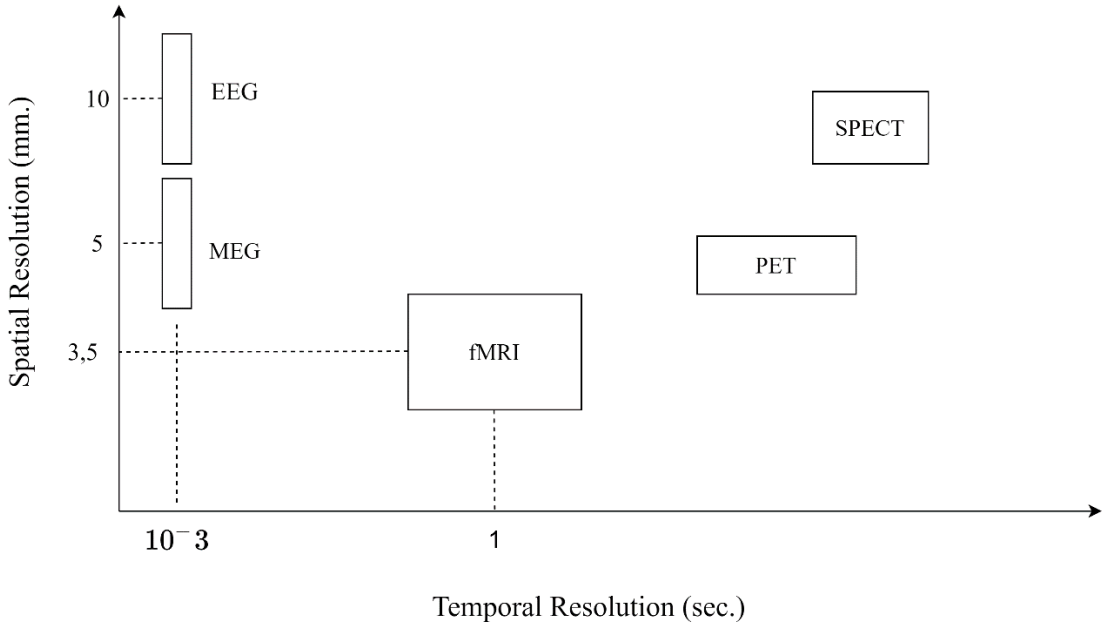

Figure 2. Spatial and temporal resolutions of the most appealing brain activity monitoring/recording methods. (Source: (Lenartowicz and Poldrack 2010))

1.1.1. Control Signal Types used in BCI and Brain Activity Characterization Studies

The use of EEG signals in BCI frameworks enables researchers to acquire temporally-resolved dynamics of the electrical activities of the brain that contains the information that are related to the intentions/thoughts of individuals. The most used control signal types in BCI settings are provided in Table 1. The brief descriptions for each control signal type are provided in this section.

Table 1. The commonly used BCI control signals and their psychological phenomenon.

Control Signal	Psychological Phenomenon
VEP	Frequency-modulated brain activity (flickering visual object)
P300	Positive deflections mainly observed at 300ms after target stimulus have been observed (oddball paradigm)
SCP	Slow cortical voltage oscillations (voltage shifts)
Sensorimotor Rhythms	Modulations of signals in 8-30 Hz frequency band (due to real or imagery motor functions)

1.1.1.1. Visual Evoked Potentials (VEP)

The visual evoked potentials (VEP) are the brain oscillations observed at occipital regions of the brain (Dreyer and Herrmann 2015). The common methodology of the usage of visual-evoked brain responses is that the participants concentrate on one of the flickering visual objects which they select from a computer screen. The flickering frequency of the concentrated visual object affects the frequency of the electrical brain oscillations that are acquired via occipital region electrodes. The concentrated visual object can then be estimated by analyzing the frequency response of these occipital brain oscillations. Depending upon the flickering frequency of the visual object, VEP can also be categorized as steady-state visual evoked potentials (SSVEP) and transient visual evoked potentials (TVEP).

The high signal-to-noise ratio (SNR) of VEP signals enables the BCI researchers to use it in brain-computer communication (Dreyer and Herrmann 2015). One important disadvantage of using VEP as a BCI control signal is that the participants had to maintain his/her concentrate on the visual objects for a long time (may last for minutes to hours) which may become tiring for the participants as the experiment time goes on.

1.1.1.2. P300

The P300 signal is a transient positive deflection that emerges almost ~300 ms after the presentation of less frequent (often referred to as the target) auditory, visual, or somatosensory (tactile) stimuli (oddball paradigm) (J. Jin et al. 2012). This short-lasting brain oscillation is thought to carry a cognitive component that is related to the presented stimulus. The typical application of P300 type BCI is the matrix speller BCI which is proposed by Farwell and Donchin in 1988 (Farwell and Donchin 1988).

The P300 type BCI applications are not preferred due to their low SNR and low information transmission rate (ITR) problems. Many different solutions were proposed to increase the performance and also the usability of P300 signals. Martens et al. changed the stimulus presentation type and observed that this change enhances the performance of P300 BCI (Martens et al. 2009). Another improvement is achieved by Jin et al. They offered using the combination of both "P300" and "SSVEP" to increase the communication rate of P300 type BCI systems (J. Jin et al. 2012).

1.1.1.3. Slow Cortical Potentials

The slow cortical potential signal (SCP) is another important control signal type utilized in BCI systems. It is known as the slowest signals of all scalp recorded EEG activities. It is basically referred to as the mean cortical voltage shifts of EEG activities and their oscillating frequencies are typically below than 1Hz. In the literature, it was highlighted that negative and positive SCP oscillation refers to mental preparation and mental inhibition (Tallgren et al. 2005). Although its relation to the mental processes, many SCP-related BCI systems use combination of different features to achieve a brilliant recognition performance (Wolpaw et al. 2002; Salyers, Dong, and Gai 2019). Another methodology for increasing the SCP-based BCI performance is to use the convex-concave feature extraction method (Hou, Sun, and Meng 2019). The popularity of the SCP signals in BCI experiments comes from the fact that people can learn to modulate their SCP activities in response to given feedback in BCI training sessions.

1.1.1.4. Sensorimotor Rhythms

Beyond a doubt, sensorimotor signals are the most preferred control signal type in the majority of commercial and clinical BCI applications. Its popularity comes from the fact that SMR signals offer the highest level of control capability (i.e. degree of freedom) than the other type of BCI control signals (Yuan and He 2014). Sensorimotor rhythms are of great importance associated with the control of the motor imagery-based BCI systems. Despite its wide usage, it is known that the motor imagination is the most difficult mental simulation type among the other alternatives such as mental rotation, word association, auditory imagination, mental math operation, spatial navigation, and face perception. That is why %20 of total BCI participants cannot learn how to modulate their SMR signals (Friedrich, Scherer, and Neuper 2012; Allison and Neuper 2010). In addition to these, nearly around ~%50 of people do not elicit clear SMR modulation/demodulation characteristics (Solis-Escalante et al. 2012).

The main reason for choosing the SMR as a control signal is that the majority of BCI user can easily learn how to modulate their sensorimotor rhythms given feedback information related to their motor imagery performances (Christa Neuper et al. 2009a). Another reason is that the brain generates similar sensorimotor rhythm changes (i.e., amplitude modulation patterns both during upper as well as lower limb movements) during both real and imagery motor tasks. The similarity of the activity patterns is thought to be the result of both motor imagery and motor execution tasks uses similar brain regions to achieve neural coordination dynamics during motor preparation and programming (Marc Jeannerod 2001; M. Jeannerod et al. 1995; Morash et al. 2008). Many studies in the literature have analyzed similarities/dissimilarities of these activation patterns that emerged during real and imagery motor movements. Llanos et al. performed an experiment to observe the distinctiveness of the sensorimotor rhythms of motor activity-related cortical areas. They found that the sensorimotor oscillations have a unique characteristic and that oscillatory patterns acquired for both real and imagery movement produce similar neural activity patterns within similar brain regions (Llanos et al. 2013). On the contrary, several studies have highlighted the differences of brain activity patterns emerged in imagery and execution cases (Kraeutner et al. 2014; Xu et al. 2014). He et al. analyzed the different perspectives of SMR signals in motor imagery functions and stated

that the SMR signals are known to be the most robust oscillatory responses that provide reproducible brain patterns embedded in the EEG activity (B. He et al. 2015).

The neural mechanism of SMR signals has been a well-studied subject (Halder et al. 2011). SMR signals generally show significant spectral modulations in 8-13 Hz (μ rhythms) and also in 14-30 Hz (β rhythms) during both in imagery and real movement tasks in contralateral region to the movement in the brain (GASTAUT 1952; Yuan and He 2014; Höller et al. 2013; G. Pfurtscheller et al. 2006). It was demonstrated that analysis of higher frequency oscillations elicited more activity-specific spectral patterns (Miller et al., 2010). In general, the amplitudes of Rolandic μ and β are known to start to decrease before the movement onset and lasts until the task finishes (G. Pfurtscheller et al. 1998). This decrease in amplitude is referred to as the event-related desynchronization (ERD). After the task finishes, the amplitude of both μ and β rhythms increase to its initial value which is referred to as event-related synchronization (ERS). These rhythms (i.e., β and μ band oscillations) has been a subject of detailed biophysical analysis for a long time. As a result of these researches, it has been understood that the β oscillations take place in cortical setting/resetting which states the inhibition of the information processing in underlying neuronal networks (G. Pfurtscheller and Lopes Da Silva 1999; G. Pfurtscheller et al. 2005). Furthermore, the α (i.e., μ for sensorimotor cortical oscillations) are responsible for functional inhibition of task-irrelevant cortical pathways for optimal cognitive task performances (Jensen and Mazaheri 2010). On the contrary to μ and β rhythms, vast amount of literature proved that the ERS in the γ band (i.e. > 30 Hz) amplitude which is observed with task initiation (Grosse-Wentrup, Schölkopf, and Hill 2011; Başar et al. 2001).

Gastaut et al. showed that the similar μ and β ERD/ERS patterns was also observed in amputee subjects (Gastaut, Naquet, and Gastaut 1965). For both normal and amputee subjects, these ERD and ERS patterns in both μ and β band primarily observed in contralateral regions of the sensorimotor/primary motor cortices. Ince et al. demonstrated that imagination of foot movement desynchronizes the μ and β band activity in foot area of the brain but synchronizes the activity in hand area in the sensorimotor cortex and vice versa (Firat Ince, Arica, and Tewfik 2006). This antagonist behavior of event-related synchronization and desynchronization is known as the “focal ERD/surround ERS” phenomenon. This phenomenon describes the organization mechanism of the thalamo-cortical structure of the brain (C. Neuper and Pfurtscheller

2001). The antagonist ERD/ERS behavior of the brain forces the focal cortical activation of relevant brain region by simultaneous deactivation (i.e., inhibition) of other regions of the brain (Z. Zhou and Wan 2012). Also, μ rhythm desynchronization in contralateral sensorimotor cortex during a motor imagery task is observed while there is a significant α band ERS in parieto-occipital cortex. This mechanism enhance the discrimination capacity of localized changes of the sensorimotor rhythms for BCI systems (G. Pfurtscheller et al. 2006).

In general, the ERD during motor imagery task in corresponding cortical areas states the reactivity of the corresponding brain regions. The ERS after the ERD is known as the inhibition/deactivation of cortical networks involved in motor imagery (Christa Neuper, Wörtz, and Pfurtscheller 2006) . Note that, the β band synchronization following the imagery/real movement is named as post-movement β rebound (G. Pfurtscheller et al. 2005). Pfurtscheller et al. observed that the most discriminative spectral component is the μ band and the electrodes that elicited most discriminative patterns are C3, Cz, and C4 EEG electrodes. These electrodes collect the electrophysiological activity mainly from left and right sides of the motor/sensorimotor cortex (G. Pfurtscheller et al. 1998; Munzert, Lorey, and Zentgraf 2009a). Neuper et al. stated that the ERD/ERS patterns observed in μ and β bands during the sensory, motor, or cognitive tasks represents the status of the underlying cortical networks. The power of μ rhythm can be used as an indicator of the activation level of cortical areas that allocates the resources for processing the information peculiar to the specific cognitive tasks (Christa Neuper et al. 2009a; 2005). Note that the amount of ERD in the task-specific frequency bands is generally modulated by task complexity, participant's concentration level, intelligent quotient scores and so forth (Llanos et al. 2013). In the same vein, Mashat et al. discovered that the increase in the motor imagery task complexity provides larger ERD/ERS changes (Mashat, Lin, and Zhang 2019). These amplitude modulations are believed to be the signature of thalamo-cortical as well as the cortico-cortical information transfer between distributed neuronal networks that are interconnected with feedback loops (C. Neuper and Pfurtscheller 2001).

1.2. The Literature Overview

After the discovery of the effectiveness of the electrophysiological activities for communication and control, a vast amount of novel brain activity analysis methods and BCI approaches have been proposed (F. Lotte et al. 2007; Abiri et al. 2019). In this section, we give a literature overview related to BCI studies. We provided it by dividing the studies into subsections according to the used for signal processing/feature extraction methods for a better understanding of the logic of the proposed brain activity characterization methods in this thesis. Also note that, in this section, we did not restrict ourselves to the literature that only related to the motor imagery activity recognition studies. We tried to provide an extensive overview that includes the other types of mental imagery (non-BCI) as well as brain activity characterization studies to make a general insight about adopted perspectives when characterizing the brain activities. Note that, the mathematical details of these methods described in the below subsections is given in the second chapter of this thesis.

1.2.1. Autoregressive Modelling Studies

One of the most popular parametric methods for brain activity characterization are the autoregressive (AR), moving average (MA) and autoregressive moving average (ARMA) modelling (Haykin and Widrow 2005). Among them, autoregressive modelling by far the one of the most appealed method for EEG signal analysis. Briefly, autoregressive model is a linear forward prediction filtering model that estimates the signal sample by using the weighted combinations of the past samples of the corresponding signal (Troughton and Godsill 1998). The weights (i.e., the model coefficients) serve information about the signal characteristics. Two types of AR modelling approaches, named as univariate and multivariate modelling, can be found. The AR model coefficients were used as discriminating feature in many brain activity characterization frameworks. In here, we briefly summarized some of brain activity characterization studies that uses the AR model coefficients as characteristic features. Anderson et al. used both univariate and multivariate AR modelling based method to

characterize different types of mental tasks which was collected by Keirn and Aunon (Keirn and Aunon 1990). They achieved satisfactory recognition performance with the autoregressive model coefficients of six EEG channels. One important outcome of this study is that, unlike the merits of multivariate AR model, univariate autoregressive modelling is more effective in both computation time and recognition performance (Anderson, Stolz, and Shamsunder 1998). Pfurtscheller et al. adopted using adaptive AR model coefficients obtained for each time instant to capture the transient changes in the brain dynamics against its dynamically changing nature (G. Pfurtscheller et al. 1998) The adaptive AR coefficients calculated for each of the EEG channels placed on the sensorimotor cortices. Authors calculated the adaptive AR model coefficients via recursive least squares method. Arnold et al. offered using a Kalman filter to estimate and update the multivariate and univariate AR model coefficients for each time instant. This approach is adopted by the authors that it is beneficial to incorporate the nonstationary and dynamical changing characteristics of brain activity (Arnold et al. 1998). The proposed approach was tested on EEG signals and observed that the coefficient update procedure is critical to capture the relevant features to characterize the cognitive task in the dynamically changing nature of the brain. Huan et al. compared the performance of the 6 different AR modelling approach and two different classification (linear discriminant analysis (LDA), multilayer perceptron with back propagation (MLP-BP)) methods using a two-state mental task imagery characterization framework. They used least squares (LS) method, Burg method, adaptive autoregressive (AAR) method with least mean squares with and without signal segmentation. In contrast to the prior works, they found that AR-LS without signal segmentation with LDA classifier achieved the best classification performances in mental task characterization study (Huan and Palaniappan 2004). Chen et al. proposed an AR forward prediction based methodology to accurately estimate phase and frequency of the narrow-band brain oscillations for clinical applications. The main reason for estimating instantaneous phase and frequency accurately and send transcranial magnetic/electric pulses is to observe the exact changes of memory performance of the subjects under different phase and frequency organization of respective cortical areas. They tested their algorithm on two patients while they were performing Sternberg memory task. They achieved clinically as well as biophysically acceptable phase-locking performances during memory task obtained via the intracranial EEG signals (L. L. Chen et al. 2013). Krusienski et al. conducted an AR-based online cursor control study and evaluated the computer control performances of method with

different AR model orders. In that study, authors observed that the increase of the AR model order causes a gradual increase in the control performance of the subjects and stated that when different frequency bands are utilized for BCI purposes, choosing of band-specific model orders would be beneficial. One important thing -also discussed in (McFarland and Wolpaw 2008)- is that minimizing the penalty term introduced by model order estimation methods is not directly related to the activity recognition performances of the AR-based BCI systems. The model order must be determined by considering the user's control performance in training phase of the BCI experiments. Schlögl et al. used four different classification methods namely minimum distance analysis (MDA), support vector machine (SVM), linear discriminant analysis (LDA) and k-nearest neighborhood (kNN) to determine the best classification method when using adaptive AR modelling for motor imagery activity recognition framework. The overall results show that SVM achieved a better recognition performance in both single channel and multivariate AR modelling frameworks (Schlögl et al. 2005). Similarly, Hettiarachchi et al. compared short-time moving window and Kalman filtering methods in estimating the adaptive autoregressive model coefficients in a motor imagery BCI scenario. They found that Kalman filtering approach is better in extracting adaptive AR and MVAR model coefficients (Hettiarachchi, Nguyen, and Nahavandi 2016).

Besides the motor imagery related brain activity characterization, AR models can be used the detect neurological deteriorations. In that context, Altunay et al. proposed an autoregressive error prediction filtering approach to determine the epilepsy onsets (Altunay, Telatar, and Erogul 2010). They filtered the EEG activity and observed the forward prediction error for epilepsy detection. EEG signals usually subject to external and physiological disturbances such as movement artifacts, eye blinks and so forth. Li et al. considers L_p norm ($p \leq 1$) instead of L_2 norm as objective function for calculating the AR model for EEG analysis to reduce the effects of outliers on model coefficients (Peiyang Li et al. 2015). Another approach to filter out the subject-generated non-EEG components such as jaw clenching, eye blinking, eyebrow moving and head rotation approach was developed by Lawhern et al. (Lawhern et al. 2012). They modelled the different types of artifacts via AR modelling and used SVM classifier to determine the categories of the disturbance accurately. Authors claimed that the AR coefficients obtained for each different type of artifacts may be used for cleaning the EEG activity and thus obtaining better EEG characterization. Also, the removal of the artifacts via the

method proposed by Lawhern et al. may help to obtain exact dipole-source modelling of EEG activity (Lawhern et al. 2012).

1.2.2. Time-Frequency Analysis Studies

Besides the autoregressive modelling, a vast amount of literature utilized the time-frequency decomposition methods for analyzing the EEG signals for brain activity recognition/characterization purposes. Time-frequency methods can decompose the signals into several time-frequency atoms to unveil the discriminative patterns. In Figure **3**, we provided an illustrative example of time-frequency energy distributions of right foot and right hand motor imagery activities.

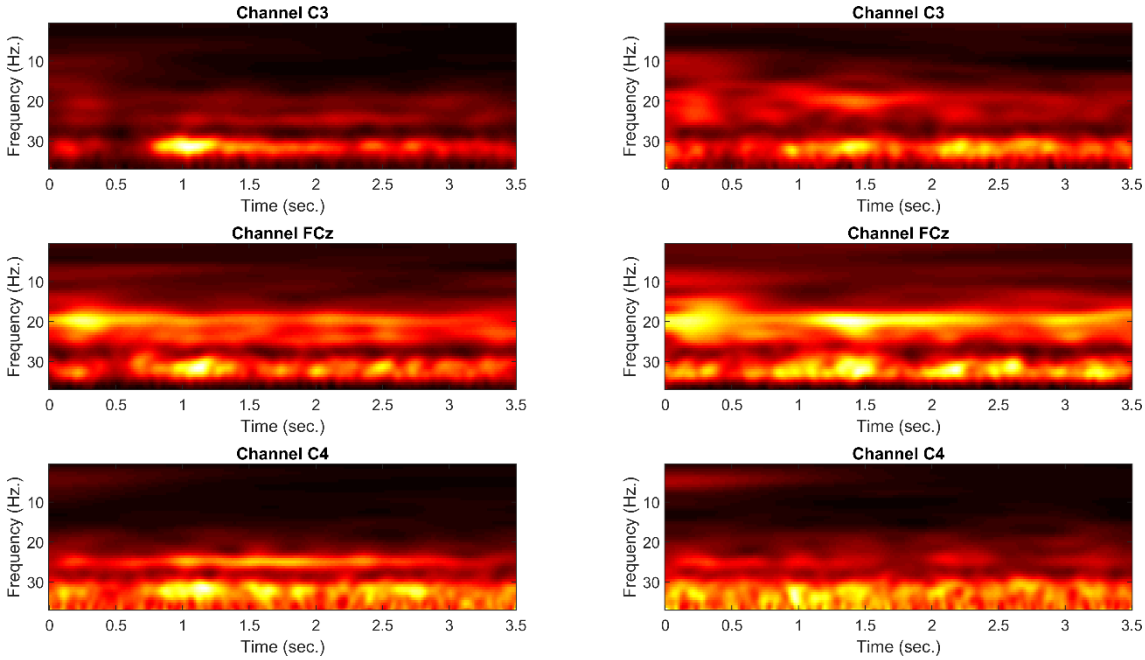

Figure 3. The time-frequency distribution of different motor imagery-related electrophysiological activities. The time-frequency energy distributions in the left column represents the of right foot motor imagery activity and the right column represents the right hand motor imagery activities.

This exemplary figure shows that different cognitive tasks produce conspicuously different energy concentrations at each time-frequency point. After the discovery of the discriminative strength of time-frequency methods, several brain-computer interface studies were started to adopt these methods for feature extraction purposes (Hsu 2011; Ince, Tewfik, and Arica 2007; Salyers, Dong, and Gai 2019).

In line with this, Zhou et al. offered a wavelet packet independent component analysis method to extract activity-specific frequency-resolved ERD/ERS patterns from the EEG activity to characterize the complex motor imagery tasks such as standing up, right/left imagery foot movement with homolateral imagery hand movement (Z. Zhou and Wan 2012). Ince et al. proposed finding and using multiple informative time-frequency patterns captured using dyadic tree segmentation of time and frequency axis. Authors used discrete cosine transform to decompose the brain signals. The captured electrophysiological patterns during the motor imagery tasks were mainly the time and frequency localized sensorimotor ERD/ERS features (Ince, Tewfik, and Arica 2007). They claimed their proposed method can extract subject-specific localized time-frequency patterns and also takes the hemispheric asymmetry of the brain dynamics induced during motor imagery tasks into account. A non-dyadic segmentation version of the previous time-frequency method proposed by Ince et al. to get rid of the limitations of the dyadic time segmentation procedure. They observed that the non-dyadic segmentation method captured more discriminative as well as time-sensitive ERD/ERS features for motor imagery activity recognition (Firat Ince, Arica, and Tewfik 2006). An improved version of the time-frequency segmentation approach described above proposed by Ince et al (Ince et al. 2009). The improved version of the method identifies the electrodes that elicit most informative time-frequency features and discards the uninformative ones. They again used the most informative time-frequency features for motor imagery activity characterization purposes. Their results suggest that this improved version achieved better results than two well-known benchmark method common spatial patterns (CSP) and AR. Zarjam et al. calculated the entropies of the wavelet coefficients of the source localized EEG signals and used them as features to categorize the EEG signals collected under different type of cognitive workloads (Zarjam et al. 2013). Lerga et al. used the Wigner-Ville transform and Renyi entropy methods to show that the motor functions cause short-lived spectral changes in the neural activity (Lerga, Saulig, and Mozetič 2017). Cek et al. used wavelet-based information theoretic measures to analyze the stimulus related evoked brain potentials (Emre Cek, Ozgoren, and Acar Savaci 2010).

In our past study, we used wavelet-based methods to observe the changes of the electrophysiological activity during olfactory stimulus presentation (Bilal Orkan Olcay 2014). Goksu et al. calculated the log-energy entropy of the wavelet packet transform coefficients of slow cortical potentials to achieve a satisfactory motor imagery task recognition performance (Göksu 2018). Chaudhary et al. used flexible analytic wavelet transform to decompose EEG activities into sub bands recorded during motor imagery tasks. The narrow-band brain activities for each EEG channel were used to obtain the temporal moment features to characterize the motor imagery related brain dynamics (S. Chaudhary et al. 2020). Wavelet analysis is also helpful to understand the inherent chaotic dynamics of the epileptic and normal EEG activities. Adeli et al. used wavelet decomposition to calculate the correlation dimension (CD_2) and largest Lyapunov exponent (LLE, (L_1)) values of each sub-band of EEG signals collected during seizure and seizure-free cases. The major aim of the authors is to highlight the significant difference in CD and LLE between epileptic and normal brain dynamics which is usually hidden in broad-band brain activity (Adeli, Ghosh-Dastidar, and Dadmehr 2007). Özgören et al. conducted a wavelet analysis on the responses collected during auditory stimulations for analysis of consciousness of the subjects during anesthesia administration (Ozgoren et al. 2010). Also, wavelet analysis was used to delineate the μ and β band modulation characteristics of primary motor and somatosensory cortices during movement observation cases which was due to the activation of mirror neuron system which includes these cortical regions (Muthukumaraswamy and Johnson 2004).

1.2.3. Spatial Filtering Based Studies

In the literature majority of the BCI studies utilize the common spatial patterns (CSP) method which is the most popular spatial filtering/transformation approach. In general sense, a typical motor imagery-based BCI system aims to capture the concomitant changes of electrophysiological activity due to the imagination of movements via the electrodes placed on the motor activity related cortical regions (i.e., homunculus). On the homunculus, there are several cortical representation areas of both upper and lower extremities can be found which is illustrated graphically in Figure 4.

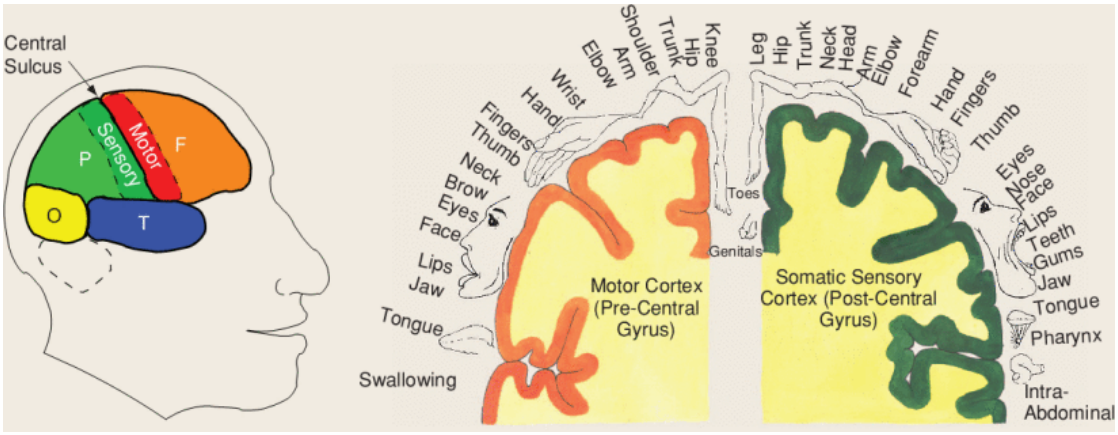

Figure 4. The illustration of representation of the extremities and non-extremities on both motor and sensory cortices (Blankertz et al. 2008). (This figure used with permissions under the *Copyright © 2008, IEEE*)

The graphical illustration of the cortical regions of the upper and lower extremities shows that each of the representation areas located as very close to each other. The tight closeness of these representation areas of each extremity as well as other non-extremity regions and the volume conduction problem makes detection of the particular modulations of each representation areas due to the motor movement/imagery using EEG signals a vexing problem. In such cases, the spatial filters are the vital signal processing methods to cope with the two aforementioned problems. Spatial filtering of the frequency-resolved EEG activities enables the researchers to distinguish the motor imagery/movement-related cortical modulations to a certain extent. In a study, diverse spatial filtering methods such as common average reference (CAR), Laplacian filtering, bipolar derivation, and CSP methods were evaluated (Blankertz et al. 2008). Among these spatial filtering techniques, the CSP method achieved the best classification performance between occipital-α and Rolandic μ rhythm. In general, the CSP method designs a spatial filter and conduct a spatial linear transformation so that the variance of resulting CSP-filtered activity belongs to one class is maximized and the variance of the other activity is minimized simultaneously (Ramoser, Müller-Gerking, and Pfurtscheller 2000; Blankertz et al. 2008). Thereafter the effectiveness of the CSP method was proved, the BCI researchers try to improve the discrimination capacity the CSP method by incorporating several different optimization criteria into the optimization problem. Common spatio-spectral patterns (CSSP) (Lemm et al. 2005), common sparse spatio-

spectral pattern (CSSSP) (Dornhege et al. 2006; W. Wu et al. 2008), Tikhonov-regularized CSP (referenced therein (F. Lotte et al. 2007; Fabien Lotte and Guan 2010)), local-temporal CSP (H. Wang and Zheng 2008), augmented complex common spatial patterns (Cheolsoo Park, Took, and Mandic 2014), and probabilistic common spatial patterns (W. Wu et al. 2015) are the well-known variants of the CSP method. Vast amount of motor imagery activity recognition studies uses the CSP and its extensions in the literature. Zhang et al. adopted a procedure that optimize both spatial and spectral filter for motor imagery based BCI frameworks (Yu Zhang et al. 2015). Ang et al. proposed to find different CSP filters to each band-pass filtered EEG activities (Ang et al. 2008). Wang et al. used CSP filter to enhance the dichotomy between EEG signals belongs to different type of motor imagery tasks (J. Wang et al. 2018). Jiao et al. used sparse group representation method (SGRM) to enhance the classification performance of target subject having insufficient number training samples. This method extracts the CSP based features from both target and nontarget subjects to generate composite dictionary matrix. Then, these vectors are used to represent each test feature vectors of target subject. The results obtained via publicly available BCI datasets showed that this method enables to reduce the demand of training task periods thus reduces the training/calibration time of BCI systems (Jiao et al. 2019). Similarly, composite CSP method were proposed by Kang et al. to handle the small training sample problem in BCI studies (H. Kang, Nam, and Choi 2009). Authors proposed two method that composes the spatial covariance matrices of different subjects for an accurate motor imagery activity recognition for target subject. Bruner et al. performed a comparison between different spatial filtering approaches (Brunner, Naeem, and Pfurtscheller 2009). The authors used four different spatial filtering approaches based on PCA and ICA methods. The classification performance results found for the case, where using PCA as preprocessing dimensional reduction purpose, showed that PCA as preprocessing did not provide any advantage for motor imagery classification. This shows that, PCA-based dimension reduction, which relies on selecting components with largest variances, did not retain the motor imagery activity related brain patterns. Furthermore, they found that using EEG channels except for frontal and occipital regions for ICA and CSP decomposition achieved satisfactory recognition performances. Liao et al. used a two different spatial filters, CSP and discriminative spatial patterns (DSP) to extract relevant features from both movement related cortical potentials and sensorimotor rhythms for imager finger movement classification (Liao et al. 2007). Mishuhina et al. proposed a complex CSP method that captures spectral, spatial, and

temporally relevant features for a successful recognition (Mishuhina and Jiang 2021). Several strategies were adopted to improve both accuracy and information transfer rate of EEG-CSP based BCI systems. One important approach in the literature is exhibited by Khalaf et al. that combines EEG derived CSP features with fTCD (functional transcranial Doppler)-derived wavelet features (Khalaf, Sejdic, and Akcakaya 2019).

1.2.4. Connectivity Based Studies

The majority of the analysis methods, as well as BCI frameworks, have achieved notable recognition performance by extracting and using relevant brain patterns from the neural activities acquired from distinct regions of the brain. However, it is also known that the brain is organized as a dynamical complex network in which the neural information is continuously processed and transferred between different regions of the brain (Olaf Sporns et al. 2004; S. H. Jin, Lin, and Hallett 2012; C. J. Stam and Van Dijk 2002). Contemporary brain mapping techniques, models, and theories, which was putted forward to delineate the brain functioning, signifies the collective behavior of distinct cortical regions (Mišić and Sporns 2016). Distinct regions that take part in this complex network are in continuous interaction with each other functionally in a nonlinear as well as dynamic fashion (O. Sporns, Tononi, and Edelman 2000; Rubinov and Sporns 2010; Marinazzo et al. 2011; Bullmore and Sporns 2009). These interaction patterns are thought to be generated during information transmission between different regions of the brain (please see Figure 5).

Two types of statistical interactions, also termed statistical connectivity, have been proposed to take place between brain regions (Fingelkurts, Fingelkurts, and Kähkönen 2005; C. J. Stam and van Straaten 2012). Functional connectivity refers to temporal synchronization and effective connectivity refers to the causal synchronization between the electrophysiological/hemodynamic signals, also referred to as the undirected and directed interaction, respectively (Bowyer 2016). Note that these terms will be explained in detail in the upcoming chapter. Brain connectivity appears to be central to understanding the systematic information processing organization of the brain for cognitive, sensory as well as other processes (Tognoli and Kelso 2009; Harrison, Penny,

and Friston 2003). It offers a fundamental insight into the functional network organization of the brain (Hipp et al. 2012).

In the literature, these interaction patterns are tried to captured and used to derive network-theoretic features (i.e., centrality, clustering coefficient, characteristic path length,…) to understand the organization of the brain network and network topology for different cognitive tasks (Telesford et al. 2011; Rubinov and Sporns 2010). However, these graph-theoretic measures may not be applicable to fully characterize the whole brain dynamics without capturing the true interaction dynamics. It is clear that there is an urgent need for advanced synchronization calculation methods to understand the true interaction dynamics of the brain. However, the exact model of the synchronization among the brain regions and its functional role in cognitive, sensory, and motor tasks is still unclear (Marinazzo et al. 2011). In the last few years, researchers have spent substantial effort to develop more advanced mathematical methods to elucidate details of these complex brain interactions during cognitive tasks (Sargolzaei et al. 2015; Meunier, Lambiotte, and Bullmore 2010).

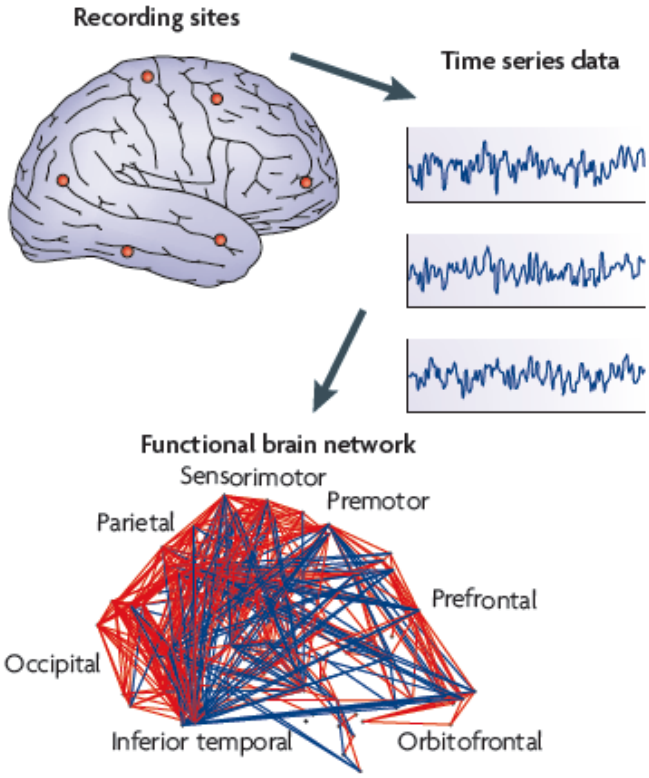

Figure 5. Typical flow of the functional connectivity-based brain network inference (Source: Fadlallah, 2015).

In this sense, various model-based and model-free synchronization methods have been proposed and used to disentangle the underlying true cortical interactions (Duckrow and Albano 2003; Pereda, Quiroga, and Bhattacharya 2005; Sakkalis 2011; Greenblatt, Pflieger, and Ossadtchi 2012; Bakhshayesh et al. 2019b; 2019a; B. Orkan Olcay and Karaçalı 2019; Kaminski et al. 2016; Jalili, Barzegaran, and Knyazeva 2014). Along with this perspective, researchers adopted to use these advanced brain connectivity estimation methods for motor imagery/execution -based studies to capture and use the task-related brain synchronizations as features. Gonuguntla et al. classified motor imagery tasks by using the task-specific phase couplings between remote brain regions (Gonuguntla, Wang, and Veluvolu 2016). Rocca et al. calculated magnitude squared coherences (MSC) between EEG signals as a biomarker for a person identification purpose (Rocca et al. 2014). Billinger et al. proposed using directed transfer function (DTF) to identify the causal interaction between EEG sources obtained during motor imagery tasks (Billinger, Brunner, and Müller-Putz 2013). Siuly et al. offered a cross-correlogram based method that calculates the correlation between EEG signals and extract several statistical features to characterize the right hand/right foot motor imagery tasks (Siuly and Li 2012). Li et al. proposed joint distribution entropy method to capture the coupling dynamics of electrophysiological activity collected from different regions of the brain (Peng Li et al. 2016). Faes et al. used a compensated transfer entropy analysis to capture volume conduction-free information flow between EEG channels (Faes et al. 2016). Brunner et al. offered using the phase coupling between EEG channels to design an online BCI framework (Brunner et al. 2006). Wei et al. performed a phase coupling based motor imagery activity recognition study to find the brain regions that elicit significant connectivity patterns during motor imagery tasks (Q. Wei et al. 2007). Daly et al. proposed using frequency-resolved phase coupling statistics for an accurate detection of motor imagery task (Daly, Nasuto, and Warwick 2012). Makarov et al. used wavelet bi-coherence method to observe the frequency-resolved task-specific pairwise brain synchronization modulations during motor movement/imagery tasks (Makarov et al. 2018). Wang et al. utilized phase coupling statistics between specialized brain regions (Supplementary Motor Area (SMA) and Primary Motor Cortex (M1)) during right/left motor imagery hand movement (Yijun Wang et al. 2006) which are demonstrated to play key role during motor imagery tasks (Halder et al. 2011). Gao et al. used relative wavelet entropy to determine the changes in the functional brain network topology to characterize the fatigue during driving task (Z. Gao et al. 2019). Babiloni et al. used Directed Transfer

Function (DTF) to reveal the directional information transfer among different brain regions during finger movement task (Babiloni et al. 2005).

Besides the BCI studies described above, the notion of brain connectivity has also been used for clinical researches. Calhoun et al. extracted connectivity features from the brain activity for detecting the schizophrenia disorder (Calhoun, Kiehl, and Pearlson 2008). Sarmukadam et al. proposed connectivity based approach to observe the effects of autism spectrum disorder (Sarmukadam et al. 2020). Olcay et al. proposed a mutual information-based technique that determines the functional channel clusters in the brain to determine the type of tactile stimulus (Bilal Orkan Olcay et al. 2017). Melia et al. used several connectivity methods such as mutual information, cross-correntropy to determine the changes in the brain connectivity patterns in sleep related disorders (Melia et al. 2014; 2015). Vergara et al. calculated inter-regional brain synchronizations for different spatial scales to observe the differences between healthy individuals and schizophrenia patients (Vergara et al. 2019). Skidmore et al. offered using wavelet-based connectivity features to capture the alterations of the interactions of distinct brain regions (Skidmore et al. 2011). Gurkan et al. multivariate autoregressive model based method (i.e. generalized Partial Directed Coherence (gPDC)) to analyze the effects of propofol injection on the changes of connectivity of distinct regions of the brain (Gürkan, Akan, and Seyhan 2014). All the connectivity-based studies mentioned above helped researchers to uncover the inter-regional cross-talk among the brain regions during cognitive activities to a certain extent.

In the literature, a large number of the synchronization (i.e. connectivity)-based brain activity characterization studies disregard the dynamically changing characteristics of the brain and assume that the inter-regional synchronization profile among the brain regions remains constant throughout the cognitive task periods (Makarov et al. 2018; Yijun Wang et al. 2006; Brunner et al. 2006; Gonuguntla, Wang, and Veluvolu 2016; Olejarczyk et al. 2017; Van de Steen et al. 2019). However, as previously stated, despite its fixed anatomical structure, brain exhibits a dynamically changing as well as nonlinear synchronization characteristics, which introduces an additional challenge in elucidating the cognitive dynamics (Rabinovich and Muezzinoglu 2010; C. J. Stam 2005; Ince et al. 2009; Cornelis J. Stam et al. 2003; Hutchison et al. 2013; Andre M. Bastos, Vezoli, and Fries 2015; Fries 2005). The intermittent characteristics of the inter-regional brain synchronizations were demonstrated to be the results of transient (i.e. short-lived) activations/synchronizations of localized neuronal ensembles (Cornelis J. Stam et al.

2003). Few studies that try to extract and interpret the intermittent dynamical characteristics of the brain activity for modelling cognitive tasks/states. Lu et al. analyzed short-lived functional interactions of EEG channels via time-frequency cross mutual information analysis. They observed the dynamical changes of the channel synchronizations with regard to the changes of the task demands accordingly (C. F. Lu et al. 2011). Hipp et al. demonstrated that transiently changing perceptual (visual perception) stimuli causes emergence of dynamically changing task-specific cortical synchronization patterns at task-specific frequency and spatial locations (Hipp, Engel, and Siegel 2011). Baker et al. used Hidden Markov Model (HMM) to capture consistent short-lived brain states that are emerged with transiently coherent spatial networks to characterize the behavior of the brain during idling conditions (Baker et al. 2014). Santamaria et al. identified the short-lived phase synchronized states during motor imagery tasks and used them for activity recognition purposes (Santamaria and James 2019). Rosario et al. used motif synchronization method to discover the time-varying brain networks during a visual experiment (Rosário et al. 2015). Pfurtscheller et al. highlighted the emergence of short-lived somatotopically-specific brain states during motor imagery activities (G. Pfurtscheller et al. 2008). Gu et al. used time-frequency decomposition for EEG signal collected during lower extremity motor imagery tasks and observed short-lived frequency-specific the ERD/ERS patterns (Gu et al. 2020). Ambrosi et al. proposed a particle filtering-based method to analyze the temporal variations of brain synchronization (Ambrosi et al. 2019). Hansen et al. addressed the transient nature of the synchronization between brain regions during the rest state (Hansen et al. 2015). Ren et al. analyzed the fluctuations of information integration/segregation via dynamic graph metrics and showed that during cognitive tasks, dynamic small world architecture emerges in the brain (Ren et al. 2017). Karamzadeh et al. used a dynamic time warping based approach to track and analyze the characteristics of time-varying brain synchronization due to auditory and visual stimulus presentation (Karamzadeh et al. 2013). Li et al, proposed a conditional Granger causality analysis to track the dynamic connectivity between brain regions (Y. Li et al. 2019). Spiegler et al. analyzed the frequency-specific time-varying phase coupling characteristics of tongue-movement imagery activity on the time-frequency domain (Spiegler, Graimann, and Pfurtscheller 2004). Dimitriadis et al. proposed a scheme that discretizes the captured short-lived phase-synchronized microstate patterns to analyze the transitory behavior of brain regions during task periods (S. I. Dimitriadis, Laskaris, and Tzelepi 2013). Schack et al. captured

the activity-specific short-lived cortical connectivity profiles during abstract and concrete noun processing (Schack, Weiss, and Rappelsberger 2003).

All these studies stress the importance of considering the dynamic nature of the brain in characterizing electrical activity during any kind of cognitive task (D. Vidaurre et al. 2018; G. Pfurtscheller et al. 2008). Additional studies stressed another related phenomenon; the emergence of systematic timing organization of synchronization between the electrical activity of the brain during cognitive tasks (Jeong, Gore, and Peterson 2001; Na et al. 2002; Ktonas and Mallart 1991; Boeijinga and Lopes da Silva 1989; A. Adhikari et al. 2010; Roelfsema et al. 1997; B. Orkan Olcay and Karaçalı 2019; Dawson 2004). The studies that consider the systematic timing organization of brain synchronization is based on the premise that the brain coordinates the information routing between its regions by re-organizing the synchronization timings between the particular brain regions for each different type of cognitive task according to the task demands (Dawson 2004; S. H. Jin, Lin, and Hallett 2012; Alais, Blake, and Lee 1998; Lin et al. 2020). Hereby, the brain integrates the localized neural activities by creating a short-lived communication window at different temporal and spatial scales between different brain regions by reciprocally modulating the inter-areal synchronization of the neural activities at activity-specific timings during the information routing (Palmigiano et al. 2017). This hypothesis is called the communication-through-coherence (CTC) hypothesis (Fries 2005). Also, it has been demonstrated that the timing organization between the brain regions at different spatial scales significantly enrich the repertoire of cognitive dynamics (Madadi Asl, Valizadeh, and Tass 2018). Supporting this hypothesis, Kirschner et al. identified the task-specific brain synchronization patterns that are consistently emerged during the particular cognitive task and these synchronization patterns remains more active than some of the inter-regional synchronizations observed within the default mode network (Kirschner et al. 2012). In a face recognition study, Wang et al. realized that the phase coherence simultaneously increases at infra-slow frequency bands between task-specific brain regions during face recognition task. Also, between the brain regions, the synchronization lag among the oscillatory activities becomes smaller for faster and accurate inter-regional communication. Additionally, they realized that the inter-regional synchronization lag flexibly re-organized to adapt to the requirements of cognitive activities (Yifeng Wang et al. 2019).

The issue of synchronization timing has also been analyzed in neuronal level. Vibert et al. and Asl et. al. performed several analyses on the inter-neural synchronization

delays and stated that the inter-neural synchronization timing is crucial to consider when characterizing the neural-level network behavior since synchronization timing is a controlling factor of brain functioning (Vibert, Pakdaman, and Azmy 1994).

1.2.5. Brain Activity Characterization Studies Using Different Methods

There are many BCI as well as brain activity characterization studies that uses different approaches than given above. Some approaches adopted parametric and non-parametric EEG modelling approaches. Tzovara et al. modelled the voltage topographies of different tasks and used this approach in a BCI framework (Tzovara et al. 2012). Mateo et al. used Volterra modelling for analysis for a brain activity characterization purpose (Mateo et al. 2013). Using same Volterra modelling approach, authors try to suppress the eye movement artifacts (Mateo et al. 2015). As a nonlinear signal processing method, entropy has proven to be a crucial method to capture vital features of the electrophysiological signals. Up to now, several different entropy methods was proposed. Approximate entropy (Pincus 1991), sample entropy (Richman and Moorman 2000), Renyi entropy (Principe 2010), bubble entropy (Manis, Aktaruzzaman, and Sassi 2017) are the most popular ones that are used in electrophysiological activity analysis. Arunkumar et al. used three different entropy measures to capture the dichotomy between the normal EEG and focal EEG activities (Arunkumar et al. 2017). Authors used for entropy features for classification purposes. They achieved brilliant recognition performances via non-nested generalized exemplars classifier. Raghu et al. proposed an epileptic activity classification method that calculates the sigmoid entropy of sub-bands of EEG activities (Raghu et al. 2019). Srinivasan et al. used approximate entropy to detect epileptic activity from EEG signals (Srinivasan, Eswaran, and Sriraam 2007). Sun discriminated the healthy people and stroke patients by detecting the changes of the cortical dynamics during motor observation task via fuzzy Approximate entropy (R. Sun et al. 2017). Olcay et al. used entropy to discriminate somatosensory stimulations presented to different hands (Bilal Orkan Olcay et al. 2017). Guducu et al. used an entropy estimation method to detect and separate the normal and anosmic subjects by evaluating the entropies of the different time intervals of EEG-derived potentials (Güdücü et al. 2019). Zeng et al. used multivariate multiscale permutation entropy method to track the

transient dynamics of the multichannel brain activity during interictal, pre-ictal and ictal periods (Zeng et al. 2018). The authors concluded that including the inter-regional interactions rather using only localized activity provides a better understanding of inherent nature of generation of absence epilepsy. Entropy has been used to uncover the significant changes in the brain dynamics during meditation (Vivot et al. 2020). Authors found that meditation induces considerable entropic changes in gamma band in the frontal brain regions and in alpha bands across all regions of the brain. In addition to these, brain complexity measures show a significant correlation with the brain functional connectivity (D. J. J. Wang et al. 2018b; Nobukawa et al. 2020). These two different perspectives (i.e., complexity and functional connectivity) are strongly related to the information processing capacity of the brain and can be used together the changes of neural behavior due to the diseases (Nobukawa et al. 2020). In this sense, McDonough et al. stated that the greater entropy is related to the greater neural activity complexity which possesses great potential for information processing especially at larger spatial scales (McDonough and Nashiro 2014). Previous studies have demonstrated that distinct pathological cases, as well as cognitive status, produce distinct nonlinear dynamics on physiological signals which can be detected by entropy measures (Labate et al. 2013; Zeng et al. 2018).

Besides the entropy, some other nonlinear signal analysis methods were employed to extract salient features from electrophysiological signals. Bola et al. used several fractal dimension determination methods to observe the changes of synchronization of local as well as distant brain regions during visual stimulus presentation (Bola, Gall, and Sabel 2015). Swiderski et al. characterized the short-lived epileptic brain oscillations by calculating the Lyapunov exponents (Swiderski, Osowski, and Rysz 2005). Vidaurre et al. used time domain statistical features for brain activity characterization (C. Vidaurre et al. 2009).

1.2.6. Brain Activity Characterization Studies Using Transfer Entropy

As stated above, the information transfer between the brain structures is realized by selective inter-regional functional synchronizations. These interactions should occur in a systematic timing organization for efficient and economical information transfer (Bullmore and Sporns 2012). Capturing these time-sensitive synchronizations requires

considering causality in synchronization pattern analyses. In this manner, several causality analysis methods were proposed to capture these causal interactions such as dynamic causal modelling (DCM) (K. J. Friston et al. 2019), Granger Causality (GC) (Granger 1969), kernel Granger Causality (Marinazzo et al. 2011), local linear nonlinear autoregressive model (LLNAR) (Freiwald et al. 1999). Among these methods, transfer entropy is one of the most crucial causality analysis approaches that has been frequently used to identify both linear and nonlinear causal interactions (Schreiber 2000). In essence, transfer entropy is a model-free and information-theoretic-based effective connectivity analysis method (Vicente et al. 2011) that should be carefully considered. In that sense, we opened a separate subsection for causality and transfer entropy.

Many studies employed transfer entropy to capture the causal synchronization patterns during the cognitive, motor, and perceptual processes (Vicente et al. 2011; S. Dimitriadis et al. 2016; Faes et al. 2016). Besides, Montalto et al. and Lindner et al. proposed transfer entropy calculation toolboxes for enabling wide usage of this method (Montalto, Faes, and Marinazzo 2014; Vicente et al. 2011). Although there are numerous merits of transfer entropy underlined in the previous literature, however, there some important drawbacks that must be considered. The most important one is that the transfer entropy requires a large number of signal samples and assumes stationarity for calculation. This means, transfer entropy inherently neglects the dynamical (i.e., transient) nature of the brain. This means that the transfer entropy method cannot consider the short-lived driver-response relationship between EEG channels. To cope with this drawback, Herrero et al. proposed a novel formulation of transfer entropy assessing the transient coupling dynamics of the brain regions (Gómez-Herrero et al. 2015). Although this method partially overcomes the stationarity assumption, it requires a large number of EEG trials for accurate estimation.

1.3. Objectives of the Thesis

In the literature, the methods, as well as the frameworks proposed either for brain-computer interfacing or other types of brain activity characterization studies, adopt using either the pairwise brain synchronization features or the features extracted from localized brain activities. The majority of these approaches assumes that the brain shows a

stationary behavior especially during cognitive activities which does not consistent with the dynamically changing nature of the brain. Besides, the studies that consider the transient and dynamically changing nature of the brain, however, mainly disregard the systematically adjusted timing organization that emerge among the brain regions.

Brain functional organization is flexible and economic which lead to a dynamic modulations of functional interactions among brain structures by changing its coordination dynamics due to changing cognitive conditions accordingly (Tognoli and Kelso 2009; C. F. Lu et al. 2011). Taking these transient coordination dynamics into consideration may elicit an accurate brain activity characterization for cognitive, perceptual, and motor processes. Additionally, Hermanto et al. hypothesized that the brain should generate similar neural responses as well as synchronization patterns at similar timings among its regions for each of every trial of a particular cognitive task to meet the task-specific demands (Hermanto et al. 2013). By considering these two important statements which refer to both the dynamic nature of the brain coordination and the systematic timing organization, an accurate characterization of the cognitive tasks can thus be obtained by capturing and using activity-specific timings at which the systematic, as well as characteristic inter-regional short-lived brain patterns (Danielle S. Bassett et al. 2006; S. H. Jin, Lin, and Hallett 2012).

In this thesis, we intend to obtain the timings of the activity-specific short-lived (i.e., transient) brain patterns for cognitive activity characterization. The brain patterns that we identify the timings are 1) pairwise inter-regional brain synchronizations, 2) localized brain activities. We figured out the importance of considering the systematic timing organization during cognitive activity characterization in a motor imagery activity characterization framework. We selected this framework due to its popularity in the neuroscience area. The methods proposed in this thesis can be used to characterize any type of cognitive activity.

To sum up, the main message of this thesis is that the brain generates cognition/behavior by adaptively changing the timing organization of both synchronizations between different regions and local information encoding. In that sense, the characterization of brain activity by using entire task periods are not meaningful. In order to obtain a logical and reliable characterization accuracy, one must consider the systematically adjusted temporal dynamics of the brain.

Please note that, the performances, especially obtained using PhysioNet dataset, were relatively low when comparing with the performances of existing BCI literature. It

is important to highlight that, as stated above, the common approach for removing the muscular or other type of artifacts is to decompose the EEG signal via independent component analysis method (Varsehi and Firoozabadi 2021). This kind of approach may not be applicable in a real-time BCI setting since it enhances the recognition time dramatically. So, in this thesis, we did not use any blind signal source separation method as preprocessing.

1.4. Organization of the Thesis

We start our discussion in Chapter 2 by introducing the definitions of EEG. Then, we give some information about the neurophysiological basis of motor imagery, the notion of brain connectivity. Then, we provided the mathematical expression of the methods that we used throughout this thesis. Next, we described the motor imagery based EEG datasets that we used for evaluating the proposed BCI models.

In Chapter 3, we proposed a novel motor imagery activity recognition framework. In this framework, we captured the activity-specific time lags (τ) between the EEG channels by using the task periods in the training dataset. We then used this time lags to calculate the inter-channel synchronizations for each training and test task periods. We compared the recognition performance of the method with well-known method CSP. In the last section of this chapter, we discussed the significant points of the outcomes.

In Chapter 4, we extend the perspective in the previous chapter by introducing two more timing parameters (i.e., Δt and w) for brain activity characterization. In this chapter, we propose a heuristic search strategy to find activity-specific timing parameter triplets (i.e., $\Delta t, \tau$, and w) for each EEG channel pair and cognitive activity type. We then characterized each motor imagery task in dataset by calculating the inter-channel synchronization by using the timing parameter triplets and performed a classification analysis. We again compared the performance results with CSP method and univariate AR modelling method.

In Chapter 5, we characterized the motor imagery activities by clustering transiently synchronized EEG channel pairs according to their synchronization values. Note that the inter-channel synchronizations are calculated at activity-specific timings. The channel clusters that elicited P-values are then used for feature for recognition

purposes. We provided and discussed both recognition performances and the statistically significant clusters in the last part of this chapter.

In Chapter 6, we proposed a brain activity characterization method that finds and uses the timings of the short-lived brain oscillations where the entropies of the brain oscillations are appeared as activity-specific. In order to find these timings parameters, we adopted a heuristic-probabilistic search strategy. We provided the classification performances as well as the biophysical outcomes with necessary discussion at the end of this chapter.

In Chapter 7, we proposed a novel autoregressive modelling for cognitive activity recognition purposes. This method incorporates both channel interactions and internal channel dynamics into a single model. In order to construct this combined model, we used both multivariate (channel interactions) and univariate AR modelling (internal channel dynamics) together to obtain a representative model for each type of cognitive activity. The performances show that, we achieved a better activity recognition performances than the previously presented methods and benchmark BCI methods.

In Chapter 8, we provided a general conclusion related to the results obtained in this thesis and also some future directions that may contribute an important insight to the timing organization of the brain.

CHAPTER 2

BACKGROUND

Any man could, if he were so inclined,
Be the sculptor of his own brain
-Santiago Ramon y Cajal-

In this chapter, we provide the background information for the important topics related to content of this thesis. Throughout this thesis, we proposed different brain activity characterization methods and we evaluated their performances on the publicly available two EEG datasets collected under different motor activity imagery experiments. We provide the details of these datasets in the upcoming subsections. We first give some brief information about EEG and generation of EEG signal. Then in the next subsection, we give details of neurophysiological basis of motor imagery and notion of brain connectivity. Thereafter, we give the details of the mathematical methods and the datasets that we used in this thesis.

2.1. Electroencephalogram (EEG)

The EEG is the brain's electrical activity that is collected via electrodes on the scalp (Sanei and Chambers 2013). It mainly reflects the oscillations produced by ensembles of cortical-pyramidal neurons. The recording of electrical oscillations was done by Richard Caton in 1875 (Caton 1875). This experiment was conducted on monkeys' and rabbits' brains by using a simple galvanometer. Shortly after, Caton performed similar experiments on the human brain. In 1929, Hans Berger was the person who conducted an experiment on the human brain via a powerful Siemens double-coil galvanometer (Berger 1929). This experiment was assumed as the milestone of system neuroscience since important findings were discovered that shed light on many mysteries of the brain. The "EEG" terminology was put forward in these years. A few months later,

Berger conducted another experiment on the human brain via a bipolar recording from frontal-occipital sites and concluded that alpha oscillations are major oscillation components within the brain.

Thereafter, many developments came through. The importance of multichannel EEG recordings was noticed by Kornmüller (Kornmüller 1935). The EEG was used to investigate the brain rhythms of human brain during sleep by Hallowel and Davis. Thereafter, Loomis and friends conducted mathematical analysis to sleep EEG patterns. First intracerebral EEG recordings was performed by Mayer and Hayne in 1948, and first intracortical EEG recording was conducted by Phillips in 1961.

Berger and Dietch performed Fourier analysis to EEG recordings in 1932. This attempt was used to investigate sleep related disorders by Kleitman. In 1960, it was realized that the evoked potentials embedded in EEG signals contains vital information about mental status.

2.1.1. Generation of EEG Signals

As provided, the EEG signal is the measurement of current flows during synaptic excitations of pyramidal cortical neurons. This current is generated by motion of positive (i.e., Na^{+}, K^{+} and, Ca^{++}) and negative ions (i.e., Cl^{-}). This motion of ions is mostly governed by changes of membrane potentials of neural cells.

The human head consist of three main layers. These are scalp, skull, and the brain. We presented the resistivity values of each layer in Figure 6. There are many different thin layers between these layers. The EEG activities and many other noise components were low-pass filtered and attenuated while travelling from neuronal tissue through scalp. Approximately, there are more than 100 billion of neurons inside the brain and each one of them is interconnected to ten thousands of other neurons (Eagleman 2019). Note that the number of neurons and their synaptic connection amounts may alter during life span due to several reasons such as aging, changes in health condition, and some other environmental/genetic factors.

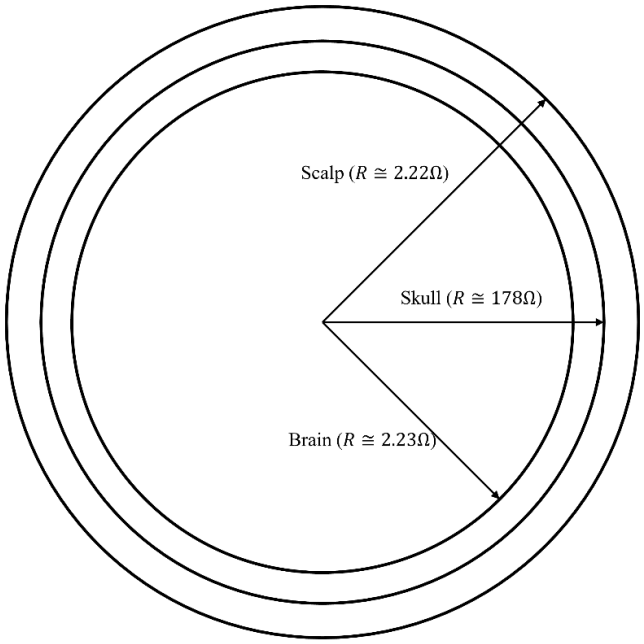

Figure 6. The three main layers and their resistivity values
(Source: Sanei and Chambers, 2013).

The brain processes are known to be highly complex and manifests itself in multiple frequency bands (J. Li et al. 2016). For analysis and diagnosis purpose, the EEG signal is divided into smaller frequency bands according to their inherent characteristics (Başar et al. 2001; Klimesch 1996; Sanei and Chambers 2013). The name and corresponding frequencies of these bands are provided in Table 2.

Table 2. The major frequency bands and their frequencies

Band Name	**Corresponding Frequency Range**
Delta (δ)	0.5-4 Hz
Theta (θ)	4-7.5 Hz
Alpha (α)	8-13 Hz
Beta (β)	14-28 (~30) Hz
Gamma (γ)	Upper than 30 Hz

In the literature, there are vast number of studies have analyzed the relationship between these frequency bands and cognitive activities/status (Klimesch, Sauseng, and Hanslmayr 2007; Sauseng et al. 2005; Klimesch 2012; 1996; Ozgoren et al. 2010). We will not provide the details of this relationships since this topic is out of the scope of this thesis. Interested readers may look at the references provided herein.

2.1.2. EEG Measurement

In order to collect the electroencephalography signals, different EEG recording systems and setups were developed. Basically, these systems have similar structure. The EEG system generally consist of four different subsystems. These are:

- Electrodes
- Amplifier with filters
- Analog-to-digital converter
- Recording

The very first step in EEG signal collection procedure is the electrodes and their montages on the scalp surface. The electrodes should be attached to the participants according to previously adopted standards. There are several electrode types that can be listed as:

- Disposable electrodes (gel-less, and pre-gelled types)
- Reusable electrodes (gold-, silver-made)
- Electrode caps and head bands
- Saline-based electrodes
- Needle electrodes

For both clinical and research purposes, in general, electrode caps are preferred where multichannel EEG recordings are required (Teplan 2002). The electrodes are placed onto had surface according to a standardized positioning system. In 1958, the 10/20 system were adopted as standard for electrode placement. According to this system, the head surface is separated into the corresponding proportional distances (i.e., %10-%20) by considering important landmarks such as inion, nasion, and preauricular points

(Teplan 2002). Please note that apart from 10/20, there are several widely adopted electrode positioning systems can be used such as 10/10, 10/5, 5/5 (Jurcak, Tsuzuki, and Dan 2007). In Figure 7, we provided an illustration of electrode cap with 64 electrodes placed in 10/10 system. Note that the electrodes are pre-gelled type electrodes represented in this figure.

Figure 7. The illustration of 64 electrodes on a head model placed according to 10/10 recording system.

The collected EEG signals should initially be amplified and filtered to enhance the visibility of the neural activities for further processing before recording. The basic requirements of the EEG amplifiers are (Nagel 2003; Teplan 2002):

- Amplifier should not distort the neural activity
- Amplifier should clearly separate neural activity and unwanted noise components
- Amplifiers should have a power protection against electric shocks
- Amplifiers should protect itself from high input voltage shocks.

The conversion of amplified and filtered analog EEG activities into a digitized form is called analog-to-digital conversion. The repetition of this conversion in a second determines the sampling frequency of the digitized signal. The sampling frequency of EEG signals is of great importance for extracting meaningful information (B. Orkan Olcay and Karaçalı 2019).

The quantization of EEG signals is related to the accuracy of the signal amplitudes. The majority of EEG recording systems adopt 16-bit quantization (Schalk et al. 2004). Besides, 24-, 32- and 64-bit systems is available in market (Guger 2018).

Besides the traditional *in-lab* EEG recording systems, mobile EEG recording systems are attracting technology nowadays. These systems provides unprecedented flexibilities to the researchers to develop new strategies for studying neurodevelopmental cognitive disorders (Lau-Zhu, Lau, and McLoughlin 2019). These systems use, in general, dry electrodes, light-weight amplifiers, and wireless transmission which are important for portability. These systems can be used in any purpose such as analyzing the event-related potentials (P300, N1, N2), brain-computer interfacing, analyzing the functional connectivity patterns for various neurophysiological disorders. Mobile EEG systems can analyze the data with advanced analytical approaches such as time-frequency methods, statistical subspace decomposition methods (e.g., ICA, PCA), causality methods to extract biomarkers for various scientific aims.

2.2. The Neurophysiological Basis of Motor Imagery

Motor imagery is arguably one of the most remarkable and interesting, even referred to as “embodied cognition” to study brain functioning (Höller et al. 2013; Hanakawa 2016). It includes specific brain regions related to cognitive control and movement planning and generation (Decety 1996). As Jeannerod stated, motor imagery can be thought of as a dynamic preparation phase of the brain before the real motor execution (M. Jeannerod et al. 1995). In this preparation phase, several movement-related parameters, duration, and motor programs are adjusted. As evidence, the majority of neuroimaging studies related to motor imagery/execution highlighted that the consciously performed motor imagery and motor preparation phases activate similar brain regions. This argument may explain the reason for the similarity of activated neural structures both

in motor execution and imagery tasks. This similarity can also be observed physiologically. Shaw et al. observed that, during the imagery weightlifting task, linear relationship was observed between the weight and amplitude increase of electromyography (EMG) signals collected from the forearm. This significant outcome stresses that the neural organization of motor imagery is not the result of having an ability of movement execution. In order to gain a better insight related to the regions of the brain we provided a graphical illustration that presents the brain regions to achieve a general overview of which regions are responsible for motor imagery functioning in the upcoming part of this subsection (please see Figure 8).

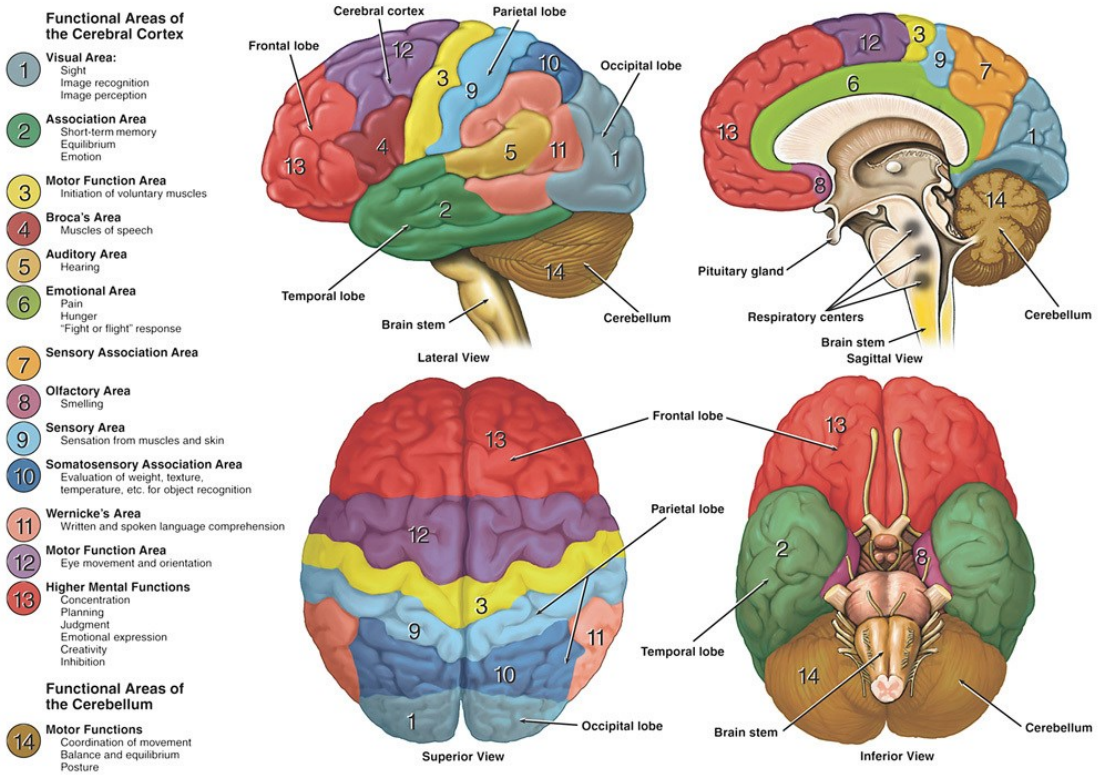

Figure 8. An illustration of regions of the brain (Sukel Kayt 2019)
(Source: dana.org/article/neuroanatomy-the-basics)

Motor imagery functions, in general, is controlled by the frontal regions of the brain. One of the crucial brain regions is the primary motor cortex (M1) for both motor execution and imagery. This brain region is located in the dorsal portion of the frontal lobe. Its functional roles are planning and executing the motor actions. During motor task,

contralateral M1 demonstrates strong desynchronization (i.e., ERD) which indicates the reactivity of this region. Several studies in the literature stressed the activation of M1 region but some of them were not (Dechent, Merboldt, and Frahm 2004). According to the Lotze et al., the major reason of such inconsistent results may be the relatively small amount of and shorter time of M1 regions than that of during execution (Lotze and Halsband 2006). From the biophysical point of view, M1 region in separated into two distinct subregions. One of the subregions (dorsal part of M1) is closely related to the pure motor execution tasks, another one in close interaction with BA6 area of the brain which plays active role especially in complicated motor execution/imagery tasks. The type and complexity of imagery movements may be another reason of this inconsistent activation profile of M1.

Another important brain region is cerebellum. This area is responsible for reciprocal information transform the internal (i.e., neural) image of the movement into actual physical conditions for execution/imagery. Neuroimaging studies demonstrated that the cerebellum and other important structures such as prefrontal cortex, premotor cortex, and basal ganglia show significant activation simultaneously. The anterior part of the cerebellum elicits significant activation during sensorimotor exploratory movement tasks, and it shows strong functional correlation with contralateral M1 region for facilitation. The other parts of cerebellum such as Purkinje cells, however, have inhibitory impact on contralateral motor cortex to prevent the efferent impulses reach to target muscles (Cengiz and Boran 2016). Movement/imagery related information is conveyed by corticopontino-cerebellar tract. This structural connection links cerebellum to the supplementary motor area (SMA) and premotor area (PMA) which means this connection carries vital motor imagery related to information (Wheaton et al. 2005).

SMA and PMA are known as the most crucial brain areas for motor imagery tasks (Kasess et al. 2008). Studies that analyzes the neural correlates of motor imagery captured strong and consistent activation from these two brain regions (Q. Gao, Duan, and Chen 2011; Hanakawa 2016). SMA is mainly responsible for processing the aspects of movement during preparation phase. In the literature, it is pointed that some parts of the SMA regions plays active role in selection of correct movement prior to the preparatory phase. Kasess et al. stated that functional connectivity between SMA and M1 may be due to the inhibition of M1 activity to avoid unwanted muscular movement during motor imagery (Kasess et al. 2008). Similarly, PMA region is one of the key brain regions for motor imagery tasks. It is stated in the literature that different motor imagery strategies

(kinesthetic / visual modalities) activate different portions of PMA. Also, it elicited significant activation during language production and movement observation.

Superior parietal lobe (SPL), inferior parietal lobe (IPL) and precuneus also play key role in motor imagery tasks. They are responsible for processing spatial information of the movement execution/imagery. The processed spatial information of motor movement/imagery is transferred and stored into premotor cortex. SPL are functionally linked to posterior part of SMA and also premotor cortex.

The dorsolateral prefrontal cortex and prefrontal cortex are of great importance in motor imagery tasks. They reciprocally interact and adjust the timing of the overt/covert movements (Petrides 1994). Rather than these brain regions, basal ganglia, anterior cingulate cortex, inferior frontal gyrus may play significant roles in motor imagery activity preparation. Please note that we aimed to provide general information and activation profiles of motor imagery-related brain regions. In the upcoming chapters, we will provide extra information about activated brain regions and compare the resulting brain regions with existing biophysical literature.

2.3. Brain Connectivity Phenomenon

There are two main types of connectivity appears in the brain. These are connectivity types are as follows:

- Anatomical (structural) connectivity
- Statistical connectivity

A central paradigm in modern neuroscience points that the anatomical and statistical connections are adapted in a way for optimal information processing. As the result of this optimality, the brain regions are organized as spatially distributed and but functionally connected regions (Lang et al. 2012).

In the previous chapter, we simply mentioned the notion of statistical connectivity and related studies. Anatomical connectivity refers to the physical connections between brain structures. It simply connects different neuronal tissues by fiber tracts. The bunch of many of those fiber tracts forms the white matter of the brain. As depicted in the previous chapter, the statistical connectivity is related to the instantaneous correlation of

electrical/hemodynamical activities of different brain regions (Fingelkurts, Fingelkurts, and Kähkönen 2005). The statistical connectivity can be divided into two categories as:

- Functional Connectivity
- Effective Connectivity

Functional connectivity refers to the undirected temporal correlation between activities of brain regions. Effective connectivity describes the directed correlation of the activity of a brain region that exerts on another, which refers to the causal relationship between these brain activities.

The statistical connectivity phenomenon accommodates the mechanism of coordination of interactions of brain activity emerged from different neuronal populations. In the recent past, however, statistical connectivity was understood as an elusive concept due to the fact that the perspectives and theories put forward by neuroscientist were enormously different. As time went on, these debates have arrived at a unique solution. The researchers realized that the major source of occurrence of statistical connectivity is the brain plasticity. Simply, brain plasticity is the term that describes the rewiring of the structure of the brain itself for adaptation, learning, and so forth (Costandi 2016). After a while, researchers understood that brain plasticity is too slow to explain the fast changes of statistical connectivity within the brain during cognitive and perceptual processes (Fingelkurts, Fingelkurts, and Kähkönen 2005). A detailed understand of brain operations has now become possible with the realization of exact meaning of the notion of statistical connectivity. It is therefore clarified that further understanding of the brain operations from correlated neural events rely on suitable mathematical methods.

2.4. The Mathematical Expressions of the EEG Analysis Methods

In this section, we give the mathematical expressions of each method that were used in this thesis. Note that, we provided the formulations of entropy as well as synchronization methods without introducing any timing parameter for the sake of simplicity. Note also that, we used these methods in upcoming chapters by introducing these parameters into these formulations.

2.4.1. Entropy Estimation

The notion of entropy has been proved its effectiveness in EEG signal analysis studies. It is powerful information-theoretic method to quantify the brain functioning ranging from functional interactivity between brain regions to quantification of state of consciousness (Keshmiri 2020). Various type of entropy definitions has been proposed for brain research studies. We described these entropy methods and related studies in the previous chapter.

In this thesis, we adopted quantifying differential entropy of EEG signals. The mathematical expression of differential entropy is given as

$$H(X) = -\int_{\infty}^{+\infty} f_X(x) \log f_X(x)\ dx \tag{2.1}$$

where $f_X(x)$ is the marginal probability density function (pdf). The equation given above says that, calculating the differential entropy requires probability density function of signal X. However, calculating the density function of the corresponding signal from its limited number of observations is not straightforward. In the literature, there two estimation methods, K-L (Kozachenko and Leonenko 1987) and Vasicek's estimator (Vasicek 1976). Due to its computation speed and slightly better accuracy, we used Vasicek's unbiased entropy estimation method to estimate the entropy of EEG signals. The mathematical expression of the Vasicek's entropy estimator $\widehat{H}(\cdot)$ is given as (Ibrahim Al-Omari 2014)

$$\widehat{H}(X) = \frac{1}{N}\sum_{k=1}^{N} \log\left(\frac{N}{2m}\right)\left(\tilde{X}_{(k+m)} - \tilde{X}_{(k-m)}\right) - \left(\log(N) - \log(2m) + \left(1 + \frac{2m}{N}\right)\psi(2m) - \psi(N+1) + \frac{2}{N}\sum_{i=1}^{m}\psi(i+m-1) \right) \tag{2.2}$$

where N is the total number of samples of X, m denotes the neighborhood used for entropy estimation, $\psi(\cdot)$ denotes the digamma function, and $\tilde{X}$ denotes the sample-ordered version of the signal X. Note that, we used the first neighborhood statistics (i.e., $m = 1$) when calculating the entropies.

2.4.2. Synchronization Measures

In this thesis, one of our major aim is to capture the timing parameters of the characteristic brain synchronization patterns. To that end, we used ten different synchronization metrics throughout this thesis to determine which synchronization measure is good at capturing biophysically relevant synchronization patterns as well as provides useful synchronization features for a satisfactory recognition performance. Note that each of these measures has its own advantages and disadvantages. Besides these measures, there are many different measures that was reviewed in the literature (André M. Bastos and Schoffelen 2016; H. E. Wang et al. 2014). We provided the mathematical expressions of each one of the individual synchronization metrics in detail below. Note that we treat the signals x and y as realizations of random variables X and Y.

2.4.2.1. Mutual Information

The mutual information is a well-known synchronization measure that calculates the common statistical uncertainty shared between two signals X and Y. The mutual information between signals can be expressed as

$$S_{MI}(X,Y) = \int_{-\infty}^{\infty}\int_{-\infty}^{\infty} f_{XY}(x,y)\ \log\frac{f_{XY}(x,y)}{f_X(x)\,f_Y(y)}\ dx\ dy \tag{2.3}$$

where $f_X(x)$ and $f_Y(y)$ are the respective first-order marginal probability density functions, and $f_{XY}(x,y)$ is the corresponding joint probability density function. However, obtaining the probability densities above from a limited number of samples is not straightforward. A common approach is to partition the samples into several bins and calculate histograms. Another well-known strategy is to use kernel-based density estimators (Hill 1985; Principe 2010). Yet, these methods need large sample sets to provide an accurate mutual information estimation. As an alternative approach, Kraskov et al. proposed a method based on neighborhood statistics of the data samples given by

$$S_{kraskovMI}(X,Y) = \psi(k) - \langle\psi(n_x+1) + \psi\big(n_y+1\big)\rangle + \psi(N) \tag{2.4}$$

where $\psi(\cdot)$ is the derivative of gamma function (i.e. digamma function) (Kraskov, Stögbauer, and Grassberger 2004). The parameters $n_x,\ n_y$ denote the number of points whose distances are less than $\epsilon(i)/2$ to points x_i and y_i respectively, while $\epsilon(i)/2$ is the maximum of the Euclidean distance between x_i and y_i and their k^{th} neighbor, N is the number of samples, and $\langle\cdot\rangle$ represent the calculation of average over i.

2.4.2.2. Cross-Correntropy

Correntropy is a measure of similarity that calculates the similarity of two signals X and Y by utilizing both the probability and the time domain structures. (Santamaría, Pokharel, and Principe 2006; Liu, Pokharel, and Principe 2007; Principe 2010). The formulation of the cross-correntropy measure between the signals X and Y is given in terms of their samples (x_i, y_j) for $i, j = 1,2,..,N$ as

$$S_{correntropy}(X,Y) = \frac{1}{N}\sum_{i=1}^{N} \kappa_{Laplacian}(x_i, y_i) \tag{2.5}$$

where N is the number of data samples and $\kappa_{Laplacian}(\cdot,\cdot)$ denotes the Laplacian kernel function. This kernel function can be defined as (M. Rao et al. 2011)

$$\kappa(x_i, y_i) = \exp(-|x_i - y_i|) \tag{2.6}$$

where $\exp(\cdot)$ denotes the exponential function.

2.4.2.3. Phase Locking Value

The PLV method calculates the stability of the phase difference between two oscillations by averaging the instantaneous phases across trials (Lachaux et al. 1999; Varela et al. 2001; Lachaux et al. 2002; Aviyente et al. 2011). The instantaneous phases can be calculated via wavelet transform, Fourier transform, and Hilbert transform (Brunner et al. 2006). In this thesis, we calculated the instantaneous phases by taking the Hilbert transform of the signals. For the signal x, the Hilbert transform is calculated as

$$\tilde{x}(t) = \frac{1}{\pi}\, PV \int_{-\infty}^{\infty} \frac{x(t')}{t - t'}\, dt' \tag{2.7}$$

where *PV* indicates the Cauchy Principal Value. The instantaneous phase of the signal $x(t)$ can then be calculated using

$$\theta_x(t) = \arctan \frac{\tilde{x}\{(t)}{x(t)} \tag{2.8}$$

In our analysis, we obtained the phase locking value between the EEG signals X and Y as

$$S_{PLV}(X, Y) = \frac{1}{N} \left| \sum_{i=1}^{N} \exp\left\{ j\left(\theta_{x_i} - \theta_{y_i}\right)\right\} \right| \tag{2.9}$$

where N is the common signal length and θ_{x_i} and θ_{y_i} represent the instantaneous phases of the corresponding signals (Daly, Nasuto, and Warwick 2012; Gonuguntla, Wang, and Veluvolu 2016; Brunner et al. 2006). The PLV equals 1 if the phase difference is 0, and the PLV attains 0 when the phase difference shows a random distribution across trials.

2.4.2.4. Phase Coherence Value

The phase coherence value between the signals X and Y can be obtained by calculating the entropies of their instantaneous phase differences (Bakhshayesh et al. 2019b; Tass et al. 1998; Ziqiang and Puthusserypady 2007). The phase coherence value can be calculated as

$$S_{PCV}(X,Y) = \frac{H_m - \widehat{H}(\theta_x - \theta_y)}{H_m} \tag{2.10}$$

where $\widehat{H}(\cdot)$ is the Vasicek's entropy estimation function, $H_m = \log(NF_s)$, F_s is the sampling frequency, N is the common length of the used signals. Note also that, when the phase difference shows a regular behavior, PCV based synchronization between the signal segments approaches to 1, when phase difference shows a random behavior PCV decays to 0.

2.4.2.5. Cosine-based Similarity

The cosine-based similarity method simply calculates the angle of energy-normalized correlation of two signals X and Y and subtracts from π. The mathematical expression of cosine-based similarity is given as (Sargolzaei et al. 2015; Herff et al. 2019)

$$S_{cosine}(X,Y) = \pi - \arccos\left(\frac{\langle x,y\rangle}{\|x\|\|y\|}\right) \tag{2.11}$$

where $\langle\cdot,\cdot\rangle$ and $\|\cdot\|$ represent the inner product and the Euclidean norm operators, respectively. The maximum synchronization between signals occurs when the correlation angle between them is zero. For the signals $z_1(t)$ and $z_2(t)$, the dot product $\langle z_1, z_2\rangle$ is calculated as

$$\langle z_1, z_2\rangle = \int_{-\infty}^{\infty} z_1(t) z_2(t)\ dt \tag{2.12}$$

providing an expression for the signal norm

$$\|z\| = \sqrt{\langle z, z \rangle} \tag{2.13}$$

In the implementation, the discrete versions of the above expressions were used to suit the digitally recorded EEG data using sums instead of the integrals.

2.4.2.6. Cross-Correlation

The cross-correlation method measures the linear statistical dependency between two signals X and Y. The sample estimate of the cross-correlation can be calculated as

$$S_{xcorr}(X, Y) = \frac{1}{N} \sum_{i=1}^{N} x_i y_i \tag{2.14}$$

The sign of the cross-correlation is an indicator of the direction of the correlation. Note, however, throughout this study, we take the absolute value of the resulting correlation value to find the activity-specific synchronization based on magnitude of the resulting correlation only.

2.4.2.7. Linearized Mutual Information

Although the Kraskov's mutual information estimation methods achieved a notable success, calculation of mutual information via this method requires huge amount of computation time. A simplified approach is to assume that the signal segments are Gaussian distributed with zero mean and unity variance (Kraskov, Stögbauer, and Grassberger 2004; S. H. Jin, Lin, and Hallett 2010; Montalto, Faes, and Marinazzo 2014). In this case, the mutual information between the signals X and Y can be calculated as

$$S_{linearMI}(X,Y) = -\frac{1}{2}\log(1-\rho_{XY}^2) \tag{2.15}$$

where ρ_{XY} is denoted as the correlation coefficient between the signals X and Y. The correlation coefficient can be calculated as

$$\rho_{XY} = \frac{\mathrm{cov}(X,Y)}{\sigma_X\,\sigma_Y} \tag{2.16}$$

where $\mathrm{cov}(X,Y)$ is the function that calculates the covariance between X and Y σ_X is the standard deviation of X. Note that, the linearized mutual information uncovers the second-order correlation statistics between X and Y. However, the mutual information estimation methods (i.e., Kraskov's method) can consider higher order correlation statistics when calculating the synchronization. We tried linearized mutual information to observe if there is an advantage of assuming the Gaussianity for the distribution of the signals which is usually reasonable for the short-lasting quasi-stationary EEG activities (Lemm, Schäfer, and Curio 2004). Another reason for using linearized mutual information is its advantage in computational speed.

2.4.2.8. Nonlinear Interdependency

Consider the time series data of the signals X and Y collected into phase space vectors $\boldsymbol{x_i} = \left(x_i, x_{i-d}, \dots, x_{i-(m-1)d}\right)^T$ and $\boldsymbol{y_j} = \left(y_j, y_{j-d}, \dots, y_{j-(m-1)d}\right)^T$ where m and d parameters represent the phase space dimension and the time delay defined in phase space, respectively, and x_i and y_j are the samples of the time series. Then, the average Euclidean distance between n^{th} phase space vector of observation X and its first k nearest neighbors is given as

$$R_n^k(X) = \frac{1}{k}\sum_{p=1}^{k} \left\| \boldsymbol{x_n} - \boldsymbol{x_{r_{n,p}}} \right\|^2 \tag{2.17}$$

where $r_{n,p}$ represents the indices of the nearest neighbors of n^{th} phase space vector of observation x_i. Likewise, the Y-conditioned average Euclidean square distance to its k nearest neighbor of the vectors of observation X is

$$R_n^k(X|Y) = \frac{1}{k}\sum_{p=1}^{k} \left\| \boldsymbol{x_n} - \boldsymbol{x_{s_{n,p}}} \right\|^2 \tag{2.18}$$

where $s_{n,p}$ denotes the indices of the nearest phase space vectors of Y. The nonlinear interdependence measure between the time series X and Y (Arnhold et al. 1999) is defined as

$$S_{nonlinearInt}(X,Y) = \frac{1}{N}\sum_{n=1}^{N} \frac{R_n^k(X)}{R_n^k(X|Y)} \tag{2.19}$$

By construction, $R_n^k(X|Y^\tau) \geq R_n^k(X)$, so the result is between 0 and 1. The parameter N denotes the sample size. In this study, we selected k as 10, dimension m of phase space vectors as 6, and delay for phase space representation as 1 as initially suggested by Bandt and Pompe (C. Bandt and Pompe 2002; Román Baravalle, Rosso, and Montani 2018; Roman Baravalle, Rosso, and Montani 2018).

2.4.2.9. Wavelet Bi-Coherence

The continuous wavelet transforms of the signals X and Y can be calculated as (Mallat 2009)

$$W_x(a,t) = \int_{-\infty}^{\infty} x(\bar{t}) \frac{1}{\sqrt{a}} \phi^* \left(\frac{\bar{t}-t}{a} \right) d\bar{t} \tag{2.20}$$

and

$$W_y(a,t) = \int_{-\infty}^{\infty} y(\bar{t}) \frac{1}{\sqrt{a}} \phi^* \left(\frac{\bar{t}-t}{a} \right) d\bar{t} \tag{2.21}$$

where $\phi(\cdot)$ is the mother wavelet function of choice, a and t are the scale and translation parameters, respectively. In this thesis, we used complex-valued Morlet function as mother wavelet which is the most used wavelet function in biological signal analysis (Alexander E. Hramov et al. 2015; Makarov et al. 2018). The scale to frequency conversion can be done by using the formula (Emre Cek, Ozgoren, and Acar Savaci 2010)

$$f = \frac{F_c \, F_s}{a} \tag{2.22}$$

In the above equation F_c denotes center frequency of the mother wavelet function, F_s represent the sampling frequency of the EEG signal. The real and imaginary part of the complex wavelet coefficients can be represented as $W_x(f,t) = m_x(f,t) + in_x(f,t)$ and $W_y(f,t) = m_y(f,t) + in_y(f,t)$. The real and imaginary part of the mutual wavelet spectrum $\gamma_{X,Y}$ from their individual wavelet coefficients can be calculated as (Makarov et al. 2018; Alexander E. Hramov et al. 2015)

$$Re\left[\gamma_{X,Y}(f,t)\right] = \frac{m_x(f,t)\, m_y(f,t) + n_x(f,t)\, n_y(f,t)}{\sqrt{m_x^2(f,t) + n_x^2(f,t)}\sqrt{m_y^2(f,t) + n_y^2(f,t)}} \tag{2.23}$$

and

$$Im\left[\gamma_{X,Y}(f,t)\right] = \frac{n_x(f,t)\, m_y(f,t) - n_y(f,t)\, m_x(f,t)}{\sqrt{m_x^2(f,t) + n_x^2(f,t)}\sqrt{m_y^2(f,t) + n_y^2(f,t)}} \tag{2.24}$$

The time average of the real and imaginary parts of the mutual wavelet spectrum is expressed as

$$Re\left[\gamma_{X,Y}(f)\right]_{TA} = \frac{1}{N}\int Re\left[\gamma_{X,Y}(f,t)\right]dt \tag{2.25}$$

and

$$Im\left[\gamma_{X,Y}(f)\right]_{TA} = \frac{1}{N}\int Im\left[\gamma_{X,Y}(f,t)\right]dt \tag{2.26}$$

The magnitude of the time-averaged wavelet spectrum can be calculated as

$$\gamma_{X,Y}(f) = \sqrt{\left\{Re\left[\gamma_{X,Y}(f)\right]_{TA}\right\}^2 + \left\{Im\left[\gamma_{X,Y}(f)\right]_{TA}\right\}^2} \tag{2.27}$$

We then averaged the magnitude of the time-averaged mutual wavelet spectrum across the frequency tones and obtained the wavelet bi-coherence between the signals as

$$S_{WaveletBiCoh}(X,Y) = \frac{1}{\Delta f}\int_{f_i}^{f_j} \gamma_{X,Y}(f)\, df \tag{2.28}$$

where Δf represents the length of the interval of frequency of interest. In this study, we took f_i = 8 Hz and f_j = 30 Hz.

2.4.2.10. Kendall's Tau Correlation

Kendall's tau correlation coefficient is a rank-based correlation method that simply uses the total number of pairs of the signs of the difference of signal samples with their successive ones for calculating the synchronization (M. G. Kendall 1946; M. Kendall 1938). The mathematical expression of Kendall's tau correlation can be given as

$$S_{Kendall}(X,Y) = \left|\frac{2K_{XY}}{N(N-1)}\right| \tag{2.29}$$

where K_{XY} is the total number of signal samples that their difference with upcoming signal sample have similar signs, and N is the total number of signal samples. The parameter K_{XY} can be calculated as

$$K_{XY} = \sum_{i=1}^{N-1}\sum_{j=i+1}^{N} \operatorname{sgn}\Big(\big(x_i - x_j\big)\cdot\big(y_i - y_j\big)\Big) \tag{2.30}$$

2.4.3. Autoregressive Modelling

The autoregressive models are denoted as linear predictive models so that their observations are obtained by filtering the past samples of a stochastic processes. There are two types of AR processes, univariate, and multivariate AR. The generic formulation of a univariate AR process is expressed as

$$u(n) = a_1 u(n-1) + a_2 u(n-2) + \cdots + a_M u(n-M) + v(n) \tag{2.31}$$

where $a_1, a_2, \ldots, a_M$ are the AR model coefficients, $v(n)$ is the residual term (i.e. sometimes referred to as error or innovation term) which is generally accepted as normally distributed (Haykin and Widrow 2005; Haykin 2001). The current value of the signal $u(n)$ is obtained by summing the linear combinations of the past samples of $u(n)$ (i.e., $u(n-1), u(n-2), \ldots u(n-M)$). The AR model parameters can be estimated by adopting the methods of least squares, Yule-Walker, Burg, maximum likelihood estimation, modified covariance method (Kuruoğlu 2002; Golub and Saunders 1970; Subasi 2007). In this thesis, we used the methods of least squares to estimate the model parameters (Kuruoğlu 2002; Billinger, Brunner, and Müller-Putz 2013). The initial point of methods of least squares for estimating the model coefficients is minimization of the mean squared error

$$E\{|v(n)|^2\} = E\{|u(n) - \hat{u}(n)|^2\} \tag{2.32}$$

where $\hat{u}(n) = \sum_{k=1}^{M} a_k u(n-k)$. The term $v(n) = u(n) - \hat{u}(n)$ can be written in matrix-vector form as

$$v(n) = \begin{bmatrix} u(M+1) \\ u(M+2) \\ \vdots \\ u(N) \end{bmatrix} - \begin{bmatrix} u(M) & u(M-1) & \cdots & u(1) \\ u(M+1) & u(M) & \cdots & u(2) \\ \vdots & \vdots & \vdots & \vdots \\ u(N-1) & u(N-2) & \cdots & u(N-M+1) \end{bmatrix} \begin{bmatrix} a_1 \\ a_2 \\ \vdots \\ a_M \end{bmatrix} \quad (2.33)$$

The first and second terms of the right-side of the above equality can be represented as $\boldsymbol{u}$ and $\boldsymbol{Ua}$, respectively. The minimization of the error term $\|\boldsymbol{u} - \boldsymbol{Ua}\|^2$ can be obtained by

$$\boldsymbol{a} = -(\boldsymbol{U^T U})^{-1} \boldsymbol{U^T u} \quad (2.34)$$

where the bold symbols represent the matrices and the vectors, the exponent symbol T represents transpose operation.

Similarly, we used the formulation for estimating the coefficients of the multivariate AR model in (Gürkan, Akan, and Seyhan 2014). Assume that for an M-channel EEG system the multivariate AR model is expressed as

$$U(n) = A_1 U(n-1) + A_2 U(n-2) + \cdots + A_p U(n-p) \quad (2.35)$$

where $U(n) = \begin{bmatrix} u_1(n) \\ u_2(n) \\ \vdots \\ u_M(n) \end{bmatrix}$ and $A_k = \begin{bmatrix} a_{11}(k) & \dots & a_{1M}(k) \\ \vdots & \ddots & \vdots \\ a_{M1}(k) & \dots & a_{MM}(k) \end{bmatrix}$. For the first term of $U(n)$, we can easily write the autoregressive model as

$$u_1(n) = A_1(1,:)U(n-1) + A_2(1,:)U(n-2) + \cdots + A_p(1,:)U(n-p) \quad (2.36)$$

We can reorganize the Eq.(2.36) in a matrix form as

$$u_1(n) = [U^T(n-1) \quad U^T(n-2) \quad \cdots \quad U^T(n-p)] \begin{bmatrix} A_1^T(1,:) \\ A_2^T(1,:) \\ \vdots \\ A_M^T(1,:) \end{bmatrix} \tag{2.37}$$

For $n = p+1, \ldots, N$, we write equations in matrix form as

$$\underbrace{\begin{bmatrix} u_1(p+1) \\ u_1(p+2) \\ \vdots \\ u_1(N) \end{bmatrix}}_{\boldsymbol{b}} = \underbrace{\begin{bmatrix} U^T(p) & U^T(p-1) & \cdots & U^T(1) \\ U^T(p+1) & U^T(p) & \cdots & U^T(2) \\ \vdots & \vdots & \ddots & \vdots \\ U^T(N-1) & U^T(N-2) & \cdots & U^T(N-p) \end{bmatrix}}_{\boldsymbol{U}} \underbrace{\begin{bmatrix} A_1^T(1,:) \\ A_2^T(1,:) \\ \vdots \\ A_M^T(1,:) \end{bmatrix}}_{\boldsymbol{A_1}} \tag{2.38}$$

For the first channel (i.e., $u_1(n)$) the corresponding multivariate AR coefficients can be calculated by using methods of least squares as in univariate case. The solution can be obtained as

$$\boldsymbol{A_1} = \left(\boldsymbol{U^T U}\right)^{-1} \boldsymbol{U^T b} \tag{2.39}$$

This procedure should be repeated for each channel to find the remaining AR coefficients (i.e., $A_2, A_3, \ldots, A_M$).

The optimum model order identification is critical for AR-based studies. Up to now, several model order identification approaches have been proposed. These approaches are Recursive Jump Markov Chain Monte Carlo (RJMCMC) (Karakus, Kuruoglu, and Altinkaya 2015; Troughton and Godsill 1998), Akaike Information Criterion (Akaike 1969), Bayesian Information Criterion (Mariani, Giorgetti, and Chiani 2015), information complexity (Aşikgil 2011), Minimum Description Length (Haykin 2001). These approaches, in general, selects the model order which minimizes *a priori* defined cost function (especially prediction error power). For the BCI frameworks, however, a fixed and relatively long model order is selected for each task period since each training task period requires a largely different model order. (Übeyli 2010; Anderson, Stolz, and Shamsunder 1998). Although this approach is mainly falls at odds

with the minimum prediction error principle as adopted in other types of EEG signal processing approaches (Subasi 2007), the most crucial thing for the BCI frameworks discussed by McFarland et al. is that the minimum error criterion is proved to be something different than the classification/recognition performance (McFarland and Wolpaw 2008).

2.4.4. Common Spatial Patterns

CSP is an effective supervised data-driven method and it plays a crucial role in motor imagery (MI) signal processing (Blankertz et al. 2008). The CSP calculates spatial filters for the multi-channel dataset that optimizes the variances of the signals for an efficient task discrimination (Ramoser, Müller-Gerking, and Pfurtscheller 2000; Dornhege et al. 2004). It is demonstrated that CSP filtering provides better discrimination capacity than Laplacian, common average referencing (CAR) and bipolar derivations (Blankertz et al. 2008).

Suppose that the task periods in the filtered M-channel EEG data

$$\boldsymbol{x}[n] = \begin{bmatrix} x_1[n] \\ x_2[n] \\ \vdots \\ x_M[n] \end{bmatrix} \tag{2.40}$$

are collected into $m \times n$ data matrices X_i, where m denotes number of channels and n denotes the time samples that are collected for each task period. Given the index pair $\left(n_i^b, n_i^e\right)$ that denote the beginning and ending time samples of the i^{th} task period, the data matrices X_i are constructed using

$$X_i = \left[\boldsymbol{x}\left[n_i^b\right] \boldsymbol{x}\left[n_i^b + 1\right] \ldots \boldsymbol{x}[n_i^e]\right] \tag{2.41}$$

In addition, let the motor imagery activity type associated with each task indexed by i is represented by the labels $Y_i \in \{1,2\}$ for the two activity types, respectively. The methodology for CSP first calculates the covariance matrices Σ_1 and Σ_2 for the two activities using

$$\Sigma_1 = \frac{1}{\ell_1} \sum_{i \in I_1} X_i X_i^T \tag{2.42}$$

and

$$\Sigma_2 = \frac{1}{\ell_2} \sum_{i \in I_2} X_i X_i^T \tag{2.43}$$

where $I_1 = \{i | Y_i = 1\}$ and $I_2 = \{i | Y_i = 2\}$ with $\ell_1 = |I_1|$ and $\ell_2 = |I_2|$ denoting the number of activity periods associated with the two activity types, respectively. The spatial filters are then calculated by solving the generalized eigenvalue problem in terms of eigenvectors w_j and eigenvalues λ_j for which the equality

$$\Sigma_1 w_j = \lambda_j \Sigma_2 w_j \tag{2.44}$$

is satisfied, for $j = 1,2, \ldots, M$. Finally, CSP selects the eigenvectors w_j with the largest and the smallest λ_j that characterize the latent channels over which the ratio of average energies is maximized and minimized, respectively, across the task periods of the two activity types. Note that the latent channels corresponding to a weighted linear combination sum of existing electroencephalography channels with weights determined by the coefficients of selected eigenvectors. Note also that by convention, a typical CSP uses the three maximal eigenvalue channels along with three minimal eigenvalue channels to characterize the discriminative electroencephalography profiles associated with the two activity types (i.e. $m = 3$) (Blankertz et al. 2008). Adopting same

convention, we have collected the six eigenvectors associated with the top and bottom three eigenvalues into a matrix W and calculated the latent channel signals $\tilde{\boldsymbol{x}}[n]$ using

$$\tilde{\boldsymbol{x}}[n] = W^T \boldsymbol{x}[n] \tag{2.45}$$

for all task periods i.

Please note that besides the two class discrimination, there are several multiclass extension approaches of CSP method have been proposed in the literature (Grosse-Wentrup and Buss 2008; W. Wei, Xiaorong, and Shangkai 2005).

2.5. The Classification Methods

There are many classification methods that have been used to evaluate the performance of the extracted features via brain activity characterization methods. Among them, there are three outperforming classification methods named as, Fisher's linear discriminant, linear support vector machines and nonlinear support vector machines. We used these classifiers in this thesis to evaluate the performance of the proposed brain activity characterization methods. In below, we give brief information about these classification methods.

2.5.1. Fisher's Linear Discriminant (FLD)

The Fisher's linear discriminant classifier is known as simple linear classifier that utilizes the covariance information of the feature vectors. For this classification method, the idea is to find a projection vector that maximizes the differences of the mean values of samples of different classes, at the same time minimizes sum of within class variances of the projected samples. This can be expressed in mathematical manner as (Fisher 1936)

$$J(v) = \frac{|\tilde{\mu}_1 - \tilde{\mu}_2|^2}{\tilde{s}_1^2 + \tilde{s}_2^2} \tag{2.46}$$

where $J(\cdot)$ denotes the cost function to be maximized, $\tilde{\mu}_1$, $\tilde{\mu}_2$ and $\tilde{s}_1^2, \tilde{s}_2^2$ are the mean and scatter values of the projected samples (i.e., $v^T x_i$) that are belong to class-1 and class-2, respectively (please see Figure 9). By using several mathematical operations, we can express the cost function as (Duda and Hart 2000)

$$J(v) = \frac{v^T S_B v}{v^T S_W v} \tag{2.47}$$

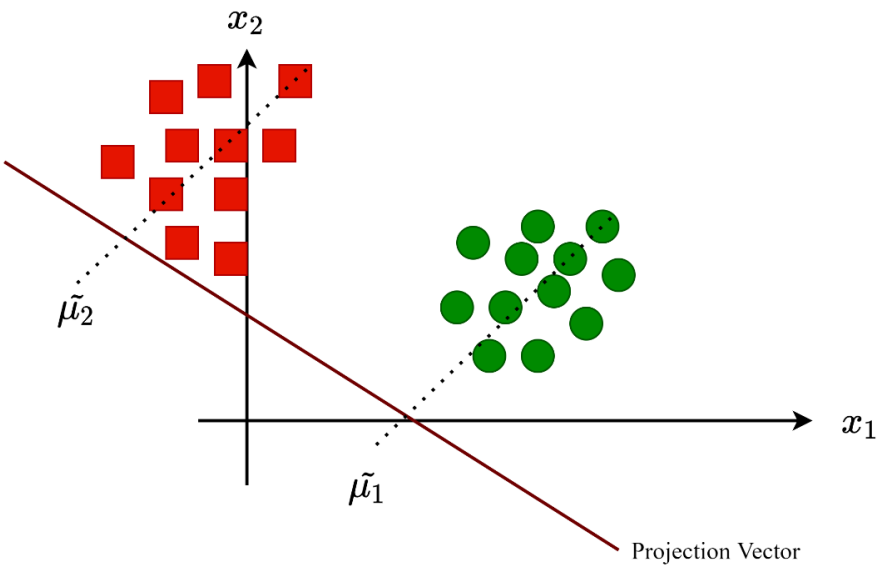

Figure 9. The illustration of the projection vector for a FLD classifier. The parameters $\tilde{\mu}_1$ and $\tilde{\mu}_2$ represents the projected mean values of the samples belongs to class-1 and class-2.

where v is the projection vector, S_B and S_W are the between and within class scatter matrices, respectively. From this equation, we can obtain the weight vector v by solving a generalized eigenvalue problem as

$$v = (\mathrm{S}_1 + \mathrm{S}_2)^{-1}(\mu_1 - \mu_2) \tag{2.48}$$

where S_1, S_2 denote scatter matrices and μ_1, μ_2 denote mean vectors of the samples belongs to class-1 and class-2, respectively. The functional form of FLD classifier is then expressed as

$$f(x) = \mathrm{sgn}(v^T x + v_0) \tag{2.49}$$

where the parameter v_0 is the bias parameter that minimizes the classification error on the training set.

2.5.2. Support Vector Machines (SVM)

There are many linear classifications method type can be used in any pattern recognition problem. Each linear classifier generates a hyperplane (or a threshold value) to discriminate the samples into classes. Among the linear classifiers, linear support vector machine classifier maximizes the margin (distance between hyperplane and nearest samples). This linear machine can be termed as optimal separating hyperplane. The optimum separating hyperplane is so that it classifies the samples correctly and the distance to the nearest sample for each category is maximal (please see Figure 10). The optimum separating hyperplane can mathematically be expressed as (Vapnik 2000)

$$\min_i \left| \langle v, x^i \rangle + b \right| = 1 \tag{2.50}$$

where v denotes the separating hyperplane and b denotes the bias term which is be calculated in training vectors so that training error of the support vector classification is minimal.

The optimum separating hyperplane can be obtained via optimization techniques based on the premise that the norm of weight vector v should be equal to the inverse of the distance of the nearest point in training data to the hyperplane. We can obtain the corresponding weight vector using the mathematical formula of the distance between margins and nearest samples

$$\begin{aligned}\rho(v,b) &= \min_{x^i:y^i=-1} d\left(v,b;x^i\right) + \min_{x^i:y^i=+1} d\left(v,b;x^i\right) \\ &= \min_{x^i:y^i=-1} \frac{\left|\langle v,x^i\rangle + b\right|}{\|w\|} + \min_{x^i:y^i=+1} \frac{\left|\langle v,x^i\rangle + b\right|}{\|w\|} \\ &= \frac{1}{\|w\|}\left(\min_{x^i:y^i=-1}\left|\langle v,x^i\rangle + b\right| + \min_{x^i:y^i=+1}\left|\langle v,x^i\rangle + b\right|\right) \\ &= \frac{2}{\|w\|}\end{aligned} \tag{2.51}$$

Finally, the optimally separating hyperplane can be obtained by adopting a minimization of the function

$$\Phi(w) = \frac{1}{2}\|w\|^2 \tag{2.52}$$

The weight vector and bias term can be obtained via methods of Lagrange multipliers (Haykin 1995; Duda and Hart 2000). Thus, the hard classification function can be expressed as

$$f(x) = \mathrm{sgn}(\langle v^*, x\rangle + b^*) \tag{2.53}$$

where terms v^* and b^* are optimum weight vector and bias for optimum classification.

However, many real-world classification problems are linearly non-separable problems (Özbek 2009; F. Lotte et al. 2007). In such cases, to minimize the classification error, a generalization may be beneficial for linear classifier formulated above. The

generalization to the linear SVM formulation can be done by introducing slack variables. The mathematical expression for obtaining the optimum separating hyperplane after introducing the slack variables is then becomes

$$\Phi(v, \xi) = \frac{1}{2}\|v\|^2 + C\sum_{i=1}^{n}\zeta_i \tag{2.54}$$

where C is known as the regularization parameter and ζ_i is the slack variable introduced for generalization of the hard linear classifier detailed above.

Alternatively, for a linearly non-separable classification problem, kernel functions can be adopted. Simply, kernel functions are used to map input pattern vectors into a higher dimensional feature space where a linear separation can be achieved (see Figure 11). A kernel function $\kappa(\cdot,\cdot)$ selected for this nonlinear mapping is simply a dot product operator in feature space which can be expressed as

$$\kappa(x, y) = \langle \phi(x), \phi(y) \rangle \tag{2.55}$$

where $\phi(\cdot)$ is the mapping operator. The classification function can be expressed as

$$f(x) = \text{sgn}\left(\sum_{i \in SV} \alpha_i \, \kappa(x, x_i) + b\right) \tag{2.56}$$

where SV represents support vectors. The most used kernels and their functional forms are presented in Table 3. In this thesis, for nonlinear classification, we used radial basis function kernel to evaluate the performance of synchronization and entropy based features extracted for brain activity characterization purposes. We calculated the kernel parameter γ as

$$\gamma = \sqrt{\frac{1}{L(L-1)} \sum_{i=1}^{L-1} \sum_{j=i+1}^{L} \|\xi_i - \xi_j\|^2} \tag{2.57}$$

where L is number of training feature vectors which are represented by ξ.

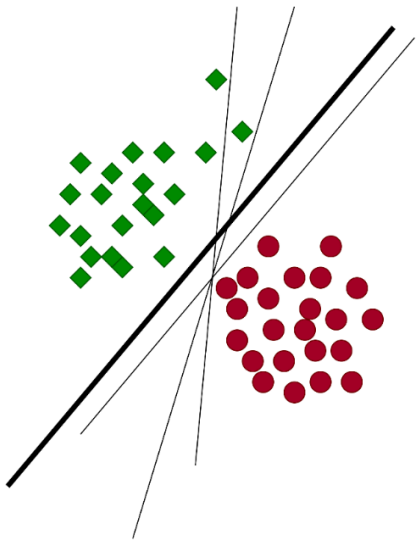

Figure 10. The illustration of importance of choosing optimal separating hyperplane. The thickest separating plane should be chosen as optimal hyperplane for minimizing the misclassification risk.

Table 3. Summary of kernels (Haykin 1995)

Type of Kernel	**Functional Form**	**Some Comments**
Polynomial	$(x^T x + 1)^p$	Power p must be determined *a priori*
Radial-basis function	$\exp(-\gamma \|x - y\|^2)$	Kernel parameter γ should be specified *a priori*
Hyperbolic	$\tanh(\beta_0 x^T x + \beta_1)$	Mercer's theorem satisfies only for some β_0 and β_1

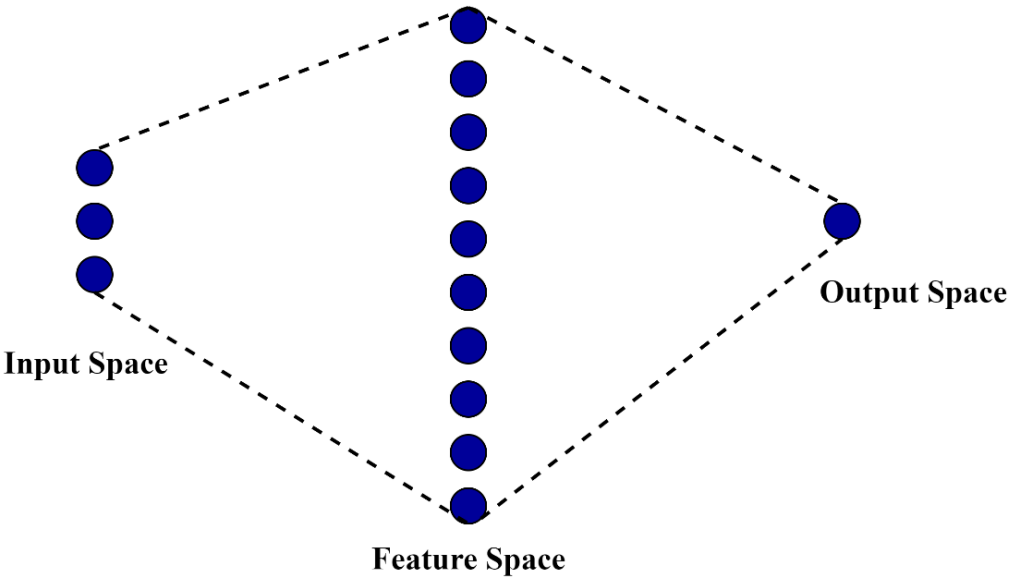

Figure 11. Mapping input space into a high dimensional feature space via kernel methods.

2.6. Feature Ranking/Selection Method

We used feature ranking to quantify and select the most informative features to reduce the dimension before the classification. In the literature, various feature ranking/selection methods can be (Malan and Sharma 2019; Yijun Sun 2007; Kira and Rendell 1992; Ang et al. 2012; Gosset 1908; Pudil, Novovičová, and Kittler 1994). We adopted Fisher's ratio method for quantifying the discrimination power of each extracted feature (Duda and Hart 2000; Fisher 1936). Simply, Fisher's ratio calculates separability power of each feature indexed by α by using its mean and standard deviation values for different classes. The mathematical expression of calculation of Fisher's ratio can be given as

$$F(\alpha) = \frac{\left|\mu_{\alpha,A_1} - \mu_{\alpha,A_2}\right|}{\sigma_{\alpha,A_1} + \sigma_{\alpha,A_2}} \tag{2.58}$$

where μ_{α,A_1}, μ_{α,A_2} are the mean and σ_{α,A_1}, σ_{α,A_2} values denote the mean and standard deviations calculated for the classes A_1 and A_2. As for the feature selection, we first

calculated each features Fisher ratio by using the training vectors, then we selected the features that has higher Fisher ratio than mean plus two times standard deviation of Fisher ratio values calculated for all features.

2.7. The Datasets Used in this Thesis

In this study, comparative performance evaluations were carried out on two different motor imagery datasets, BCI Competition-III IVa and PhysioNet Motor Movement/Imagery Dataset. The former dataset comprises EEG recordings of 5 subjects as they perform 140 right hand and 140 right foot imagery activity in a randomized order (Blankertz et al. 2006). This dataset was collected using 118 electrodes according to extended international 10/20 system at a sampling frequency of 1000 Hz (Dornhege et al. 2004). During each trial, subjects performed the imagery activities approximately for 3.5 seconds. Note that we used the 100 Hz down-sampled version of this dataset which is also available online on the competition website.

The latter dataset comprises EEG signals of 109 subjects recorded under real and imaginary motor tasks (Goldberger et al. 2000). EEG signals were collected via a BCI2000 system with 160 Hz sampling frequency (Schalk et al. 2004). The recording system was international 10/10 system with 64 electrodes. The electrode montages used for the collection of the corresponding dataset is presented in Figure 12.

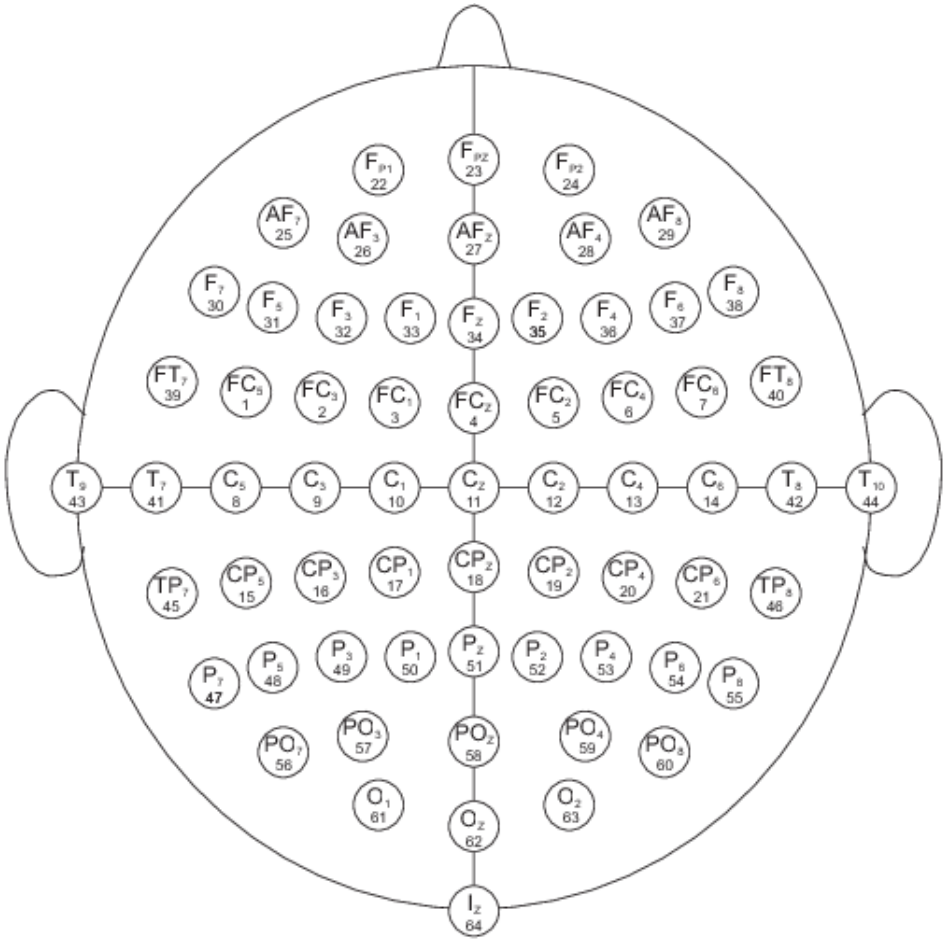

Figure 12. The illustration of the 10/10 electrode montage with 64 electrodes used for collecting the EEG signals (PhysioNet Motor Movement/Imagery dataset).

For each subject, the experiment was composed of 14 separate sessions, beginning with two eyes open/eyes closed sessions. The progression of the remaining 12 sessions is given in Table 4. Note that each task period lasted about 4.1 seconds, followed by a rest period with a duration of 4.2 seconds. We illustrated the sequence of task and rest periods for a session in Figure 13.

Table 4. Content of remaining 12 sessions with real/imagery task

Task Name	**Real Motor Activity Sessions**	**Imaginary Motor Activity Sessions**
Right/Left Fist	3, 7, 11	4, 8, 12
Both Fist/Both Feet	5, 9, 13	6, 10, 14

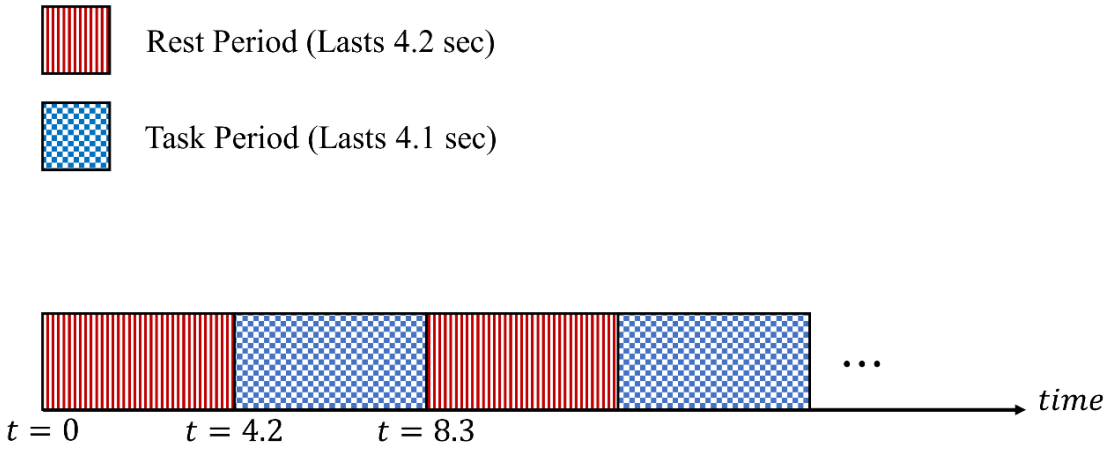

Figure 13. Illustration of timing diagram of a session with rest and task periods (PhysioNet Dataset).

Each session contains a total of 30 mixed blocks of task and rest periods. Please note that, we evaluated the performance of the proposed activity recognition frameworks using the EEG recordings of right fist versus left fist motor imagery task sessions of the first 20 subjects in the dataset throughout this thesis.

As a preprocessing step, for both datasets, we re-referenced the signals to the common average to reduce the effect of volume conduction (Olejarczyk et al. 2017; Fabien Lotte 2008; McFarland et al. 1997). The mathematical formulation of the common average referencing (CAR) is expressed as

$$s_i(t) = s_i(t) - \frac{1}{M}\sum_{j=1}^{M} s_j(t) \tag{2.59}$$

where $s_i(t)$ represents the EEG signal recording at i^{th} channel, M represents the total number of channels used for collecting EEG signals, and t denotes the time. Basically, CAR filter enhances the signal-to-noise ratio of the channels by removing the noises common to all EEG channels. It transforms EEG signal distributions into a zero-mean scalp voltage distribution. Thereafter, to avoid the phase distortion, we used a finite-impulse response (FIR) band-pass filter with a passband of 8-30 Hz to filter the signals into SMR related frequency band (see Figure 14) (Fabien Lotte 2008; Jian, Chen, and McFarland 2017). Finally, by using the task initiation indices given in these datasets, we extracted the task periods of the EEG signals with the corresponding task label indicating the type of motor imagery activity.

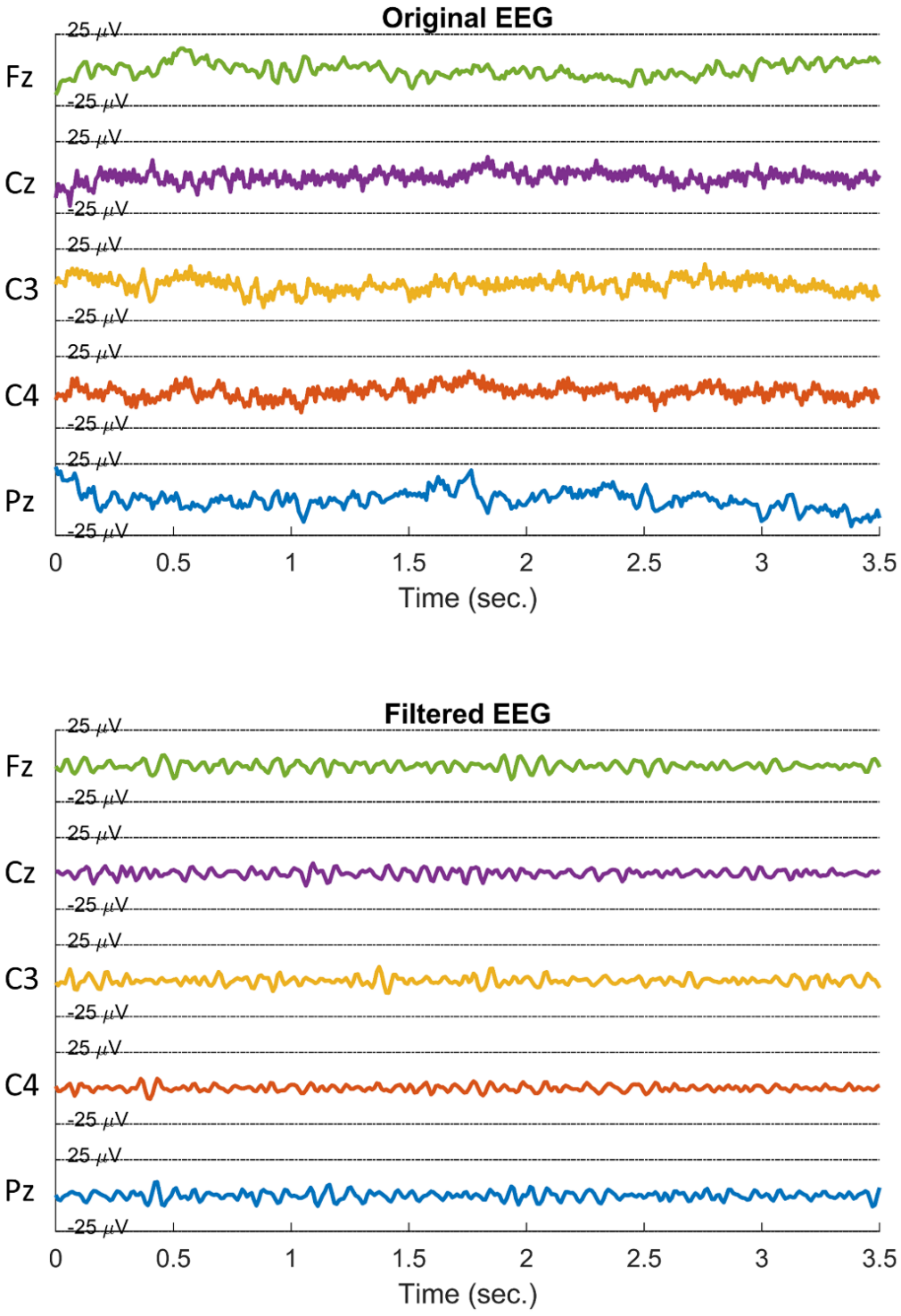

Figure 14. Illustration of the original EEG signals and the filtered EEG signals of a subject during right-hand motor imagery activity (BCI Competition-III dataset IVa).

CHAPTER 3

TIME-LAGGED SYNCHRONIZATION BETWEEN EEG CHANNELS FOR COGNITIVE TASK RECOGNITION

May be the human brain is an object beyond the reach of metaphor,
for the simple reason that is the only object capable of creating metaphors to describe itself…
-Luke Dittrich-

3.1. Introduction

In this chapter, we propose a novel approach for cognitive task recognition that captures and uses the activity-specific inter-channel synchronization timings between distant brain regions. As timing parameter, we used only the time lag (τ). Basically, our approach proposed in here is based on the premise that during a particular cognitive tasks, selective interactions between distant brain regions arise at a time lag profile that is specific to and characteristic of the task at hand (Chen, Guanrong and Dong 1998; Shahverdiev, Sivaprakasam, and Shore 2002; O. Sporns, Tononi, and Edelman 2000; Wibral et al. 2011; Pampu et al. 2013).

In the literature, several studies exploit the time lag as the only parameter of timing organization of maximal information transfer in detecting functional impairment in the analysis of brain activity via information theoretic methods (Jeong, Gore, and Peterson 2001; Na et al. 2002). In addition, time lag between EEG channels has been used to identify the epileptic foci (Gotman 1983; Ktonas and Mallart 1991). Similarly, Bandt et al. showed that the epilepsy disorder significantly alter the physiological lag organization among the brain regions (S. K. Bandt et al. 2019). Van Bergen estimated and analyzed the time lag by calculating the mutual information between EEG signals for brain activity characterization (Bergen 1986). Boeijinga and Lopez da Silva estimated lag between EEG channels to identify the propagation direction of beta activity in the cat brain (Boeijinga and Lopes da Silva 1989). Adhikari et. al. evaluated a study on mice and discovered consistent time lag organization by applying a cross-correlation analysis to envelope of

instantaneous amplitudes of local field potentials recorded from medial prefrontal cortex and ventral hippocampus during awake state (A. Adhikari et al. 2010). Mijalkov et al. studied delayed correlations between distant brain regions to identify the exact structural connections (Mijalkov, Pereira, and Volpe 2020). Authors in this study demonstrated that the functional synchronizations of distant brain regions are dependent on the sequential activations as well as the activation degree of individual brain regions which can be detected by delayed correlations of the brain regions.

All these studies given above stress that there is an inherent time lag organization in the synchronization of distinct areas of the brain during particular cognitive states due to the activation sequence of individual brain regions. If that is the case, brain synchrony between different regions that arise in accordance with cognitive or motor tasks may go undetected by an approach that does not consider the inherent time lag. Indeed, it is highly possible that the conspicuous lack of synchrony-based task recognition studies is due to the inability of establishing the synchrony using methods that disregard this time lag. So as the initial step, we addressed this issue by carrying out a comparative evaluation of well-known synchronization measures to assess activity specific time lag organization between EEG channels in a motor imagery activity recognition scenario. Note that the approach adopted in this chapter can also be easily adapted to analyze other types of cognitive tasks/states.

The remainder of this chapter is organized as follows: In the Section 3.2, the properties of the EEG datasets used in this study are described, accompanied by an operational pipeline of the proposed method. Next, the definitions and formulations of coherence measures are provided. In Section 3.3, the classification and the novel cross validation schemes are summarized, and performance results obtained via the proposed method are presented. In Section 3.4, we elaborate on the merits and drawbacks of the approach and the obtained results in comparison with a benchmark method.

3.2. Proposed Method

In this section, we first describe the operational pipeline of the proposed method is given, along with the calculation of the activity specific time lag and construction of

training and test feature vectors generated from both training and test datasets. Finally, the definitions and formulations of the applied synchronization measures are presented.

3.2.1. Synchronization Metrics Used for Capturing Lagged Brain Synchronization

We estimated the time lag between the brain regions by capturing the time lag at which the maximum synchronization occurs as adopted in (Govindan et al. 2005). The lagged synchronization between EEG channels was calculated using six different methods that are listed as:

- Cross-correntropy (I. Park and Príncipe 2008; Principe 2010; Santamaría, Pokharel, and Principe 2006)
- Mutual information (Altermann and Kuhn 1994; Kraskov, Stögbauer, and Grassberger 2004)
- Phase locking value (Lachaux et al. 1999)
- Cross-correlation (Stoica 1997)
- Nonlinear interdependency (Arnhold et al. 1999)
- Cosine-based similarity (Sargolzaei et al. 2015; Herff et al. 2019) (B. Orkan Olcay and Karaçalı 2019).

It is important to note that, by using different time lags τ ranging from $-125\,ms$ to $125\,ms$ (B. Orkan Olcay and Karaçalı 2019), we calculated the synchronization value between the signals that falls into the time window illustrated with dashed lines in Figure 15. In the proposed method section, we represent the discretized and delayed signal $s_{j-f_s\tau}$ as s_j^{τ}. In here, τ represents the time lag, an integer multiple of $1/f_s$ in milliseconds, and f_s denotes the sampling frequency in Hertz. In Figure 16, we presented an exemplary illustration of the evolution of average synchronization between C3-C4 channels during left fist imagery activity on EEG signals of three sessions of subject S001 in the PhysioNet dataset for varying time lags according to the synchronization measures listed above.

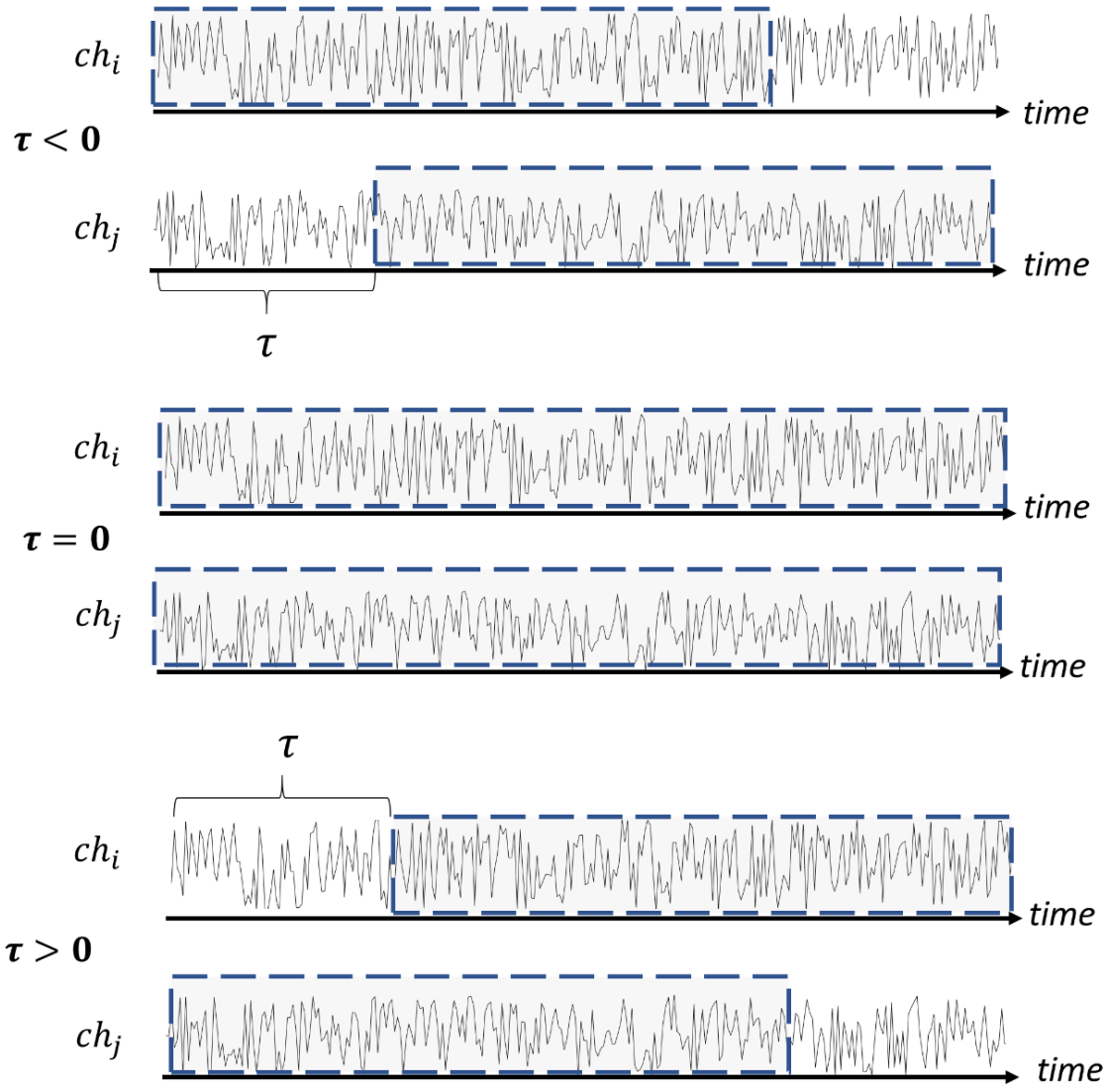

Figure 15. The signal segments in the yellow and green time windows were used in the calculation of inter-channel synchrony for $\tau < 0$, $\tau = 0$ and $\tau > 0$.

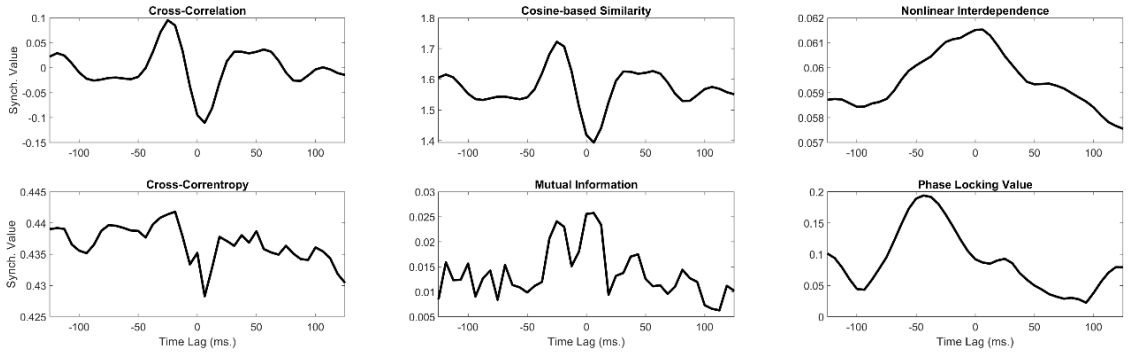

Figure 16. The time lag versus average synchronization value of all six methods included in this study for the C3-C4 channel pair of subject *S001* (exemplary demonstration from left fist imagination-PhysioNet Dataset).

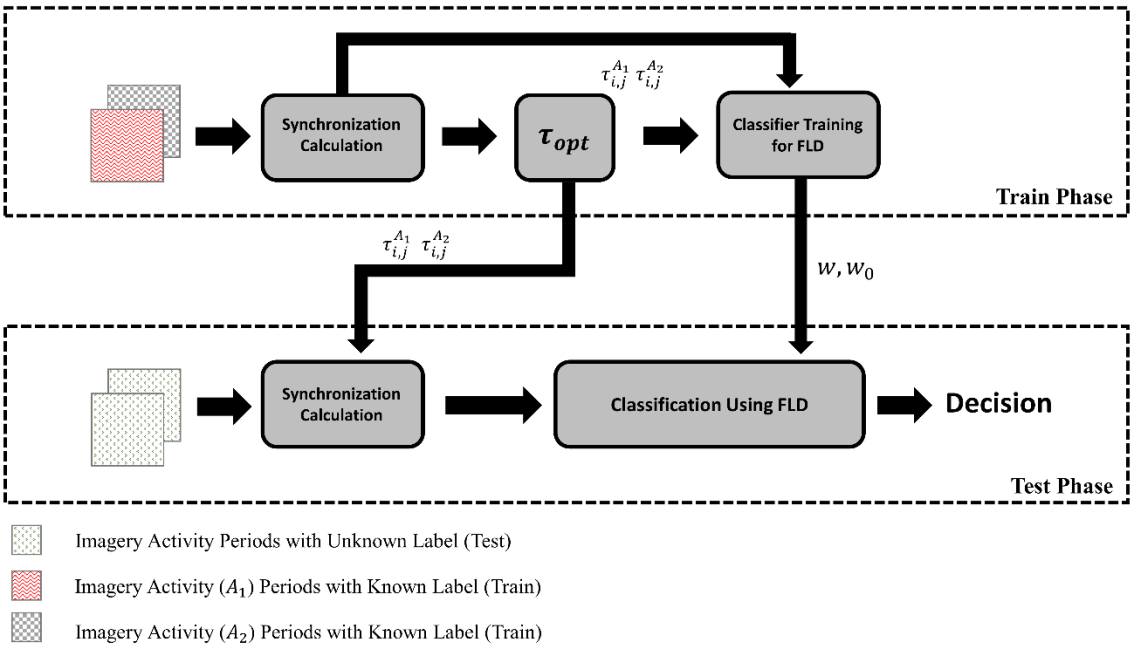

Figure 17. Flow diagram of the proposed framework (τ-based method).

3.2.2. The Recognition Framework

The operational flow diagram of the proposed brain activity recognition framework is given in Figure 17. The details of both training and test phases are described

below. In the training phase of the proposed framework, we calculated the synchronization values between EEG signals between each channel pair for different time lags τ running from $-125ms$ to $125ms$ in the *Synchronization Calculation* block, for the training task periods of each type of imagery activity (B. Orkan Olcay and Karaçalı 2019; Gotman 1983). Then, in the τ_{opt} block, for each type of imagery activity (say A_1 and A_2), the optimum time lags $\tau_{i,j}^{A_1}$ and $\tau_{i,j}^{A_2}$ that maximize the average synchronization value between channels i and j are determined as the activity-specific time lag. We calculate the inter-channel activity-specific time lags $\tau_{i,j}^{A_1}$ and $\tau_{i,j}^{A_2}$ for each channel pair (i,j) and each type of imagery task using

$$\tau_{i,j}^{A_1} = \underset{\tau}{\operatorname{argmax}} \left(\frac{1}{N_{A_1}} \sum_{k \in I_{A_1}} S\left(s_{i,k}, s_{j,k}^{\tau}\right) \right) \tag{3.1}$$

and

$$\tau_{i,j}^{A_2} = \underset{\tau}{\operatorname{argmax}} \left(\frac{1}{N_{A_2}} \sum_{\ell \in I_{A_2}} S\left(s_{i,\ell}, s_{j,\ell}^{\tau}\right) \right) \tag{3.2}$$

where k and ℓ are the indices of the period, I_{A_1} and I_{A_2} represent the indices of the respective imagery task periods in the training set, and N_{A_1} and N_{A_2} denote the corresponding number of periods. Furthermore, $s_{i,k}$ is the EEG signal from the i^{th} channel of the k^{th} imagery activity period. Note that we used training task periods for calculating the activity-specific inter-channel time lags. Note also that $\arg\max_{\rho} q(\rho)$ returns value ρ^* over which the function $q(\cdot)$ is maximized. Finally, $S\left(s_i, s_j\right)$ denotes the synchronization measure of choice that measures the interrelation between the signals s_i and s_j. Then, in the *Classifier Training for FLD* block, for the subsequent recognition of each imagery activity period k in the training dataset, the feature vector ξ_k that contains

synchronization values between EEG signals were constructed at time delays $\tau_{i,j}^{A_1}$ and $\tau_{i,j}^{A_2}$ as

$$\xi_k = \begin{bmatrix} S\left(s_{1,k}, s_{2,k}^{\tau_{1,2}^{A_1}}\right) \\ S\left(s_{1,k}, s_{3,k}^{\tau_{1,3}^{A_1}}\right) \\ \vdots \\ S\left(s_{M-2,k}, s_{M,k}^{\tau_{M-2,M}^{A_1}}\right) \\ S\left(s_{M-1,k}, s_{M,k}^{\tau_{M-1,M}^{A_1}}\right) \\ S\left(s_{1,k}, s_{2,k}^{\tau_{1,2}^{A_2}}\right) \\ S\left(s_{1,k}, s_{3,k}^{\tau_{1,3}^{A_2}}\right) \\ \vdots \\ S\left(s_{M-2,k}, s_{M,k}^{\tau_{M-2,M}^{A_2}}\right) \\ S\left(s_{M-1,k}, s_{M,k}^{\tau_{M-1,M}^{A_2}}\right) \end{bmatrix} \tag{3.3}$$

by collecting inter-channel synchronization values calculated at activity-specific inter-channel time lags from contending cognitive activities into a column vector. In the expression above, M represents the number of channels. Note that the number of channels $M = 118$ for the BCI Competition-III dataset IVa, $M = 64$ for the PhysioNet Motor Movement/Imagery datasets. We obtained the feature vectors for each training task period of size $M(M-1) \times 1$. We calculated the weight vector and bias parameters of the Fisher's linear discriminant classifier by using the training feature vectors (Fisher 1936).

In the test phase, we obtained a feature vector ξ using the inter-channel synchronization values calculated at same activity-specific time lags and organized into a matching column vectors in the *Synchronization Calculation* block, for each task period of interest characterized by EEG signals $s_1, s_2, \ldots, s_M$. The feature vector constructed for a test period can be represented as

$$\xi = \begin{bmatrix} S\left(s_1, s_2^{\tau_{1,2}^{A_1}}\right) \\ S\left(s_1, s_3^{\tau_{1,3}^{A_1}}\right) \\ \vdots \\ S\left(s_{M-2}, s_M^{\tau_{M-2,M}^{A_1}}\right) \\ S\left(s_{M-1}, s_M^{\tau_{M-1,M}^{A_1}}\right) \\ S\left(s_1, s_2^{\tau_{1,2}^{A_2}}\right) \\ S\left(s_1, s_3^{\tau_{1,3}^{A_2}}\right) \\ \vdots \\ S\left(s_{M-2}, s_M^{\tau_{M-2,M}^{A_2}}\right) \\ S\left(s_{M-1}, s_M^{\tau_{M-1,M}^{A_2}}\right) \end{bmatrix} \tag{3.4}$$

In the *Classification Using FLD* block, the imagery activity period in question was then decided upon by conducting a Fisher's linear discriminant analysis using the formula given in Eq. (3.4), assigning test feature vectors to either first or second category of imagery activity (i.e., A_1 or A_2).

3.3. Results

In order to determine the way in which recognition performance varies in response to varying size of the training set, we chronologically partitioned the dataset in two different ways as follows:

- In scenario-1, for PhysioNet dataset, imagery activity periods in session-4 were used for training, imagery activity periods in session-8 and session-12 were used for testing purposes. For BCI Competition-III dataset, the first 94 imagery activity periods were used for training, and the remaining 186 imagery activity periods used for testing purposes. For each dataset, this corresponds to using the first

%33,3 of total imagery activity periods for training, and the remaining %66,7 of total imagery activity periods for testing.

- In scenario-2, for PhysioNet dataset, imagery activity periods in session-4 and session-8 were used for training while imagery activity periods in session-12 were used for testing purposes. For BCI Competition-III dataset, the first 186 imagery activity periods were used for training, and the remaining 94 imagery activity periods used for testing. For each dataset, this corresponds to using the first %66,7 of total imagery activity periods for training, and the remaining %33,3 for testing.

Note also that this kind of partitioning of the data in training and test sets is also more realistic compared to a typical n-fold cross validation scheme with randomly selected training and test sets, since training naturally precedes testing in real applications. We will use this cross-validation approach throughout this thesis. In addition, it is also useful to evaluate how much improvement can be expected by increasing the amount of training data.

Prior to classifier construction, to reduce the dimensionality, we have applied feature selection according to each feature's Fisher ratio (Dat and Guan 2007; Guyon 1998; Duda and Hart 2000). In each chronological cross validation scenario, we selected the features that had higher Fisher ratio values than the mean plus two times the standard deviation of all Fisher ratios across all features. For each scenario, the average classification performance results over 20 subjects from the PhysioNet dataset and the average performance over all 5 subjects of BCI Competition-III dataset are given in Table 6 and Table 7, respectively.

For comparison purposes, we also evaluated the recognition performance using a priori selected channel pairs that were identified to be meaningful for right hand versus left hand imagery activity discrimination in previous EEG connectivity-based studies. Krusienski et al. has proposed to use 9 channels (producing 36 channel pairs) to elucidate the merits and drawbacks of the phase locking value (PLV) method for imagery activity recognition (Krusienski, McFarland, and Wolpaw 2012). The performance of additional electrode subsets were also compared for PLV-based activity recognition (Q. Wei et al. 2007). Daly et al. argued for the importance of using all spatial and spectral information in the connectivity-based BCI framework which amounts to using all channel pairs (Daly, Nasuto, and Warwick 2012). Wang et al. also proposed using a large number of electrode pairs to couple up the motor-activity related brain regions for activity recognition (Yijun

Wang et al. 2006). Rathee et al. proposed three channel pairs arguably offering the greatest contribution for right hand/left hand imagery activity recognition (Rathee, Cecotti, and Prasad 2017). Hamedi et al. identified additional channel pairs for right- and left-hand imagery activity recognition (Hamedi et al. 2015). These a priori channel pairs are listed in Table 5 below. Note, however, these channels/channel pairs were identified for right fist versus left fist recognition; thus, we applied them for performance evaluation on PhysioNet dataset only and not on BCI Competition dataset as it contains right hand versus right foot imagery activity periods. A similar analysis using a priori selected channels for right hand/right foot recognition was not possible as a comparable list of channels that discriminate between right hand and right foot activities is lacking from the literature. In (Gaxiola-Tirado, Salazar-Varas, and Gutierrez 2018), authors identified EEG channel networks for BCI Competition-III IVa dataset claimed to be highly discriminative for right foot/right hand motor imagery activity. However, these channel networks are highly subject and frequency specific, and thus, not viable for performance comparison across different subjects (see (Gaxiola-Tirado, Salazar-Varas, and Gutierrez 2018) and Table I therein). As a result, we did not include these channels. The performance results obtained using this a priori selected right hand versus left hand connectivity features are also given in Table 6 and Table 7 for scenario-1 and scenario-2, respectively.

Finally, we compared the performance of the cognitive task recognition framework evaluating the various synchronization measure with a well-known BCI strategy, CSP (Ramoser, Müller-Gerking, and Pfurtscheller 2000). In the training phase, we filtered the signals with 8-30 hertz FIR band-pass filter and obtained the CSP filter ($m = 3$). We then applied the CSP filter on both training and test periods. We calculated the log-variance features from CSP-filtered activity periods for recognition purpose.

Table 5. The *a priori* selected channel pairs given in previous studies for right fist/left fist recognition

	# **Pairs**	# **Channels**	**Channels / Channel Pairs**
Krusienski et. al.	36	9	[T7, F3, P3, C3, Cz, C4, P4, F4, T8]
Wei-CW et. al.	45	10	[C5, FC3, CP3, C3, C1, C2, C4, FC4, CP4, C6]
Wei-CB1 et. al.	25	10	[C5, FC3, CP3, C3, C1] ↔ [C2, C4, FC4, CP4, C6]
Wei-CB2 et. al.	50	15	[AFz, Fz, FCz, F1, F2] ↔ [C5, FC3, CP3, C3, C1] [AFz, Fz, FCz, F1, F2] ↔ [C2, C4, FC4, CP4, C6]
Wang et. al.	3	3	[FCz, C3, C4]
Rathee et. al.	3	5	[CP1 ↔ C4], [C3 ↔ FC1], [C4 ↔ Cz]
Hamedi et. al.	5	6	[C3 ↔ C4], [C1 ↔ Cz], [C2 ↔ Cz], [C1 ↔ C2], [C2 ↔ CPz]

Table 6. The average performance results of subjects for different datasets for Scenario-1. The rows marked with an asterisk represents the a *priori* selected channel pairs (Right/Left Hand) from the literature.

		Average Performances of Different Synch. Measures (%)					
		Mutual Information	**Cosine**	**PLV**	**Nonlinear Int.**	**Correlation**	**Correntropy**
PhysioNet Motor Imagery Dataset (Right/Left Fist Imagery)	**Fisher ratio**	58.33 ± 10.57	56.83 ± 10.17	54.67 ± 10.83	57.0 ± 11.44	55.67 ± 8.02	56.16 ± 15.07
	***Krusienski, 2012**	53.83 ± 10.66	54.16 ± 8.15	55.16 ± 11.96	53.0 ± 7.1	51.67 ± 8.95	53.17 ± 10.45
	***Wei-CW, 2007**	54.0 ± 13.35	54.67 ± 9.75	53.67 ± 10.97	56.16 ± 12.29	59.83 ± 11.96	56.67 ± 9.85
	***Wei-CB1, 2007**	53.67 ± 6.65	54.33 ± 10.71	51.33 ± 8.94	54.0 ± 6.89	53.5 ± 9.07	52.5 ± 7.78
	***Wei-CB2, 2007**	58.5 ± 9.14	52.33 ± 10.71	53.5 ± 10.0	53.33 ± 8.71	54.5 ± 9.74	50.83 ± 9.48
	***Wang, 2006**	53.17 ± 6.7	55.33 ± 8.67	54.83 ± 8.12	52.16 ± 8.67	53.5 ± 9.39	53.17 ± 11.67
	***Rathee, 2017**	55.0 ± 10.0	53.17 ± 11.41	54.83 ± 8.94	52.0 ± 10.39	56.5 ± 11.21	54.67 ± 9.32
	***Hamedi, 2016**	53.33 ± 9.97	50.5 ± 6.76	52.83 ± 9.13	51.83 ± 9.08	54.0 ± 6.89	53.16 ± 9.64
BCI Comp. III	**Fisher ratio**	76.69 ± 12.88	70.52 ± 9.0	68.08 ± 8.7	72.55 ± 9.65	72.65 ± 8.77	75.95 ± 11.56

Table 7. The average performance results of subjects for different datasets for Scenario-2. The rows marked with an asterisk represents the a *priori* selected channel pairs (Right/Left Hand) from the literature.

		Average Performances of Different Synch. Measures (%)					
		Mutual Information	**Cosine**	**PLV**	**Nonlinear Int.**	**Correlation**	**Correntropy**
PhysioNet Motor Imagery Dataset (Right/Left Fist Imagery)	**Fisher ratio**	59.33 ± 15.12	61.0 ± 10.2	59.67 ± 15.06	60.67 ± 13.83	60.33 ± 15.37	59.33 ± 16.17
	***Krusienski, 2012**	58.67 ± 13.26	56.0 ± 13.22	57.67 ± 17.34	57.33 ± 15.2	57.33 ± 12.12	55.67 ± 11.9
	***Wei-CW, 2007**	51.0 ± 20.55	57.0 ± 15.81	56.67 ± 16.11	55.67 ± 17.06	58.67 ± 12.34	51.67 ± 21.61
	***Wei-CB1, 2007**	55.33 ± 15.0	52.0 ± 11.15	53.33 ± 10.59	56.67 ± 13.42	54.67 ± 13.08	48.33 ± 12.4
	***Wei-CB2, 2007**	55.0 ± 8.88	53.33 ± 16.32	56.0 ± 13.74	55.33 ± 16.9	53.0 ± 10.0	58.33 ± 16.31
	***Wang, 2006**	47.33 ± 15.43	56.33 ± 11.94	54.67 ± 12.9	54.67 ± 12.72	54.0 ± 8.62	56.33 ± 15.51
	***Rathee, 2017**	54.33 ± 15.48	55.33 ± 14.36	50.0 ± 10.92	53.33 ± 14.66	56.0 ± 12.86	55.33 ± 17.58
	***Hamedi, 2016**	51.0 ± 11.9	54.3 ± 10.65	51.33 ± 10.61	51.67 ± 13.48	53.67 ± 10.91	52.67 ± 11.0
BCI - III	**Fisher ratio**	75.76 ± 12.3	76.0 ± 8.43	68.41 ± 11.98	70.73 ± 8.79	68.83 ± 9.72	72.0 ± 13.07

Table 8. Comparison of average performances (Our method versus CSP)

Method	Average Performances (%)			
	PhysioNet Dataset		BCI Competition-III Dataset	
	Scenario-1	Scenario-2	Scenario-1	Scenario-2
CSP ($m = 3$)	53.83 ± 4.87	55.65 ± 9.97	82.33 ± 11.46	84.67 ± 15.38
Our method (Cosine-based)	56.83 ± 10.17	61.0 ± 10.2	70.52 ± 9.0	76.0 ± 8.43

The classification was evaluated again using a FLD analysis. We demonstrate the average performance results in Table 8.

3.4. Discussion

The immediate observation on the performance results (i.e., presented in Table 6 and Table 7 for both scenarios) is the stark discrepancies between the recognition performances achieved on the PhysioNet and BCI Competition-III IVa datasets. Based on the performance evaluation criteria proposed by Müller (Müller-Putz et al. 2007), this appears to be a common trait of the PhysioNet dataset as observed in similar studies that report results only on a limited, well-performing subset of the subjects (please see Table 9) (Cheolsoo Park, Took, and Mandic 2014; Kim et al. 2016; Handiru and Prasad 2016; Tolić and Jović 2013; Athif and Ren 2019). While this can be justified to a certain extent by arguing that poor-performing subjects belonged to a presumed BCI-illiterate category, it falls at odds with the original premise of independent experimental validation. Our results, however, have been obtained from the first 20 subjects in PhysioNet dataset, without any performance-related exclusion criteria in order to avoid such controversies. Another important point is that, in general, the BCI studies using PhysioNet Motor Movement/Imagery dataset which elicited brilliant recognition performances uses independent component analysis-based methods as preprocessing to filter out the non-neural artifacts from each task period (Varsehi and Firoozabadi 2021). This approach may

not be applicable in real-time BCI systems. So, in this study, we did not adopt any statistical noise removal approach. The average performances on BCI Competition-III dataset IVa given in Table 6 (in Scenario-1) reveals that Kraskov's mutual information method can better capture the task specific time lags when the size of the training dataset is small. However, with a larger training dataset (in scenario-2), cosine-based similarity captured the task specific time lags more accurately and achieved the best average performance on both PhysioNet and BCI Competition-III datasets (please see Table 7). Performance of both mutual information-based and cosine similarity-based methods for both scenarios for different BCI Competition-III subjects shown in Table 10 indicate that for three well-performing subjects, the recognition accuracies are in the %70-%90 interval, while the accuracies for the other two is around %60-%65.

Table 9. Performance demonstration styles of studies that use the PhysioNet dataset

Author	**Proposed Method**	**Performance Demonstration Style**
Park et al. (Cheolsoo Park, Took, and Mandic 2014)	Augmented Complex CSP	Eliminates subjects with performance below the %64
Handiru et al. (Handiru and Prasad 2016)	Optimized Bi-Objective Chan. Selection Method	Uses 35 best performing subjects
Athif et al. (Athif and Ren 2019)	Wavelet transform and CSP filtering based method	Eliminates subject with performance below the %64
Kim et al. (Kim et al. 2016)	Complex CSP with Strong Uncorrelating Transformation	Eliminates subjects with performance below the %64

To see the ranking of the proposed method, by using original train and test dataset sizes given in the competition website, we also compared our recognition performances with the performances presented in the BCI Competition-III winner tables (performance rankings are given in the competition website). The mutual information-based and the cosine-based activity recognition methods ranked the 7^{th} place and 11^{th} places, respectively.

Table 10. Individual performances of BCI Competition-III dataset IVa subject for Scenario-1 and Scenario-2. The subjects *al, aw* and *ay* are the well-performing subject.

	Scenario-1 Performances (%)		**Scenario-2 Performances (%)**	
Subject	**Mutual Inf.**	**Cosine**	**Mutual Inf.**	**Cosine**
aa	64.36	67.55	70.52	73.68
al	90.95	82.97	92.63	84.21
av	62.23	60.1	64.21	64.21
aw	79.78	65.95	66.31	73.68
ay	86.17	76.06	84.21	84.21

Note also that, further developments may be expected on the recognition performance with some additional efforts such as elimination of the background activity (Hyvärinen and Oja 2000; Von Bünau et al. 2009; Jolliffe 1986) or using tailored spatial filters (Carvalhaes and De Barros 2015; Song and Epps 2007). The average performance can also be improved by increasing the size of the training set (BCI Competition-III dataset IVa contains more imagery activity periods than PhysioNet dataset). This suggests that using larger training sets or longer training sequences may lead to better learning and a higher recognition rate than obtained here.

In this study, our main aim was to highlight the potential of the inter-channel activity specific time lags in a cognitive task recognition scheme. The feature vectors obtained using these activity-specific time lags were expected to be an indicator of the dichotomy between different cognitive tasks (right/left hand motor imagery for PhysioNet, right hand/right foot for BCI Competition-III dataset). In that spirit, we used FLD analysis as a benchmark classifier. However, for the highest recognition performance, more sophisticated classification methods such as support vector machine (SVM) (Vapnik 2000), extreme learning machine (G. Bin Huang, Chen, and Siew 2006), kernel based extreme learning machine (Yu Zhang et al. 2018) or sparse Bayesian learning machine classifiers (Z. Jin et al. 2018) can certainly be evaluated.

Yet, an extended analysis involving linear and nonlinear SVM classifiers on both Scenario-1 and Scenario-2 that we have carried out reveals interesting results (please see Table 11 and Table 12 below). Linear SVM outperformed the FLD analysis, especially on the BCI Competition-III dataset IVa, in all synchronization measures while performance dropped using a radial basis function kernel. This suggests that a linear classification approach is more reliable in this instance, potentially due to high number of features against a low number of training samples. Furthermore, a conspicuous superiority of linear maximum margin classification on FLD analysis indicates that the generalization ability of FLD analysis is worsened when training samples are low in number, possibly due to the inability to calculate class covariance matrices with sufficient accuracy.

We tested our lagged synchronization-based framework with two datasets having 160 Hz. (PhysioNet) and 100 Hz. (BCI Competition-III dataset IVa) sampling frequencies. Note that, the sampling frequency of the EEG signals constitutes a fundamental limitation for the method that calculates and uses the inter-channel time lags that emerge between EEG signals during particular cognitive tasks. Actually, it is possible that the true inter-channel time lags deviated from those calculated by the synchronization measures evaluated here due to the low sampling frequency. It is evident that, increasing the sampling frequency may be expected to lead to an increase the accuracy of the activity-specific time lags that emerge between channels are calculated, as it would provide more data points for the calculation. However, it should also be noted that a higher sampling frequency would cause a sharp increase in computation time.

In this study, even for a low sampling frequency, we showed that the inter-channel time lags that maximizes the average synchronization values for each EEG channel pairs (i.e., activity-specific time lags), have potential in characterizing the cognitive task-related neural activity during a task period. Another limitation, the present framework disregards the subject-specific frequency bands. In general sense, filter bank strategy overcomes the subject-specific frequency band identification problem by incorporating different band-pass filters and identifies most discriminative frequency-specific features before the classification (S. H. Park, Lee, and Lee 2018; Higashi and Tanaka 2013; Ang et al. 2008; Gysels, Renevey, and Celka 2005). For our framework, instead of using 8-30 Hertz frequency band, incorporating a filter bank structure can be used in this method before the determination of activity-specific time lags.

Table 11. The comparison of the classification methods for Scenario-1

		Average Performances (%)					
		Cosine	**Cross Corr.**	**Non. Int.**	**Corr.**	**Mutual Inf.**	**PLV**
FLD	**PhysioNet**	56.83 ± 10.17	55.67 ± 8.02	57.0 ± 11.44	56.16 ± 15.07	58.33 ± 10.57	54.67 ± 10.83
	BCI Comp.	70.52 ± 9.0	72.65 ± 8.77	72.55 ± 9.65	75.95 ± 11.56	76.69 ± 12.88	68.08 ± 8.7
Linear SVM	**PhysioNet**	57.83 ± 10.38	58.17 ± 10.73	50.17 ± 2.28	50.17 ± 9.93	58.5 ± 10.78	60.5 ± 10.99
	BCI Comp.	74.46 ± 9.52	72.97 ± 10.93	77.65 ± 11.89	77.34 ± 9.5	77.97 ± 10.35	70.31 ± 10.58
Nonlinear SVM	**PhysioNet**	58.83 ± 11.0	55.83 ± 11.54	58.16 ± 9.58	55.67 ± 14.71	59.83 ± 9.33	58.83 ± 10.21
	BCI Comp.	71.7 ± 8.07	72.12 ± 8.33	76.38 ± 12.36	77.02 ± 8.42	75.0 ± 10.52	69.78 ± 8.22

Table 12. The comparison of the classification methods for Scenario-2

		Average Performances (%)					
		Cosine	**Cross Corr.**	**Non. Int.**	**Corr.**	**Mutual Inf.**	**PLV**
FLD	**PhysioNet**	61.0 ± 10.2	60.33 ± 15.37	60.67 ± 13.83	59.33 ± 16.17	59.33 ± 15.12	59.67 ± 15.06
	BCI Comp.	76.0 ± 8.43	68.83 ± 9.72	70.73 ± 8.79	72.0 ± 13.07	75.76 ± 12.3	68.41 ± 11.98
Linear SVM	**PhysioNet**	59.33 ± 16.02	61.67 ± 14.8	51.0 ± 10.43	62.33 ± 16.51	59.33 ± 14.96	59.67 ± 15.36
	BCI Comp.	79.57 ± 9.52	77.26 ± 9.75	81.05 ± 8.93	80.21 ± 10.35	81.89 ± 11.8	75.15 ± 13.03
Nonlinear SVM	**PhysioNet**	58.67 ± 12.53	58.66 ± 14.28	62.0 ± 13.36	65.33 ± 17.91	59.67 ± 15.21	60.0 ± 14.82
	BCI Comp.	74.73 ± 5.47	74.1 ± 4.85	78.1 ± 7.85	80.0 ± 6.69	77.89 ± 10.26	70.94 ± 8.1

This enables us to calculate and use the frequency-resolved activity-specific time lags may also be expected to improve recognition performance, albeit in expense of computation time (Goldhacker et al. 2018). Still, once the salient subject-specific frequency bands are identified, activity-specific time lags can easily be calculated and used for subsequent recognition purposes (Kumar, Sharma, and Tsunoda 2017).

In the present study, we aimed to determine the most powerful synchronization method among six different methods that captures the most appropriate time lag (activity-specific time lag) between EEG channels that the synchronization (evaluated at this lag) is characteristic to the particular cognitive tasks. In the literature, many different synchronization measures were proposed and subjected to performance comparison using various types of synthetic and real datasets collected under various experimental conditions (Bakhshayesh et al. 2019b; Dauwels et al. 2010; Duckrow and Albano 2003; M. H. Wu, Frye, and Zouridakis 2011). However, the main outcome of these studies indicates that there is no universal synchronization measure that works better than all others. It appears a general consensus that different measures calculate the synchronization by taking different feature types of the input signals into consideration (Bakhshayesh et al. 2019b; Sakkalis 2011). During cognitive tasks, the brain presents dynamically changing electrophysiological characteristics and also, the functional connectivity between distant regions is affected from these dynamical changes. Each of the different synchronization methods used in this study attempts to find the activity-specific time lags between electrophysiological signals as captured by the method itself. Since each method evaluates a different aspect of the signals, it is not surprising to observe dissimilar time lags. In the absence of full knowledge of exact time lags between the signals, it is impossible to tell which method appeared to be more accurate in calculating the time lag of interest.

In addition to those evaluated in this study, further synchronization estimation methods exist in the literature. Notably, the transfer entropy has been frequently used in both sensor space and source space connectivity studies (Faes et al. 2016; Olejarczyk et al. 2017; Wibral et al. 2013; Pampu et al. 2013; Montalto, Faes, and Marinazzo 2014; Schreiber 2000). However, due to the high computational requirements during its calculation, transfer entropy does not appear to be a viable method for brain activity recognition. As a result, it was not included in this work. Even then, calculating the mutual information, correntropy and nonlinear interdependency measures for 20 subjects in PhysioNet dataset and 5 subjects for BCI Competition-III dataset IVa took several days.

However, for PhysioNet dataset, the required computation time for cross-correlation and cosine-based similarity are about 15,6 seconds and 13,7 seconds per subject, respectively. As for BCI Competition-III dataset IVa, for five subjects, the corresponding computations took 154,7 seconds and 202,2 seconds per subject. While these computation times are not extensive, with the high speed and parallel computing architectures, cosine similarity-based measure stands out as the more practical synchronization evaluation method for a real time cognitive status analysis.

The recognition performance results for the PhysioNet dataset, given in both Tables 6 and 7 show that we did not achieve the minimum reliable communication rate (%70). These low performances may be due to relatively small training sample size or low-quality of EEG recordings. For the small sample size problem of FLD and/or SVM classifiers, increasing the number of training samples may require long training sequences which then very tiring and therefore challenging for the participants. Pooling and using informative feature vectors from all other subjects may also improve the classification performance of the proposed framework. Jiao et al. proposed sparse group representation method (SGRM) to reduce the required training time without any performance degradation for motor imagery brain computer interface approaches (Jiao et al. 2019). Briefly, this method identifies and uses informative feature vectors (also features) from a dictionary matrix constructed using both non-target subjects' and target subject's training feature vectors. For our study, as proposed in (Jiao et al. 2019), exploiting the informative features and feature vectors obtained from both target and non-target subjects' training task periods (for each subject, feature vectors are constructed via inter-channel synchronization values evaluated at activity-specific time lags) may improve the recognition performances especially obtained for PhysioNet dataset. Similar sparse representation approach for frequency-resolved informative feature identification was proposed and can be applied to our framework (Yu Zhang et al. 2015). Another problem, since we do not accurately know when the subject begins and ends the imagination of the motor movement task, we used whole task period EEG signals to calculate the activity-specific time lags. For an accurate brain activity characterization, an extended approach that jointly optimizes the time window and the frequency band can also be adopted in our framework before the inter-channel activity-specific time lag estimation (Yu Zhang et al. 2019).

For both PhysioNet and BCI Competition-III dataset IVa datasets, we listed the electrode pairs that provide meaningful differences between two cognitive tasks along

with five most significant electrode pairs that achieve maximum separability among different type of motor imagery activities in Table 13 (for scenario-2). We observed that on the BCI Competition-III dataset, all synchronization measures identified couplings between similar group of electrode pairs. However, on the PhysioNet dataset, the groups of electrode pairs identified to be in synchrony differed for the different synchronization measures. While this makes the interpretation of identified couplings challenging meaningful comparisons can still be made as follows,

A first-look analysis on PhysioNet dataset (right fist versus left fist imagination) reveals that cosine-based similarity captured mostly the parietal-central electrode couplings, cross-correlation the parietal-parietal electrode couplings, nonlinear interdependency central-parietal electrode pairs, mutual information the frontal and parietal electrode couplings, correntropy the frontal electrode couplings and finally PLV the parietal-parietal electrode couplings.

As for the BCI Competition-III dataset IVa (right hand versus right foot imagination), we observed that all synchronization measures consistently captured the left fronto central-central, left central-centro parietal and left fronto central-centro parietal connectivity. By taking both results into consideration, mutual information method can better unveil motor imagery task related connectivity patterns than the other synchronization methods. These electrode couplings result for each dataset shows that, for both datasets, mutual information can better unveil motor imagery task related connectivity patterns than the other synchronization measures.

For the right/left fist motor imagery task, mutual information captured the synchronization patterns that reflect the functional connectivity of left premotor area-right premotor area, supplementary motor area-left sensorimotor cortex, right premotor area-right sensorimotor cortex, and right-left parietal regions. In the literature, these brain regions have already been identified to be strongly associated with hand motor imagery tasks. While the right and left premotor areas are responsible for the integration and processing of information collected from other regions of the brain (Xu et al. 2014; Luppino and Rizzolatti 2000), sensorimotor cortex plays a role in spatial control and motor planning (Porro et al. 1996). In (H. Chen et al. 2009), authors found that both sensorimotor cortices and premotor area are simultaneously activated with supplementary motor area during hand motor imagery activity. In a later study, the same group identified connectivity patterns between similar regions for right- and left-hand motor imagery task (Q. Gao, Duan, and Chen 2011).

Table 13. The 5 most frequent electrode pairs obtained for both PhysioNet Motor Movement/Imagery and BCI Competition-III dataset IVa (for scenario-2)

	Cosine	**Correlation**	**Non. Int.**	**Corr.**	**Mutual Information**	**PLV**
PhysioNet Dataset	Fc3-P5	C6-AF3	C4-Po4	Fcz-Ft8	F5-F8	Tp8-Po7
	Fc6-Ft7	Cp3-Fp1	C6-Po4	F7-O1	Tp8-Po3	P5-P8
	C1-P7	Cp6-Po3	Cp5-O2	Fc1-Ft8	P8-Po7	P1-P8
	Cp5-P2	P5-P8	Cp1-Po4	Fcz-F8	Fc4-Tp8	Fc3-Ft7
	Cp6-Iz	P3-P8	Ft8-Po4	Fcz-Ft7	C5-F1	C4-P8
BCI Competition-III Dataset	Fc1-C1	Fc1-C1	Fc1-C1	Fc1-C1	Fc1-C1	CFC1-CCP3
	F3-CCP5	Fc1-CCP3	CFC1-Cp3	CFC1-Cp3	Fc1-CCP3	Cz-CCP3
	F1-CCP3	CFC1-CCP3	F7-CCP5	Cz-CP3	CFC1-CCP3	Fc1-CCP3
	F1-CCP5	Cz-CCP3	F5-CCP5	F1-CCP5	Cz-CCP3	Fcz-CCP3
	F1-Cp5	Cz-Cp1	FFC7-CCP5	F1-CCP3	Cz-Cp1	FFC1-CCP3

Cognitive, sensory and motor functions require interconnectivity of anatomically as well as functionally different regions of the brain (Y. Gao et al. 2019). Basically, these regions reciprocally process and exchange neural information for each specific brain activity (Rangaprakash 2014). So far, in the literature, a great deal of brain activity recognition/characterization studies analyzed and used power-based features of electrophysiological data obtained from focal cortical activity of the brain with notable success (Ramoser, Müller-Gerking, and Pfurtscheller 2000; Fabien Lotte and Guan 2011; Yu Zhang et al. 2015; 2019). However, as also depicted in many other studies, a complete assessment of brain function requires a detailed evaluation of the interaction between electrophysiological data collected from distinct regions of the brain (Sakkalis 2011; Rocca et al. 2014; Greenblatt, Pflieger, and Ossadtchi 2012). Indeed, this perspective forms the main premise of the current study.

Yet, for a more concrete comparison of CSP-based power features and synchronization-based features, it may be helpful to recognize that, CSP essentially calculates the power of the latent channels obtained as weighted linear combinations of actual EEG signals. In case where synchronization occurs through concurrent power increase or decrease that is preserved through the prescribed linear weighting by the CSP, the resulting power features can be expected to be useful for task recognition. However, there is no clear indication on how synchrony manifests between different brain regions during tasks of interest. This, in fact, was the main reason for evaluating a battery of potential synchronization measures in a cognitive task recognition scenario in this manuscript. Consequently, CSP-based power features may be insensitive to synchronization modes that do not survive weighted linear average over a large number of brain regions, that may also explain their apparent weakness in the recognition problem considered here.

For right fist/left fist motor imagery recognition, performances obtained from a *priori* selected channel pairs show that the channel pairs proposed by Krusienski et al. (Krusienski, McFarland, and Wolpaw 2012) generally achieves better accuracy than the other ones. From a biophysical point of view, these channel pairs constitute inter- and intra-hemispheric connections and collect electrophysiological activity from premotor, primary motor, sensorimotor and central-parietal regions. In the literature, these brain areas are listed among the critical brain for regions and constitute the functional network related with the right/left hand/finger motor imagination tasks (Xu et al. 2014). In line with the previous studies that examine the intra- and inter-hemispheric interactions, stated

that these electrodes mainly manifest the electrical activity of parietal, central and premotor regions during right and left hand motor imagination (Q. Gao, Duan, and Chen 2011; Solodkin et al. 2004). A study accomplished by L. A. Wheaton et al. further stated that the increase of synchronization between premotor and parietal cortices are the signature of motor preparation task for praxis hand movements (Wheaton et al. 2005). Since right/left fist imagination is not a fully praxis movement, it is reasonable to expect that these channel pairs demonstrate better recognition performance than the other ones. Another study that evaluates the functional networks during finger tapping imagination identified eight connections that are mainly observed between premotor and motor cortices (Xu et al. 2014). Yet, the results in Table 6 and Table 7 show that automatically selected channel pairs outperform these a *priori* determined channel pairs for imaginary motor activity recognition. Clearly, the issue of which channel pairs are useful for which activity is to be elucidated further. One possible avenue of research may be to evaluate which channel pairs are often selected across the subjects of a large cohort. The current study forms the initial stage of a funded project that addresses a connectivity-based brain activity characterization. We are currently seeking to capture the characteristic short-lived synchronization patterns that emerge during the cognitive task in different time lags as well as in different latency values. This, however, entails a 3-parameter optimization (i.e., $\Delta t, \tau$ and w) with additional algorithmic and computational challenges and is studied in the next chapter.

CHAPTER 4

SHORT-LIVED SYNCHRONIZATION BETWEEN EEG CHANNELS FOR CHARACTERIZATION OF COGNITIVE ACTIVITIES

It is necessary to study not only parts and processes in isolation,
but also, to solve the decisive problems found in organization and order unifying them,
resulting from dynamic interactions of parts, and making the behavior of the
parts different when studied in isolation or within the whole…
-Ludwig won Bertalanffy-

4.1. Introduction

In this chapter, we propose a novel brain activity characterization framework that tries to improve the characterization ability of the method presented in the previous chapter (Orkan Olcay, Özgören, and Karaçalı 2021). Our approach in this chapter is based on the premise that the activity-specific synchrony between EEG channels may emerge and vanish in a short period of time. The method presented here identifies and uses the timing parameter triplets of the activity-specific short-lived synchronizations between the EEG channels emerged for each specific mental task. We captured the timings of maximal average short-lived synchronization for characterization of brain activities. Note that the short-lived maximal synchrony between the brain electrical signals during a cognitive task can be thought of evidencing cognitive task-specific information exchange/flow between brain regions and possibly also in specific frequency bands (Maars and Lopes Da Silva 1983; Gonuguntla, Wang, and Veluvolu 2016; Wibral et al. 2011; Zanon, Borgomaneri, and Avenanti 2018), which may further signify the presence of an activity-specific functional integration mechanism (Rubinov and Sporns 2010; S. H. Jin et al. 2006). The three timing parameters we use to calculate pairwise channel synchrony are:

- Δt for latency of maximally synchronized signal segments from activity onset ($t = 0$).

- τ for the time lag between maximally synchronized signal segments.
- w for the length of the maximally synchronized signal segments.

The graphical illustration of these timing parameters is presented in Figure 18. To identify the three timing parameters of the activity-specific synchronization for each type of motor imagery activity and each EEG channel pair, we adopted a heuristic optimization that evaluates the channel synchronizations calculated using a fixed-length sliding time window. Simply, the optimization method captures and evaluates the significant synchronization patterns (i.e., candidate patterns) aligned on Δt axis emerged for different τ parameters. Next, we evaluated the significance of each candidate synchronization patterns by conducting one-sample t-tests to identify the most significant synchronization timings. The timing parameter triplet that elicited the most significant synchronization (i.e., the smallest P-value) among all candidate timing parameter triplets is identified as the activity-specific timing parameter triplet for the corresponding motor imagery activity type and channel pairs duely. The activity-specific timing parameter triplet can be represented by $\{\Delta t_{i,j}^{A}, \tau_{i,j}^{A}, w_{i,j}^{A}\}$ for motor imagery activity type A and for channel pair (i, j).

After finding the activity-specific timing parameter triplets for each channel pair and each type of motor imagery activity, we evaluated the discrimination ability of the activity-specific timing parameter triplets both in a motor imagery activity recognition framework and statistical tests. To that end, we used the activity-specific timing parameter triplets to calculate and use the inter-channel short-lived synchronizations as features.

We expect that the inter-channel short-lived synchronizations calculated using the corresponding activity-specific timing parameter triplets for the respective activity periods will be significantly distinct from those calculated with the same parameters for other types of activity periods. We conducted these analyses for six different synchronization measures to specify the most successful measure at capturing the timings of characteristic pairwise channel synchronizations (H. E. Wang et al. 2014; Sakkalis 2011; Greenblatt, Pflieger, and Ossadtchi 2012).

The remainder of this chapter is organized as follows: In Section 4.2, we provided the synchronization measures and the details of the proposed method along with the heuristic optimization approach adopted in this study. In Section 4.3, we present the recognition performance results that compare channel synchronization values obtained

for different tasks calculated using the activity-specific timing parameter triplets. In Section 4.4, we discuss the classification performances and the biophysical findings obtained from the motor imagery activity recognition framework adopted for testing the proposed method.

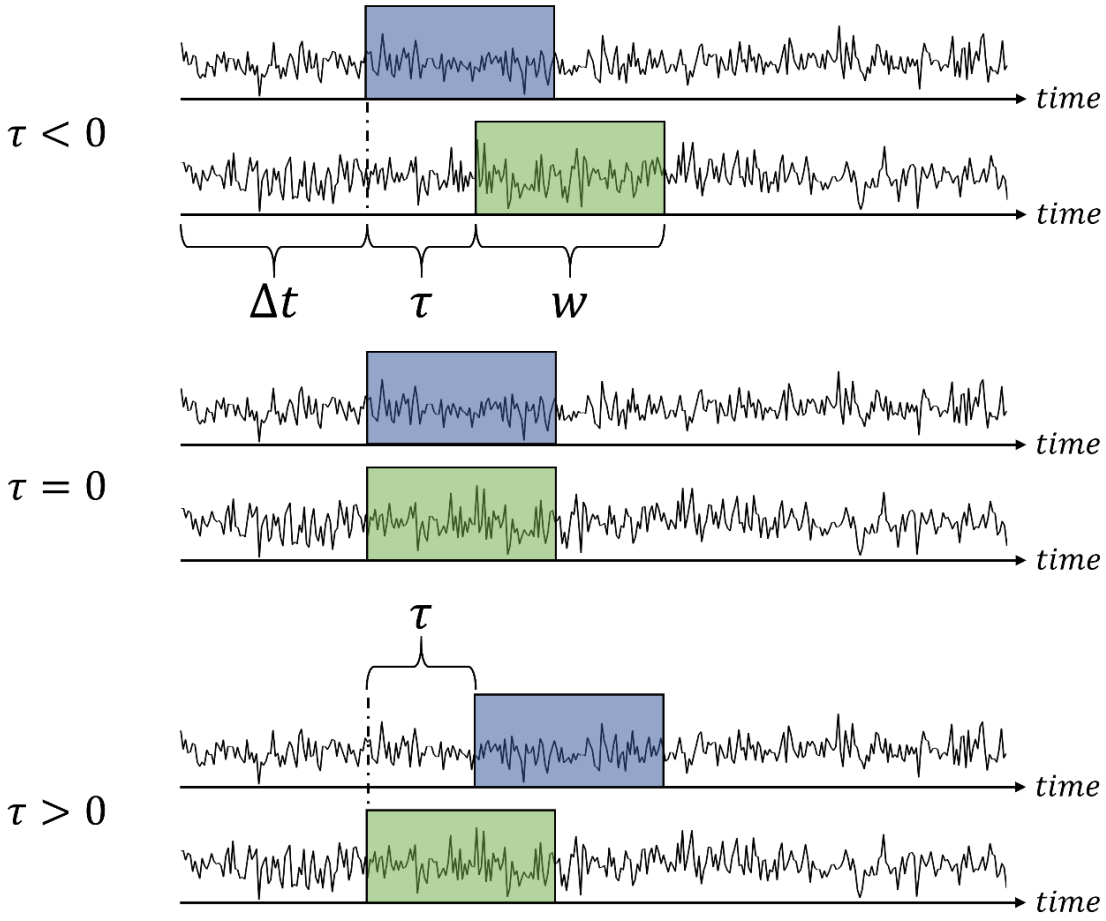

Figure 18. The illustration of the timing parameters Δt, τ, and w used to determine pairwise short-lived synchronization between two EEG channels. Δt stands for latency of characteristic synchronization from activity onset, τ for time lag between synchronized signal segments, and w for duration of characteristic synchronization. We demonstrated the three cases which time-directional synchronization calculated for $\tau < 0$, $\tau = 0$, and $\tau > 0$.

4.2. Proposed Method

In order to capture the timings of the activity-specific short-lived synchronization between the EEG channels, we used six different synchronization measures. The measures that we used in this framework are:

- Cosine-based similarity (B. Orkan Olcay and Karaçalı 2019; Sargolzaei et al. 2015; Herff et al. 2019)
- Wavelet bi-coherence (Makarov et al. 2018)
- Phase locking value (Lachaux et al. 1999; Varela et al. 2001)
- Phase coherence value (Tass et al. 1998; Ziqiang and Puthusserypady 2007; Bakhshayesh et al. 2019b)
- Linearized mutual information (S. H. Jin, Lin, and Hallett 2010; Montalto, Faes, and Marinazzo 2014)
- Cross-correntropy (Santamaría, Pokharel, and Principe 2006; Liu, Pokharel, and Principe 2007; Principe 2010)

We adopted Vasicek's entropy estimation method (Ibrahim Al-Omari 2014; Vasicek 1976) to estimate the entropies of the phase difference signals for the phase coherence value method. Furthermore, we used complex Morlet wavelets, which is the most used wavelet function in biological signal analysis, to calculate the wavelet transforms of the EEG signals for the wavelet bi-coherence method (Alexander E. Hramov et al. 2015). Also, we used linearized mutual information due to the computation speed issues faced using Kraskov's method. As a note, the linearized mutual information uses the linear correlation coefficient when calculating the synchrony between the short-lived signals.

Prior to the synchronization calculation, we extracted the signal segments of each task period from each channel represented by $s_{i,n}^{\Delta t,w} = s_i(t)|_{t\in[t_n+\Delta t,\ t_n+\Delta t+w]}$ where the signal segments extracted from task period n and channel i that starts at Δt milliseconds from the activity onset t_n and lasts for w milliseconds. Similarly, $s_{j,n}^{\Delta t+\tau,w} = s_j(t)|_{t\in[t_n+\Delta t+\tau,\ t_n+\Delta t+\tau+w]}$ represents the signal segment extracted from task period n and channel j that starts at $\Delta t + \tau$ milliseconds from the activity onset t_n and lasts for w milliseconds (please see Figure 19). Note that while τ can take positive or negative

values, Δt takes values that are greater than or equal to zero only. Consequently, $s_{j,n}^{\Delta t+\tau,w}$ may lead or lag $s_{i,n}^{\Delta t,w}$ on the time axis.

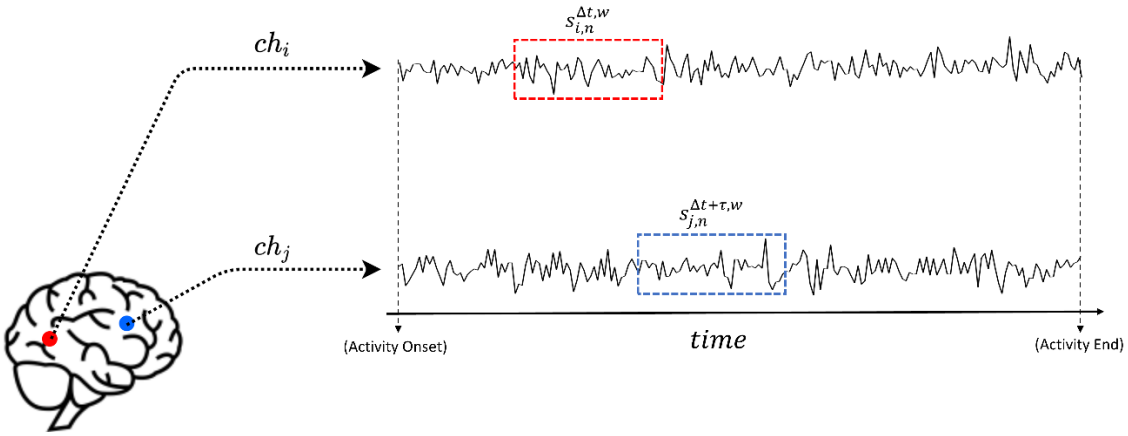

Figure 19. Illustration of short-lived signal segments obtained from EEG channels *i* and *j* for task period indexed by n. Note that in here, τ takes a positive value, suggesting that the i[th] channel leading the j[th] channel.

4.2.1. Heuristic Search Method for Determining the Activity-Specific Timing Parameters

Our main aim here is to determine the activity-specific timing parameter triplets for each specific cognitive activity and channel pairs. To that end, we adopted the heuristic parameter search strategy described in detail below to capture these timing parameter triplets. Since the EEG signals as well as their short-lived synchronization estimates are quite noisy, using well-known search methods such as gradient descent, Nelder-Mead (i.e., simplex search), simulated annealing, leads to an erroneous parameter triplet estimation.

In order to determine the activity-specific timing parameter triplets $\{\Delta t, \tau, w\}$ for each channel pair and each type of cognitive activity, we adopted a sliding time window based search method with a fixed length of 300ms as in (Roelfsema et al. 1997) and (Bola, Gall, and Sabel 2015). In this method, we first calculated the short-lived synchronization between the signal segments obtained for each channel pair (i, j) and training task period

n for varying $\Delta t \in [0ms, 2000ms]$ as in (Chung, Kang, and Kim 2012; Christa Neuper et al. 2009a) and $\tau \in [-125ms, 125ms]$ as in (B. Orkan Olcay and Karaçalı 2019) at a fixed duration of 300ms as

$$D_{i,j}(\Delta t, \tau, n) = S\left(s_{i,n}^{\Delta t, 300ms}, s_{j,n}^{\Delta t+\tau, 300ms}\right) \tag{4.1}$$

where $S(\cdot,\cdot)$ denotes the synchronization measure of choice. We then calculated the average synchronization across the training task periods of the same cognitive activity type for each channel pair (i, j) as

$$\overline{D}_{i,j}^{A_{1/2}}(\Delta t, \tau) = \frac{1}{\left|I_{1/2}\right|} \sum_{n \in I_{1/2}} D_{i,j}(\Delta t, \tau, n) \tag{4.2}$$

where $\overline{D}_{i,j}^{A_{1/2}}(\Delta t, \tau)$ is the average synchronization matrix calculated across the corresponding training task periods, and I_1 and I_2 are the indices of the training task periods belonging to activity types A_1 and A_2, respectively. Since the aim of this study is to analyze the short-lived brain interactions, we adopted a quantile (or alternatively percentile) based thresholding to capture the important synchronization dynamics as in (Zink, Mückschel, and Beste 2020). Next, we thresholded the average synchronization values $\overline{D}_{i,j}^{A_{1/2}}(\Delta t, \tau)$ with respect to the %99 quantile of the cumulative distribution functions of all values of $\left\{\overline{D}_{i,j}^{A_{1/2}}(\Delta t, \tau)\right\}$ for all combinations of Δt and τ. This revealed candidate short-lived synchronization patterns that extend the along the Δt axis, that were then subjected to statistical evaluation.

For the statistical evaluation, we identified the timing parameter triplets that correspond to each of candidate short-lived synchronization patterns. Note that a synchronization pattern observed at $\tau = \tau_0$ and $\Delta t_1 \leq \Delta t \leq \Delta t_2$ suggests significant synchronization between $s_{i,n}^{\Delta t_1, \Delta t_2 - \Delta t_1 + 300ms}$ and $s_{j,n}^{\Delta t_1 + \tau_0, \Delta t_2 - \Delta t_1 + 300ms}$ (see Figure 20). The statistical test evaluated the channel synchronizations obtained from corresponding task periods observed for each such triple timing parameter against zero for each channel

pair (i, j) in case multiple patterns emerged and selected the one with the lowest P-value observed as a result of t-test. Consequently, we identified the activity-specific timing parameter triplet that maximizes the statistical significance of channel synchronizations for each activity type and for each channel pair separately.

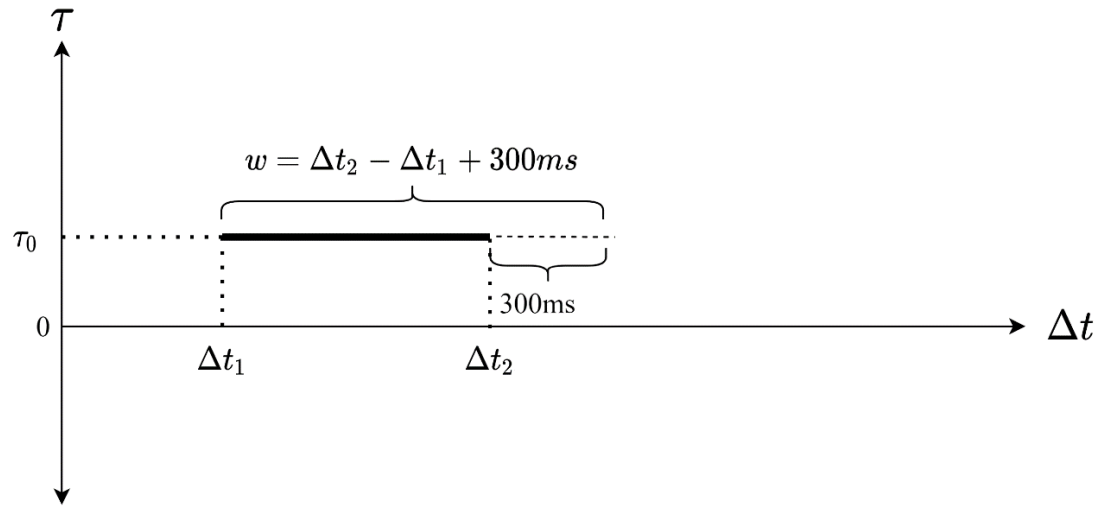

Figure 20. An exemplary illustration of timings of the three candidate maximal synchronization patterns obtained after thresholding for a channel pair (i, j). We determined the latency (Δt) of the candidate signal segment as Δt_1, time lag (τ) between the candidate signal segments as τ_0, and the duration of signal segments (w) as $\Delta t_2 - \Delta t_1 + 300ms$.

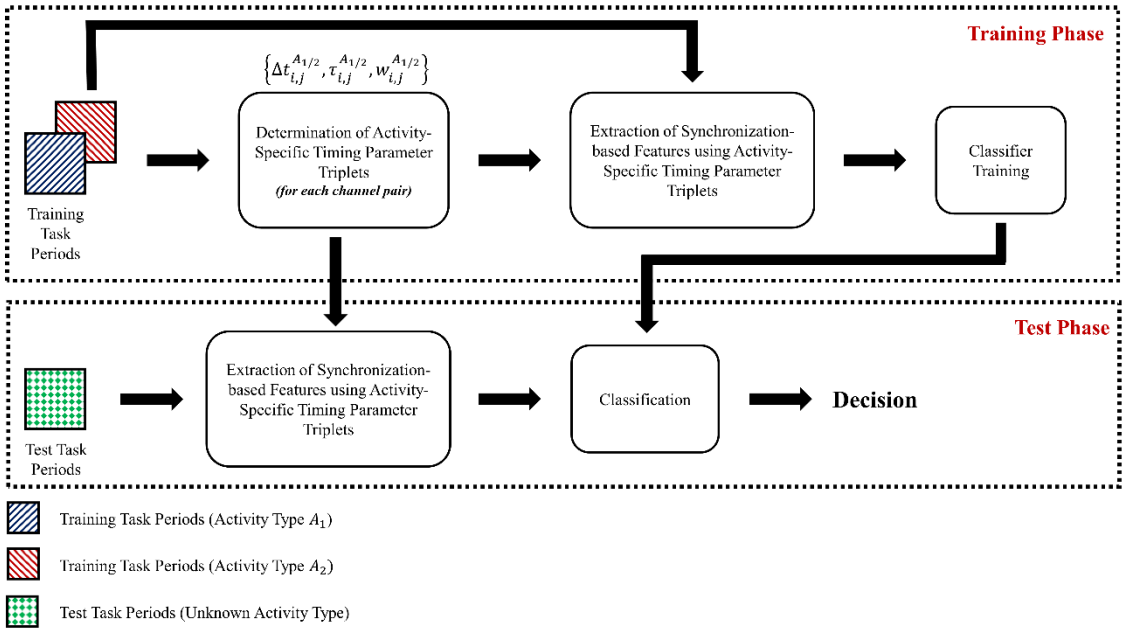

Figure 21. The illustration of the operational flow diagram of the short-lived synchronization based proposed method.

4.2.2. The Proposed Cognitive Activity Recognition Method

In this section, we provided the details of operational flow diagram of the brain activity recognition scheme in Figure 21. In the training phase, we determined the activity-specific timing parameter triplets $\left\{\Delta t_{i,j}^{A_{1/2}}, \tau_{i,j}^{A_{1/2}}, w_{i,j}^{A_{1/2}}\right\}$ for cognitive activities A_1 and A_2 for each channel pair (i,j). Next, we used the activity-specific timing parameter triplets to calculate inter-channel characteristic synchronization values and then collected these synchronization values into a feature vector for each training task period. Thus, the training feature vector ξ_ℓ for the training task period indexed by ℓ is constructed as

$$\xi_\ell = \begin{bmatrix} S\left(s_{1,\ell}^{\Delta t_{1,2}^{A_1}, w_{1,2}^{A_1}}, s_{2,\ell}^{\Delta t_{1,2}^{A_1}+\tau_{1,2}^{A_1}, w_{1,2}^{A_1}}\right) \\ S\left(s_{1,\ell}^{\Delta t_{1,3}^{A_1}, w_{1,3}^{A_1}}, s_{3,\ell}^{\Delta t_{1,3}^{A_1}+\tau_{1,3}^{A_1}, w_{1,3}^{A_1}}\right) \\ \vdots \\ S\left(s_{M-2,\ell}^{\Delta t_{M-2,M}^{A_1}, w_{M-2,M}^{A_1}}, s_{M,\ell}^{\Delta t_{M-2,M}^{A_1}+\tau_{M-2,M}^{A_1}, w_{M-2,M}^{A_1}}\right) \\ S\left(s_{M-1,\ell}^{\Delta t_{M-1,M}^{A_1}, w_{M-1,M}^{A_1}}, s_{M,\ell}^{\Delta t_{M-1,M}^{A_1}+\tau_{M-1,M}^{A_1}, w_{M-1,M}^{A_1}}\right) \\ S\left(s_{1,\ell}^{\Delta t_{1,2}^{A_2}, w_{1,2}^{A_2}}, s_{2,\ell}^{\Delta t_{1,2}^{A_2}+\tau_{1,2}^{A_2}, w_{1,2}^{A_2}}\right) \\ S\left(s_{1,\ell}^{\Delta t_{1,3}^{A_2}, w_{1,3}^{A_2}}, s_{3,\ell}^{\Delta t_{1,3}^{A_2}+\tau_{1,3}^{A_2}, w_{1,3}^{A_2}}\right) \\ \vdots \\ S\left(s_{M-2,\ell}^{\Delta t_{M-2,M}^{A_2}, w_{M-2,M}^{A_2}}, s_{M,\ell}^{\Delta t_{M-2,M}^{A_2}+\tau_{M-2,M}^{A_2}, w_{M-2,M}^{A_2}}\right) \\ S\left(s_{M-1,\ell}^{\Delta t_{M-1,M}^{A_2}, w_{M-1,M}^{A_2}}, s_{M,\ell}^{\Delta t_{M-1,M}^{A_2}+\tau_{M-1,M}^{A_2}, w_{M-1,M}^{A_2}}\right) \end{bmatrix} \tag{4.3}$$

where M denotes the total number of channels (i.e., $M = 118$ for BCI Competition-III dataset IVa, $M = 64$ for PhysioNet dataset). After constructing the training feature vectors, we performed a feature selection procedure to determine the most discriminative features. To that end, we calculated the Fisher's ratio of each feature as in the previous chapter. We selected the features that elicited a Fisher's ratio higher than the mean plus two times the standard deviation of the Fisher's ratios of all features. Finally, we trained classifiers on the reduced training feature vectors. In this study, we used three different classification methods, namely Fishers' linear discriminant (FLD), linear support vector machines (linear SVM), and nonlinear (radial basis function) support vector machines (nonlinear SVM). The kernel width parameter for nonlinear SVM classifier was calculated using the Eq. (2.57).

In the test phase, we constructed the test feature vectors ξ for each test task periods using the activity-specific timing parameter triplets obtained in the training phase as

$$\xi = \begin{bmatrix} S\left(s_1^{\Delta t_{1,2}^{A_1}, w_{1,2}^{A_1}}, s_2^{\Delta t_{1,2}^{A_1}+\tau_{1,2}^{A_1}, w_{1,2}^{A_1}}\right) \\ S\left(s_1^{\Delta t_{1,3}^{A_1}, w_{1,3}^{A_1}}, s_3^{\Delta t_{1,3}^{A_1}+\tau_{1,3}^{A_1}, w_{1,3}^{A_1}}\right) \\ \vdots \\ S\left(s_{M-2}^{\Delta t_{M-2,M}^{A_1}, w_{M-2,M}^{A_1}}, s_M^{\Delta t_{M-2,M}^{A_1}+\tau_{M-2,M}^{A_1}, w_{M-2,M}^{A_1}}\right) \\ S\left(s_{M-1}^{\Delta t_{M-1,M}^{A_1}, w_{M-1,M}^{A_1}}, s_M^{\Delta t_{M-1,M}^{A_1}+\tau_{M-1,M}^{A_1}, w_{M-1,M}^{A_1}}\right) \\ S\left(s_1^{\Delta t_{1,2}^{A_2}, w_{1,2}^{A_2}}, s_2^{\Delta t_{1,2}^{A_2}+\tau_{1,2}^{A_2}, w_{1,2}^{A_2}}\right) \\ S\left(s_1^{\Delta t_{1,3}^{A_2}, w_{1,3}^{A_2}}, s_3^{\Delta t_{1,3}^{A_2}+\tau_{1,3}^{A_2}, w_{1,3}^{A_2}}\right) \\ \vdots \\ S\left(s_{M-2}^{\Delta t_{M-2,M}^{A_2}, w_{M-2,M}^{A_2}}, s_M^{\Delta t_{M-2,M}^{A_2}+\tau_{M-2,M}^{A_2}, w_{M-2,M}^{A_2}}\right) \\ S\left(s_{M-1}^{\Delta t_{M-1,M}^{A_2}, w_{M-1,M}^{A_2}}, s_M^{\Delta t_{M-1,M}^{A_2}+\tau_{M-1,M}^{A_2}, w_{M-1,M}^{A_2}}\right) \end{bmatrix} \tag{4.4}$$

After the construction of the test feature vectors, we extracted the features that were identified in the training phase, applied the classifiers constructed earlier on the reduced test feature vectors and correspondingly assigned the associated cognitive task period either to A_1 or A_2.

To be clearer, we constructed the algorithmic steps in tabular form (please see Tables 14 and 15) to capture the activity-specific timing parameter triplets, and the classification framework that we adopted in this chapter.

Table 14. The algorithmic steps for finding activity-specific timing parameter triplets.

Algorithm-1:	Finding Activity-Specific Timing Parameter Triplets
Step-1	For the channel pair (i,j), calculate inter-channel synchronizations for $\Delta t \in [0ms\ 2000ms], \tau \in [-125ms\ 125ms]$ via $w = 300ms$ length sliding time window for each training task period of activity A.
Step-2	Calculate the average the synchronization values across training task periods of activity A.
Step-3	Set the threshold to %99 quantile of average synchronization values. Then, compare each entry of average synchronization matrix with the threshold.
Step-4	Determine the timings of each of synchronization patterns remaining after thresholding. Use each one of these candidate timings to extract the signal segments from corresponding training task periods.
Step-5	Calculate the synchronization between the extracted signal segments. Apply t-test to these synchronization values to determine P-value of each timing parameter.
Step-6	Identify the timing parameter triplet for channel pair (i,j) and activity A, which elicited the smallest P-value as activity-specific timing parameter triplet (i.e., $\{\Delta t_{i,j}^{A}, \tau_{i,j}^{A}, w_{i,j}^{A}\}$). Repeat these calculations from the steps 1-6 for all channel pairs.

Table 15. The algorithmic steps of the classification framework.

Algorithm-2:	The Classification Framework
Step-1	Use 8-30 Hz bandpass filter and CAR to filter the data spectrally and spatially.
Step-2	Use **Algorithm-1** to obtain the A_1 activity-specific timing parameter triplets for each channel pair.
Step-3	Use **Algorithm-1** to obtain the A_2 activity-specific timing parameter triplets for each channel pair.
Step-4	Use both A_1 and A_2 activity-specific timing parameter triplets to construct training feature vectors.
Step-5	Calculate the Fisher ratio of each feature. Identify the features that elicited higher than mean plus two standard deviation of Fisher ratios of all features.
Step-6	Train the classifiers by using reduced training feature vectors.
Step-7	Use both A_1 and A_2 activity-specific timing parameter triplets to construct reduced test feature vectors.
Step-8	Determine the category of each test feature by using the classifier trained in step-6

4.2.3. Comparative Analysis Using Benchmark BCI Methods

We employed conventional CSP and AR modelling methods to compare the performance of the proposed method. We calculated the CSP filters on the training task periods by setting the number of eigenvectors $m = 3$ in accordance with the literature and filtered all training and test task periods by CSP filters (Blankertz et al. 2008). Then, we extracted the log-variance features from CSP-filtered task periods. For AR modelling, we used a least-squares method to calculate the univariate model coefficients over signal segments of one-second sliding time windows with %50 percent overlap and concatenated them together to incorporate the dynamic changes of the spectral information of the electrophysiological activity as adopted in past literature (Ince, Tewfik, and Arica 2007; Gürkan, Akan, and Seyhan 2014; Kuruoğlu 2002; Golub and Saunders 1970). We set the AR model order of each channel to six as in (Ince, Tewfik, and Arica 2007; Anderson, Stolz, and Shamsunder 1998) unlike in (McFarland and Wolpaw 2008) due to the limited number of signal samples in the sliding time window. Next, we selected the most informative AR modelling features via Fisher's ratio as adopted for the proposed method. We then trained the classifiers using the reduced training AR features. A similar feature extraction procedure was adopted for the test task periods. We finally used the reduced features for constructing the test feature vectors for performance evaluation.

4.3. Results

We used two distinct chronological cross-validation scenarios (i.e., scenario-1 and scenario-2) to evaluate the performance of our brain activity characterization method for different training set sizes as in (B. Orkan Olcay and Karaçalı 2019). We determined the activity-specific timing parameter triplets for each type of motor imagery activities by using the training task periods for each subject individually in both BCI Competition-III dataset IVa (i.e., right hand/right foot imagery movement) and PhysioNet dataset (right/left fist imagery movement). Afterwards, we constructed the synchronization-based feature vectors by using these parameters as in Eq. (4.3) and (4.4) and carried out

training and testing procedures as described earlier. Average classification performances are shown in Table 16 and the performance comparison results are presented in Table 17.

In Table 16, we presented the average performances obtained using the six different synchronization measures obtained via three different classifiers. In Table 17, we provided the maximum performances obtained via the currently proposed method, the earlier τ-based method developed by our group (B. Orkan Olcay and Karaçalı 2019), the common spatial patterns (CSP) method (Ramoser, Müller-Gerking, and Pfurtscheller 2000; Blankertz et al. 2008), and the univariate autoregressive (AR) modelling based method (Anderson, Stolz, and Shamsunder 1998). Note that the last two are the popular benchmark methods in the mental imagery activity related brain activity recognition literature (G. Pfurtscheller et al. 2000; Coyle, Prasad, and McGinnity 2005). The results show that the proposed method trails the earlier τ-based and CSP methods on the BCI Competition-III dataset IVa dataset while surpassing them significantly on the PhysioNet dataset. Interestingly, the univariate AR model-based method no better than random classification for the most parts.

In order to provide additional insights on these results, we identified the most frequently selected channel pairs during feature selection in scenario-2 that has a larger collection of training task periods. We then carried out unpaired two-tailed t-tests among the synchronization values between contending motor imagery task periods and obtained the P-values of these synchronizations for each subject. We corrected the P-values of the channel synchronizations via Benjamini-Hochberg's (B-H) method to minimize the type-I error rates observed during statistical testing (Benjamini and Hochberg 1995). Finally, we calculated the geometric means of the corrected P-values of the synchronization values for each channel pair across all subjects.

Table 16. Average correct classification rates obtained across 5 subjects for BCI Competition-3 dataset IVa and first 20 subjects for PhysioNet Motor Movement/Imagery datasets. S1 and S2 represents scenario-1 and scenario-2, respectively.

			Performances of Synch. Measures (%)					
			Cosine	**Wavelet-BiCoh**	**PLV**	**PCV**	**Linear MI**	**Corr.**
BCI Competition-III dataset IVa	**FLD**	**S1**	62.97 ± 8.84	62.12 ± 6.86	55.42 ± 4.04	61.48 ± 8.18	65.63 ± 9.8	65.85 ± 9.1
		S2	73.04 ± 8.97	63.69 ± 8.26	62.61 ± 5.62	66.95 ± 11.77	71.95 ± 11.04	73.91 ± 9.19
	Linear SVM	**S1**	65.95 ± 8.68	66.06 ± 7.32	60.0 ± 5.60	62.97 ± 6.23	67.02 ± 10.91	67.55 ± 7.67
		S2	76.52 ± 6.85	64.34 ± 7.66	66.3 ± 7.37	69.56 ± 10.92	76.52 ± 13.34	75.43 ± 12.82
	Nonlinear SVM	**S1**	65.53 ± 9.53	66.48 ± 5.92	60.85 ± 5.71	61.7 ± 6.05	67.97 ± 11.05	65.95 ± 9.74
		S2	73.69 ± 8.22	70.21 ± 9.11	63.26 ± 7.26	69.78 ± 9.19	75.0 ± 12.46	73.91 ± 8.48
PhysioNet Motor Movement/Imagery Dataset	**FLD**	**S1**	56.33 ± 10.19	52.83 ± 7.11	50.67 ± 5.14	52.83 ± 6.94	55.33 ± 11.2	55.34 ± 6.87
		S2	61.0 ± 10.65	58.0 ± 8.94	54.67 ± 13.43	53.67 ± 16.11	59.33 ± 13.66	58.0 ± 12.44
	Linear SVM	**S1**	62.0 ± 15.3	55.33 ± 10.33	52.67 ± 7.76	54.0 ± 6.45	58.33 ± 14.69	60.0 ± 14.18
		S2	63.67 ± 13.76	59.0 ± 10.87	54.33 ± 10.2	57.33 ± 8.75	63.67 ± 13.41	64.0 ± 15.04
	Nonlinear SVM	**S1**	63.5 ± 15.08	55.0 ± 10.05	53.33 ± 6.75	54.16 ± 6.74	60.33 ± 14.62	59.83 ± 14.72
		S2	65.33 ± 13.61	57.0 ± 11.74	54.67 ± 10.5	58.0 ± 10.16	60.67 ± 13.13	64.33 ± 14.87

Table 17. Average correct classification rates of best performing configurations of maximum average performances obtained from currently proposed $\Delta t, \tau, w$ method along with τ-based, CSP, and autoregressive methods.

		Performance Comparison of Different Approaches (%)							
		$\{\Delta t, \tau, w\}$-based Method (Linear MI for BCI Comp-III, cosine similarity for PhysioNet)		**τ-based Method** (B. Orkan Olcay and Karaçalı 2019) (With Kraskov's Mutual Information for both dataset)		**CSP** (Ramoser, Müller-Gerking, and Pfurtscheller 2000) (With log-variance features)		**Univariate AR Model** (With model order as 6)	
		S1	**S2**	**S1**	**S2**	**S1**	**S2**	**S1**	**S2**
BCI Competition-IIIdataset IVa	**FLD**	65.63 ± 9.8	71.95 ± 11.04	76.69 ± 12.88	75.76 ± 12.3	82.33 ± 11.46	84.67 ± 15.38	54.68 ± 6.16	56.73 ± 5.17
	Linear SVM	67.02 ± 10.91	76.52 ± 13.34	77.97 ± 10.35	81.89 ± 11.8	80.0 ± 11.45	83.91 ± 17.33	55.63 ± 5.47	60.86 ± 4.0
	Nonlinear SVM	67.97 ± 11.05	75.0 ± 12.46	75.0 ± 10.52	77.89 ± 10.26	82.12 ± 12.61	84.13 ± 18.23	54.14 ± 4.22	54.78 ± 1.97
PhysioNet Motor Movement/Imagery Dataset	**FLD**	56.33 ± 10.19	61.0 ± 10.65	58.33 ± 10.57	59.33 ± 15.12	53.83 ± 4.87	55.65 ± 9.97	52.0 ± 8.47	53.67 ± 14.74
	Linear SVM	62.0 ± 15.3	63.67 ± 13.76	58.50 ± 10.78	59.33 ± 14.96	57.66 ± 14.11	62.88 ± 15.91	51.83 ± 10.84	50.33 ± 13.58
	Nonlinear SVM	63.50 ± 15.08	65.33 ± 13.61	59.83 ± 9.33	59.67 ± 15.21	60.11 ± 14.0	64.0 ± 16.47	51.0 ± 12.47	48.0 ± 12.72

The most significant three channel pairs and their corrected P-values obtained for BCI Competition-III dataset IVa were CCP5-CP3 ($p < 0.001$), C3-CCP3 ($p < 0.001$) and C5-CCP5 ($p < 0.001$) for right foot motor imagery, F3-CFC3 ($p < 0.001$), FFC3-FC3 ($p < 0.001$), and FC1-C3 ($p < 0.001$) for right hand motor imagery tasks. The three channel pairs that reveals the most significant short-lived synchronization for the PhysioNet Motor Movement/Imagery dataset were FPz-FT7 ($p > 0.05$), FP2-FT7 ($p > 0.05$), and FP1-FT7 ($p > 0.05$) for left fist motor imagery, FPz-T10 ($p > 0.05$), FP2-F8 ($p > 0.05$), and FP2-T10 for right fist motor imagery tasks. All the P-values obtained from the PhysioNet dataset are well above the significance threshold ($p < 0.05$). We performed second evaluation on the PhysioNet dataset by discarding the subjects that elicited the performance below 64% in scenario-2 in accordance with (Müller-Putz et al. 2007; Athif and Ren 2019; Cheolsoo Park, Took, and Mandic 2014) revealed channel pairs with significant task-specific synchronizations: The three channel pairs that elicited the most significant synchronizations were FPz-FT7 ($p < 0.05$), FP2-FT7 ($p < 0.05$), and FP1-FT7 ($p < 0.05$) for left fist motor imagery, FP2-F8 ($p < 0.05$), FPz-F8 ($p < 0.05$), and FPz-T10 ($p < 0.05$) for right fist motor imagery tasks.

In order to elucidate the temporal dynamics of task-specific short-lived channel synchronizations, we plotted the average synchronizations patterns that emerge on the CCP5-CP3 channel pair for right foot and the F3-CFC3 pair for right hand motor imagery activity obtained at different $\{\Delta t, \tau\}$ combinations for the subject al of the BCI Competition-III dataset IVa during scenario-2. On the upper rows of Figure 22 and Figure 23, we presented the average synchronization values calculated using different $\{\Delta t, \tau\}$ parameters for the right foot and right hand motor imagery activities. On the lower rows, we presented the candidate synchronization patterns with a black pattern that exceeded the threshold value. The plots in these figures reveal that maximal synchronization is observed for this subjects CCP5-CP3 channels for $\tau = 0$ and Δt varying between 1540-1860ms, corresponding to a timing parameter triplet of $\{\Delta t, \tau, w\} = \{1540\text{ms}, 0\text{ms}, 620\text{ms}\}$. Similarly, the synchronization pattern observed for channels F3-CFC3 corresponded to the timing parameter triplet $\{\Delta t, \tau, w\} = \{580\text{ms}, 0\text{ms}, 1240\text{ms}\}$.

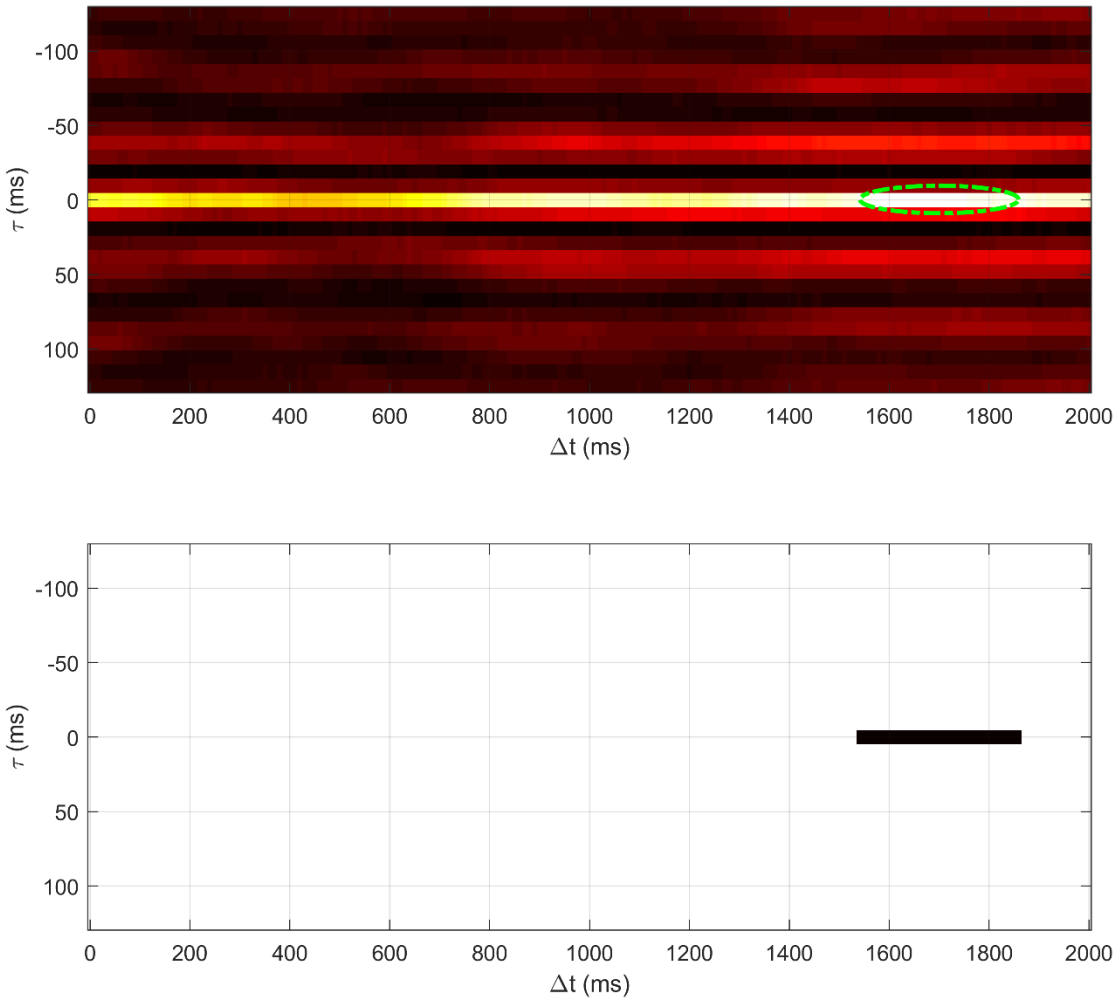

Figure 22. (upper) The illustration of the averaged synchronization values between CCP5-CP3 channels calculated for each $\{\Delta t, \tau\}$ combination for right foot motor imagery activity. The green ellipse represents the candidate maximal synchronization pattern. (lower) The illustration of the candidate maximal synchronization pattern after thresholding. We used linearized mutual information method to calculate the synchronization values of subject al who elicited the most successful recognition performance for BCI Competition-III dataset. The darker colors and the lighter colors in the upper figure representing low and high synchronization values, respectively.

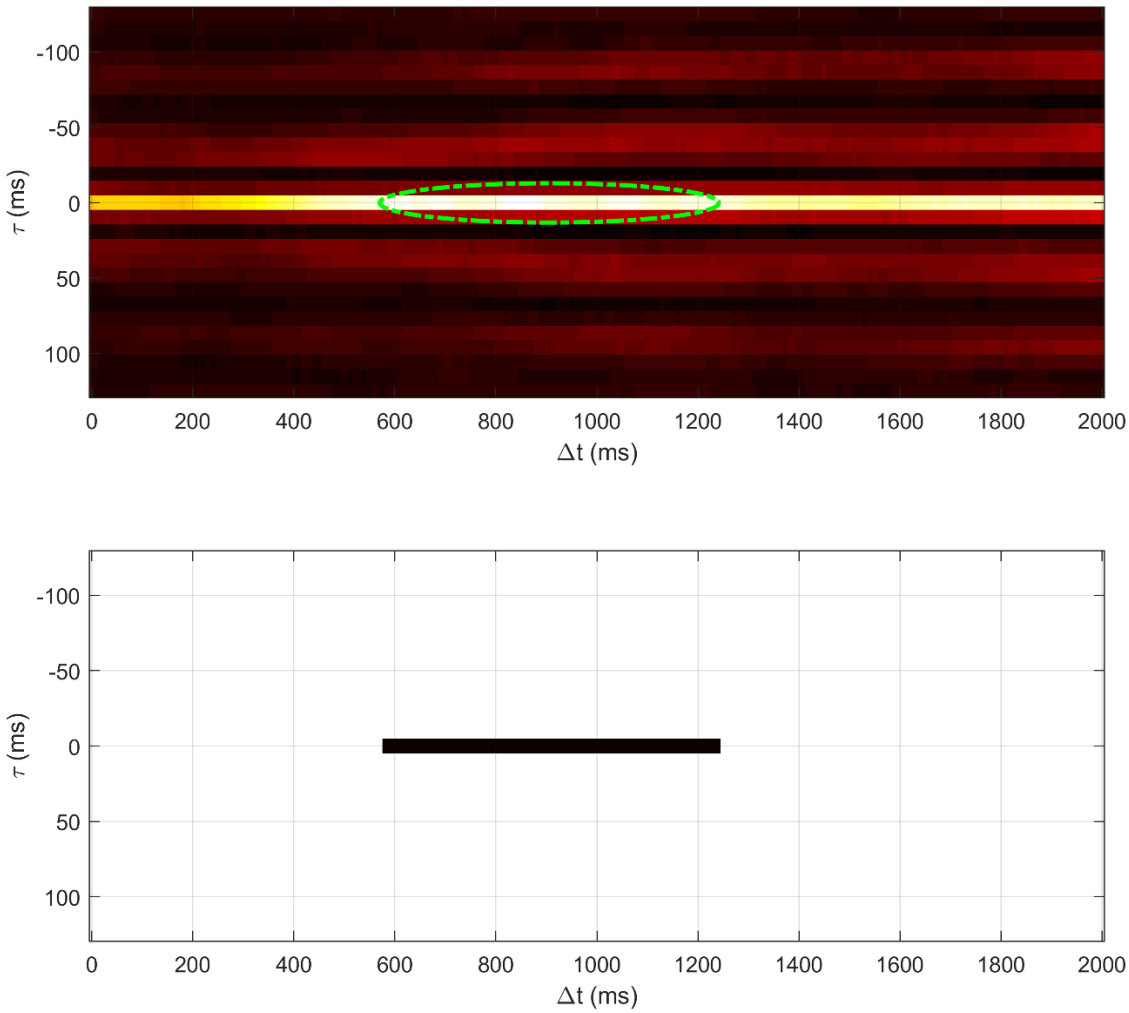

Figure 23. (upper) The illustration of the averaged synchronization values between F3-CFC3 channels calculated for each $\{\Delta t, \tau\}$ combination for right hand motor imagery activity. The green ellipse represents the candidate maximal synchronization patterns. (lower) The illustration of the candidate maximal synchronization patterns after thresholding. We used linearized mutual information method to calculate the synchronization values of subject al who elicited the most successful recognition performance for BCI Competition-III dataset. The darker colors and the lighter colors in the upper figure representing low and high synchronization values, respectively.

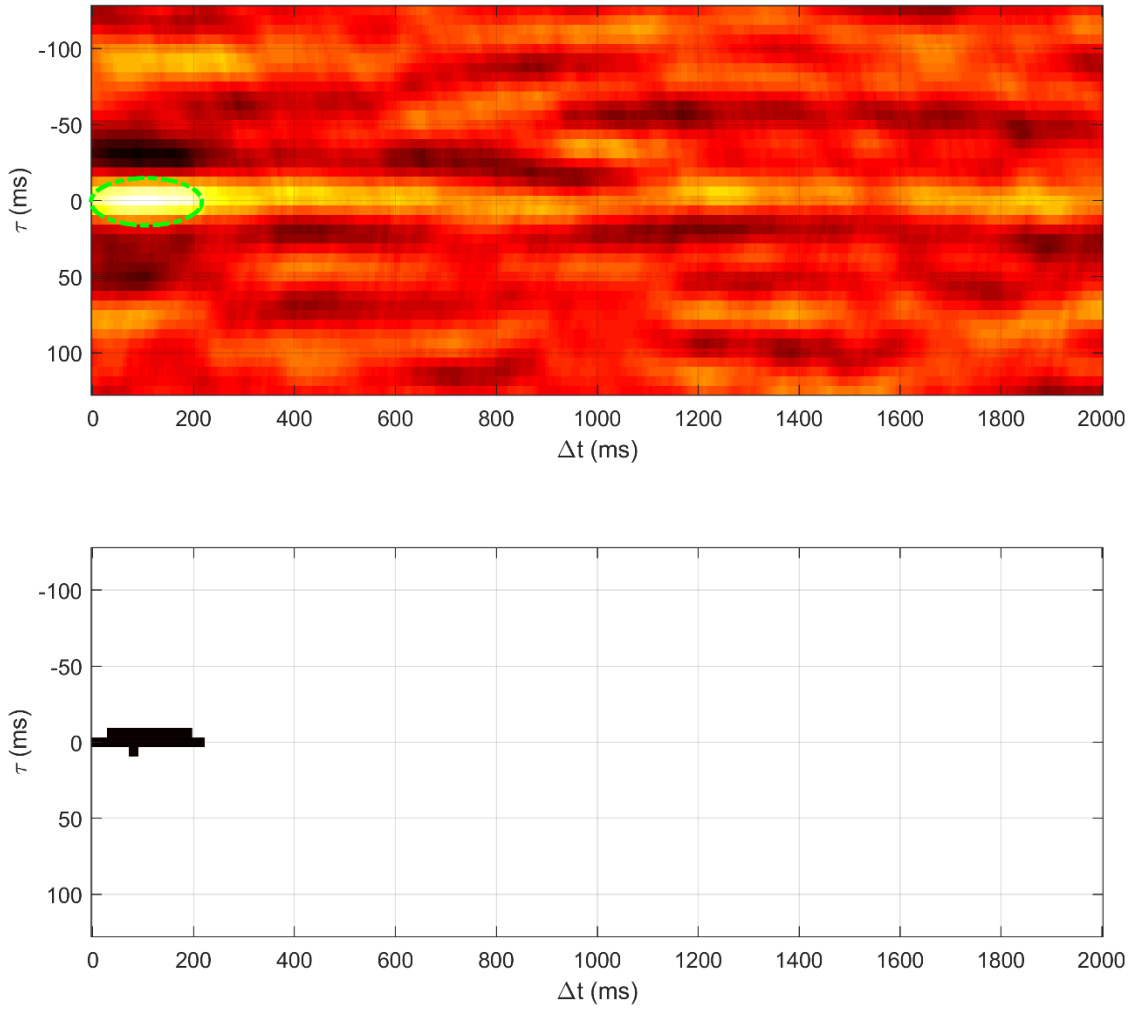

Figure 24. (upper) The illustration of the averaged synchronization values between FPz-FT7 channels calculated for each $\{\Delta t, \tau\}$ combination for left fist motor imagery activity. The green ellipse represents the candidate maximal synchronization patterns. (lower) The illustration of the candidate maximal synchronization patterns after thresholding. We used cosine similarity method to calculate the synchronization values of subject S004 who elicited the one of the most successful recognition performances for the PhysioNet Motor Movement/Imagery dataset. The darker colors and the lighter colors in the upper figure representing low and high synchronization values, respectively.

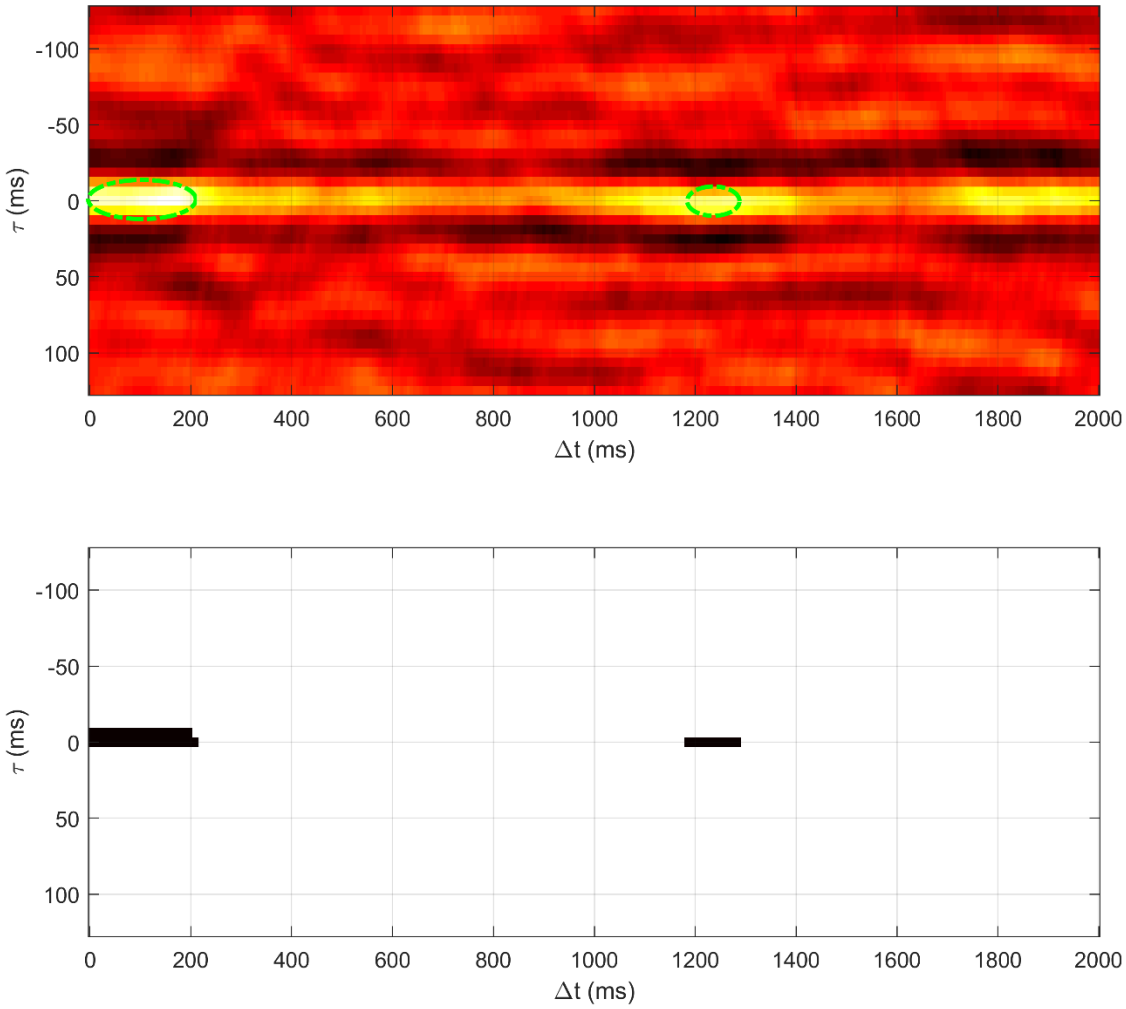

Figure 25. (upper) The illustration of the averaged synchronization values between FP2-F8 channels calculated for each $\{\Delta t, \tau\}$ combination for right fist motor imagery activity. The green ellipse represents the candidate maximal synchronization patterns. (lower) The illustration of the candidate maximal synchronization patterns after thresholding. We used cosine similarity method to calculate the synchronization values of subject S004 who elicited the one of the most successful recognition performances for the PhysioNet Motor Movement/Imagery dataset. The darker colors and the lighter colors in the upper figure representing low and high synchronization values, respectively.

Likewise, we demonstrated both average synchronization values as well as the candidate synchronization patterns between channel pairs Fp2-F8 and FPz-FT7 of the best performer PhysioNet subject (S004) for both right and left fist motor imagery activity in Figure 24 and in Figure 25, respectively. Note that compared to the averaged synchronization patterns observed for the BCI Competition-III dataset IVa (subject al), these patterns are much noisier and the distinction between maximal synchronization pattern and the rest is much less clear.

It is important note that the black lines observed for each different time lag are the candidate synchronization patterns obtained for different type of motor imagery tasks presented above. In Table 18 and Table 19, we presented the activity-specific timings for the most significant channel pairs identified for different motor imagery tasks for both BCI Competition-III dataset IVa and PhysioNet Motor Movement/Imagery dataset, respectively. Note that we presented the timings of all of the five subjects in former dataset; however, and we presented the timings of the subjects which exceeds 64% recognition performance in the latter.

Table 18. The activity-specific timing parameter triplets obtained during scenario-2 using linearized mutual information metric for CCP5-CP3 channel pair for right foot and F3-CFC3 for right hand motor imagery activity (BCI Competition-III dataset IVa).

Subject ID	**Right Foot Imagery Activity-Specific Timing Parameter** (CCP5-CP3)			**Right Hand Imagery Activity-Specific Timing Parameter** (F3-CFC3)			**Performance** (at scenario-2)
	Δt (ms)	**τ (ms)**	**w (ms)**	**Δt (ms)**	**τ (ms)**	**w (ms)**	
aa	1590	0	520	220	0	580	67.39%
al	1540	0	620	580	0	960	91.30%
av	800	0	560	360	0	550	60.86%
aw	1280	0	450	1730	0	570	73.91%
ay	770	0	360	1460	0	820	89.13%

Table 19. The activity-specific timing parameter triplets obtained during scenario-2 using linearized mutual information for FPz-FT7 channel pair for left fist motor imagery activity and for FP2-F8 for right fist motor imagery activity (PhysioNet Motor Movement/Imagery dataset). We used the most successful eight subjects that elicited more than 64% performance (Müller-Putz et al. 2007).

Subject ID	**Left Fist Imagery Activity-Specific Timing Parameter** (FPz-FT7)			**Right Fist Imagery Activity-Specific Timing Parameter** (FP2-F8)			**Performance** (at scenario-2)
	Δt **(ms)**	τ **(ms)**	w **(ms)**	Δt **(ms)**	τ **(ms)**	w **(ms)**	
S001	0	0	563	0	0	518.8	73.33%
S002	1912	0	387.5	31.3	0	493.8	80%
S004	31	6.25	462.5	0	-6.25	500	86.67%
S006	231	0	575	0	0	818.8	73.33%
S007	0	0	493.8	0	0	650	73.33%
S015	118.8	0	487.5	12.5	0	662.5	86.87%
S018	0	0	512.5	0	-6.25	443.8	80%
S020	225	-6.25	462.5	12.5	-6.25	431.3	73.33%

4.4. Discussion

Our main motivation for proposing this method is based on the premise that the brain regions transiently interact with each other during periods of cognitive activity (Fries 2005; Andre M. Bastos, Vezoli, and Fries 2015). These reciprocal interactions may carry critical neural information which is vital for the generation of task-specific neural patterns within the brain. In our previous study, we calculated only the synchronization lags (τ) between the channel pairs which was found to be useful for characterizing the cognitive activity (B. Orkan Olcay and Karaçalı 2019). However, according to Bastos et al. and Fries et al., the activity-specific inter-regional interactions emerge and vanish in relatively short time intervals within the task periods. In order to track this behavior, in this study, we extended our earlier approach with the addition of two new timing parameters (i.e., the latency of maximal synchronization between channel pairs from activity onset (Δt), and duration of maximal synchronization among channel pairs (w)) to characterize the cognitive activities.

Since we do not know which synchronization measure would capture the actual neural synchronization patterns that emerge within the brain better, we tried six different synchronization measures and evaluated their performance in a motor imagery activity recognition framework. The reason for using these synchronization measures is that they elicited a better characterization performance in the past literature and that they had favorable computational properties. In the literature, there are many additional synchronization methods that have been used in various types of brain activity characterization studies. We believe that the six measures we have evaluated in our study covers the range of prominent and effective similarity measures well.

Lastly, the majority of brain activity characterization studies in the literature use the entire task periods to calculate connectivity-based features. As depicted above, there is evidence in the literature that the task-related information is embedded within the signal pairs only for a limited duration. These finite-length signal pairs can thus be used to calculate several features such as common spatial patterns (CSP), power-based features, time domain features … etc. to further improve task recognition performances.

In the light of these motivations, our method presented in this chapter determines and uses the activity-specific timing parameter triplets of the characteristic short-lived synchronization for each channel pair and each type of cognitive activity. In order to

determine the activity-specific timing parameter triplets for each channel pair and each type of cognitive activity, we adopted a heuristic search method that uses a 300ms-length sliding time window to calculate average the channel synchronizations across all task periods for different $\{\Delta t, \tau\}$ parameter combinations. As a note, the timing parameter search that we adopted in this chapter increases the computation time in a quadratic manner in comparison with the previous chapter. We then evaluated the usefulness of the channel synchronizations calculated at activity-specific timing parameter triplets in a motor imagery task recognition setting by using them as features as well as via statistical comparisons of the channel synchronizations between the different cognitive tasks. Prior to the classification, we selected the most discriminative synchronization features for a better classification. We observed that, for both dataset, both adjacent and non-adjacent channel pairs remained after the feature selection which is in line with the fact that many different brain regions are involved to integrate information during cognitive tasks (Telesford et al. 2011; Mišić and Sporns 2016; Uhlhaas et al. 2009). The recognition performances as well as the statistical test results reveal several insights on connectivity based brain activity characterization as discussed below.

4.4.1. Performance Evaluation and Comparison

The average recognition performances obtained for six different synchronization metrics for both BCI Competition-III dataset IVa (right-foot / right-hand imagery) and PhysioNet Motor Movement/Imagery (right-fist / left-fist imagery) in Table 16 show that the linear mutual information and cosine-based similarity methods demonstrated the top-ranking average performances for BCI Competition-III dataset IVa and PhysioNet datasets, respectively. This outcome indicates that these two synchronization metrics capture the timings of the characteristic synchronizations of the channel pairs more accurately than the other methods used in this chapter.

In comparative performance evaluation, the CSP-based method ranked supreme on the BCI Competition-III dataset IVa as expected since a CSP-based approach was the winner of the competition. On the PhysioNet dataset, the proposed method surpasses CSP recognition performance which suggests that the CSP method may be overfitted to the BCI Competition data and may not necessarily do as well in other instances. In a detailed

manner, the CSP method exhibits satisfactory recognition performances when there is a conspicuous dichotomy between the spatio-spectral patterns (i.e., band powers of spatially localized activities) for contending cognitive activities. Unfortunately, the differences in the band powers are not clearly observed for the most cases of motor imagery-based BCI experiments. In such circumstances, the CSP method unable to show its discrimination ability. In comparison, the performance of the proposed method was more stable on both datasets. The univariate AR model based method, on the other hand, did not perform well despite its popularity in the literature.

Note that the most likely reason for performances lower than 70% on the PhysioNet dataset may be the small number of task periods considering that even 30 task periods for training in scenario-2 may not be sufficient to extract reliable discriminative content. In the specific case of CSP these results suggest that the method could not find appropriate spatial filters to discriminate between different cognitive activities due to inaccurate estimates of spatial covariance matrices. Another possible reason for low performances on the PhysioNet dataset may be a low signal-to-noise ratio. In the literature, the studies that employs the PhysioNet dataset, in general, use noise/artifact removal methods to filter out the non-neural signals (Varsehi and Firoozabadi 2021). In such a case, it may be helpful to use various denoising techniques in the preprocessing step to identify and hopefully remove the noise component from the EEG signals (Hyvärinen and Oja 2000; Von Bünau et al. 2009; Jolliffe 1986). Despite these problems, it is noteworthy that the proposed method achieved the best performance among the four competing approaches on the PhysioNet dataset, indicating robustness against various pitfalls associated with changes in EEG procedures, equipment, or signal recording quality. Note also that, in the literature, the majority of the motor imagery activity recognition studies on the PhysioNet dataset report the performance results of only the well-performing subjects with recognition performances over 64% (Handiru and Prasad 2016; Cheolsoo Park, Took, and Mandic 2014; Tolić and Jović 2013; Kim et al. 2016; Athif and Ren 2019). Note that, in this study, we showed the average performances of the first 20 subjects without any performance related elimination criteria to clarify the pros and cons of the proposed method along with the alternative techniques.

The reason for the slightly lower performances obtained from the BCI Competition-III ($f_s = 100$ Hz) dataset may probably be the result of an insufficient number of signal samples since we used only 30 samples (i.e., 300ms) for short-lived synchronization calculation. During calculation, using low number of samples lead to an

underestimation of synchronization (Fraschini et al. 2016; Sideridis et al. 2014). As an evidence, for the PhysioNet Motor Movement/Imagery dataset ($f_s = 160$ Hz), our $\{\Delta t, \tau, w\}$-based method achieved a better recognition performance than the other three methods. This result suggests that using an EEG recording system with a greater sampling frequency increases the resolution of the timing parameters to be captured for each channel pair and each activity type and also, inherently increases the number of samples in the 300ms-length time window which avoids underestimation of short-lived synchronization quite likely.

In this comparison, the autoregressive modelling achieved the worst performance among the four methods used here. In the literature, several brain activity characterization studies underwent performance comparison with AR modelling-based method. As an example, Ince et al. compared the performance of their proposed method with AR modelling on the BCI Competition-III dataset IVa (Ince et al. 2009). During performance comparison, they adopted the procedure in (Song and Epps 2007). The performance results show that the AR modelling based method achieved a success rate of nearly ~%80. The main reason for the performance differences obtained during performance comparison via AR modeling method is that they adopted using separate frequency bands and different signal length for features extraction as in (Dornhege et al. 2004).

4.4.2. Effect of Number of Training Task Periods

It is apparent in Table 16 that as the number of training task period increases (in scenario-2), the performance of the proposed method increases considerably for most of the synchronization measures. This indicates that increasing the number of training task periods provides accurate capturing of the timing parameters of characteristic short-lived patterns. In the past BCI literature, a considerable amount of effort has been spent to overcome the problem caused by an insufficient number of training task periods (Jiao et al. 2019; Azab et al. 2019; H. Kang, Nam, and Choi 2009). The outcomes of the past literature suggest that the motor imagery related neural activity characterization methods requires a considerable number of training task periods to achieve a reliable performance.

4.4.3. Biophysical Relevance of the Significant Channels Pairs

We provided the top three significant channel pairs as well as their geometric means of corrected *P*-values of timings of the activity-specific channel synchronizations obtained from training task periods of the BCI Competition-III dataset IVa and the PhysioNet Motor Movement/Imagery dataset in scenario-2. The most significant channel pairs identified for right foot motor imagery activity task mainly include the left central and left centro-parietal electrode pairs. As for right hand motor imagery activity, the most significant channel pairs include left frontal, left fronto-central and left central electrodes/electrode pairs. The analysis results suggests that, for right hand/foot imagery activities, the majority of the electrodes that constitute the significant pairs across all 5 subjects are mainly located on the left hemisphere, which is consistent with the existing literature (Chung, Kim, and Kim 2011; Gonuguntla, Wang, and Veluvolu 2016; Chung, Kang, and Kim 2012). It is important to note that the determined channel pairs are located in contralateral region of performed imagery movement which is also consistent with the past literature (G. Pfurtscheller and Berghold 1989; Gert Pfurtscheller and Neuper 1997).

The frontal electrodes obtained for BCI Competition-III dataset IVa during hand motor imagery activity collect electrophysiological activity mainly from prefrontal regions such as supplementary motor area (SMA), precentral motor area (PMA), inferior frontal gyrus (IFG), medial precentral gyrus (hand representation area), middle frontal gyrus (MFG) which are known to be higher order information processing and coordination (Hétu et al. 2013; Ehrsson, Geyer, and Naito 2003; Chung, Kang, and Kim 2012; Lotze et al. 1999), and motor planning and preparation centers of the hand movement imagination (Chang hyun Park et al. 2015; Hanakawa 2016; Halder et al. 2011; Lotze et al. 1999). Among these regions, PMA is declared as to be the most critical region on performance of hand and foot motor imagery as well as motor execution in motor imagery training studies (H. Zhang et al. 2011; Pilgramm et al. 2016). The activity levels of the aforementioned regions was shown to be strongly correlated with SMR-related BCI performance (Halder et al. 2011).

The central electrodes mainly collect electrophysiological activity from the primary motor (M1) and sensorimotor (S1) regions (Dechent, Merboldt, and Frahm 2004) that are generally believed to be activated during hand motor imagery task periods (Lotze

et al. 1999; Xu et al. 2014; Carrillo-de-la-Peña, Galdo-Álvarez, and Lastra-Barreira 2008; Q. Gao, Duan, and Chen 2011).

The parietal regions obtained during both hand and foot motor imagery tasks including the inferior parietal lobule (IPL), superior parietal lobule (SPL), precuneus, and postcentral gyrus also play important roles such as sensory integration hub, online movement/imagination control, motor attention (especially in motor planning), and motor imagery activity production (Xu et al. 2014; Hétu et al. 2013; H. Zhang et al. 2011; Pilgramm et al. 2016). Among these regions, the postcentral gyrus and precuneus regions play a central role in episodic memory retrieval which is thought to be critical especially in visual motor imagery modality (H. Zhang et al. 2011), and the activity levels of IPL and SPL are known to vary according to the specific type of hand actions (Pilgramm et al. 2016).

As for the PhysioNet dataset, we presented the frequently observed significant channel pairs and their geometric means of *P*-values for the first 20 subjects for left fist motor imagery activity are generally the left frontal, left fronto-temporal and left temporal electrodes. Similarly, the frequently observed significant channel pairs for the first 20 subjects during right fist imagery activities include right and left frontal and right frontal as well as temporal electrodes, respectively. Although these biophysical as well as statistical findings mainly falls at odds with the current biophysical literature on the right/left hand motor imagery activity that points to the significance of the contralateral connectivity patterns during motor imagery tasks, there are several important biophysical studies that found ipsilateral activations/synchronization profiles as significant (Q. Gao, Duan, and Chen 2011; Kraeutner et al. 2014; Brunner et al. 2006; Alanis-Espinosa and Gutiérrez 2020) especially for the novice participants (Milton et al. 2007).

These ipsilateral synchronization patterns that observed both in our study and some of the past literature might be due to several reasons. The first reason may be due to the excessive information flow from parietal to frontal regions. Menicucci et al. realized that a significant amount of information flow occurs towards the frontal areas to compensate for the imagination inability during kinesthetic motor imagery task (Menicucci et al. 2020). These information overflow may produce several unexpected short-lived synchronization patterns within the frontal/fronto-temporal electrodes. Similarly, another reason of observing frontal synchronization patterns is the increased activity of dorsolateral prefrontal cortex, which is a key brain region of central executive network, during cognitively demanding tasks (C. F. Lu et al. 2011). As another viewpoint,

the reason for the emergence of synchronization/activation of rarely or never observed channel pairs may be due to an inability to plan or execute motor imagery properly or failure to perform kinesthetic/visual motor imagery (Bauer et al. 2015; Gu et al. 2020). Another reason may be the insufficient number of training task periods available used in statistical analysis: in the PhysioNet dataset, there are only 45 motor imagery activity task periods for each subject. With a greater number of motor imagery task periods, more reliable and consistent as well as biophysically relevant channel pairs may be expected to emerge. Furthermore, as also suggested by Xie et al., subject-specific but task un-specific synchronization modulations may be present and associated with the emergence of unanticipated channel pairs (Xie et al. 2018). Similarly, Demuru et al. speculated that the aperiodic parts of EEG signal contains subject-specific activation/synchronization patterns (Demuru and Fraschini 2020). It is possible that task-specific synchronization modulations as well as the task relevant channel pairs can be obtained by filtering the subject-specific modulations (Allen et al. 2014).

Besides the biophysical factors, there are some important subjective factors for this ambiguity. The results obtained from PhysioNet dataset may be affected from the inherent condition of the human brain. The participants' "mind sets" cannot be expected to be fully isolated from internal (e.g., concentration, focusing momentarily on other issues, some accompanying thoughts, etc.) or external (any minor external trigger etc.) factors, which may then cause the electrophysiological organization of the brain to fluctuate substantially between successive task periods. Alternatively, change of the imagination strategy such as from kinesthetic imagery to visual imagery or vice versa by the participants during the experiment may significantly alter the information processing scheme and thus inter-regional synchronization timings of the brain which may cause performance deterioration as illustrated in (Christa Neuper et al. 2005).

4.4.4. Effect of Time Lag on the Characterization Performance

We presented the average synchronization, and the candidate synchronization patterns in Figures 22-25. Interestingly, these figures and also the timings parameters (see Table 18 for BCI Competition-III dataset IVa and Table **19** for PhysioNet results) show that the short-lived synchronization patterns are emerged and vanished at different

timings but more importantly, the time lag between the corresponding signals segments is near or exactly equal to zero. This suggests that the brain systematically organizes the synchronization between the primarily task-related regions at zero-lag for effective as well as efficient information transfer during a cognitive task. Similar outcomes were observed in (Roelfsema et al. 1997) that the brain itself dynamically adjusts the synchronization lag between its visual-specific regions to zero during visual stimulus presentation to integrate the neural information into coherent representational states. The zero-lagged synchronization between task-related regions may constitute evidence of the information relaying mechanism that organizes the synchrony dynamically to transfer the neural information among the cortical and subcortical structures reliably via thalamocortical and/or hippocampal circuits. This mechanism overcomes the delay interference induced by information transfer between distant structures of the brain (Vicente et al. 2008).

The channel pairs that we identified as the most significant for BCI Competition-III dataset IVa (CCP5-CP3 for right foot activity, and F3-CFC3 for right hand activity), and for PhysioNet Motor Movement/Imagery dataset (FPz-F7 for left fist activity, and FP2-F8 for right fist activity) are relatively close to each other as demonstrated in Figure 26.

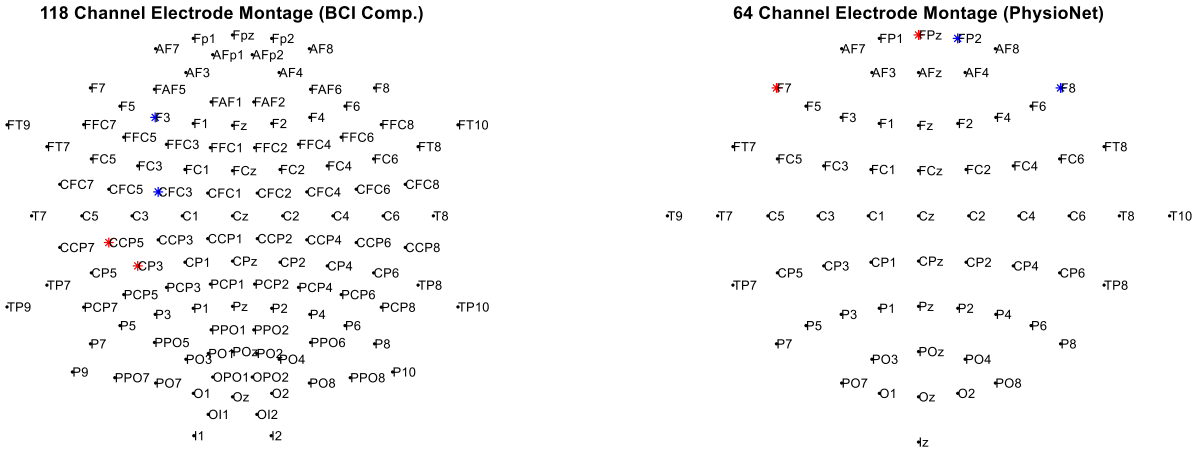

Figure 26. Illustration of the electrode montages of both PhysioNet and BCI Competition-III dataset IVa. The electrodes that marked with red star was found as significant channel for one cognitive activity, and the electrodes marked with blue star was found as significant for another cognitive activity.

Since the aforementioned electrodes are placed relatively close to each other, they tend to collect the electrophysiological activities from overlapping cortical structures. In this circumstance, the most probable reason why the time lag between these channel pairs is near or equal to zero for each subject is the volume conduction problem which hampers the actual time lag between these channel pairs (André M. Bastos and Schoffelen 2016; Tognoli and Kelso 2009). To minimize the effects of volume conduction, we used the common average referencing (CAR) method before the short-lived synchronization calculation (McFarland et al. 1997; Tsuchimoto et al. 2021). However, as Cohen stated, there is no perfect method that completely eliminates the effects of volume conduction (M. X. Cohen 2015). In order to achieve a slightly better characterization performance, more advanced spatial filtering techniques are required albeit with a greater computational cost (Rathee et al. 2017).

Although the volume conduction appeared as the primary reason, we actually do not know the exact timings ($\Delta t, \tau$, and w) of the activity-specific synchronization for each channel pair. In our results, we observed zero-lagged short-lived synchronization for the most significant channel pair which is not necessarily completely due to volume conduction phenomena. For instance, Witham et al. observed in the monkeys that the movement-related cortical synchronization between relatively close areas emerges at zero time lag (Witham, Wang, and Baker 2007).

It is important to highlight that, not all channel pairs synchronize at zero time lag. The channel pairs presented in Tables 18 and 19 in this study, were the most statistically significant in terms of their short-lived interactions (as the result of t-tests), and also, these channels are the one of most frequently selected channel pairs as features (according to the Fisher ratio) for each activity type. In addition to these channel pairs, there are also other channel pairs that elicit significant synchronization with an inter-channel time lag different from zero.

We performed an extra analysis and observed that not only adjacent but also non-adjacent channels may elicit zero-lag synchronization. We used several channel pairs that were used in previous motor imagery activity recognition studies. We determined the activity-specific timings of these channel pairs for each different cognitive activity, and we calculated the channel synchronizations to use in a motor activity recognition framework. In a previous synchronization-based motor imagery activity characterization study, both adjacent and non-adjacent channel pairs were used (Q. Wei et al. 2007). In that study, the channels Fz and its neighbors (Cluster-1), C3 and its neighbors (Cluster-

2), and C4 and its neighbors (Cluster-3) achieved the best recognition accuracy. These electrodes are known to collect the electrophysiological activity from left and right primary motor, sensorimotor, premotor and prefrontal cortices which are actively engaged in motor imagery tasks (Decety 1996; Chung, Kang, and Kim 2012; Munzert, Lorey, and Zentgraf 2009b). We paired the channels (i.e., Cluster-1 ↔ Cluster-2, Cluster-1 ↔ Cluster-3, and Cluster-2 ↔ Cluster-3) contained in different clusters without considering the intra-cluster channel pairs, providing a total of 85 non-adjacent channel pairs (please see Table 20 for the channels). Please note that since the EEG recording system that was used to collect BCI Competition-III dataset IVa did not contain the AFz electrode, we included both AF3 and AF4 electrodes instead of AFz.

Table 20. The electrode clusters of BCI Competition-III dataset IVa and PhysioNet dataset according to CB2 subset. This clusters contain C3, C4, and Fz channels and their nearest neighbors.

Cluster-1	**Cluster-2**	**Cluster-3**
Fz	C3	C4
AF3	FC3	FC4
AF4	CP3	CP4
F1	C5	C6
F2	C1	C2
FCz	-	-

We showed the time lags of the channel synchronizations for each of the 85 pairs during right hand motor imagery activity in Figure 27. Note also that, for synchronization calculation, we used linear MI which appeared as the most successful measure for BCI Competition-III dataset IVa on the average. The "*" symbol above or below the time lag bars indicates that the timing parameter triplet elicited statistically significant synchronization for that channel pair for right hand motor imagery activity.

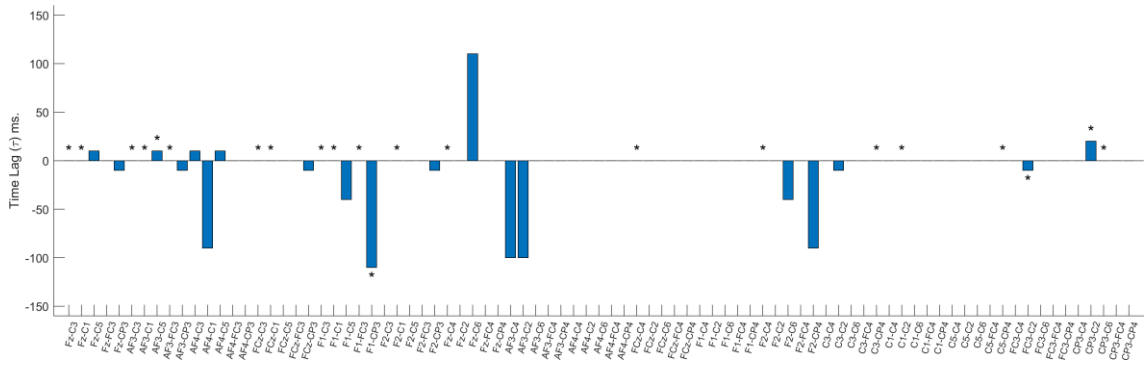

Figure 27. The illustration of time lag parameters for short-lived synchronization of non-adjacent channels for right hand motor imagery activity for subject al (for linear MI). Note that the '*' symbol above or below the lag representation bar plots denotes that the synchronization of corresponding channel pair is statistically significant ($P < 0.05$).

We repeated the time lag estimation for the correntropy method for the subject *al* for which we observed the highest performance (93.47%). We showed the correntropy results in Figure 28 below.

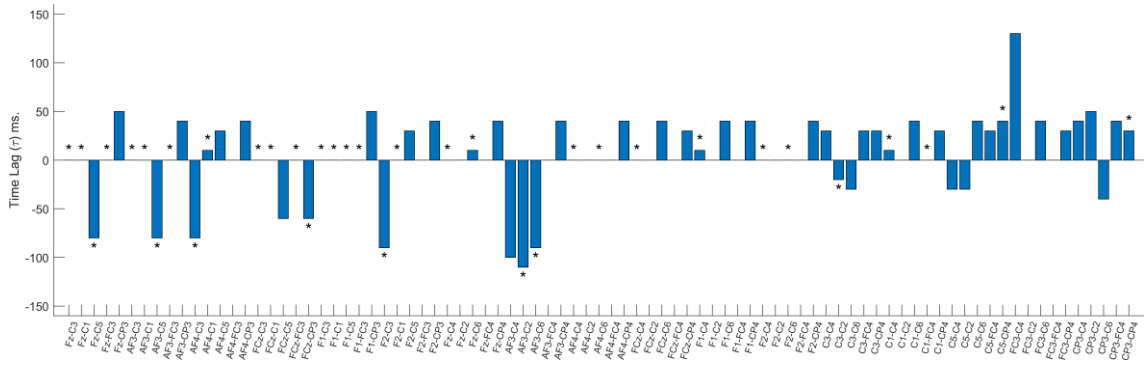

Figure 28. The illustration of time lag parameters for short-lived synchronization of non-adjacent channels for right hand motor imagery activity for subject al (for correntropy). Note that the '*' symbol above or below the lag representation bar plots denotes that the synchronization of corresponding channel pair is statistically significant ($P < 0.05$).

In these figures, it is clear that not only the adjacent channel pairs synchronized at zero lag but also several non-adjacent channel pairs significantly synchronized at zero-lag along with several other pairs for which activity-specific synchronization occurred at non-zero time lags.

In addition to the above analysis, we obtained 1452 pairwise short-lived synchronizations as significant. Among these synchronizations 391 of them demonstrated non-zero time lag for linear mutual information method. Furthermore, for the correntropy method, out of the 1757 significant pairwise synchronizations, 1017 of them demonstrated non-zero time lag. These results points that the main source of lag between the EEG signals as identified by the synchronization measure of choice is the delay between electrophysiological signals generated by the brain during cognitive tasks according to a timing organization (Hari and Parkkonen 2015).

This shows that the brain adjusts the timings of the synchronizations according to the task demands in the associated regions with communication-through-coherence hypothesis. This hypothesis suggests that the brain generates temporal communication windows by maximizing the temporal synchronization among its regions for task-specific neural information transfer (Andre M. Bastos, Vezoli, and Fries 2015; Fries 2005). These inter-areal communication windows integrate the processed segregated information. We observed that the timings of the short-lived maximal synchronization elicited significantly different synchronizations for different types of motor imagery activities. The differences of the timing parameters triplets are thought to be the result of different neural mechanisms taking place for different activities. In (Z. Gao et al. 2019), it was demonstrated that neural synchronizations calculated at normal conditions show a significant difference when calculated in a fatigue mood. This shows that neuronal conditions exhibit significant alteration between different brain states, and this alteration affects the neural synchronization dynamics. In a similar vein, Salyers et al. showed that different task conditions requires different network coordination (Salyers, Dong, and Gai 2019).

Another possible mechanism, which characterizes the organization of the zero lagged synchrony between cortical circuits, is the spike-timing dependent plasticity (STDP). Basically, the STDP interplay the synchronization regimes between the sender-receiver brain regions (i.e. delayed synchronization (DS) and anticipated synchronization (AS)) to organize the information transfer lag (i.e., synchronization lag) by altering the

activation degree of inhibitory neural structures placed within the information-receiving-end regions (Matias et al. 2015).

Besides the above descriptions pointing the significance of zero-lagged brain synchronizations among primarily task-related regions, we previously provided that there exist a systematic time lag organization between the brain regions which means that not all pairs of brain regions simultaneously synchronized at zero lag (B. Orkan Olcay and Karaçalı 2019). To stress the necessity of considering a time-lag analysis, we urgently conducted another classification analysis using the same datasets. In this analysis, we neglected the time lag (i.e., τ) between the EEG channels and assumed that the maximal channel synchrony always occurs simultaneously (i.e., at $\tau = 0$) and at specific latency (Δt) and time window (w) for each channel pair and each type of motor imagery activity. The performance results presented in Table 21 shows that the recognition performances obtained using $\{\Delta t, \tau, w\}$-based method is greater than the performances obtained by considering zero time lag (i.e., considering only $\{\Delta t, w\}$). These results suggest that not all of the brain regions synchronized at zero-lag during cognitive tasks. This outcome stresses the importance of the considering time-lagged synchronization between the brain regions during characterization.

Another interesting thing that was observed in Figures 22 and 23 is that, apart from the time-lag that the maximal short-lived synchronization emerged, there are short-lived synchronization patterns that emerged at different time-lags which are observed as periodic red colors at different time lags. These red-colored synchronization patterns emerged at different time lags throughout the motor imagery tasks may indicate an inter-areal communication patterns in both feedforward and feedback directions which may also supports the hypothesis of the communication through coherence with inter-areal time lags (Andre M. Bastos, Vezoli, and Fries 2015). Further analysis should be conducted to uncover the exact mechanism of these inter-areal communication patterns.

Table 21. The recognition performances obtained when inter-channel time lags are/are not considered.

		Average Recognition Performances (%)					
		FLD		**Linear SVM**		**Nonlinear SVM**	
		S1	**S2**	**S1**	**S2**	**S1**	**S2**
PhysioNet (cosine)	$\{\Delta t, \tau, w\}$	56.33 ± 10.19	61.0 ± 10.65	62.0 ± 15.33	63.67 ± 13.76	63.5 ± 15.08	65.33 ± 15.08
	$\{\Delta t, w\}$	58.5 ± 12.54	58.67 ± 13.08	61.16 ± 13.07	60.0 ± 14.98	61.83 ± 13.44	65.67 ± 14.55
BCI Comp.-III (Linear MI)	$\{\Delta t, \tau, w\}$	65.63 ± 9.8	71.95 ± 11.04	67.02 ± 10.91	76.52 ± 13.34	67.97 ± 11.05	75.0 ± 12.46
	$\{\Delta t, w\}$	65.0 ± 9.38	71.08 ± 11.74	67.12 ± 9.0	74.78 ± 12.01	65.95 ± 10.71	74.13 ± 11.59

4.4.5. Biophysical Evidences for Considering Latency (Δt) and Duration (w) Parameters

The electrophysiological signals acquired from controlled biophysical experiments show that the brain activation/synchronization patterns from any external (or internal) stimulation would continue for hundreds of milliseconds (Güdücü et al. 2019; Bilal Orkan Olcay et al. 2017; Schack, Weiss, and Rappelsberger 2003). For instance, it was shown during dichotic auditory stimulations that intra-hemispheric reciprocal auditory processing occurs first, followed by inter-hemispheric communication across the corpus callosum, and finally by the posterior-frontal communication to evaluate the complex nature of the stimulus (Bayazit et al. 2009). Similar results were obtained in the literature that the visual input is processed reciprocally between different brain regions which produces a complex short-lived synchronization patterns on the alpha band. The temporal complexity of the inter-areal synchronization may point the importance of adaptive organization of neural information processing (Bola, Gall, and Sabel 2015).

Similarly, comparison of motor imagery and motor execution tasks shows that different temporal brain dynamics arise for each type of task (Solomon et al. 2019). In a similar manner, a single pulse TMS-EEG (transcranial magnetic stimulation) study reveals that during the finger movement, inferior frontal cortex establishes causal synchronization first with fronto-parietal regions and then with the default mode network (Zanon, Borgomaneri, and Avenanti 2018). This shows, among other things, that the bottom-up stimulus/cognitive task processing is embraced with top-down higher-level content assessment. But more importantly, it signifies that the reactions of different and distant brain regions to stimulus/cognitive task manifest according to a temporal order (Dawson 2004). The temporal order of short-lived synchronization between brain regions may be a signature of the transitory behavior of the changes of synchronization between brain areas which sub-serve an efficient short-lasting brain coordination (S. I. Dimitriadis, Laskaris, and Tzelepi 2013). These discussions point the importance of considering latency (Δt) as well as duration (w) parameters during the analysis of characteristic brain synchronization.

As an important point, it was presented in Tables 18 and 19, the latency (Δt) and duration (w) parameters vary considerably across the subjects. According to the information provided by the two datasets that we used in our study; these subjects performed only motor imagery tasks associated with the command provided by the experimenter (Goldberger et al. 2000; Dornhege et al. 2004).

The variation of these parameters is thought to be due to the different mental strategies adopted by the subjects during these tasks (Friedrich, Scherer, and Neuper 2012; Kilintari et al. 2016). Differences in mental strategies among the subjects can be observed in the timing parameter triplets identified for each mental task and channel pair. Please note that the latency (Δt) and duration (w) parameters are thought to be indicators of temporal processing of the task-related information in the brain. The timing parameters (Δt, τ, and w) are systematically adjusted according to the mental strategies that the subjects adopt.

It is important to note that the subject's condition may also have a significant impact on these parameters in addition to the task requirements. Especially the latency Δt parameter is inevitably affected by several important factors such as the subject's command perception time, and initialization time to motor imagination, which may cause random variations from trial to trial during motor imagery tasks.

Our reasoning in seeking the optimal timing parameters using the average synchronization values is based on the premise that since perception and task initiation are subjective parameters and vary randomly according to the aforementioned reasons, averaging of synchronization values ought to minimize these task-unspecific (i.e., subject-specific) variations and allow capturing the task-specific timing parameters. The performance results, which we presented in the manuscript, show that, especially in scenario-2 that uses a greater number of training task periods, we elicited a better recognition performance than obtained in scenario-1.

4.4.6. Using Different Synchronization Measures

We tried six different synchronization measures to evaluate which synchronization measure captures the timings of the most informative short-lived synchronization. We used cosine based similarity (Sargolzaei et al. 2015; B. Orkan Olcay and Karaçalı 2019; Herff et al. 2019), phase locking value (Lachaux et al. 1999; Varela et al. 2001), phase coherence value (Tass et al. 1998; Bakhshayesh et al. 2019b), wavelet bi-coherence (Makarov et al. 2018; Alexander E. Hramov et al. 2015), linearized mutual information (S. H. Jin, Lin, and Hallett 2010; Montalto, Faes, and Marinazzo 2014), cross-correntropy (Liu, Pokharel, and Principe 2007; Santamaría, Pokharel, and Principe 2006; Principe 2010). The choice of these similarity metrics to evaluate channel synchronization was also in part due to its computational efficiency, along with its success both in past studies and also in our previous study as revealed by the recognition performances. The differences observed in the recognition performances for each metric (please see Table 16 and performance results in (B. Orkan Olcay and Karaçalı 2019)) is due to the differences of the timing parameters captured by each of the synchronization method. The main reason of such diversity of captured triple parameters is that each method extracts and uses different aspects of the signal features to calculate the synchronization in mathematical manner.

Alternative measures can also be evaluated such, phase lag index (PLI) (Cornelis J. Stam, Nolte, and Daffertshofer 2007), imaginary part of coherency (imCOH) (Nolte et al. 2004), transfer entropy (TE) (Wibral, Vicente, and Lindner 2014; Wibral et al. 2013; Schreiber 2000), coherence (COH) (Rocca et al. 2014; Wendling et al. 2009;

Bakhshayesh et al. 2019a; Greenblatt, Pflieger, and Ossadtchi 2012; Sakkalis 2011), cross-sample entropy (Gomez et al. 2016), eigenvalue-based synchrony measures (Jalili, Barzegaran, and Knyazeva 2014) and synchronization likelihood (C. J. Stam and Van Dijk 2002). The short-lived synchronization calculation adopted here can also be calculated via Kraskov's mutual information estimation method (Kraskov, Stögbauer, and Grassberger 2004) which elicited the best performance in our previous study (B. Orkan Olcay and Karaçalı 2019). However, calculating the mutual information between the signal segments via Kraskov's method requires huge amount of computation time which may be unsuitable for a short-lived synchronization-based BCI application. However, advanced parallel computing architectures as well as efficient computation algorithms can be incorporated here to overcome the computation speed issues of the Kraskov's mutual information estimation.

4.4.7. Future Directions of the Proposed Method

As for the potential extension of the methodology proposed here to brain-computer interfacing applications, it should be noted that the core of the method relies on identifying the channel pairs with significantly different synchronization characteristics during different activities in terms of optimal activity-specific timing parameters. Clearly, once the activity-specific timing parameter triplets and channel pairs are identified from a training set, they can be used as features in a connectivity-based BCI framework. First and foremost, filtering of the EEG signals into 8-30 Hz frequency band is consistent with many BCI studies where the motor imagery related information is sought within the frequency range of 8-30 Hz (Yuan and He 2014; Lafleur et al. 2013; McFarland and Wolpaw 2008). Several studies used a filter-bank structure or wavelet-based methods prior to the feature extraction to obtain frequency-resolved features for motor imagery related brain activity characterization (Kumar, Sharma, and Tsunoda 2017; S. H. Park, Lee, and Lee 2018; Higashi and Tanaka 2013). Clearly, a filter-bank strategy or maximally overlap discrete wavelet transform analysis may also be incorporated here prior to the synchronization calculation, allowing analysis of different frequency bands in the sense of the activity-specific timing parameter triplets and the related channel pairs (S. H. Park, Lee, and Lee 2018; Ang et al. 2008; Walden and Contreras Cristan 1998).

For instance, the role of μ and β bands during motor imagery activity was revealed in earlier studies (Gu et al. 2020; Athanasiou et al. 2018). Also, Gu et al. found that during lower extremity motor imagery trials, right and left foot imagination revealed significantly different μ and β band networks/subnetworks (Gu et al. 2020). Also, the μ rhythm dynamics have been associated with the motor imagery related information processing among the motor cortical regions (Başar et al. 2001; Llanos et al. 2013). However, increase in the spectral resolution entails substantial computational cost, requiring repeated calculations for each frequency band. Alternatively, since wavelet-based methods have also been used in the brain activity analysis (O. A. Rosso et al. 2006; Emre Cek, Ozgoren, and Acar Savaci 2010; Osvaldo A. Rosso et al. 2001; Nguyen-Ky et al. 2012), frequency-resolved activity-specific short-lived synchronization can also be identified over time-frequency scalograms of the EEG channels (Z. Gao et al. 2019; Osvaldo A. Rosso et al. 2001), albeit with a similar computational cost.

As an extension, our method can reliably be considered in human-computer interaction such as gesture recognition applications. Up to now, many different conspicuous efforts have been spent to increase the accuracy of gesture recognition applications (G. Li, Li, et al. 2019; Ying Sun et al. 2020). In this respect, brain synchronization/activation features can additionally be adopted to increase the recognition accuracy. Once the important EEG channel pairs and the corresponding movement-specific inter-regional synchronization timings are determined in training phase, our method can reliably be used in conjunction with current surface EMG-based gesture recognition methods to achieve improved movement identification performances and thus be used in hand motion controlled devices. In a similar manner, the proposed timing-based brain activity analysis method can also be used to detect brain lesions, which may cause significant alterations of inter-regional communication patterns (G. Li, Jiang, et al. 2019).

On a final note, it should be emphasized that, the approach presented here deviates significantly from the majority of the brain activity characterization studies in the literature that aim to extract characteristic synchronization-based features for different motor imagery tasks using whole activity periods (Anderson, Stolz, and Shamsunder 1998; Feng et al. 2018; Lemm et al. 2005). Notably, a critical issue can arise when using the whole activity periods to determine activity-specific brain patterns. Although the exact time of initiation and end cue for motor imagery activity is known in synchronous BCI experiments, the initiation and end time of the reciprocal information processing can

be different for each different pairs of brain regions (Curran and Stokes 2003). That means the activity-related localized activation/synchronization dynamics may emerge and disappear in a short period of time thanks to the activity-specific timing organization. In the literature, few studies address this issue. Zhang et al. proposed a temporally constrained sparse group spatial pattern method to locate the time window where the short-lived frequency-specific patterns emerge (Yu Zhang et al. 2019). Ang et al. proposed an information-theoretic method to determine the optimal time window and frequency band simultaneously to characterize the motor imagery periods accurately (Ang et al. 2012). Wang et al. proposed a Kullback-Liebler divergence based method to identify the most informative time segment for EEG signal classification (J. Wang et al. 2020; 2018). Hsu et al. adopted a wavelet-based active segment selection strategy to isolate the most informative features from the EEG signals recorded over sensorimotor regions (Hsu et al. 2007). Feng et al. proposed a correlation-based optimal time segment selection for CSP based BCI applications (Feng et al. 2018). These studies, however, used time windows of fixed duration, usually 1 or 2 seconds, and calculated features to be used in a classification setting to decide which time window is the most informative based on their discrimination ability. This approach may assume that the statistics of EEG activity do not change in a considerable extent (Bullmore and Sporns 2009). Furthermore, this strategy disregards variations in the duration of the brain's responses. In this chapter, optimal latency (Δt), time lag (τ) and duration (w) of the coupling were determined to capture activity-specific inter-channel synchronization for each motor imagery activity type and each channel pair, addressing both issues listed above to their full complexity.

CHAPTER 5

COGNITIVE ACTIVITY RECOGNITION BY USING CLUSTERS OF TRANSIENTLY SYNCHRONIZED EEG CHANNELS

The brain is the citadel of the senses,
This guides the principles of thoughts
-Pliny the Elder-

5.1. Introduction

In the previous chapters, following the similar way of Friston et al. (Karl J. Friston 2000), we highlighted the importance of considering the time-sensitive brain synchronization analysis to reveal how the cognitive functions are generated (Burgess 2011). The main outcomes of the previous chapter tell us that brain systematically adjusts the timings of inter-regional synchronizations to generate desired cognitive processes.

It is argued that the characteristic inter-regional synchronization may constitute a hierarchical organization among the brain regions (Ravasz and Barabási 2003). The hierarchical clusters that emerged within the brain regions constitutes the transient neural communication channels for information integration and segregation (C. Zhou et al. 2006; Miraglia, Vecchio, and Rossini 2018). Along with these findings, in this chapter, we aimed to capture this transiently synchronized activity-specific hierarchical channel networks and use them for a cognitive activity characterization.

In this method, we initially captured the activity-specific inter-channel synchronization timings (i.e., $\left\{\Delta t_{i,j}^{A_{1/2}}, \tau_{i,j}^{A_{1/2}}, w_{i,j}^{A_{1/2}}\right\}$). To that end, we used the same optimization method described in Chapter 4. Next, we used agglomerative hierarchical clustering method to obtain the channel groups (i.e., clusters) by considering their average short-lived activity-specific synchronizations. We characterized these channel groups via first order statistical features. We used unpaired two-tailed t-tests to determine the

activity-specific transiently synchronized channel groups. We used activity-specific channel groups to recognize the cognitive task.

5.2. Proposed Method

In this chapter, we again used six different synchronization measure to calculate short-lived brain synchronizations. The synchronization measures are listed as follows:

- Cosine-based similarity (B. Orkan Olcay and Karaçalı 2019; Sargolzaei et al. 2015; Herff et al. 2019)
- Linearized mutual information (S. H. Jin, Lin, and Hallett 2010)
- Kendall's tau correlation (M. Kendall 1938; M. G. Kendall 1946)
- Phase locking value (Lachaux et al. 1999)
- Phase coherence value (Tass et al. 1998; Bakhshayesh et al. 2019b)
- Cross-correntropy (Liu, Pokharel, and Principe 2007; Santamaría, Pokharel, and Principe 2006)

Note that we used the same heuristic optimization procedure as in Chapter 4 to determine the inter-channel activity-specific timing parameter triplets.

5.2.1. Determination of Hierarchical Channel Clusters

We used the activity-specific timing parameter triplets, which was calculated in the previous chapter $\left(\text{i.e.,}\left\{\Delta t_{i,j}^{A_1}, \tau_{i,j}^{A_1}, w_{i,j}^{A_1}\right\} \text{and} \left\{\Delta t_{i,j}^{A_2}, \tau_{i,j}^{A_2}, w_{i,j}^{A_2}\right\}\right)$, to calculate the pairwise synchronizations matrices Σ for each corresponding training task period and channel pair (i, j). The mathematical expression of the synchronization matrices is given as

$$\Sigma^{A_1|A_1}(i,j;k) = S\left(s_{i,k}^{\Delta t_{i,j}^{A_1}, w_{i,j}^{A_1}}, s_{j,k}^{\Delta t_{i,j}^{A_1} + \tau_{i,j}^{A_1}, w_{i,j}^{A_1}}\right)$$

$$\Sigma^{A_2|A_2}(i,j;m) = S\left(s_{i,m}^{\Delta t_{i,j}^{A_2}, w_{i,j}^{A_2}}, s_{j,m}^{\Delta t_{i,j}^{A_2} + \tau_{i,j}^{A_2}, w_{i,j}^{A_2}}\right) \tag{5.1}$$

where $\Sigma^{A_1|A_1}(i,j;k)$ denote the synchronization calculated for the training task $k \in I_{A_1}$ ($m \in I_{A_2}$) by using the A_1-specific timing parameter triplet for the channel pair (i,j) and, I_{A_1} denote the indices of the training task periods belongs to A_1 activity. After finding the pairwise synchronization matrices, we calculated their average as

$$\bar{\Sigma}^{A_1|A_1}(i,j) = \frac{1}{\left|I_{A_1}\right|} \sum_{k \in I_{A_1}} \Sigma^{A_1|A_1}(i,j;k)$$
$$\bar{\Sigma}^{A_2|A_2}(i,j) = \frac{1}{\left|I_{A_2}\right|} \sum_{m \in I_{A_2}} \Sigma^{A_2|A_2}(i,j;m) \tag{5.2}$$

where $\left|I_{A_{1/2}}\right|$ denote the total number of training task periods belong to $A_{1/2}$ activity. We then applied agglomerative hierarchical clustering to averaged synchronization matrices to obtain the channel clusters. We used all the three linkage methods since we do not know the actual hierarchical organization among the brain regions. The cluster similarity between channel groups I and J can be calculated for the complete linkage as

$$S(I,J) = \min_{i \in I, j \in J} \bar{\Sigma}(i,j) \tag{5.3}$$

for the single linkage as

$$S(I,J) = \max_{i\in I, j\in J} \bar{\Sigma}(i,j) \tag{5.4}$$

and finally, for the average linkage as

$$S(I,J) = \frac{1}{M_I M_J} \sum_{i\in I, j\in J} \bar{\Sigma}(i,j) \tag{5.5}$$

where M_I and M_J are the total number of EEG channels inside the clusters I and J. For the BCI Competition-III dataset IVa, we obtained 117 clusters for each different linkage method and activity type which are represented as $\left\{C_{linkage}^{A_{1/2}}(x)\right\}_{x=1}^{117}$. For the PhysioNet dataset, we obtained 63 clusters. In this study, we use three linkage methods which means we obtained 351 and 189 clusters for each activity type for BCI Competition-III dataset IVa and PhysioNet datasets, respectively. Note that, among the 351 clusters obtained for the BCI Competition-III dataset (189 for PhysioNet), some of the clusters may appear similar to each other. In such a case, we kept one replica of the similar clusters and throw the other replicas out.

5.2.2. Activity Recognition Framework

The flow diagram of hierarchical clustering based activity recognition framework is presented in Figure 29. In the training phase of the proposed method, in the first step, we captured the activity-specific timing parameter triplets for each channel pair and activity type $\left(\text{i.e., } \left\{\Delta t_{i,j}^{A_1}, \tau_{i,j}^{A_1}, w_{i,j}^{A_1}\right\} \text{ and } \left\{\Delta t_{i,j}^{A_2}, \tau_{i,j}^{A_2}, w_{i,j}^{A_2}\right\}\right)$ as in the previous chapter. In the second step, we obtained the hierarchical channel clusters for each activity type as described above. In the third step, for each training task period, the pairwise synchronizations between the channels in each cluster obtained for $A_{1/2}$ activity was calculated using the timing parameters specific to respective channel pairs for $A_{1/2}$ activity. Then, these pairwise synchronizations were used to calculate six statistical

features (i.e., mean, maximum, minimum, %75 quantile, median, %25 quantile) to characterize the corresponding clusters. The feature vector ξ_ℓ for the training task period ℓ can be expressed as

$$\xi_\ell = \begin{bmatrix} F_{mean}\left(\Sigma^{A_1}(i,j;\ell)\middle|C^{A_1}(1)\right) \\ F_{max}\left(\Sigma^{A_1}(i,j;\ell)\middle|C^{A_1}(1)\right) \\ \vdots \\ F_{q25}\left(\Sigma^{A_1}(i,j;\ell)\middle|C^{A_1}(1)\right) \\ F_{mean}\left(\Sigma^{A_1}(i,j;\ell)\middle|C^{A_1}(2)\right) \\ \vdots \\ F_{q25}\left(\Sigma^{A_1}(i,j;\ell)\middle|C^{A_1}(2)\right) \\ \vdots \\ F_{q25}\left(\Sigma^{A_1}(i,j;\ell)\middle|C^{A_1}(M-1)\right) \\ F_{mean}\left(\Sigma^{A_2}(i,j;\ell)\middle|C^{A_2}(1)\right) \\ F_{max}\left(\Sigma^{A_2}(i,j;\ell)\middle|C^{A_2}(1)\right) \\ \vdots \\ F_{q25}\left(\Sigma^{A_2}(i,j;\ell)\middle|C^{A_2}(1)\right) \\ F_{mean}\left(\Sigma^{A_2}(i,j;\ell)\middle|C^{A_2}(2)\right) \\ \vdots \\ F_{q25}\left(\Sigma^{A_2}(i,j;\ell)\middle|C^{A_2}(2)\right) \\ \vdots \\ F_{q25}\left(\Sigma^{A_2}(i,j;\ell)\middle|C^{A_2}(M-1)\right) \end{bmatrix} \tag{5.6}$$

where $F(\Sigma|C)$ calculates the feature by using the pairwise synchronizations Σ of the channel pairs that is contained in the cluster C. At the end of these feature extraction step, we obtained 1404-dimensional training feature vectors for the BCI Competition-III dataset, and 756-dimensional for the PhysioNet. As feature selection, we performed a two-tailed unpaired t-test between the statistical features calculated from the synchronization values calculated using $A_{1/2}$-specific timing parameter triplets and clusters separately. Then, we used Benjamini-Hochberg to correct the resulting P-values against multiple comparison problem (Benjamini and Hochberg 1995). We selected and used the significant features (i.e., $P < 0.05$) for classifier training.

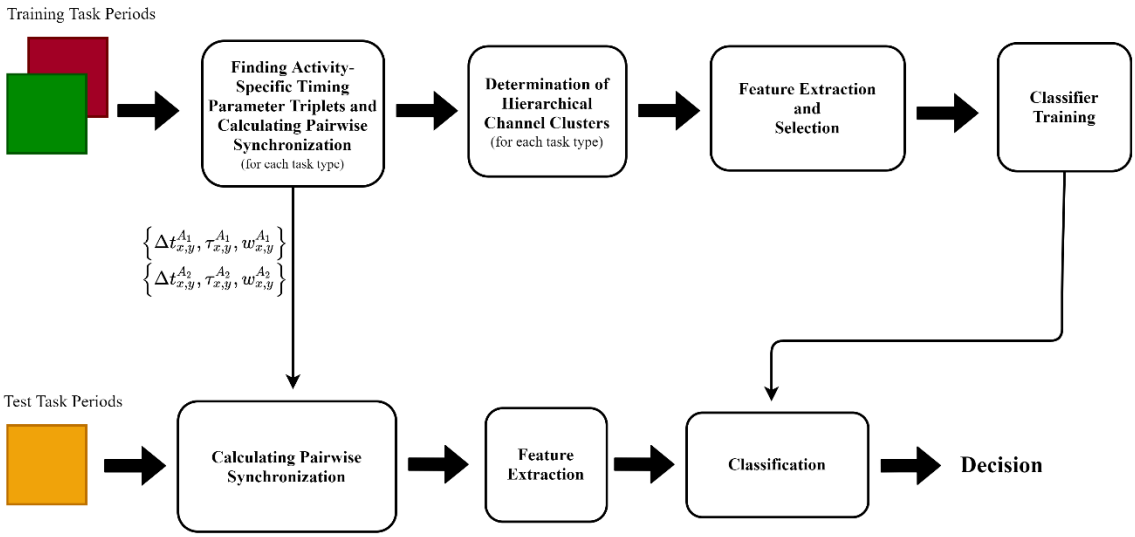

Figure 29. The demonstration of the block diagram of the proposed brain activity characterization method. Red and green square represented the training task periods with known classes while yellow square representing the test task periods with unknown class.

In the test phase of the proposed recognition framework, we used activity-specific timing parameter triplets to calculate short-lived pairwise synchronization values for each test task period. For each test period, we obtained the feature vector ξ as

$$\xi = \begin{bmatrix} F_{mean}\left(\Sigma^{A_1}(i,j)\middle|C^{A_1}(1)\right) \\ F_{max}\left(\Sigma^{A_1}(i,j)\middle|C^{A_1}(1)\right) \\ \vdots \\ F_{q25}\left(\Sigma^{A_1}(i,j)\middle|C^{A_1}(1)\right) \\ F_{mean}\left(\Sigma^{A_1}(i,j)\middle|C^{A_1}(2)\right) \\ \vdots \\ F_{q25}\left(\Sigma^{A_1}(i,j)\middle|C^{A_1}(2)\right) \\ \vdots \\ F_{q25}\left(\Sigma^{A_1}(i,j)\middle|C^{A_1}(M-1)\right) \\ F_{mean}\left(\Sigma^{A_2}(i,j)\middle|C^{A_2}(1)\right) \\ F_{max}\left(\Sigma^{A_2}(i,j)\middle|C^{A_2}(1)\right) \\ \vdots \\ F_{q25}\left(\Sigma^{A_2}(i,j)\middle|C^{A_2}(1)\right) \\ F_{mean}\left(\Sigma^{A_2}(i,j)\middle|C^{A_2}(2)\right) \\ \vdots \\ F_{q25}\left(\Sigma^{A_2}(i,j)\middle|C^{A_2}(2)\right) \\ \vdots \\ F_{q25}\left(\Sigma^{A_2}(i,j)\middle|C^{A_2}(M-1)\right) \end{bmatrix} \tag{5.7}$$

We reduced the feature vector by selecting the similar features that was found as significant in feature selection step of training phase. At the final step, we determined the category of corresponding test period by classifying its reduced feature vector.

5.3. Results

In order to evaluate the performance of the proposed method for varying sizes of the training task periods, we performed a chronological partitioning on the datasets as in previous chapters. The recognition performances for different synchronization measures for both scenario-1 and scenario-2 are provided in Table 22. We also provided the most three successful performances using correntropy method for BCI Competition-III dataset IVa, and linearized mutual information for PhysioNet Motor Imagery datasets in Table 23.

Table 22. The average performances of the proposed clustering based framework calculated across 5 subjects from BCI Competition-III dataset IVa and first 20 subjects from PhysioNet Motor Movement/Imagery datasets. We again used three different classifiers, FLD, Linear SVM, and Nonlinear (Gauss) SVM.

		Scenario-1 Performances (%)			**Scenario-2 Performances (%)**		
		FLD	**Linear SVM**	**Gauss SVM**	**FLD**	**Linear SVM**	**Gauss SVM**
BCI Competition-III dataset IVa	**Cosine**	59.89 ± 7.75	64.04 ± 8.93	65.42 ± 8.88	69.78 ± 10.2	70.86 ± 9.94	70.43 ± 9.61
	Linear MI	68.93 ± 5.48	69.14 ± 8.23	66.06 ± 5.85	69.56 ± 9.69	70.0 ± 11.74	68.26 ± 8.5
	Correntropy	63.08 ± 6.69	67.12 ± 6.88	67.87 ± 5.24	67.17 ± 5.77	71.73 ± 9.72	69.34 ± 9.04
	PLV	56.06 ± 6.07	61.80 ± 5.65	62.34 ± 5.92	63.91 ± 7.42	65.21 ± 8.93	66.95 ± 6.27
	PCV	62.23 ± 5.43	62.02 ± 4.82	65.53 ± 7.89	61.73 ± 9.64	63.91 ± 13.47	62.17 ± 11.12
	Kendall	61.14 ± 4.87	66.44 ± 6.26	65.49 ± 6.01	67.51 ± 7.21	67.09 ± 8.78	66.36 ± 7.41
PhysioNet Motor Movement/Imagery	**Cosine**	55.17 ± 8.41	59.83 ± 11.82	61.5 ± 10.78	57.33 ± 12.86	62.67 ± 15.65	64.0 ± 16.52
	Linear MI	57.83 ± 10.55	62.33 ± 12.38	61.83 ± 11.26	59.33 ± 9.40	63.0 ± 15.36	60.67 ± 13.49
	Correntropy	57.67 ± 10.15	60.5 ± 13.16	61.67 ± 12.86	56.0 ± 11.11	61.67 ± 15.87	60.0 ± 16.61
	PLV	52.17 ± 5.85	54.0 ± 7.91	53.17 ± 7.91	52.67 ± 11.0	54.67 ± 9.07	56.0 ± 10.0
	PCV	51.83 ± 5.45	55.67 ± 8.72	54.67 ± 7.61	59.33 ± 9.88	60.0 ± 12.97	60.33 ± 11.74
	Kendall	54.12 ± 7.41	59.54 ± 9.72	58.62 ± 8.85	56.74 ± 9.64	60.05 ± 11.34	59.54 ± 10.63

Table 23. The highest three performances obtained for BCI Competition-III dataset IVa and PhysioNet Motor Movement/Imagery datasets.

		Scenario-1 Performances (%)			Scenario-2 Performances (%)		
Dataset	**ID**	**FLD**	**Linear SVM**	**Nonlinear SVM**	**FLD**	**Linear SVM**	**Nonlinear SVM**
BCI Competition-III (Correntropy)	***al***	68.61	76.06	75.0	67.39	79.34	72.87
	av	63.29	63.82	65.95	73.91	75.0	64.13
	ay	70.44	72.87	71.27	71.73	81.52	83.69
PhysioNet (Linear MI)	**S002**	73.33	70.0	73.33	66.67	80.0	73.33
	S007	63.33	56.67	66.67	60.0	86.67	73.33
	S015	66.67	93.33	86.67	86.67	80.0	86.67

The average recognition performance results obtained for both datasets show that the proposed clustering based method is no better than the performances of the methods described in previous chapters. We also showed, however, that the method achieved satisfactory recognition performances (especially in scenario-2) for some of the subjects both in BCI Competition-III dataset IVa and PhysioNet Motor Movement/Imagery datasets.

We also demonstrated the most selected three clusters as characteristic features for the subjects that elicited the highest performances for both datasets in Figures 30-35. Note that, in these figures, the EEG electrodes inside the corresponding cluster are marked by a red star on the location where the corresponding electrode located. The black dots represent the remaining electrodes. We organized the cluster plots in these figures from up to down according to their significance level.

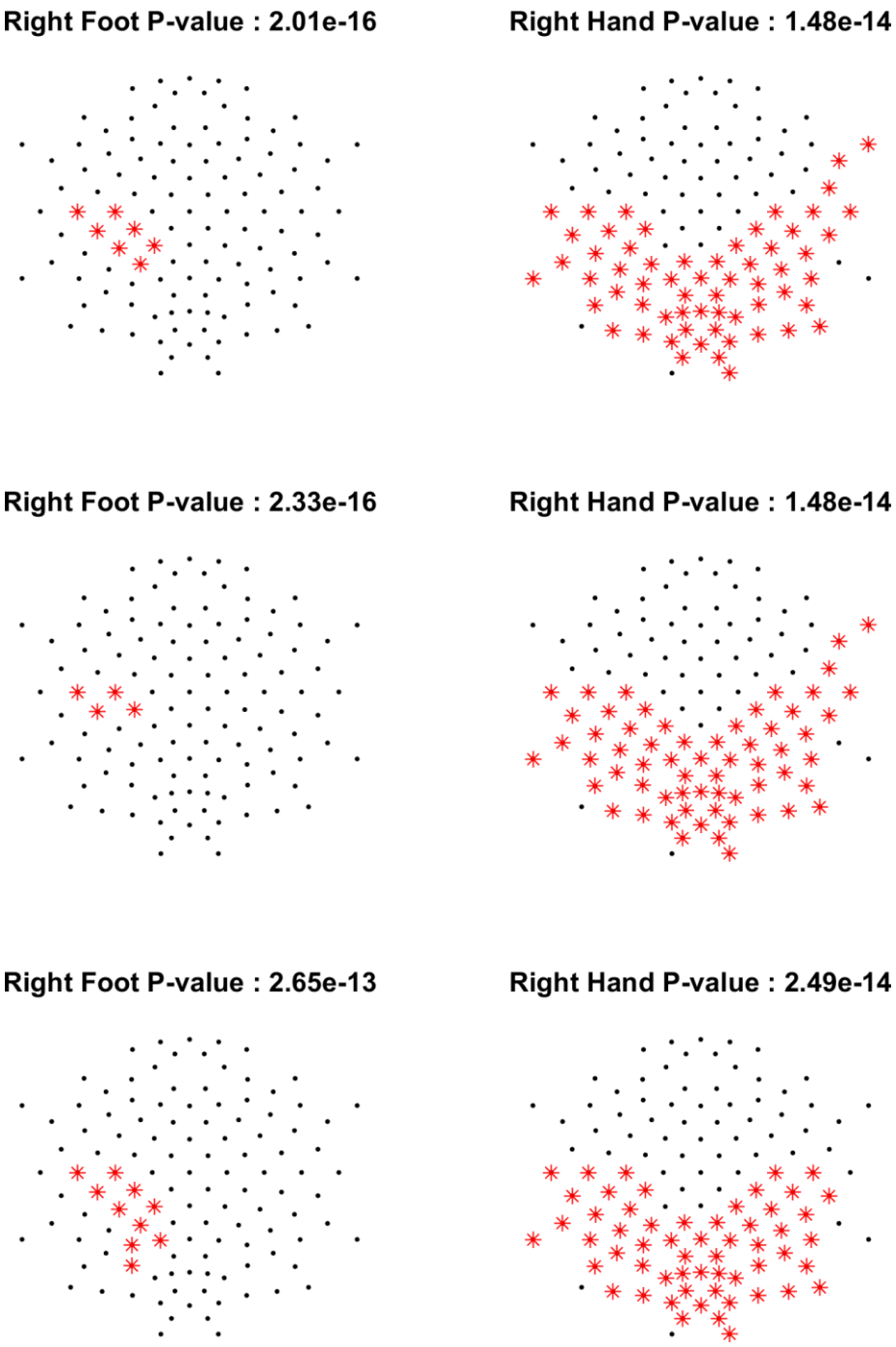

Figure 30. The first three significant cluster obtained subject *al* of BCI Competition-III (scenario-2).

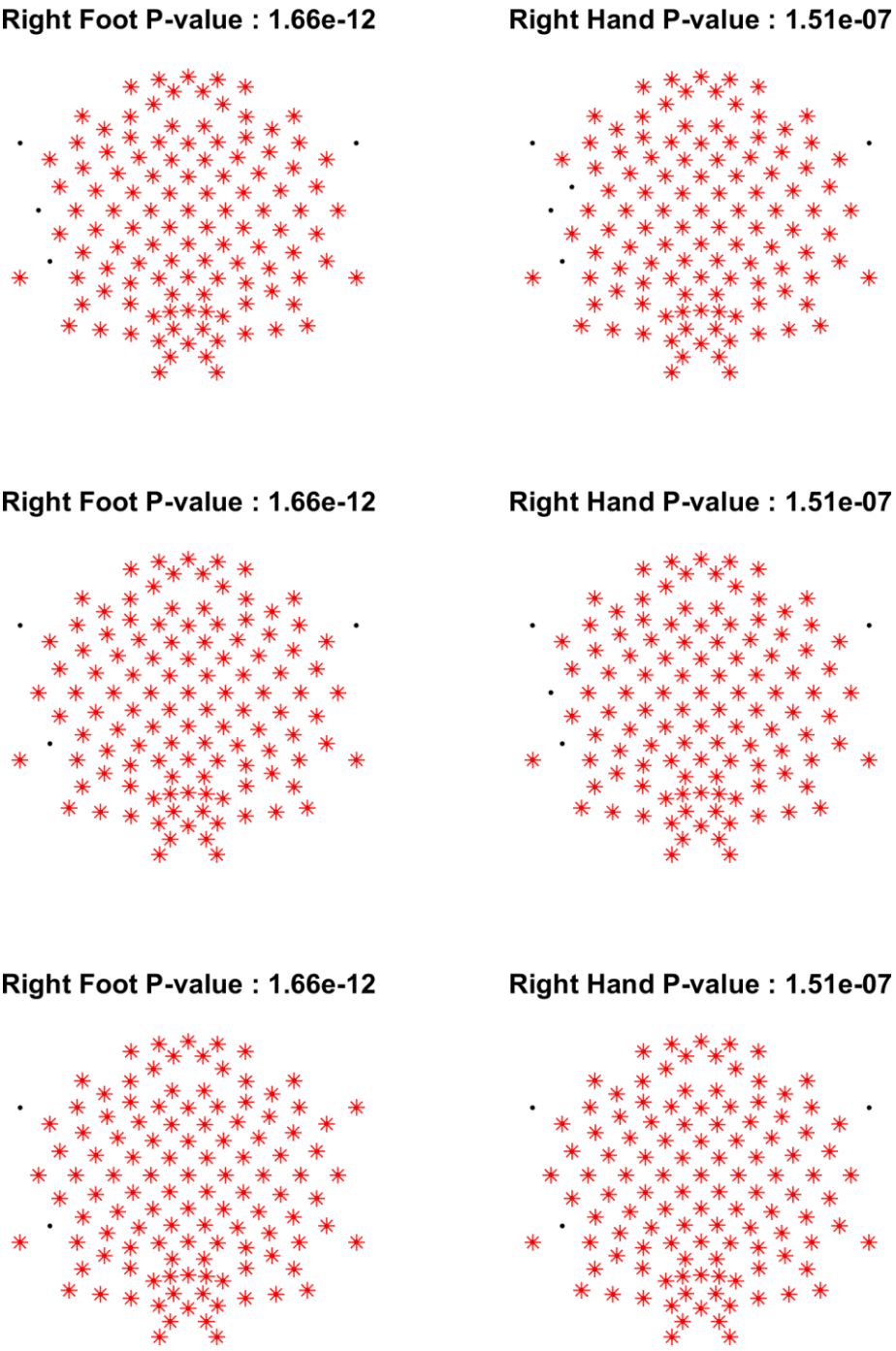

Figure 31. The first three significant cluster obtained subject *av* of BCI Competition-III (scenario-2).

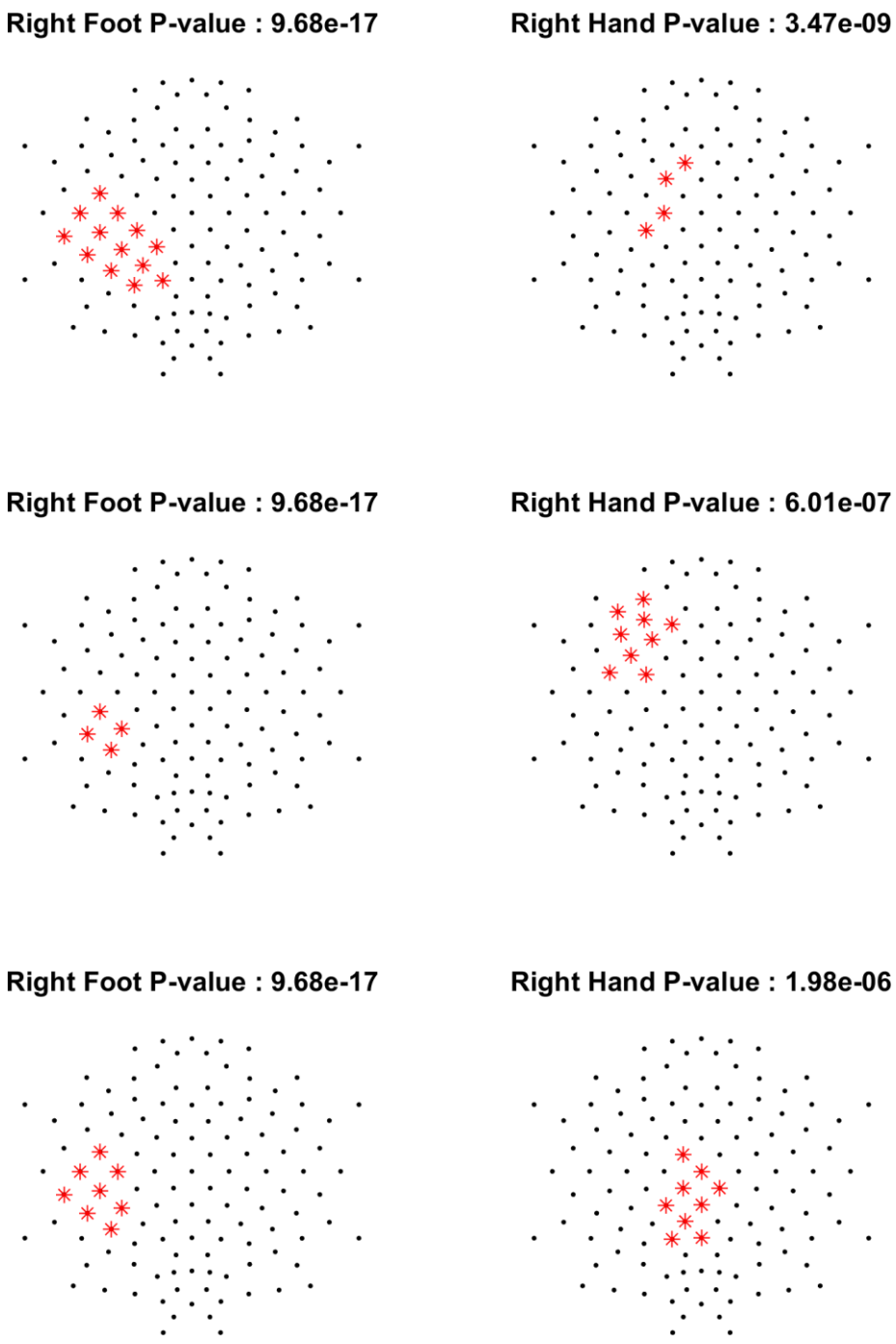

Figure 32. The first three significant cluster obtained subject *ay* of BCI Competition-III (scenario-2).

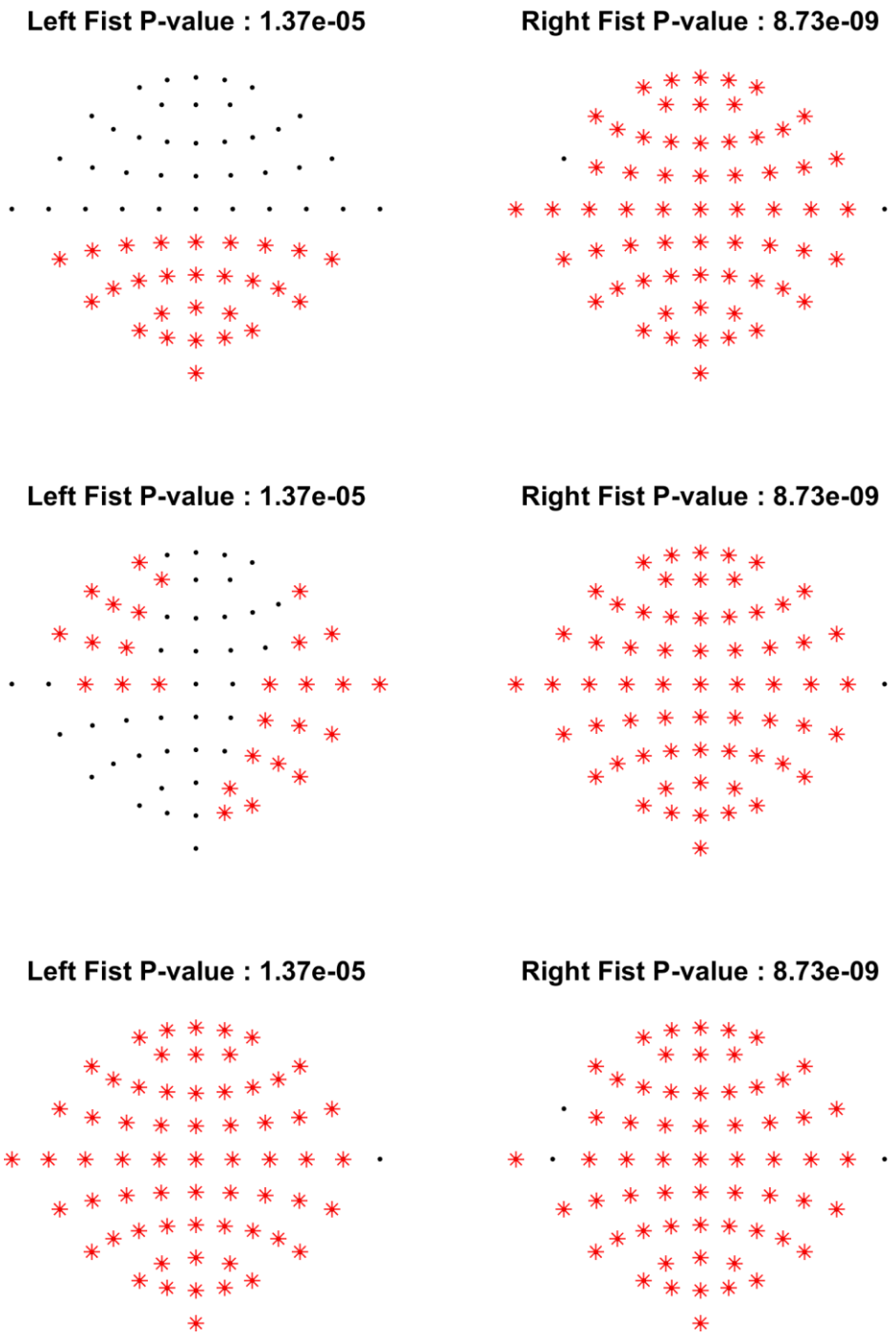

Figure 33. The first three significant cluster obtained subject *S002* of PhysioNet dataset (scenario-2).

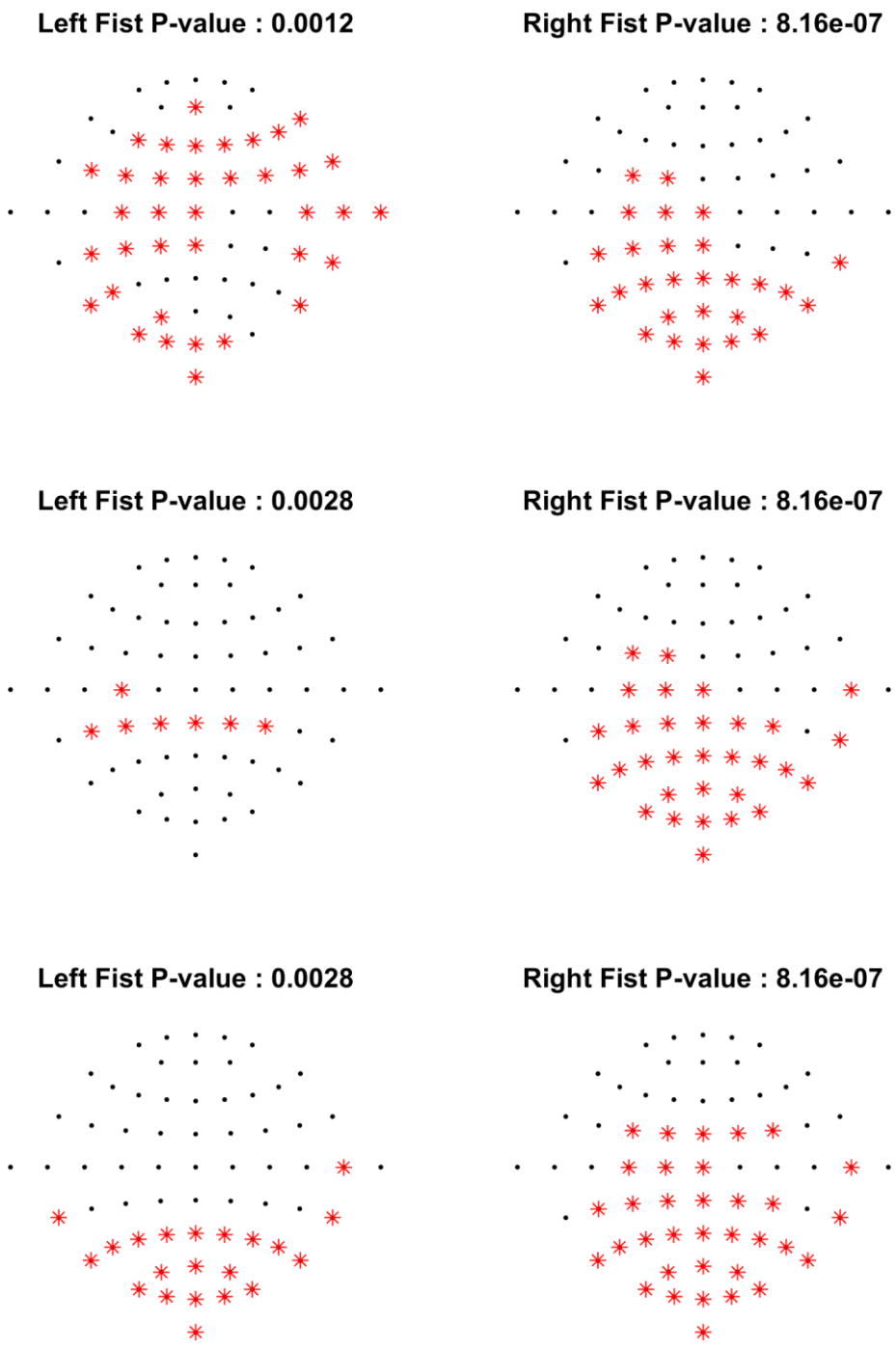

Figure 34. The first three significant cluster obtained subject *S007* of PhysioNet dataset (scenario-2).

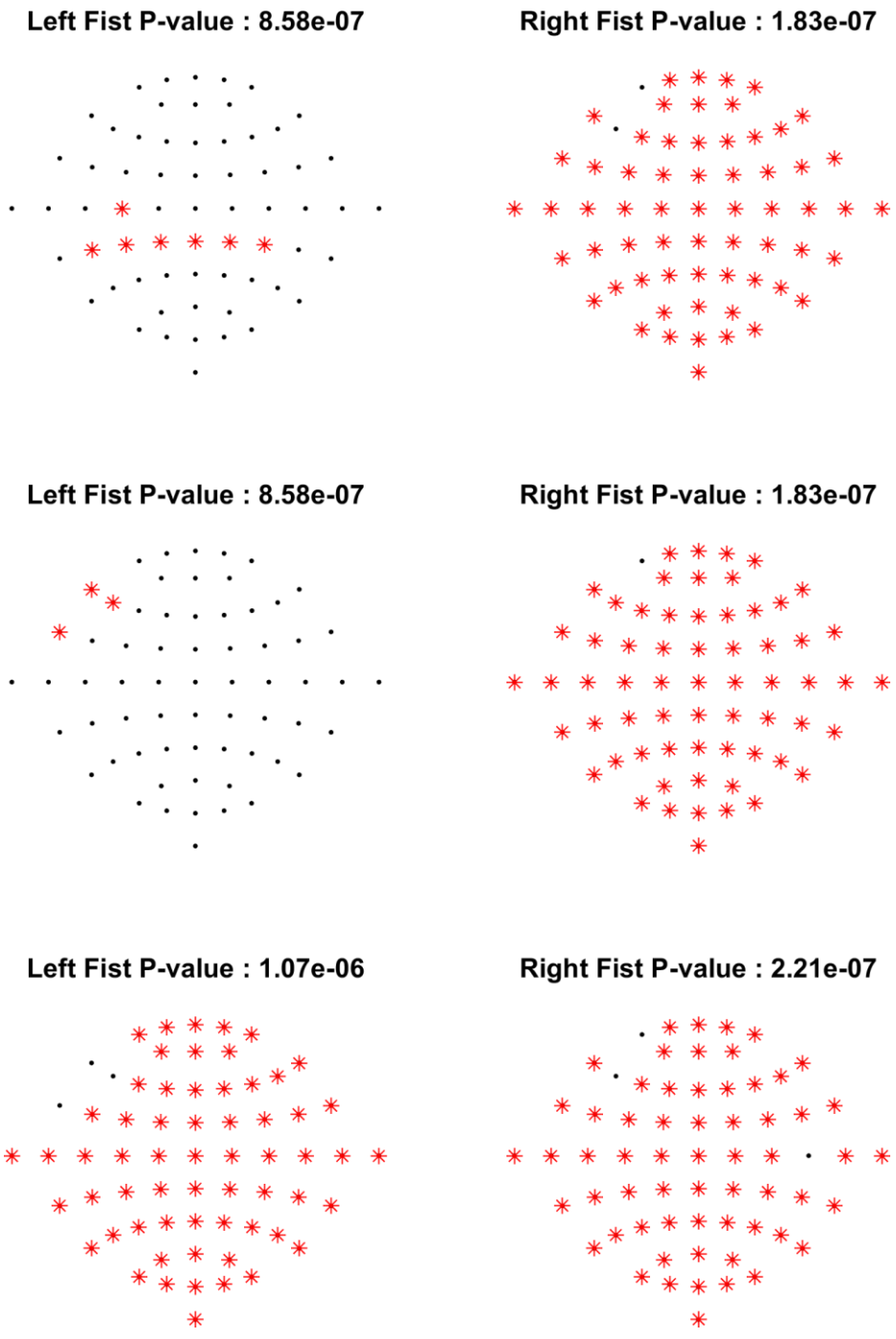

Figure 35. The first three significant cluster obtained subject *S015* of PhysioNet dataset (scenario-2)

We finally analyzed the selected (i.e., significant) clusters and observed that the 25% quantile statistical feature appeared as the most prominent feature that makes the channel clusters as the most statistically significant one.

5.4. Discussion

In this chapter, we studied a novel cognitive activity characterization framework that finds and uses the channel clusters according to their short-lived pairwise synchronizations of the EEG channels. To this end, we first determined the activity-specific timing parameter triplets for each channel pair and activity type as in the previous chapter. Then, we calculated the task-specific average synchronization matrices. These matrices were then used to obtain the hierarchical channel clusters. We characterized these clusters with several statistical features and determined the activity-specific features via two-tailed unpaired t-tests. In order to evaluate the characterization performance of the proposed method, we tested our method in a motor imagery activity recognition framework as in previous chapters. We presented the average performances results across five subjects for BCI Competition-III dataset IVa and, the first 20 subjects for PhysioNet Motor Movement/Imagery datasets in Table 22. These results show that correntropy and linearized mutual information methods achieved better recognition performances for the BCI Competition-III dataset IVa and the PhysioNet Motor Movement/Imagery dataset, respectively. As an important point, the recognition performances in scenario-2 apparently higher than the performances in scenario-1 which means our method may elicit satisfactory recognition performances for larger training sets.

In comparison with the performances of the cognitive task recognition methods proposed in previous chapters, however, the clustering-based method achieved slightly lower performances. It is apparent that the shortcomings (i.e., low sample size, low signal-to-noise ratio, …) noticed in the previous chapters can be the source of these low recognition performances obtained here. In addition to these, it may be another significant reason that the synchronization measures found as successful in this study was not the same measures found in the previous chapter.

Here, we captured the activity-related channel clusters from the training task periods by only considering the average short-lived pairwise channel synchronization

values. In the analysis of the synchronization timings of channel pairs, we observed that the majority of the channel pairs synchronized at distinct time instants. In that context, the characterization of the bunch of synchronized channels in activity-related clusters by disregarding the timings failed to provide accurate task recognition performance. As a solution, the channel clustering criteria (only the short-lived synchronizations) may be upgraded by inserting a criterion of "synchronization timing of channel pairs" for capturing the clusters with collectively synchronized channels.

It is obvious that the maximal performance obtained from both datasets was significantly different from each other. Among the other reasons, the difference in the number of EEG channels used for collecting electrical activity may have an influence on this performance difference (Wierzgała et al. 2018). This may suggest that using an EEG system having much denser electrodes may provide spatially more detailed synchronization features that is expected to provide biophysically meaningful clusters of synchronized channels.

Another reason for the low recognition performance obtained from the PhysioNet dataset is maybe the session-to-session variability problem mainly faced in BCI systems. We used a chronological cross validation (training sessions and test sessions are different) to simulate a realistic brain activity recognition scenario. In the literature, many studies addressed the difficulties of the recognition of cognitive tasks collected at different sessions which impose challenges on brain activity characterization due to the alteration of the dynamics of the EEG signal across different recording sessions (Gowreesunker et al. 2009; Saha et al. 2018a).

As depicted in previous chapters and in (Olcay and Karaçalı, 2019), the common approach of the BCI studies that employs the PhysioNet dataset is the elimination of the performances which are lower than ~64% (Athif and Ren 2019; Kim et al. 2016; Cheolsoo Park, Took, and Mandic 2014) or adopting blind signal decomposition methods as preprocessing (Varsehi and Firoozabadi 2021). Again, in here, we neither applied any performance elimination criteria not adopted using blind signal decomposition methods. Besides the average performance results, we presented the most three successful performances for both the PhysioNet and BCI Competition-III dataset in Table 23 to examine the powerful sides of our method. The performances obtained for the subjects *S002, S007* and, *S015* for PhysioNet, and al, aw, and ay for BCI Competition-III datasets show that the proposed method somehow captured relevant features during

characterization of imagery movement of upper and lower extremities for a limited number of subjects.

The clusters captured from three successful subjects for the BCI Competition-III dataset mainly contain left central, left centroparietal electrodes for the right foot, and left central, frontocentral, and centroparietal regions for right hand motor imagery activity. It is important to note that, except the subject av, while the right foot clusters obtained from these subjects are appeared to be more localized in the sense of contained electrodes, the right hand clusters are comprised of electrodes from several regions of the brain which means that our method could not capture the right hand-specific clusters.

The contralaterality of the obtained foot channels/channel clusters obtained for BCI Competition-III dataset IVa were similarly observed in previous chapter and in past literature (Chung, Kim, and Kim 2011; Gonuguntla, Wang, and Veluvolu 2016). Also, the importance and related functionality of the electrodes captured for right foot clusters (left centro-parietal and central electrodes) were described in previous chapter (Dechent, Merboldt, and Frahm 2004; Q. Gao, Duan, and Chen 2011; Xu et al. 2014; Hétu et al. 2013; Sirigu et al. 1996). For the PhysioNet dataset, however, we could not capture consistently localized and biophysically relevant electrodes for both right and left fist motor imagery activities since the clusters of all successful subjects contain majority of all EEG electrodes.

As an improvement, this study may be repeated by using a frequency-resolved EEG signals to capture frequency-specific clusters for each activity type since different cognitive processes evoke the exhibit inter-regional communication in different frequency tones (Rahman and Fattah 2020; Ziaeemehr et al. 2020). For our study, it is beneficial to calculate frequency-specific timing parameter triplets as well as significant channel clusters to reveal more informative activity-specific features. However, in such a case the time required to obtain the timing parameters and clusters from the training data would increase.

In this study, we tried to identify the activity-related channel clusters that exhibit significant short-lived functional interactions between the among the constituent channels. This approach can be assumed as a channel subset selection procedure which can used channel subset selection for accurate characterization (Royer et al. 2010; J. Jin et al. 2019; Varsehi and Firoozabadi 2021). As an improvement, adopting upgraded channel clustering method may both improve the characterization performance and greatly reduces the time required to extract connectivity-based features.

We observed that the 25% quantile feature was mostly selected feature type for characterizing the clusters obtained for the right foot, and minimum for the right hand motor imagery activities. However, the linkage methods of the significant clusters were dependent on the subjects (i.e., subject-specific) (Jeunet et al. 2015). In order to capture subject-unspecific channel clusters, some filtering operations may be required to for capturing activity-specific clusters (Xie et al. 2018; Allen et al. 2014).

CHAPTER 6

CAPTURING THE TIMINGS FOR ENTROPIC CHARACTERIZATION OF COGNITIVE ACTIVITIES

As long as our brain is a mystery, the universe,
the reflection of the structure of the brain will also be a mystery
-Santiago Ramon y Cajal-

6.1. Introduction

In the previous chapters, we proposed several synchronization-based cognitive activity characterization methods that capture the timings of characteristic brain synchronizations. Their relatively low recognition performance and their vast amount of computation time requirements for capturing the activity-specific synchronization timings indicate that these methods are not considerable as feature extraction methods for BCI frameworks in their present form. To that end, in this chapter, we propose a novel entropy-based cognitive activity recognition frameworks. Their prominent advantages from BCI perspective are: 1) They achieve better recognition performances, 2) They require much less computation time than previously proposed methods. On the other hand, more importantly, their methodological advantages are they aim to capture the timings of frequency-resolved brain oscillations that the provides the useful information for recognition of ongoing cognitive tasks.

In this chapter, we propose a time-sensitive feature extraction perspective for cognitive activity characterization as adopted in (J. Li et al. 2016). Our method considers the fact that the characteristic features of each cognitive activity are encoded in a particular temporal region of electrophysiological signals at each different spatial location and frequency band as in (Rezaie et al. 2011; S. M. Rao, Mayer, and Harrington 2001; X. Ma et al. 2020). The motivation behind adopting this perspective is based on the premise that the brain carries out information processing transiently and also, it performs information integration by establishing reciprocal synchronizations between its regions

for a short period of time. As a result, brain regions get involved in information integration mechanisms at different timings, which reveal activity-specific patterns for characterizing the ongoing brain activity (Schack, Weiss, and Rappelsberger 2003; Hari and Parkkonen 2015; Bayazit et al. 2009). As evidence, Mishuhina et al. stated that different cognitive tasks elicit different temporal patterns. According to this fact, they proposed a method that incorporates the temporal dynamics into a CSP-based motor imagery discrimination (Mishuhina and Jiang 2021). Similarly, Gao et al. used Kolmogorov entropy features to discriminate different motor imagery tasks between them. The authors used a short-live sliding window to calculate the entropies and fed them to a support vector machine classifier. They showed that the maximal discrimination is obtained for a short duration within the task period (L. Gao, Wang, and Chen 2013).

In that context, by using the training tasks, our method presented in this chapter captures the timings of relevant temporal regions where the activity-specific patterns emerged. Then, our method extracts these characteristic features for both training and test task periods by using these timings. The timing parameters that we determine for each activity type and channel are: Δt and w parameters denote the latency and duration of the signal segment where the activity-specific features are embedded, respectively. Please note that we determined the activity-specific timings by evaluating the entropies, which proves its efficiency in the previous brain-computer interface and neurological disorder studies (Güdücü et al. 2019; X. S. Zhang, Roy, and Jensen 2001; Emre Cek, Ozgoren, and Acar Savaci 2010; Bilal Orkan Olcay et al. 2017; Vivot et al. 2020; Román Baravalle, Rosso, and Montani 2018; L. Gao, Wang, and Chen 2013; Zeng et al. 2018; Abásolo et al. 2006; Kannathal et al. 2005). Briefly, entropy provides useful information about the complexity of the underlying dynamical process associated with the ongoing cognitive activities (Osvaldo A. Rosso 2007) and some neurophysiological disorders (Thul et al. 2016). An additional point is that the neural complexity is in correlation with the brain's functional connectivity (D. J. J. Wang et al. 2018b). These two different perspectives (i.e., complexity and functional connectivity) related to the information processing capacity of the brain. In this sense, McDonough et al. stated that the greater entropy is related to the greater neural activity complexity which possesses great potential for information processing especially at larger spatial scales (McDonough and Nashiro 2014). Previous studies have demonstrated that distinct pathological cases, as well as cognitive status, produce distinct nonlinear dynamics on physiological signals which can be detected by entropy measures (Labate et al. 2013; Zeng et al. 2018).

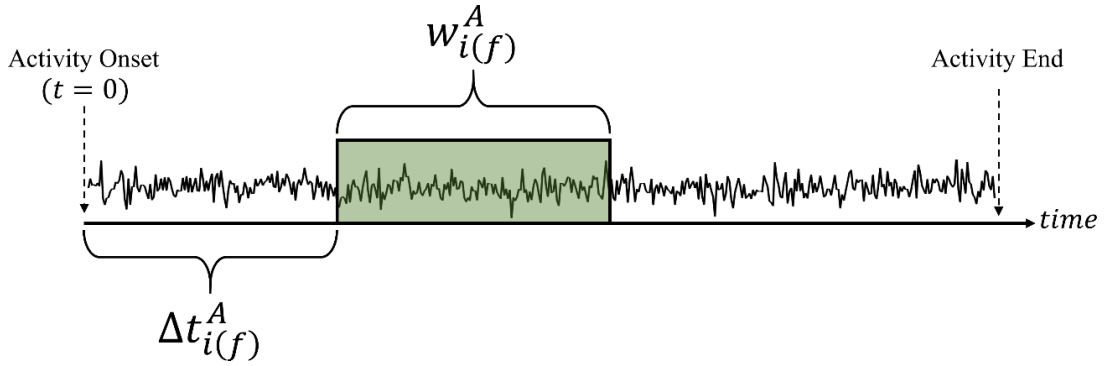

Figure 36. Illustration of activity-specific timings for activity *A* and channel *i* filtered by *f*. Note that $f \in \{f_1, f_2, \ldots, f_9\}$.

Our method adopts a heuristic optimization to determine the activity-specific timing parameter pairs (i.e., latency and duration) by evaluating the entropy calculated for each latency calculated for each channel and frequency band in a probabilistic manner as in (Lemm, Schäfer, and Curio 2004) and (Schalk et al. 2008). After the evaluations, the timings of the most significant entropy patterns were identified for each channel and frequency band. The graphical illustration of the timing parameter pairs (i.e., $\{\Delta t^A_{i(f)}, w^A_{i(f)}\}$) obtained for activity type A, channel i that was filtered by f were given in Figure 36.

Please note that, we will recall the EEG channel indexed by i that is filtered by f as channel $i(f)$ (as demonstrated in Figure 36) in the upcoming parts of this chapter. The remainder of this paper is organized as follows: In Section 6.2, we provided the details of the operational pipeline of the proposed framework and the details of capturing activity-specific timing parameter pairs. In Section 6.3, we presented the recognition performance as well as the comparative analysis results. In Section 6.4, we discuss the outcomes for the proposed framework. The final section concludes the chapter.

6.2. Proposed Method

The operational pipeline related to this proposed method is given in Figure 37. As the first step of the proposed cognitive activity characterization framework, we used a

filter bank structure with 9 finite-impulse-response (FIR) bandpass filters (S. H. Park, Lee, and Lee 2018; Ang et al. 2008). The cut-off frequencies and the names of each bandpass filter provided in Table 24.

Table 24. The frequency ranges and names of the filters used in FIR in the filter bank structure.

Filter Name	f_1	f_2	f_3	f_4	f_5	f_6	f_7	f_8	f_9
Cut-off Frequencies (Hz)	4-8	8-12	12-16	16-20	20-24	24-28	28-32	32-36	36-40

The main reason for using the FIR filter is to avoid the distortion of the activity-specific timings to be captured for each different frequency band due to the phase distortion effect during the filtering the EEG signals (Jian, Chen, and McFarland 2017). In our past study (B. Orkan Olcay and Karaçalı 2019), we filtered the EEG signals into 8-30 Hz band to obtain sensorimotor rhythms for connectivity analysis of motor imagery activities. Here, we divided the frequency spectrum into narrower frequency bands to obtain a better brain activity characterization performance as recommended in (Gysels, Renevey, and Celka 2005) since EEG dynamics associated with the cognitive tasks distributed across multiple frequency bands (Ang et al. 2008).

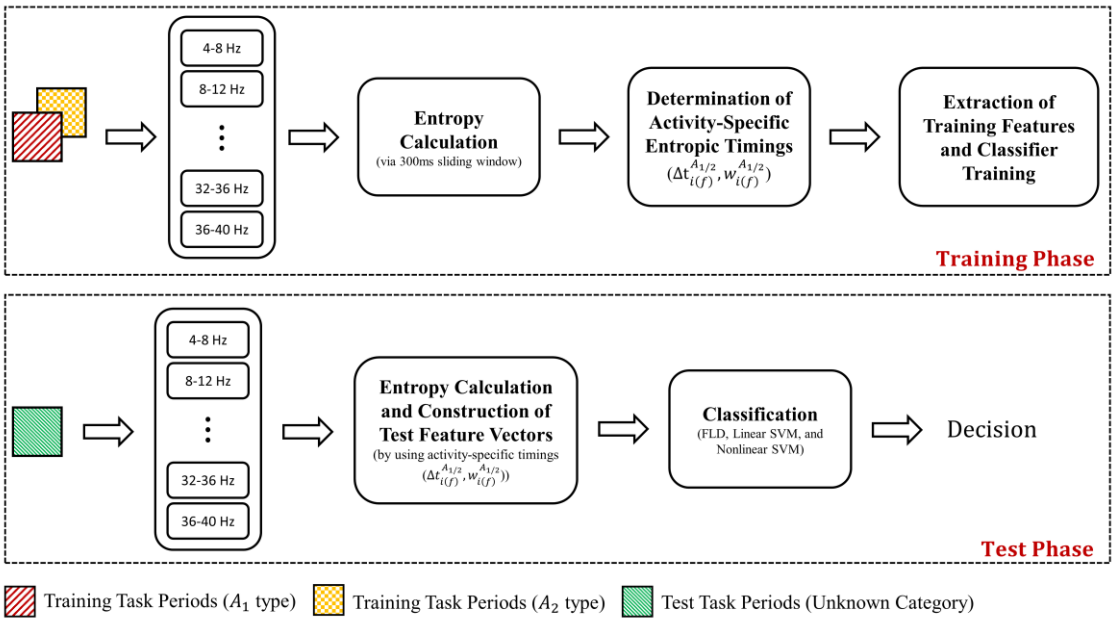

Figure 37. Illustration of flow diagram of the activity recognition framework.

In the training phase, we first filtered each channel of all the training task periods into nine distinct frequency bands (i.e., $f_1, \dots, f_9$) (please see Table 24 for the cut-off frequencies). Then, in the *Entropy Calculation* block, for each training task period ℓ and channel $i(f)$, we calculated the entropies of the signal segments that falls within the fixed-length sliding time window according to Δt parameter (please see Figure 38). Note that we set the length of the time window as 300ms as in (Bola, Gall, and Sabel 2015; Roelfsema et al. 1997). The entropy values calculated for each task period, latency and filtered channel can be expressed as

$$E_{i(f)}(\Delta t, \ell) = \widehat{H}\left(s_{i(f)}(t_\ell)|_{t_\ell \in [\Delta t,\ \Delta t+300ms]}\right) \tag{6.1}$$

where $\widehat{H}(\cdot)$ represents the entropy estimator, $E_{i(f)}(\Delta t, \ell)$ denotes the entropy value estimated for the signal segment, which is extracted from training task period ℓ, channel $i(f)$, that starts from Δt milliseconds from the activity onset (i.e., $t_\ell = 0$) and lasts for 300ms. Note that, we used Vasicek's bias-corrected estimation method when obtaining the entropies of the signal segments (Vasicek 1976; Ibrahim Al-Omari 2014). Also note

that, we maintained the entropy calculation by sliding the time window by an amount of one sample at each step starting from $\Delta t = 0ms$ (activity onset) to the $\Delta t = T - 300ms$ as illustrated in Figure 38. In here, T denotes the end time of the activity.

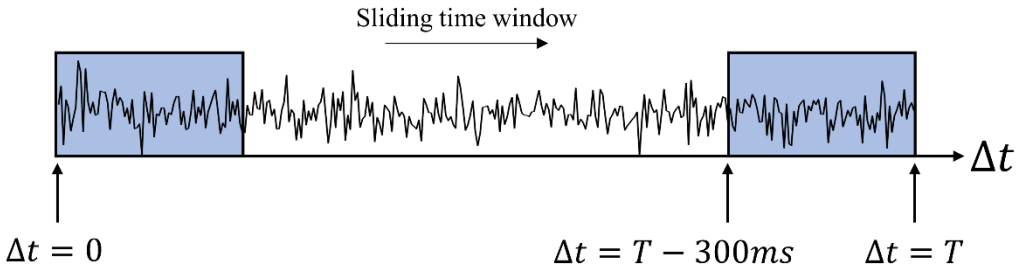

Figure 38. Demonstration of sliding time window used for calculating the entropies. Note that at each calculation step, we slide the window by an amount of one sample until the end of the window reaches the end of the task period.

In the *Determination of Activity-Specific Entropic Timings* block, we obtained the timing parameter pairs $\left(\text{i.e., } \left\{\Delta t_{i(f)}^{A_{1/2}}, w_{i(f)}^{A_{1/2}}\right\}\right)$ for each channel $i(f)$ and activity $A_{1/2}$ that addresses the signal segment which provides activity-specific entropy values. In the *Extraction of Training Features and Classifier Training* block, first, we constructed feature vector ξ_ℓ for each training task period ℓ by concatenating the entropies of the signal segments, which were extracted using the activity-specific timing parameter pairs, as

$$\xi_{\ell} = \begin{bmatrix} \widehat{H}\left(s_{1(f_1)}(t_{\ell})|_{t_{\ell}\in\left[\Delta t^{A_1}_{1(f_1)},\ \Delta t^{A_1}_{1(f_1)}+\mathrm{w}^{A_1}_{1(f_1)}\right]}\right) \\ \vdots \\ \widehat{H}\left(s_{1(f_9)}(t_{\ell})|_{t_{\ell}\in\left[\Delta t^{A_1}_{1(f_9)},\ \Delta t^{A_1}_{1(f_9)}+\mathrm{w}^{A_1}_{1(f_9)}\right]}\right) \\ \widehat{H}\left(s_{2(f_1)}(t_{\ell})|_{t_{\ell}\in\left[\Delta t^{A_1}_{2(f_1)},\ \Delta t^{A_1}_{2(f_1)}+\mathrm{w}^{A_1}_{2(f_1)}\right]}\right) \\ \vdots \\ \widehat{H}\left(s_{2(f_9)}(t_{\ell})|_{t_{\ell}\in\left[\Delta t^{A_1}_{2(f_9)},\ \Delta t^{A_1}_{2(f_9)}+\mathrm{w}^{A_1}_{2(f_9)}\right]}\right) \\ \vdots \\ \widehat{H}\left(s_{M(f_9)}(t_{\ell})|_{t_{\ell}\in\left[\Delta t^{A_1}_{M(f_9)},\ \Delta t^{A_1}_{M(f_9)}+\mathrm{w}^{A_1}_{M(f_9)}\right]}\right) \\ \widehat{H}\left(s_{1(f_1)}(t_{\ell})|_{t_{\ell}\in\left[\Delta t^{A_2}_{1(f_1)},\ \Delta t^{A_2}_{1(f_1)}+\mathrm{w}^{A_2}_{1(f_1)}\right]}\right) \\ \vdots \\ \widehat{H}\left(s_{1(f_9)}(t_{\ell})|_{t_{\ell}\in\left[\Delta t^{A_2}_{1(f_9)},\ \Delta t^{A_2}_{1(f_9)}+\mathrm{w}^{A_2}_{1(f_9)}\right]}\right) \\ \widehat{H}\left(s_{2(f_1)}(t_{\ell})|_{t_{\ell}\in\left[\Delta t^{A_2}_{2(f_1)},\ \Delta t^{A_2}_{2(f_1)}+\mathrm{w}^{A_2}_{2(f_1)}\right]}\right) \\ \vdots \\ \widehat{H}\left(s_{2(f_9)}(t_{\ell})|_{t_{\ell}\in\left[\Delta t^{A_2}_{2(f_9)},\ \Delta t^{A_2}_{2(f_9)}+\mathrm{w}^{A_2}_{2(f_9)}\right]}\right) \\ \vdots \\ \widehat{H}\left(s_{M(f_9)}(t_{\ell})|_{t_{\ell}\in\left[\Delta t^{A_2}_{M(f_9)},\ \Delta t^{A_2}_{M(f_9)}+\mathrm{w}^{A_2}_{M(f_9)}\right]}\right) \end{bmatrix} \tag{6.2}$$

where M denotes the number of channels (i.e., for PhysioNet dataset $M = 64$, and for BCI Competition-III dataset IVa $M = 118$). Next, we trained the classifier to obtain minimum classification error on the training feature vectors.

In the test phase, we initially filtered each channel of each test task period by using the filter bank. Thereafter, in the *Entropy Calculation and Construction of Test Feature Vectors* block, we calculated the entropies of the signal segments extracted from each filtered channel using corresponding activity-specific timings obtained in the training phase. Next, for each test task period, we concatenated these entropy values into a column vector form as

$$\xi = \begin{bmatrix} \widehat{H}\left(s_{1(f_1)}(\dot{t})|_{\dot{t}\in\left[\Delta t_{1(f_1)}^{A_1},\ \Delta t_{1(f_1)}^{A_1}+\mathrm{w}_{1(f_1)}^{A_1}\right]}\right) \\ \vdots \\ \widehat{H}\left(s_{1(f_9)}(\dot{t})|_{\dot{t}\in\left[\Delta t_{1(f_9)}^{A_1},\ \Delta t_{1(f_9)}^{A_1}+\mathrm{w}_{1(f_9)}^{A_1}\right]}\right) \\ \widehat{H}\left(s_{2(f_1)}(\dot{t})|_{\dot{t}\in\left[\Delta t_{2(f_1)}^{A_1},\ \Delta t_{2(f_1)}^{A_1}+\mathrm{w}_{2(f_1)}^{A_1}\right]}\right) \\ \vdots \\ \widehat{H}\left(s_{2(f_9)}(\dot{t})|_{\dot{t}\in\left[\Delta t_{2(f_9)}^{A_1},\ \Delta t_{2(f_9)}^{A_1}+\mathrm{w}_{2(f_9)}^{A_1}\right]}\right) \\ \vdots \\ \widehat{H}\left(s_{M(f_9)}(\dot{t})|_{\dot{t}\in\left[\Delta t_{M(f_9)}^{A_1},\ \Delta t_{M(f_9)}^{A_1}+\mathrm{w}_{M(f_9)}^{A_1}\right]}\right) \\ \widehat{H}\left(s_{1(f_1)}(\dot{t})|_{\dot{t}\in\left[\Delta t_{1(f_1)}^{A_2},\ \Delta t_{1(f_1)}^{A_2}+\mathrm{w}_{1(f_1)}^{A_2}\right]}\right) \\ \vdots \\ \widehat{H}\left(s_{1(f_9)}(\dot{t})|_{\dot{t}\in\left[\Delta t_{1(f_9)}^{A_2},\ \Delta t_{1(f_9)}^{A_2}+\mathrm{w}_{1(f_9)}^{A_2}\right]}\right) \\ \widehat{H}\left(s_{2(f_1)}(\dot{t})|_{\dot{t}\in\left[\Delta t_{2(f_1)}^{A_2},\ \Delta t_{2(f_1)}^{A_2}+\mathrm{w}_{2(f_1)}^{A_2}\right]}\right) \\ \vdots \\ \widehat{H}\left(s_{2(f_9)}(\dot{t})|_{\dot{t}\in\left[\Delta t_{2(f_9)}^{A_2},\ \Delta t_{2(f_9)}^{A_2}+\mathrm{w}_{2(f_9)}^{A_2}\right]}\right) \\ \vdots \\ \widehat{H}\left(s_{M(f_9)}(\dot{t})|_{\dot{t}\in\left[\Delta t_{M(f_9)}^{A_2},\ \Delta t_{M(f_9)}^{A_2}+\mathrm{w}_{M(f_9)}^{A_2}\right]}\right) \end{bmatrix} \tag{6.3}$$

In the *Classification* block, we determined the category of each test feature vector by using the classifier trained in a supervised manner in the training phase.

6.2.1. Determination of Activity-Specific Entropic Timings

In order to determine the activity-specific timing parameter pairs for each activity type and each channel $i(f)$, we adopted a heuristic optimization method which is described below. In the first step, we obtained the entropy values (i.e., $E_{i(f)}(\Delta t, \ell)$) for each latency (Δt), training task period (ℓ) and channel ($i(f)$) by using the Eq. (6.1). Next, we leaved one training task period out and we calculated the mean $\mu_{i(f)}^{A_{1/2}}(\Delta t)$ and variance $v_{i(f)}^{A_{1/2}}(\Delta t)$ of the entropy values across the remaining training task periods as

$$\mu_{i(f)}^{A_{1/2}}(\Delta t) = \frac{1}{\left|i_{A_{1/2}}\right|}\sum_{k\in i_{A_{1/2}}} E_{i(f)}(\Delta t, k)$$
$$v_{i(f)}^{A_{1/2}}(\Delta t) = \frac{1}{\left|i_{A_{1/2}}\right| - 1}\sum_{k\in i_{A_{1/2}}} \left(E_{i(f)}(\Delta t, k) - \mu_{i(f)}^{A_{1/2}}(\Delta t)\right)^2 \quad (6.4)$$

where $i_{A_{1/2}}$ represents the indices of the remaining training task periods of $A_{1/2}$ which systematically changes at each leave-one-out cycle, $|\cdot|$ denotes the cardinality of the set. Note that the mean and variance values were calculated for each latency Δt, each channel $i(f)$, and each activity type. We then used the mean and variance parameters to calculate the likelihood of the entropy values obtained for the latency Δt and channel $i(f)$ of the excluded training task period by adopting Gaussianity as in (Schalk et al. 2008)

$$p\left(E_{i(f)}(\Delta t, x)\middle|A_1\right) = \frac{1}{\sqrt{2\pi v_{i(f)}^{A_1}(\Delta t)}}\exp\left\{-\frac{\left(E_{i(f)}(\Delta t, x) - \mu_{i(f)}^{A_1}(\Delta t)\right)^2}{2v_{i(f)}^{A_1}(\Delta t)}\right\}$$
$$p\left(E_{i(f)}(\Delta t, x)\middle|A_2\right) = \frac{1}{\sqrt{2\pi v_{i(f)}^{A_2}(\Delta t)}}\exp\left\{-\frac{\left(E_{i(f)}(\Delta t, x) - \mu_{i(f)}^{A_2}(\Delta t)\right)^2}{2v_{i(f)}^{A_2}(\Delta t)}\right\} \quad (6.5)$$

where x represents the index of the excluded training task period in the leave-one-out cycle. Next, we calculated the posterior probability of the entropy value calculated for latency Δt and channel $i(f)$ of the excluded training task period as

$$p\left(A_1\middle|E_{i(f)}(\Delta t, x)\right) = \frac{p\left(E_{i(f)}(\Delta t, x)\middle|A_1\right)\cdot p(A_1)}{p\left(E_{i(f)}(\Delta t, x)\middle|A_1\right)\cdot p(A_1) + p\left(E_{i(f)}(\Delta t, x)\middle|A_2\right)\cdot p(A_2)} \quad (6.6)$$

and

$$p\left(A_2\middle|E_{i(f)}(\Delta t,x)\right) = \frac{p\left(E_{i(f)}(\Delta t,x)\middle|A_2\right)\cdot p(A_2)}{p\left(E_{i(f)}(\Delta t,x)\middle|A_1\right)\cdot p(A_1)+p\left(E_{i(f)}(\Delta t,x)\middle|A_2\right)\cdot p(A_2)} \quad (6.7)$$

where $p\left(A_1\middle|E_{i(f)}(\Delta t,x)\right)$ and $p\left(A_2\middle|E_{i(f)}(\Delta t,x)\right)$ are the posterior probabilities, $p(A_1)$ and $p(A_2)$ are the prior probabilities. It is important to note that, we repeated these calculations until each training task period excluded once. Please note that calculating and using the posterior probabilities help us to find the temporally non-overlapping brain oscillation segments, which provide task-specific entropy values, for each filtered channel.

Since we know the categories of each task period in the training set, we can safely calculate the mean of these posterior probabilities obtained for each training periods that belongs to a specific category ($A_{1/2}$). The mean of the posterior probabilities $p\left(A_1\middle|E_{i(f)}(\Delta t,x)\right)$ calculated for the excluded task periods $x \in I_{A_1}$ as

$$MP_{i(f)}^{A_1}(\Delta t) = \frac{1}{\left|I_{A_1}\right|}\sum_{x\in I_{A_1}} p\left(A_1\middle|E_{i(f)}(\Delta t,x)\right) \quad (6.8)$$

And also, the mean of the posterior probabilities $p\left(A_2\middle|E_{i(f)}(\Delta t,x)\right)$ calculated for the excluded task periods $x \in I_{A_2}$ as

$$MP_{i(f)}^{A_2}(\Delta t) = \frac{1}{\left|I_{A_2}\right|}\sum_{x\in I_{A_2}} p\left(A_2\middle|E_{i(f)}(\Delta t,x)\right) \quad (6.9)$$

where $MP_{i(f)}^{A_{1/2}}(\Delta t)$ denotes the mean posterior probability for the latency Δt and channel $i(f)$ calculated across posterior probabilities of corresponding training task periods.

After obtaining the mean posterior probabilities (i.e., $MP_{i(f)}^{A_1}(\Delta t)$ and $MP_{i(f)}^{A_2}(\Delta t)$), we compared the entries of these mean posterior probabilities with a threshold. We set the threshold as 0.5 since we are dealing with a two-class recognition problem. Afterwards, we used the entropy patterns that exceed the threshold for further analysis (please see Figure 39).

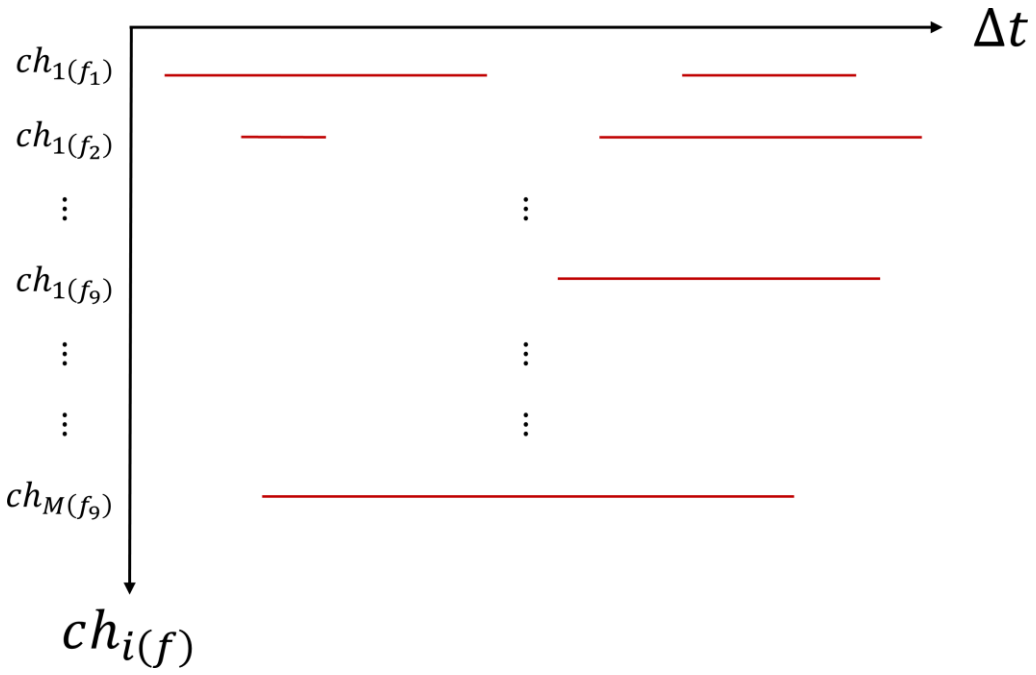

Figure 39. An exemplary illustration of entropy patterns that exceeded the threshold 0.5.

For some of the filtered channels (i.e., $i(f)$), we did not elicit any entropy pattern that exceeded the threshold value. In such a case, we did not use any feature of this filtered channel in the classification. We also encountered another important case, where we observed multiple entropy patterns along the Δt axis for some of filtered channels. In this circumstances, we first obtained the timings of each entropy pattern as demonstrated in Figure 40.

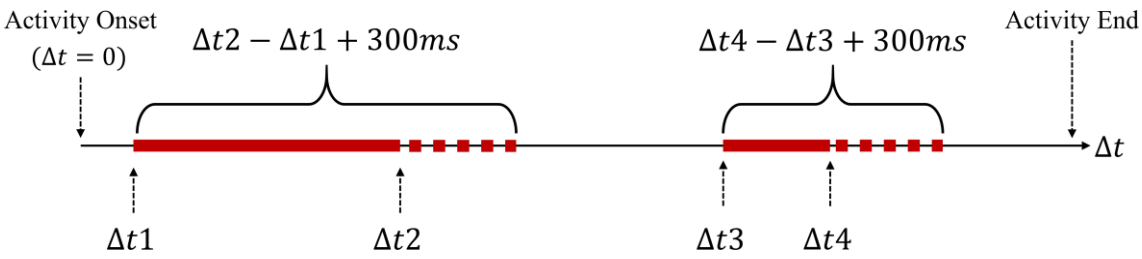

Figure 40. Obtaining the timings of the candidate entropy patterns. The timings of first candidate entropy pattern are $\{\Delta t, w\} = \{\Delta t1, \Delta t2 - \Delta t1 + 300ms\}$, and the timings of second pattern are $\{\Delta t, w\} = \{\Delta t3, \Delta t4 - \Delta t3 + 300ms\}$.

We then conducted unpaired two-tailed t-tests to determine the most significant (i.e., activity-specific) one. To that end, we used the timing parameter pairs of each entropy pattern to calculate the entropy values of both type of cognitive activities for the t-test evaluation. As a result of t-test, the entropy pattern which revealed the highest significance (i.e., lowest P-value) was identified as the activity-specific entropy pattern for the corresponding filtered channel. Thus, we used the timing parameter pairs of this entropy pattern as activity-specific timing parameter pair for cognitive task characterization (please see Figure 41).

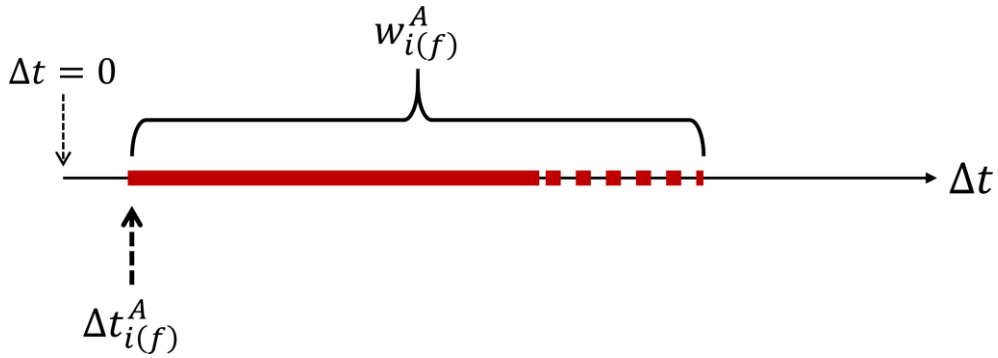

Figure 41. Illustration of entropy pattern (continuous red line) and related timing parameter pairs that achieved highest significance as a result of statistical evaluation. Note that the timings of other patterns were not used throughout this study.

6.2.2. Comparative Analysis

For a performance comparison, we used two different methods that were mainly adopted in BCI frameworks. The first method is common spatial patterns (CSP) method which simply finds a linear transformation for multichannel electrophysiological signals to calculate discriminative features (Ramoser, Müller-Gerking, and Pfurtscheller 2000; Blankertz et al. 2008). For the CSP method, we first filtered the signals into 8-30 Hz band via FIR bandpass filter. Then, we calculated the CSP filter ($m = 3$) from the training task periods. We applied the CSP filter to both training and test task periods and calculated log-variance features for task period characterization.

The second method is a wavelet-based method that was successfully used in (Khalaf, Sejdic, and Akcakaya 2019). We used this method with some slight modifications. First, we calculated the wavelet transform and thus scalograms of each task period and channel by using the complex Morlet wavelet, which is the most preferred mother wavelet function for biological data analysis (Alexander E. Hramov et al. 2015; Makarov et al. 2018). Next, for each task period and channel, we summed each scalogram that falls into the frequency bands $f_1, f_2, \dots, f_9$ separately which means we obtained $9 \times N$ dimensional scalograms for each channel and task period. Finally, we calculated *mean*, *variance*, *skewness*, and *kurtosis* features using N scalograms obtained for each frequency band. For each channel, we obtained $4 \times 9 = 36$ features. We concatenated the 36 features obtained for each channel to form a feature vector with $(36xM)x1$ dimensions to characterize each task period.

6.3. Results

We tested our recognition framework by adopting two chronological cross-validation scenarios (i.e., Scenario-1 and Scenario-2) as adopted in previous chapter and in (B. Orkan Olcay and Karaçalı 2019). Please note that, before the classification, we adopted a feature selection procedure to select the most informative features. To that end, we used the Fisher's ratio based method as in previous chapters.

We presented the average classification performances obtained from BCI Competition-III dataset IVa and the PhysioNet Motor Movement/Imagery datasets in Table 25. Also, we presented the classification performances of the features, that were calculated using the corresponding timing parameter pairs, obtained from the channels that were used for motor imagery activity recognition in the past studies (Morash et al. 2008; Q. Wei et al. 2007; Krusienski, McFarland, and Wolpaw 2012). Morash et al. used 29 channels (i.e., FC1, FC3, FC5, C1, C3, C5, FC2, FC4, FC6, C2, C4, C6, CP1, CP3, CP5, P1, P3, P5, CP2, CP4, CP6, P2, P4, P6, Fz, FCz, Cz, CPz, Pz) that contains the parietal, central, centro-parietal, and frontal channels for characterization of right/left hand, right foot, and tongue imagery movements (Morash et al. 2008). Wei et al. tested 3 different electrode clusters for calculating the connectivity-based features for motor imagery activity recognition. We used the Fz, C3, and C4 and their nearest neighbors (i.e., named as *CB2* channels), which elicited the best classification performance in (Q. Wei et al. 2007). Finally, we used the 9 electrodes (i.e., T7, F3, C3, P3, Cz, F4, C4, P4, T8) as used by Krusienski et al. in a PLV-based motor imagery recognition study (Krusienski, McFarland, and Wolpaw 2012). Note that, these channels in our study, which are mainly located at the sensorimotor, primary motor, and frontal regions, which are known to be strongly related to motor movement/imagery activities. Since the electrodes used in three different studies collects electrical activity mainly from motor imagery-related brain regions, we used the frequency bands $f_2 = [8 \quad 12]$ Hz, $f_3 = [12 \quad 16]$ Hz, $f_4 = [16 \quad 20]$ Hz, $f_5 = [20 \quad 24]$ Hz, $f_6 = [24 \quad 28]$ Hz, and $f_7 = [28 \quad 32]$ Hz that which are mainly involved in the motor imagery activity-related frequency band (Yuan and He 2014). We also compared the performance of the proposed method with the performances of two motor imagery activity recognition method (Blankertz et al. 2008; Khalaf, Sejdic, and Akcakaya 2019). The average performances of these methods were presented in Table 26. Note that we applied the similar feature selection method to the feature vectors obtained from wavelet-based method.

In order to determine the significance of the parameters that we captured during the training phase, we conducted a statistical analysis on the entropy values, which we calculated from the signal segments by applying activity-specific timings of all channels belong to both corresponding and contending activities. To be clearer, we applied $\left\{\Delta t_{i(f)}^{A_{1/2}}, w_{i(f)}^{A_{1/2}}\right\}$ parameters to both corresponding and contending training task periods. Next, we calculated the entropies of these signal segments. Finally, we conducted

unpaired two-tailed t-tests on these entropy values to determine the significance of the distinctiveness of entropies obtained via timing parameters $\left\{\Delta t_{i(f)}^{A_{1/2}}, w_{i(f)}^{A_{1/2}}\right\}$. As a result of t-tests, we obtained a P-value for each activity-specific timing parameter pairs. The aim of this statistical analysis is to show that the extracted entropic features using $A_{1/2}$ activity timing parameter pairs are more significant than the features extracted using similar timing parameters for another type of task periods. Please note that, we repeated this statistical analysis for each subject, for each filtered channel and each activity type. In Tables 27 and 28, we demonstrated the geometric means of the P-values of the most significant five filtered channels calculated across the subjects that we used in this study. Note that, prior to the geometric mean calculation, we corrected the P-values via Benjamini-Hochberg method to avoid from type-I errors (Benjamini and Hochberg 1995).

We also obtained the most selected features, which determined via the Fisher ratio method, across 5 subjects for BCI Competition-III dataset IVa, and across first 20 subject for PhysioNet Motor Movement/Imagery datasets. For the BCI Competition-III dataset IVa, the most selected five entropic features were derived from C3 (8-12 Hz), Fz (12-16 Hz), FC1 (12-16 Hz), CP3 (12-16 Hz), and C3 (20-24 Hz) channels. For the PhysioNet Motor Movement/Imagery dataset, the most selected five entropy features are from F7 (12-16 Hz), FCz (12-16 Hz), CP4 (24-28 Hz), CP6 (20-24 Hz), and AFz (24-28 Hz) channels.

Table 25. The average performance of the proposed recognition method calculated across 5 subjects for BCI Competition-III dataset IVa and across the first 20 subjects for PhysioNet Motor Movement/Imagery datasets. We also calculated the recognition performances for the 3 different channel sets that were used in previous motor imagery activity recognition studies (Morash et al. 2008; Q. Wei et al. 2007; Krusienski, McFarland, and Wolpaw 2012).

		Scenario-1 Performances (%)			**Scenario-2 Performances (%)**		
		FLD	**Linear SVM**	**Nonlinear SVM**	**FLD**	**Linear SVM**	**Nonlinear SVM**
BCI Comp.-IIIdataset IVa	**Fisher's Ratio**	62.23 ± 8.74	75.74 ± 12.39	79.46 ± 11.27	80.65 ± 9.33	85.0 ± 7.96	80.86 ± 10.32
	Morash et al. (Morash et al. 2008)	75.1 ± 11.82	78.82 ± 12.69	76.38 ± 11.78	68.69 ± 9.45	80.65 ± 9.7	78.69 ± 12.04
	Wei et al. (Q. Wei et al. 2007)	69.04 ± 10.11	71.91 ± 11.69	74.04 ± 13.45	61.95 ± 5.85	76.95 ± 12.87	77.6 ± 12.59
	Krusienski et al. (Krusienski, McFarland, and Wolpaw 2012)	60.63 ± 5.26	73.29 ± 15.3	73.51 ± 11.94	73.26 ± 13.05	75.86 ± 12.42	75.86 ± 14.0
PhysioNet Motor Movement/Imagery	**Fisher's Ratio**	54.0 ± 9.34	53.33 ± 7.87	51.83 ± 9.39	60.67 ± 11.0	62.0 ± 14.03	65.0 ± 13.99
	Morash et al. (Morash et al. 2008)	57.67 ± 13.38	57.5 ± 13.71	55.33 ± 11.51	58.0 ± 19.47	56.67 ± 18.79	55.33 ± 17.31
	Wei et al. (Q. Wei et al. 2007)	56.33 ± 8.97	56.0 ± 8.69	56.33 ± 10.36	55.67 ± 14.39	56.33 ± 15.81	56.0 ± 14.73
	Krusienski et al. (Krusienski, McFarland, and Wolpaw 2012)	52.33 ± 6.22	53.83 ± 6.14	52.83 ± 6.60	58.67 ± 13.95	60.0 ± 14.98	57.0 ± 15.81

Table 26. The demonstration of average performances of our method and the CSP method.

		Scenario-1 Performances (%)			Scenario-2 Performances (%)		
		Our Method	**CSP** ($m = 3$)	**Wavelet-Based Method**	**Our Method**	**CSP** ($m = 3$)	**Wavelet-Based Method**
BCI Comp.-IIIdataset IVa	**FLD**	62.23 ± 8.74	82.33 ± 11.46	70.31 ± 8.51	80.65 ± 9.33	84.67 ± 15.38	65.0 ± 14.36
	Linear SVM	75.74 ± 12.39	80.0 ± 11.45	76.38 ± 10.91	85.0 ± 7.96	83.91 ± 17.33	81.08 ± 13.63
	Nonlinear SVM	79.46 ± 11.27	82.12 ± 12.61	68.82 ± 10.87	80.86 ± 10.32	84.13 ± 18.23	73.69 ± 13.77
PhysioNet Motor Imagery	**FLD**	54.0 ± 9.34	53.83 ± 4.87	57.25 ± 9.05	60.67 ± 11.0	55.65 ± 9.97	59.67 ± 12.88
	Linear SVM	53.33 ± 7.87	57.66 ± 14.11	59.51 ± 8.84	62.0 ± 14.03	62.88 ± 15.91	64.0 ± 14.24
	Nonlinear SVM	51.83 ± 9.39	60.11 ± 14.0	57.74 ± 9.81	65.0 ± 13.99	64.0 ± 16.47	64.33 ± 14.39

Table 27. The most significant five filtered channels for each activity type for BCI Competition-III dataset IVa (Scenario-2).

Right Foot Motor Imagery			**Right Hand Motor Imagery**		
Channel	**Freq.**	***P*-value**	**Channel**	**Freq.**	***P*-value**
CP3	12-16 Hz	$< 10^{-3}$	CP3	12-16 Hz	$< 10^{-3}$
PCP3	12-16 Hz	$< 10^{-3}$	PCP3	12-16 Hz	$< 10^{-3}$
CCP3	12-16 Hz	$< 10^{-3}$	CCP3	12-16 Hz	$< 10^{-3}$
CCP6	12-16 Hz	$< 10^{-3}$	CCP5	12-16 Hz	$< 10^{-3}$
CCP5	12-16 Hz	$< 10^{-3}$	CCP6	12-16 Hz	$< 10^{-3}$

Table 28. The most significant five filtered channels for each activity type for PhysioNet Motor Movement/Imagery dataset (Scenario-2)

Left Fist Motor Imagery			**Right Fist Motor Imagery**		
Channel	**Freq.**	***P*-value**	**Channel**	**Freq.**	***P*-value**
P3	12-16 Hz	0.06	P3	12-16 Hz	0.0567
F8	8-12 Hz	0.091	FT8	12-16 Hz	0.0714
Cz	8-12 Hz	0.095	Cz	8-12 Hz	0.0901
FT8	12-16 Hz	0.097	F8	8-12 Hz	0.103
P7	8-12 Hz	0.110	POz	12-16 Hz	0.104

6.4. Discussion

In this study, our main aim is to develop an analytic strategy to identify task-dependent discriminative spatio-temporal entropic features which they emerged and vanished in a short period of time (Mišić and Sporns 2016). To that end, we developed a method to capture and use the timing parameter pairs, which addresses signal segments which elicits the activity-specific entropy values, for different spatial and also spectral regions. We adopted a heuristic search strategy to capture the activity-specific timing parameter pairs. At the final step, we conduct classification analysis on two publicly available motor imagery EEG dataset to evaluate the performance of our proposed method. We discuss the findings related to the proposed method below.

6.4.1. Performance Comparison

The performance results presented in Table 25 show that, especially for the BCI Competition-III dataset IVa, the performance of our method exceeded the minimum reliable communication rate (i.e., 70%) which means our method can reliably recognize the ongoing cognitive activity (Ahn and Jun 2015). For the PhysioNet dataset, however, our method did not exceed the 70% performance. There are several reasons for this unexpected performance results. The first reason is that the PhysioNet dataset contains only 30 training task periods (for training phase in scenario-2) which is extremely low for capturing the activity-specific timing parameter pairs and also, for classifier training accurately. Another reason is that the PhysioNet dataset may be collected from BCI-naïve (or BCI illiterate) subjects since the mind of the BCI experts is more focused on the directives given for imagery tasks to be done (Ahn and Jun 2015; Milton et al. 2007). The third reason may be the low signal-to-noise ratio of the PhysioNet dataset. In the literature, the successful BCI studies that used the PhysioNet dataset applied independent component analysis-based methods to each task period to remove the non-neural signal components (Varsehi and Firoozabadi 2021). For our method, it may be beneficial to use some statistical noise subspace filtering methods to unveil the accurate activity-specific timing parameter pairs and thus, motor imagery related brain patterns (Hyvärinen and Oja

2000; Von Bünau et al. 2009; Haykin and Widrow 2005). Another important thing is that, when comparing the performances with other methods using PhysioNet dataset is that (B. Orkan Olcay and Karaçalı 2019), the majority of conspicuous motor imagery recognition studies that uses PhysioNet dataset adopted performance elimination criteria when evaluating their methods (Handiru and Prasad 2016; Athif and Ren 2019; Kim et al. 2016; Cheolsoo Park, Took, and Mandic 2014) according to (Müller-Putz et al. 2007). Please note that we did not adopt a performance elimination criteria when presenting our results. An additional note for performances of PhysioNet dataset is that the training and test sessions conducted with task periods from different sessions. This may cause performance degradation in activity recognition since session-to-session variability of brain dynamics significantly affects the recognition performances (Saha et al. 2018b). For observing the exact recognition performance of our method especially on PhysioNet dataset, different cross-validation approaches (such as *N-fold* cross-validation) can be adopted.

We compared the performance of the proposed brain activity characterization method with two popular benchmark BCI methods, CSP and a wavelet-based method. The average performances in Table **26** (in scenario-2) show that on the average, our method achieved 85% performance while CSP achieved 83.91% and wavelet based method achieved 81.08% with linear SVM. For the PhysioNet dataset, on the average, our method achieved a performance as 65% when CSP achieved maximum 64% and wavelet-based method achieved 64.33% performance with nonlinear SVM classifier on the average. These results indicate that our method can characterize the motor imagery task periods better than the benchmark method in a case when the number of training samples increases, which enables capturing accurate activity-specific timings when the number of training task periods increases.

Finally, we evaluated the average performances of our method using the entropy values as features obtained from the sensorimotor rhythm frequencies (i.e., $f_2, f_3, \dots, f_7$) and the channels that was used previously in motor imagery-related studies which is provided in Table 25. Especially in scenario-2, the performance results shows that, not only motor imagery-related channels and frequencies (i.e., 8-30 Hz) but also the other brain regions and frequency bands are take place in coordinating/organizing the motor imagery-related brain dynamics (Grosse-Wentrup, Schölkopf, and Hill 2011; Başar et al. 1999).

6.4.2. Relevant Channels and Frequencies Used for Recognition

We identified the channels and corresponding frequency bands that were mostly selected as features according to their Fisher ratio. For BCI Competition-III dataset IVa, the most selected five channels are mainly collected electrophysiological activities from primary motor, sensorimotor, and premotor cortices which are known to be involved in generation of motor imagery-related brain dynamics (Halder et al. 2011; Xu et al. 2014; Q. Gao, Duan, and Chen 2011; Hanakawa 2016; Hétu et al. 2013). For the PhysioNet dataset, the most selected five channels are located on the central, frontal, and parietal regions of the brain which are also important regions for motor imagination as pointed out above for BCI Competition-III dataset IVa. More importantly, the most selected channels for the PhysioNet dataset are exactly same or very close to the channels that was selected in a previous study (Varsehi and Firoozabadi 2021). One important thing is that the significant electrodes on the frontal and fronto-temporal regions obtained in our study has not been frequently observed in the past motor imagery related studies. On the contrary to the majority of literature, some important studies that highlight the significance of the frontal electrodes, which are indicated as important nodes of central-executive (CEN) and default mode (DMN) networks, during attention increase and preparation stages for motor tasks (C. F. Lu et al. 2011).

The results obtained from the proposed methods not only considers the sensorimotor related frequencies and sensorimotor/motor related channels but also the other brain regions and frequency bands. From these results, it can be inferred that the majority of brain regions take place for coordinating/organizing the motor imagery-related brain dynamics (Grosse-Wentrup, Schölkopf, and Hill 2011; Başar et al. 1999). We demonstrated the channels and frequency bands, where the top five statistically significant entropic features are found, in Tables 24 and 25. These tables show that, for each activity types, we found similar channels and frequency bands as significant. This result points that, thanks to using the posterior probabilities, the parameter pairs captured for different activities are well-separated from each other in time domain. This inference, if this is the case, indicates that for each cognitive activity, the brain encodes the task-related neural information into the electrophysiological activity according to a systematic timing organization.

The frequency bands in which the salient features are calculated are mainly found in the range of μ and β bands. These findings are in consistent with the previous biophysical findings which stresses the importance (in both local and global properties) of these frequency bands and their respective roles in motor imagery tasks (Román Baravalle, Rosso, and Montani 2018; Athanasiou et al. 2018; Friedrich, Scherer, and Neuper 2012; Yuan and He 2014; G Pfurtscheller et al. 1997; C. Neuper and Pfurtscheller 2001; Christa Neuper et al. 2009a; G. Pfurtscheller and Solis-Escalante 2009), and in different mental tasks (D. Huang et al. 2016). The significance of μ band, which showed pronounced hemispheric asymmetry in task-related brain patterns, was illustrated in previous BCI studies which plays a crucial role peculiar to the source allocation for internal attention increase for cognition, imagination or working memory tasks (Roman Baravalle et al. 2019; Christa Neuper et al. 2009b; Pineda 2005). It was also shown that the functional connectivity between motor-related areas and the rest of the brain within the μ band directly affects both the motor imagery as well as behavioral task performance (Mottaz et al. 2015). Also, the prominent roles and generating methods of β oscillations within motor-related regions have been described in recent studies (Khanna and Carmena 2015). Another role of the β oscillations is to bind the motor-related remote brain regions together for motor task-related information integration (Canolty et al. 2010; C. F. Lu et al. 2011), and it indicates the capacity/health of cognitive function (Santos Toural, Montoya Pedrón, and Marañón Reyes 2021).

We demonstrated that using only the sensorimotor rhythms and sensorimotor cortex channels did not provide a classification performance as high as obtained when using all brain regions and frequencies. As evidence, it was observed that the complexity changes due to the cognitive tasks were observed at distributed cortical regions (Micheloyannis et al. 2003). On important thing we should emphasize, although it did not appear as significant, the frontal theta rhythm may carry a piece of information related to the cognitive task performed by subjects since it was demonstrated that frontal theta rhythm demonstrates a negative correlation with the activity of the default mode network (Scheeringa et al. 2008; 2009).

Although the majority of the relevant channels found via the Fisher ratio method are consistent with the current biophysical studies (Hardwick et al. 2018), they might fall at odds with some other existing BCI studies. These negligible deviations might be due to the feature type that we used to characterize the neural activity. A similar observation was pointed in previous literature, in which during right/left hand motor imagery tasks,

the selected band power and autoregressive (i.e., reflection coefficients) features via sequential float forward selection (SFFS) method showed significant deviations in terms of the EEG channels that they derived from (Dyson, Sepulveda, and Gan 2010).

In this study, we used nine different FIR filters to decompose the EEG signals in a spectral manner. It should be noted that not only the frequency ranges upper than 4 Hz, but lower frequency ranges may also contain significant information related to the accomplished task. As future research, besides these frequencies used here (Ang et al. 2008), analyzing the lower frequency such as 0.1-5 Hz, at which the slow cortical oscillations are found, for activity-specific features and using them may improve the characterization performance (Salyers, Dong, and Gai 2019).

6.4.3. Importance of Considering Timing Parameters

The importance of the time-sensitive feature analysis was highlighted in previous EEG classification studies. These studies demonstrated that temporal analysis of electrophysiological activities are required for effective characterization brain activity (Ince, Tewfik, and Arica 2007; Ince et al. 2009; Firat Ince, Arica, and Tewfik 2006; Daly, Nasuto, and Warwick 2012; Karamzadeh et al. 2013; Ren et al. 2017; J. Li et al. 2016). Along with this fact, several studies aim to find an activity-specific short-lived time segment that contains the most relevant localized features (Yu Zhang et al. 2019; Ang et al. 2012; J. Wang et al. 2018; Hsu et al. 2007; Feng et al. 2018). These approaches, however, use a fixed-length time window (in general, 1 or 2 seconds) with an assumption that characteristic features are embedded in a time window no longer than 1-2 seconds. Also, they assume that task-related short-lived patterns of all regions of the brain emerge/vanish at the same time with each other, which means there are no differences in timings that the characteristic brain patterns emerged and vanished at each brain region. On the contrary, in our previous study, we observed that the characteristic inter-regional brain synchrony patterns are emerges at different timings for each different brain region pairs for different cognitive tasks (B. Orkan Olcay and Karaçalı 2019).

Please keep in mind that, our method captures the time segments where the task-specific and also discriminative entropy patterns emerge. In that context, one of the main contribution of the method presented here is that it can easily be used for multiclass

cognitive task classification. It may be possible that, for the multiclass classification, the actual task-specific neural activity segments lasts longer than the patterns captured in this situation. Even in that case, our method can capture the task-specific temporal segments where the characteristic entropy patterns are emerged. For a future research, it may be beneficial to capture activity-specific timing parameter pairs by evaluating the entropy patterns of task periods and idling (i.e., rest) periods in a probabilistic manner. This approach have demonstrated to be provide a better characterization/recognition (Mashat, Lin, and Zhang 2019).

In order to stress the importance of considering activity-specific latency and duration parameters for task characterization, we performed an additional classification analysis. We used 8-30 Hz FIR bandpass filter to filter all the EEG channels into sensorimotor rhythm frequencies. Then, we calculated the entropies of EEG signal without considering any timing parameters. The performance results were given in Table 29.

The performances demonstrated in Table 29 emphasize the importance of considering the frequency-resolved analysis, and time-resolved analysis, which delineates temporal organization of brain dynamics in a better way during characterization of cognitive task-related brain activities (J. Li et al. 2016; Ince et al. 2009). One important thing that we should consider is that we identified only one timing parameter pair for each frequency-resolved channel and cognitive activity. The performance results can be improved by including more timing parameter pairs at which are emerged for some of the channels that we mentioned in methods section as Zhou et al. adopted (Z. Zhou and Wan 2012).

Table 29. The performance results when using and without using activity-specific timing parameters.

		% Perf. (Scenario-1)			% Perf. (Scenario-2)		
		FLD	**Linear SVM**	**Nonlinear SVM**	**FLD**	**Linear SVM**	**Nonlinear SVM**
BCI Comp.-III	**Our Method**	62.23 ± 8.74	75.74 ± 12.39	79.46 ± 11.27	80.65 ± 9.33	85.0 ± 7.96	80.86 ± 10.32
	Without Timing Parameters	69.57 ± 10.49	68.29 ± 9.65	69.14 ± 9.72	72.82 ± 11.12	71.08 ± 7.70	70.65 ± 7.16
PhysioNet	**Our Method**	54.0 ± 9.34	53.33 ± 7.87	51.83 ± 9.39	60.67 ± 11.0	62.0 ± 14.03	65.0 ± 13.99
	Without Timing Parameters	57.67 ± 10.6	55.5 ± 10.27	55.67 ± 12.09	57.33 ± 9.52	56.67 ± 12.51	60.67 ± 9.4

We also performed an additional analysis with frontal EEG channels to reflect the cognitive performance of subjects during motor imagery tasks. To that end, we used the well-performing and worst-performing subjects according to the performances of winner algorithm in BCI Competition-III. In this competition, the winner algorithm found that the best recognition performance belongs to subject al (100%), and the lowest performance belongs to subject av (80.6%). We used the EEG signal of these subjects to observe the difference of entropies of frontal regions (F3, Fz, and F4 channels), which were calculated using the activity-specific timings. The main reason of using the frontal region electrodes is that they mainly reflect the neural activities that reflect neural information about cognitive planning and consciousness operations (Thul et al. 2016; Liang et al. 2013). Our analysis revealed that the most pronounced discrimination in entropy values manifested in 8-12 Hz, 12-16 Hz, and 20-24 Hz frequency ranges. This result shows that the complexity of neural activity obtained from frontal regions conspicuously reflect the differences of cognitive/motor imagery task recognition ability of the subjects.

6.4.4. Using Different Type of Features

In this study, our method captured and used the timings of the signal segments that providing the most activity-specific entropies for characterization. In accordance with the past literature, we aimed that the task-related activation/synchronization patterns may emerge and vanish at different timings even for each channel and frequency band even in the case of synchronous mode BCI's (Bayazit et al. 2009; Bola, Gall, and Sabel 2015; Zanon, Borgomaneri, and Avenanti 2018; Solomon et al. 2019). In order to capture the activity-specific timing parameter pairs, we adopted an heuristic optimization that evaluates the entropy evolution in a probabilistic manner which was adopted in an asynchronous BCI study (Lemm, Schäfer, and Curio 2004). Please note that, we decided to use entropy as feature to characterize short-lived brain oscillations due to its effectiveness in previous studies.

It is possible to use a different type of features such as autoregressive model coefficients (McFarland and Wolpaw 2008), time-frequency features (Hsu and Sun 2009; Ince et al. 2009), time-domain parameters (C. Vidaurre et al. 2009), Hurst exponent (Gupta, Singh, and Karlekar 2018). However, their performances should be carefully evaluated before using them in the recognition phase. It should be noted that using different type of features may unveil different activity-specific timing parameters due to the fact that each different feature type captures different characteristics of the electrophysiological signals. For a better activity characterization, it may be possible to use multiple features in our proposed method.

In order to emphasize the characterization performance of the entropy feature, we performed an additional classification analysis by using three different time-domain parameters as features (C. Vidaurre et al. 2009). These parameters are *Activity*, *Mobility*, and *Complexity* which were inspired from Hjorth parameters (Hjorth 1970). The first one quantifies the signal band power, the second one the mean frequency of the signal and the third one the change in the signal frequency. We performed similar analysis as described in methods section but for these three parameters. In Table **30**, we presented the average performances obtained by using these three features. The results presented in Table **30** indicate the importance of using the information-theoretic features in correlating the set of behavioral and task variables with the electrical activity of the brain (Kahana 2006). Besides Vasicek's entropy estimation method, Lempel-Ziv complexity (Ibáñez-Molina et

al. 2015), fractal dimension (Loo, Samraj, and Lee 2011), bubble entropy (Manis, Aktaruzzaman, and Sassi 2017), permutation entropy and its variants (C. Bandt and Pompe 2002; Zeng et al. 2018), Renyi's quadratic entropy (Principe 2010; Kee, Ponnambalam, and Loo 2017), approximate entropy (Pincus 1991), Kolmogorov entropy (L. Gao, Wang, and Chen 2013), wavelet entropy (Osvaldo A. Rosso et al. 2001; Osvaldo A. Rosso 2007; Emre Cek, Ozgoren, and Acar Savaci 2010; Mooij et al. 2016), fuzzy entropy (Fasil and Rajesh 2019), permutation auto mutual information (PAMI) (Liang et al. 2013), and sample entropy (Arunkumar et al. 2017) can also be utilized for information-theoretic characterization of short-lived neural activities. Importantly, different entropy calculation approaches may probably delineate different complexity results since they are based on different physical hypothesis for complexity calculation which was remarked in a previous literature (J. Kang et al. 2019). In this circumstances, it is again mandatory to investigate the usefulness of different entropy methods before using them for specific purposes.

Table 30. The performances of three different features used in the proposed method.

		% Perf (Scenario-1)			**% Perf (Scenario-2)**		
		FLD	**Linear SVM**	**Nonlinear SVM**	**FLD**	**Linear SVM**	**Nonlinear SVM**
BCI Comp.-III dataset IVa	**Entropy**	62.23 ± 8.74	75.74 ± 12.39	79.46 ± 11.27	80.65 ± 9.33	85.0 ± 7.96	80.86 ± 10.32
	Activity	63.51 ± 7.87	73.29 ± 11.21	75.63 ± 10.81	73.47 ± 10.0	83.69 ± 9.66	80.21 ± 11.74
	Mobility	55.32 ± 7.29	61.27 ± 13.18	68.82 ± 13.89	68.26 ± 9.76	68.91 ± 9.36	70.65 ± 9.22
	Complexity	49.14 ± 3.29	53.61 ± 2.56	55.31 ± 4.86	50.0 ± 8.89	51.08 ± 7.95	52.82 ± 9.7
PhysioNet Motor Imagery	**Entropy**	54.0 ± 9.34	53.33 ± 7.87	51.83 ± 9.39	60.67 ± 11.0	62.0 ± 14.03	65.0 ± 13.99
	Activity	54.5 ± 10.21	54.83 ± 11.96	54.5 ± 10.66	57.67 ± 11.5	62.33 ± 15.02	60.67 ± 15.87
	Mobility	54.67 ± 7.36	57.16 ± 12.15	58.5 ± 12.06	51.33 ± 8.67	53.67 ± 15.05	56.67 ± 14.58
	Complexity	47.83 ± 7.74	49.16 ± 6.0	50.83 ± 7.24	55.0 ± 9.88	43.67 ± 11.94	43.66 ± 11.96

6.4.5. Alternative Usage of the Proposed Method

We performed an additional classification analysis to show the method presented here can also be used prior to the CSP method for the purpose of capturing relevant signal segments. We initially set the length of the search window to $w = 2$ seconds as in (Mishuhina and Jiang 2021; Yu Zhang et al. 2019). Next, we applied the same entropy and mean posterior probability calculation steps. For each channel $i(f)$ and activity type A, we determined the optimum latency parameter ($\Delta t^{A}_{i(f)}$) at which the most discriminative entropy patterns (highest mean posterior probability) emerges. Then, the latency parameters are used for extracting 2-seconds-length informative signal segments from both training and test task periods. At the final stage, the CSP filters can be obtained from the 2-second length training task periods and these filters applied for extracting log-variance features. We used large-margin classifier (linear SVM) as in (Ince et al. 2009). Our classification analysis show that, for scenario-2, we achieved 88.17% accuracy (average of five subjects) for BCI Competition-III dataset IVa. For further improvement, more shorter time windows and also several variants of CSP method or sparse CSP method can also be adopted (H. Wang and Zheng 2008; W. Wu et al. 2015; Lemm et al. 2005; Fabien Lotte and Guan 2011; Goksu, Ince, and Tewfik 2013).

The datasets that we used for performance evaluation (i.e., BCI Competition-III dataset IVa ($f_s = 100\,Hz$) and PhysioNet Motor Movement/Imagery ($f_s = 160\,Hz$)) were collected at relatively low sampling frequencies. Although our method achieved promising performances, the temporal resolution of the timings captured for brain activity characterization is relatively low (10ms resolution for BCI Competition-III dataset IVa, and 6.25ms resolution for PhysioNet Motor Movement/Imagery datasets). Our method may exhibit a better recognition performance with EEG setups having greater sampling frequencies albeit with a computational cost. An increase in the sampling frequency of EEG signals enables to use of an analysis window smaller than 300ms that enables to capture the timings more accurately. Using advanced parallel computing algorithms and advanced processor architectures, our method can reliably be used in asynchronous mode brain-computer interface applications.

On a final note, in this study we showed that, the brain encodes the task-specific information into the short-lasting electrophysiological activity segment which obeys the temporal organization dynamics as highlighted in (Z. Ma and Zhang 2018). We also

showed that emerging and vanishing of activity-specific temporal dynamics are not synchronized to activity onset within all brain regions. To sum up, our results point that obtaining the characteristic brain dynamics for each different cognitive activity requires a temporal, spatial and spectral search.

CHAPTER 7

REPRESENTATIVE AUTOREGRESSIVE MODELLING OF COGNITIVE ACTIVITIES

Biology gives you a brain,
but life turns it into a mind…
-Jeffrey Eugenides-

7.1. Introduction

In the AR modeling-based cognitive activity recognition frameworks, either univariate or multivariate autoregressive model coefficients are estimated for each task period and used as features for recognition purposes (Huan and Palaniappan 2004; Anderson, Stolz, and Shamsunder 1998). It is expected that the AR model coefficients calculated for the same type of cognitive tasks are found to be similar. However, the major problem in these studies is that the calculated model coefficients for each same type of cognitive task may significantly alter due to several internal as well as external factors such as physiological factors, movement/eye artifacts, low signal-to noise ratio and so forth. Another main reason for this alteration is thought to be the result of dynamically changing as well as nonlinear characteristics of brain activity (C. J. Stam 2005). As a result, the performance of AR modeling in capturing the inherent dichotomy between different cognitive tasks, however, remains modest (Ahn and Jun 2015; Priestley 1988; Brunner et al. 2011). This indicates that calculating the linear autoregressive model coefficients for each task period separately may not be a reasonable way for accurate recognition/characterization. Additional efforts have been spent to improve the performance of the frameworks due to the nonlinear and dynamically changing characteristics of the brain (C. J. Stam 2005), such as using both autoregressive and other different types of features together (Yong Zhang et al. 2017), calculating the AR coefficients in phase space (Fang, Chen, and Zheng 2015), calculating the autoregressive model coefficients of the wavelet transform of the signal (Yong Zhang et al. 2017), or

using complicated nonlinear classification methods (Anderson, Stolz, and Shamsunder 1998; Huan and Palaniappan 2004). Also, bilinear autoregressive modeling (Brunner et al. 2011; Priestley 1988) and time-varying autoregressive modeling have been offered to capture the inherent dichotomy from the nonlinear and dynamically evolving electrophysiological characteristics of the brain (Schlögl et al. 2005; Tarvainen et al. 2004; G. Pfurtscheller et al. 1998; Arnold et al. 1998). Although these intimate efforts achieved a conspicuous success, still some meaningful improvements are required especially for brain-computer interfacing approaches.

In this chapter, we propose an alternative AR modeling-based approach in response to the model coefficient estimation problem of conventional AR modeling described above. Basically, our method generates a representative model for each type of cognitive task by incorporating each of every task period of activity of interest into coefficient estimation for the representative models during the training phase. Note that the representative AR models generated for each cognitive activity contains both multivariate and univariate AR model coefficients. In the training phase, our method uses the CSP method as a part of preprocessing to emphasize the inherent dichotomy of different cognitive tasks (Ramoser, Müller-Gerking, and Pfurtscheller 2000; Blankertz et al. 2008). By using the CSP-filtered task periods, the representative AR models calculated for each type of cognitive task. Then, each of the CSP-filtered multichannel task periods were filtered using the representative AR models obtained for each cognitive task and obtained the forward prediction error signals. The forward prediction error signals mainly comprised of unpredicted nonlinear as well as nonstationary characteristics of the cognitive activities. In the final step, the channel-wise entropies of error signals obtained for each task period were calculated and used them as feature vectors to train a Fisher's linear discriminant (FLD) classifier.

In the test phase, we used the CSP filter, and the representative models calculated in training phase to filter each task period. The channel-wise entropies of the error signals obtained for each test period were calculated and formed as feature vectors and the trained FLD classifier were then decide the category of each test period. We tested our method on two BCI datasets available online, PhysioNet Motor Movement/Imagery Dataset and BCI Competition-III Dataset IVa. The results obtained on these two datasets show that the spatial filtering of the motor imagery task periods via CSP filter can uncover the inherent dichotomy between different types of motor imagery activities and offers a reliable representative modeling of different types of motor imagery tasks (J. Wang et al.

2018). On a final note, this approach can easily be adapted to characterize the various type of cognitive tasks.

The remainder of this paper is organized as follows: In Section 7.2, we present the details of the proposed method used in this study. In Section 7.3, we describe the performance results obtained across PhysioNet as well as BCI Competition-III datasets. In Section 7.4, we discuss the results.

7.2. The Proposed Method

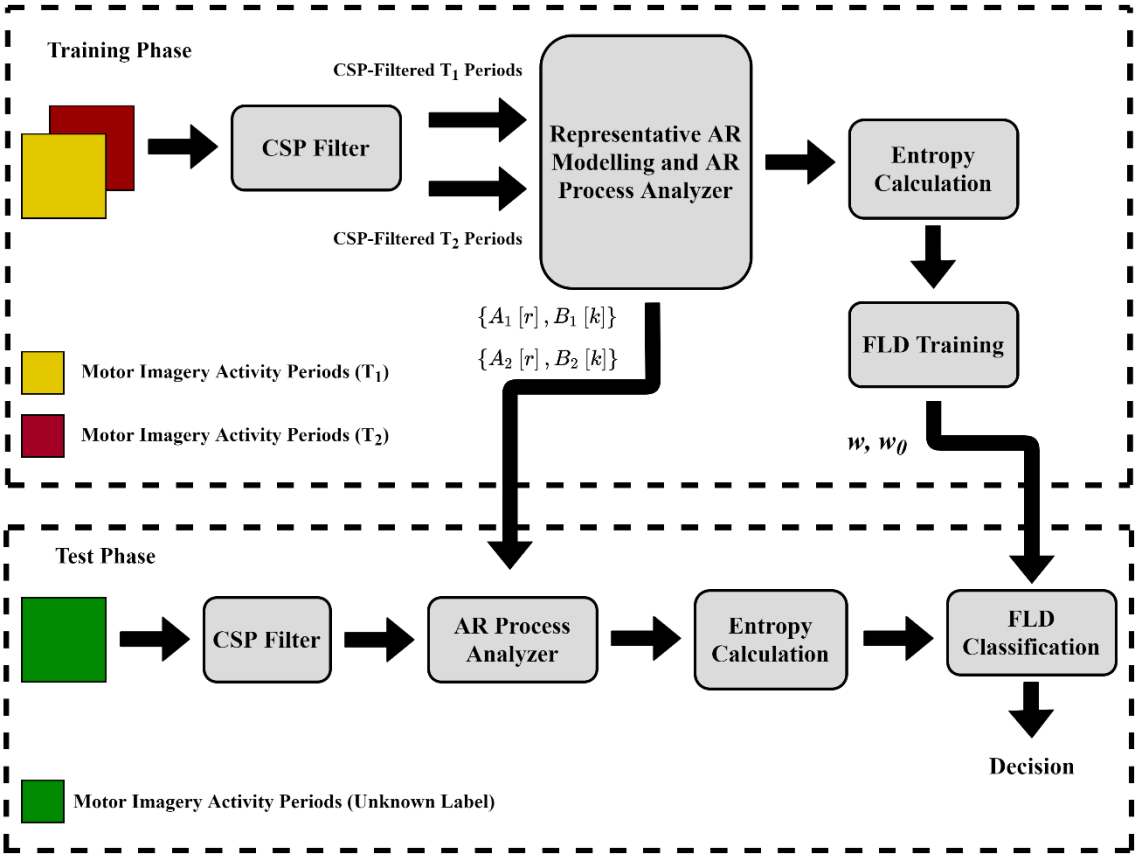

Figure 42. The illustration of the proposed AR-based method.

The operational flow diagram of the proposed framework is given. This framework was implemented following the chronological cross-validation paradigm of machine learning with exclusive training and test sets as illustrated in Figure 42.

7.2.1. Training Phase

In the *CSP Filter* block, we calculated the CSP filter W by using all the band-pass filtered motor imagery activity periods in the training set. We then filtered each of every training task period using CSP filter W. In the *Representative AR Modelling and AR Process Analyzer* block, we calculated representative model coefficient matrices $\{A_1[r], B_1[k]\}$ and $\{A_2[r], B_2[k]\}$ for each different task type (say T_1 and T_2) by using corresponding cognitive task periods. After calculating the model coefficient matrix pairs (i.e. $\{A_1[r], B_1[k]\}$ and $\{A_2[r], B_2[k]\}$), we used both models to filter each of every CSP-filtered task period indexed by i in the training set and obtained forward prediction error signals $\boldsymbol{\epsilon}_i^{A_1,B_1}[n]$ and $\boldsymbol{\epsilon}_i^{A_2,B_2}[n]$ for the task period i (Altunay, Telatar, and Erogul 2010). Note that, each error signal is $2m \times N_s$ dimensional. In here, $2m$ denotes the number of latent channels and N_s denotes the number of samples. We concatenated these error signals into a single error signal for each of every training task period indexed by i as

$$\boldsymbol{\epsilon}_i[n] = \begin{bmatrix} \boldsymbol{\epsilon}_i^{A_1,B_1}[n] \\ \boldsymbol{\epsilon}_i^{A_2,B_2}[n] \end{bmatrix} \tag{7.1}$$

Note also that, the channel size increased to $4m$ after the concatenation. In the *Entropy Calculation* block, we calculated channel-wise entropies of the error signal $\boldsymbol{\epsilon}_i[n]$ by using Vasicek's method (Vasicek 1976; Ibrahim Al-Omari 2014). The $4m \times 1$ dimensional entropic feature vectors ξ_i calculated for task period i to be used for activity recognition. The resulting entropic feature vector and class label pairs for training task period i $\{\xi_i, Y_i\}$ were then used to train a classifier to generalize the associations between the feature vectors and activity types to future task periods. In the *FLD Training* block, by using the feature vectors with known labels (i.e., $\{\xi_i, Y_i\}$), we calculated the weight and bias parameters (i.e., w and w_0) of the classifiers that minimizes the classification error obtained on the training set.

7.2.2. Test Phase

In the *CSP Filter* block, we used CSP filter matrix W calculated in the training phase to filter each test task period (i.e., $\tilde{\boldsymbol{x}}[n] = W^T \boldsymbol{x}[n]$). In the *AR Process Analyzer* block, we used the representative models (i.e., $\{A_1[r], B_1[k]\}$ and $\{A_2[r], B_2[k]\}$) to filter the CSP-filtered test task period $\tilde{\boldsymbol{x}}[n]$ and obtained error signals $\boldsymbol{\epsilon}^{A_1,B_1}[n]$ and $\boldsymbol{\epsilon}^{A_2,B_2}[n]$. We then concatenated the error signals as

$$\boldsymbol{\epsilon}[n] = \begin{bmatrix} \boldsymbol{\epsilon}^{A_1,B_1}[n] \\ \boldsymbol{\epsilon}^{A_2,B_2}[n] \end{bmatrix} \tag{7.2}$$

Then, in the *Entropy Calculation* block, we calculated the entropies of each of channel of $\boldsymbol{\epsilon}[n]$ and constructed the entropic feature vector ξ. We then decided the category of that motor imagery activity period characterized by ξ in the *FLD Classification* block.

7.2.3. Representative Autoregressive Modelling

Univariate AR modeling calculates the model coefficients for each of every EEG channel and also, multivariate AR modeling calculates the model coefficients that characterize both individual and pairwise linear relationships between EEG channels. From the biophysical point of view, multivariate modeling is more convenient since it uncovers the pairwise interaction between different brain regions albeit with requiring a large amount of sample size as well as computational cost (M. H. Wu, Frye, and Zouridakis 2011; Harrison, Penny, and Friston 2003). Note that, AR coefficient calculation step is repeated for each task period in the majority of the AR modeling studies (Huan and Palaniappan 2004).

In this study, we fitted a unique representative model for each different cognitive task type that contains both multivariate and univariate AR model coefficients together. Using a multivariate and univariate AR model together is beneficial to avoid small sample size problems faced during multivariate AR modeling (Lawhern et al. 2012). To

characterize the time evolution of the CSP-filtered latent channels for a particular task type, we have fitted a representative model separately using all the CSP-filtered task periods associated with the two activity types (i.e., T_1 and T_2). The representative models were constructed for each different type of task according to

$$\tilde{\boldsymbol{x}}_{i_1}[n] = \sum_{r=1}^{p_m} A_1[r]\tilde{\boldsymbol{x}}_{i_1}[n-r] + \sum_{k=1}^{p_u} B_1[k]\tilde{\boldsymbol{x}}_{i_1}[n-p_m-k] + \boldsymbol{\epsilon}_{i_1}[n]$$

and (7.3)

$$\tilde{\boldsymbol{x}}_{i_2}[n] = \sum_{r=1}^{p_m} A_2[r]\tilde{\boldsymbol{x}}_{i_2}[n-r] + \sum_{k=1}^{p_u} B_2[k]\tilde{\boldsymbol{x}}_{i_2}[n-p_m-k] + \boldsymbol{\epsilon}_{i_2}[n]$$

where $\tilde{\boldsymbol{x}}_{i_1}[n]$ and $\tilde{\boldsymbol{x}}_{i_2}[n]$ are the CSP-filtered task periods belongs to T_1 and T_2, i_1 and i_2 representing the indices of the task periods of T_1 and T_2, respectively. $A_x[r]$ represent the 6×6 matrices of multivariate autoregressive coefficients $B_x[k]$ represent the 6×6 matrices of univariate autoregressive coefficients calculated using task periods of T_x. Note that the $B_x[k]$ matrices are diagonal matrices that the diagonal elements are univariate autoregressive model coefficients and off-diagonal elements are zero. Following the literature (McFarland and Wolpaw 2008), the total model was chosen as 16 with multivariate order of $p_m = 1$ and univariate order of $p_u = 15$. We calculated a unique representative model for each different type of cognitive task by using all corresponding task periods at the same time. We pooled the corresponding CSP-filtered task periods into a matrix equation to calculate the task-specific model coefficients as

$$\begin{bmatrix} \boldsymbol{y}_{\ell}^{T_x,1} \\ \boldsymbol{y}_{\ell}^{T_x,2} \\ \vdots \\ \boldsymbol{y}_{\ell}^{T_x,N_{T_x}} \end{bmatrix} = \begin{bmatrix} \boldsymbol{Y}_{\ell}^{T_x,1} \\ \boldsymbol{Y}_{\ell}^{T_x,2} \\ \vdots \\ \boldsymbol{Y}_{\ell}^{T_x,N_{T_x}} \end{bmatrix} \boldsymbol{V}_{\boldsymbol{\ell}}^{\boldsymbol{T_x}} \tag{7.4}$$

where $\boldsymbol{y}_{\ell}^{T_x,i}$ represents the vectors of upcoming samples collected from channel ℓ, i represents the index of task periods belongs to cognitive task type T_x. $\boldsymbol{Y}_{\ell}^{T_x,i}$ is the matrix of signal samples that are used for calculation of upcoming sample of channel ℓ collected from i^{th} task period of cognitive task type T_x. $\boldsymbol{V}_{\boldsymbol{\ell}}^{\boldsymbol{T_x}}$ contain both multivariate and univariate model coefficients that are used for estimating the upcoming sample of channel ℓ for task type T_x. N_{T_x} represents the number of training task periods for cognitive task type T_x. We represented the Eq. (7.4) in a matrix form and calculated the model coefficients as

$$\begin{aligned} \boldsymbol{\chi}_{\boldsymbol{\ell}} &= \mathbf{H}_{\boldsymbol{\ell}}\, \boldsymbol{V}_{\boldsymbol{\ell}}^{\boldsymbol{T_x}} \\ \boldsymbol{V}_{\boldsymbol{\ell}}^{\boldsymbol{T_x}} &= \left(\mathbf{H}_{\boldsymbol{\ell}}^{\boldsymbol{T}}\mathbf{H}_{\boldsymbol{\ell}}\right)^{-1}\mathbf{H}_{\boldsymbol{\ell}}^{\boldsymbol{T}}\boldsymbol{\chi}_{\boldsymbol{\ell}} \end{aligned} \tag{7.5}$$

where superscript T represents the transpose operator. The model coefficient matrices $A_x[r]$ and $B_x[k]$ were then constructed using the estimated task-specific model coefficients by solving the matrix equation via channel-wise least squares method used in (Gürkan, Akan, and Seyhan 2014) in a way to minimize the error term $\boldsymbol{\epsilon}[n]$ (Peiyang Li et al. 2015; Kuruoğlu 2002; Golub and Saunders 1970; Frye and Wu 2011; G. Chen et al. 2011). Please note that these calculations were repeated for each channel ℓ. Note also that, the main aim of calculating representative model coefficients by using all the task periods is to obtain a common representative model for a particular type of cognitive task. The forward prediction error term can be calculated as

$$\boldsymbol{\epsilon}_i^{A_x,B_x}[n] = \tilde{\boldsymbol{x}}_{\boldsymbol{i}}[n] - \left(\sum_{r=1}^{p_m} A_x[r]\tilde{\boldsymbol{x}}_{\boldsymbol{i}}[n-r] + \sum_{k=1}^{p_u} B_x[k]\tilde{\boldsymbol{x}}_{\boldsymbol{i}}[n-p_m-k] \right) \quad (7.6)$$

$\boldsymbol{\epsilon}_i^{A_x,B_x}[n]$ is the forward prediction error signal obtained via filtering the $\tilde{\boldsymbol{x}}_{\boldsymbol{i}}[n]$ by using the model coefficient matrix pair $\{A_x[r], B_x[k]\}$, i represents the index of the task period.

7.3. Results

We compared the motor imagery activity recognition performance of our proposed method with several benchmark methods CSP (Ramoser, Müller-Gerking, and Pfurtscheller 2000), common spatio-spectral patterns (CSSP) (Lemm et al. 2005), and MVAR model (Anderson, Stolz, and Shamsunder 1998). We applied the same pre-processing steps during the performance comparison to maintaining the consistency between the benchmark methods. We selected the three largest and smallest eigenvalue channels for both CSP and CSSP methods ($2m = 6$). We selected the six most BCI related channels via a correlation-based channel selection strategy as proposed in (J. Jin et al. 2019) to maintain the equality of the number of channels between CSP and MVAR methods. We fixed the model order of MVAR to 16. We estimated the MVAR model coefficients by using the EEG signals that were collected from the channels that were identified in the channel selection strategy (J. Jin et al. 2019) and used them as features for each motor imagery activity period. For both scenario-1and scenario-2, the performance results are given in Table 31. Besides the entropy, we also calculated the root-mean-square (RMS) of the residual signals to evaluate the performances of entropy and RMS based features in the characterization of nonlinear characteristics of the residual signals. Thereafter, we used linear and nonlinear support vector machines (SVM) with Gaussian kernels as classifiers. We followed the same procedure for training as well as test phases but linear and nonlinear SVM classification. The performance results obtained for our method and the CSP for different classifier settings were provided in Table 32.

Table 31. The average performances for BCI Competition-III dataset IVa and PhysioNet Motor Movement/Imagery datasets.

		% Performance	
Method	**Dataset**	**Scenario-1**	**Scenario-2**
Proposed Method (Entropy)	PhysioNet	55.16 ± 7.04	62.33 ± 12.66
	BCI Comp.	81.69 ± 13.62	86.08 ± 12.84
Proposed Method (RMS)	PhysioNet	53.33 ± 7.33	59.33 ± 13.32
	BCI Comp.	81.27 ± 15.45	85.0 ± 14.1
CSP (Log-variance, $m = 3$)	PhysioNet	54.5 ± 6.14	58.33 ± 13.31
	BCI Comp.	82.34 ± 14.9	84.56 ± 16.4
CSSP (Log-variance, $m = 3$)	PhysioNet	50.5 ± 3.11	57.57 ± 16.08
	BCI Comp.	81.06 ± 15.66	84.34 ± 18.86
MVAR ($p_{MVAR} = 16$)	PhysioNet	47.5 ± 10.3	47.0 ± 10.91
	BCI Comp.	49.78 ± 4.88	51.52 ± 7.7

Table 32. Performance evaluation using different classifiers.

		Performances of Different Classifiers (%)					
		FLD		Linear SVM		Gauss SVM	
		S1	S2	S1	S2	S1	S2
BCI Comp.-III	Proposed	81.69 ± 13.62	86.08 ± 12.84	78.4 ± 14.36	83.25 ± 16.08	75.73 ± 12.54	81.51 ± 17.3
	CSP	82.34 ± 14.9	84.56 ± 16.4	79.9 ± 12.42	84.56 ± 17.58	80.95 ± 13.53	83.9 ± 18.5
PhysioNet	Proposed	55.16 ± 7.04	62.33 ± 12.66	58.33 ± 11.87	59.33 ± 14.65	57.83 ± 10.5	59.0 ± 14.39
	CSP	54.5 ± 6.14	58.33 ± 13.31	61.83 ± 14.03	63.0 ± 16.53	60.83 ± 14.42	65.33 ± 16.83

Apart from fixed model order approach, we tried several model order identification techniques (Akaike Information Criterion, Bayesian Information Criterion, and Mutual Information) to find optimum multivariate (i.e., p_M) and univariate (i.e., p_U) model orders for a better brain activity recognition performances (Gibson 2018; Mariani, Giorgetti, and Chiani 2015; Akaike 1969). The recognition performance results are provided in Table 33. The performances provided in Table 33 shows that the fixed model order approach which is adopted from study of (McFarland and Wolpaw 2008) achieved a higher recognition performances than the performance obtained using well-known model order identification methods.

Table 33. Average recognition performances of different model order identification techniques.

	Dataset	Scenario-1 Performances (%)	Scenario-2 Performances (%)
Fixed Order ($p_M = 1, p_U = 15$)	BCI-III	81.69 ± 13.62	86.08 ± 12.84
	PhysioNet	55.16 ± 7.04	62.33 ± 12.66
Akaike Information Criterion (AIC)	BCI-III	78.41 ± 17.59	80.02 ± 18.37
	PhysioNet	50.67 ± 10.1	57.33 ± 8.25
Bayesian Information Criterion (BIC)	BCI-III	77.82 ± 14.2	81.24 ± 16.23
	PhysioNet	51.67 ± 9.43	60.33 ± 14.42
Mutual Information (Kraskov's method)	BCI-III	78.57 ± 15.41	83.27 ± 9.06
	PhysioNet	53.67 ± 9.97	61.67 ± 12.56

7.4. Discussion

The performance evaluated in a task recognition framework highlights the capability of the proposed method. Results showed that the performance of the proposed method exceeded the minimum reliable communication rate (Ahn and Jun 2015). In Scenario-2, the proposed method achieved greater recognition performance than the well-known benchmark methods CSP, CSSP, and MVAR modeling on both datasets. The results also showed for the PhysioNet dataset that we could not achieve the minimum reliable communication rate for the motor imagery activity recognition. The common approach is the elimination of the subjects from the method evaluation who elicit poor recognition performances during the motor imagery activity recognition that uses the PhysioNet motor imagery dataset (Handiru and Prasad 2016; Athif and Ren 2019; Cheolsoo Park, Took, and Mandic 2014; Kim et al. 2016), as pointed out by Müller (Müller-Putz et al. 2007). As in our previous study (B. Orkan Olcay and Karaçalı 2019), we demonstrated the average performances calculated across the first 20 subjects from

the PhysioNet dataset and we demonstrated the average performances calculated across the five subjects BCI Competition-III dataset IVa without considering any performance exclusion criteria to clearly demonstrate the pros and cons of the proposed method. Also, we also used linear as well as nonlinear SVM classifiers. The results presented in Table 31 shows that the classification performance obtained for CSP, and our method do not demonstrate any enormous differences for both datasets when linear and nonlinear SVM classifiers are used. In this study, our main idea is not to improve the performance of CSP based motor imagery activity recognition (Ramoser, Müller-Gerking, and Pfurtscheller 2000), is to enhance the characterization capability of autoregressive modeling for motor imagery task recognition. Along with this idea, we proposed a method that utilizes the merits of CSP in the pre-processing step. We obtained a common representative model for each type of cognitive task by using all the CSP-filtered task signals. The performance results obtained using both multivariate AR modeling and the proposed method given in Table 31 show that we significantly developed the discrimination capability of the AR modeling in motor imagery activity characterization/recognition frameworks. To improve the performance of the proposed method, as the preprocessing step, different variants of the CSP method can be applied as pre-preprocessing (Fabien Lotte and Guan 2011; H. Lu, Plataniotis, and Venetsanopoulos 2009; Fabien Lotte and Guan 2010; Ashok et al. 2013; Cheolsoo Park, Took, and Mandic 2014).

The characteristics of the brain oscillations alter significantly during the epileptic seizures (Sharma, Pachori, and Acharya 2015; Padmasair et al. 2010; Altunay, Telatar, and Erogul 2010). Along with this fact, autoregressive modeling approaches used in epilepsy detection studies achieved brilliant recognition performances as the result of apparently diverging dichotomy emerged between normal and epileptic brain oscillations (Altunay, Telatar, and Erogul 2010). However, the dichotomy between two different motor imagery tasks is not apparent without using any pre-processing method in the motor imagery activity recognition case. Performance results obtained via multivariate AR modeling given in Table 31 shows that multivariate AR modeling did not achieve the minimum reliable communication rate. These results signify the inability of the autoregressive modeling to capture the activity-specific nonlinear brain dynamics emerge during cognitive tasks since it characterizes only the linear dynamics of the brain activity. For this reason, as pre-processing, we filtered the task periods via CSP filter to amplify the characteristic differences of different types of motor imagery activities that help autoregressive modeling to capture the activity-specific dichotomies (J. Wang et al.

2018). Thereafter we filtered the task periods with these linear models to obtain the nonlinear dynamics. Similar autoregressive based filtering has been proposed to detect the artifacts of the electrophysiological signals (Schlögl 2000) and epileptic activity (Altunay, Telatar, and Erogul 2010). The main idea behind this is that the autoregressive model captures the linear portion of the brain activity which can be characterized by a continuous function of frequency in power spectra. However, artifacts or transiently emerged nonlinear oscillations which are characterized by discrete narrow peaks, in general, cannot be modeled by the autoregressive model. Thus, filtering the electrophysiological activity produces the transiently emerged nonlinear characteristics of the brain activity (C. J. Stam 2005) that are assumed to be the nonlinear portion of motor imagery activity related brain processes (Pardey, Roberts, and Tarassenko 1996; Akin and Kiymik 2000; Acir and Güzeliş 2004).

The notion of entropy has proven to be an effective method in uncovering the latent nonlinear characteristics of the electrophysiological signals (Güdücü et al. 2019; Arunkumar et al. 2017; Liang et al. 2015). We calculated the channel-wise entropies of the prediction error signals to characterize the nonlinear dynamics. Many different entropy estimation methods such as approximate entropy (Pincus 1991), sample entropy (Richman and Moorman 2000), distribution entropy (Peng Li et al. 2015), bubble entropy (Manis, Aktaruzzaman, and Sassi 2017), quadratic Renyi entropy (Principe 2010) have been proposed and tested on real and synthetically generated signals. Among the several alternatives, we selected the Vasicek's entropy estimator with bias correction term (Ibrahim Al-Omari 2014). Besides the entropy, we also calculated channel-wise RMS values of the prediction error signals as features to see the effectiveness of the entropy in characterizing the prediction error signals. Performance results obtained via proposed method show that entropy-based features are better in characterizing the nonlinear dynamics of the electrophysiological signals (Güdücü et al. 2019).

To capture the dynamically changing behavior of the brain, time-varying autoregressive modeling was adopted in many studies (Tarvainen et al. 2004; G. Pfurtscheller et al. 1998; Schlögl 2000; Schloegl, Lugger, and Pfurtscheller 1997; Arnold et al. 1998; Gutiérrez and Salazar-Varas 2012). In these studies, the autoregressive model coefficients are iteratively updated to capture the instantaneous brain dynamics. Note that, these iterative updates continue either in the testing/recognition phase. The re-calculation of model coefficients for an N-channel EEG system requires a large amount of memory as well as computation power to meet the speed requirements for BCI applications in the

recognition phase. Unlike these approaches, our method calculates the activity-specific representative models only in the training phase. These representative models are then used for filtering the upcoming EEG signals which means that the testing/recognition phase does not bring any computational cost to the BCI system.

In the literature, the optimum AR model order identification (i.e. identification of p_m or p_u) is generally carried out by using Akaike information criterion (AIC) (Akaike 1969), Schwartz Bayesian information criterion (BIC), Akaike's final predictions error (FPE), minimum description length (MDL), and RJMCMC (Karakuş 2017; Troughton and Godsill 1998). Besides, information-theoretic methods such as entropy power (Bu et al. 2018), Kullback-Liebler discrepancy (Broersen and Wensink 1998), generalized information criteria (Mariani, Giorgetti, and Chiani 2015), coherence-based methods (Thuraisingham 2007) has been proposed to identify the optimum model order. The majority of these studies use both the modeling error and model complexity and calculates a penalty for each model order. The model order that exhibits the minimum penalty is selected as the optimum model order. However, the situation changes in the case of BCI studies. In (McFarland and Wolpaw 2008), McFarland et al. highlighted the importance of model order selection in sensorimotor-based motor imagery activity characterization studies. It was also stated in Refs. (Krusienski, McFarland, and Wolpaw 2006; McFarland and Wolpaw 2008), for BCI studies, minimum mean square error performance is significantly different from the BCI performance. We choose the total model order as 16 with the multivariate model order $p_m = 1$ and univariate term $p_u = 15$ in light of the results in (McFarland and Wolpaw 2008). The reason for fixing the multivariate model order as one and allowing a large number of univariate model order is twofold. The first reason is, adding one more multivariate term requires estimation of N^2 more coefficients for an N-channel dataset. The dramatic increase of the number of multivariate model coefficients may cause an erroneous estimation of model coefficients especially for small sample-sized datasets This approach facilitates avoiding erroneous estimation of AR model coefficients due to the large number of coefficients to be estimated when characterizing the cognitive tasks with a limited number of samples as pointed in Ref. (Lawhern et al. 2012). The second reason is that the univariate AR modeling elicited better cognitive activity recognition performance than multivariate AR modeling for the majority of the subjects studied in the past literature (Anderson, Stolz, and Shamsunder 1998). So, we fixed the multivariate term to one and allowed using a large number of univariate terms. Note that, we use the multivariate term as the most recent regression

term to capture the inter-channel linear relationship as it provides, to a certain extent, characterization of the pairwise channel interactions that spread from the past samples used for the estimation of the upcoming signal sample. After the multivariate term, we use the univariate terms to capture the temporal dynamics of each channel. As a final note, it is possible to acquire better recognition performance from the proposed method by evaluating different model orders to univariate part of the representative model to different channels using a recognition framework in the training phase (Bufalari et al. 2006).

In the training phase, we fitted a mixed AR model for each type of motor imagery activity by using the corresponding CSP-filtered task periods. Note that, we used entire signal samples of each CSP-filtered training tasks during model fitting. However, identifying and using the most informative segment of the task periods may have a significant influence on the recognition performances. In the literature, much effort has been spent on capturing the most informative signal segment for better motor imagery activity characterization. Zhang et al. proposed the temporally constrained sparse group spatial patterns method to extract features from the most activity-related signal segment (Yu Zhang et al. 2019). Wang et al. proposed the Kullback-Liebler divergence based method to identify the most relevant signal segment for a BCI purpose (J. Wang et al. 2018). Ang et al. proposed an information-theoretic framework to capture the optimal time window of task periods for EEG signal classification (Ang et al. 2012). As a pre-processing step, capturing and using the most informative time segment for the proposed method may be beneficial for a better recognition performance.

CHAPTER 8

CONCLUSIONS AND FUTURE DIRECTIONS

The human brain has 100 billion neurons,
each neuron connected to 10 thousand other ones,
sitting on your shoulders is the most complex object in the known universe...
-Michio Kaku-

The brain appears to operate through multi-dimensional states (Breakspear and Stam 2005). Communication among different regions, sensory and motor information processing associated areas, and frontal/prefrontal areas co-exist. The nature of asymmetrical brain response to dichotic stimulus has given some insight to trans-hemispheric and posterior-frontal axes in stimulus-specific time intervals (Bayazit et al. 2009). The operational complexity as well as the timing specialization of the brain forces us to seek novel analysis methods that can elucidate the characteristic as well as transient synchronization between distinct brain regions. Since cognition as well as other processes shows nonstationary behavior, methods that invoke stationarity assumptions on brain electrophysiology are rendered inadequate to reveal the characteristic behavior of the brain.

The major shortcoming of the classical analysis approaches is the disregard of the transient as well as the complex nature of the brain's distributed functionality in favor of model simplicity. The more adequate distributed systems approach requires new tools as the function blocks are widely distributed and the information complexity overwhelms locality to a large degree.

This thesis proposes a new perspective for analysis of brain activity that can be useful to trace and characterize the behavior of distributed information processing during cognition, perceptual, and other processes. Our perspective in this thesis is based on the premise that the brain adapts itself by re-organizing its inter-regional synchronization timings for each different cognitive activity for optimal information processing (Bullmore and Sporns 2012). In this sense, in Chapter 3, we characterized the brain activity by means of calculating the synchronization between EEG channels at task-specific time lags (i.e., τ). To that end, we applied six synchronization measures and calculated the characteristic

time lags (task-specific time lags) associated with different cognitive tasks: mutual information, correntropy, phase locking value, cross-correlation, nonlinear interdependence, and cosine-based similarity. In the training phase, the task-specific time lags were obtained and used for constructing training feature vectors. These lags maximized the average synchronization for their respective channel pairs and cognitive task types in the training set. In the test phase, we calculated the synchronization values at the same task-specific time lags calculated in the training phase and constructed the test feature vectors. Due to the high dimensionality of the feature vectors, we carried out a feature selection using Fisher ratio along with *a priori* suggested channel pairs in the literature. For recognition, we used a FLD classifier. The results in Tables 3 and 4 show that the recognition rates were below the minimum reliable communication rate (i.e. %70) for PhysioNet dataset (Ahn and Jun 2015). However, for the BCI Competition-III dataset, the average performance varied between 69%-76%.

Performance evaluation was carried out using a realistic cross validation scheme that uses a chronological partitioning of the data into training and testing sets. In classification results on the PhysioNet Motor Movement/Imagery Dataset, connectivity-based framework evaluated here outperformed a CSP-based benchmark scheme. Using BCI Competition-III dataset, it achieved a slightly lower performance than the CSP method. These results indicate that task-specific inter-regional lagged synchronization between potentially remote brain regions were used effectively to discriminate between different motor imagery tasks.

Since the synchronous type methods calculate relevant features in a pre-determined time window, the asynchronous version needs to monitor the changes in brain activity in flowing EEG data to capture the task-specific changes as quickly as possible. This refers to the need of an improved methodology that captures the short-lived activity-specific synchronization timings between brain regions.

The methodology proposed in Chapter 4 determines the timings of the short-lived characteristic synchronizations (i.e., $\{\Delta t, \tau, w\}$) among the brain regions for different cognitive activities. We again used six different synchronization measures separately to capture the activity-specific synchronization pattern between the EEG channels. In order to capture the activity-specific timing parameter triplets for each motor imagery activity and channel pair, we used a heuristic optimization to determine from the training set. As done in Chapter 3, we use these timings for calculating training and test feature vectors.

We provided both the performance results as well as the significant channel pairs, and also their statistical significance, that were mostly selected in feature selection. The performance results show that the pairwise short-lived channel synchronizations calculated at these activity-specific timings can be used for characterization of motor imagery activities. Although the classification results obtained from BCI Competition-III dataset IVa was relatively lower than the these obtained using previous method, the performances of PhysioNet datasets, in comparison with the performances of previous method, manifests the usefulness of our method. The channel pairs that were identified as significant during classification sows that, in general, our method captures biophysically meaningful channel pairs that we highlighted their relevance to motor imagery tasks.

A critical point related to this method is that the captured timing parameters for different cognitive tasks appeared to be deviated from each other to a large extent. The differences in the timings for each different cognitive activity and each different brain region indicate that the brain generates transient synchronization windows to integrate the segregated neural information to support a rich variety of cognitive processes (Zalesky et al. 2014). Additionally, these differences in the synchronization timings may constitute a "synchrony filter" to inhibit the interference of task-unspecific neural synchronizations coming from different brain regions (Patel and Joshi 2013). The cognitive task recognition performance results point to the importance of considering time-resolved cortical communication for discovering the working principles of the brain.

It has proven that the hierarchical organization is an inherent characteristic of many real complex systems such as brain networks and these elements of these networks constitute temporal communication channel by synchronizing their electrophysiological activities for global information integration and segregation (Ravasz and Barabási 2003; C. Zhou et al. 2006). In Chapter 5, we adopted this idea and try to characterize the brain activity by first finding timing parameters and thus the temporally synchronized channel clusters. We used a similar strategy for finding activity-specific timing parameter triplets as in Chapter 4. Afterward, we used these timings to calculate inter-channel synchronizations for obtaining the clusters of temporally synchronized channels. We characterized the clusters via statistical features to determine significant ones for use in activity recognition. The performance results obtained via this method were slightly lower than the performances in previous chapters. However, more importantly, the significant channel clusters identified for each successful participant fall at odds with the current

biophysical literature. These results shows that our method requires some critical methodological improvements for achieving satisfactory results.

Our proposed synchronization-based methods discussed above barely exceed the reliable communication rate (70%) which indicates the need for further improvements for use of these approaches in a BCI setting. The systematic timing organization may shape not only the pairwise brain synchronizations but also the information content of localized electrophysiological activities. To be more precise, thanks to the timing organization, the brain may encode the task-specific information content into the electrophysiological activity that emerges and vanishes in a short period for efficient as well as effective information processing. We suggest that the systematic timing organization can be captured and used for characterizing motor imagery tasks using only the localized electrophysiological activities. To validate this, in Chapter 6, we propose an information-theoretic brain activity characterization method. Our method simply captures the timings of the signal segments that provides activity-specific entropy features for activity characterization. Satisfactory performance results as well as the most selected channels and frequency bands highlights the validity of considering timing organization even for using individual brain activities. The biophysical results that we found for these methods indicates that the μ and β frequency band is appeared as vital for motor imagery organization (Román Baravalle, Rosso, and Montani 2018).

In the final section, we propose a representative model for characterizing the motor imagery activities. The representative models constructed for each different type of cognitive task is comprised of both multivariate and univariate terms. In the training phase, first, we used the CSP filter to enhance the electrophysiological dichotomy between different type of motor imagery activities. This enhancement enables the representative autoregressive model to achieve a better motor imagery activity characterization. The calculated representative model for each type of motor imagery activity is used to filter upcoming task periods. We use the errors obtained at the output of these filters for characterization the motor imagery activity periods. For characterization purpose, we calculate the channel-wise entropies of these error signals to quantify the remaining nonlinear content of the prediction errors. The entropies calculated for each task period were used to decide the category of the corresponding motor imagery activity period via FLD as well as SVM analyses. The performance results obtained on both PhysioNet Motor Movement/Imagery and the BCI Competition-III dataset IVa show that the proposed method achieved a better activity characterization

performance than the well-known benchmark methods such as CSP, CSSP, MVAR modeling frequently used in BCI literature. This suggests that our modification approach for AR-based motor imagery activity classification enhances the characterization capacity of autoregressive modeling in case of motor imagery activity recognition. With slight improvements, the proposed method can easily be used as an asynchronous BCI framework since the evaluation phase is mainly consisting of filtering operations of the upcoming EEG samples and channel-wise entropy estimation for recognition purposes.

To sum up, in this thesis, we show that the temporal organization of the brain is systematic so that this feature leads its dynamic operation towards a more optimal and economical state. We also showed that accurate characterization of brain activity is possible by putting the systematic timing organization into play.

8.1. Future Research Directions

So far, we manifest the importance of capturing and using the characteristic synchronization timings for brain activity characterization. The idea adopted here is that the activity-specific timings is critical so that at these timings the brain conducts similar neural operations for accomplishing the desired cognitive tasks. In the light of this idea, we will discuss several potential research directions that incorporate the systematic timing organization of the brain for potential scientific research avenues.

8.1.1. Synchronization Timings in Neurodegenerative Diseases

It is clear that neurodegenerative diseases and pathological problems such as Alzheimer's and Parkinson's diseases, and traumatic brain injury induces considerable deterioration of the interaction of neuronal networks within the brain (Yates 2012; McMackin et al. 2019). The recent approach is that these diseases can now be diagnosed by analyzing the inter-regional brain synchronizations calculated from electrophysiological measurements both during idling and task state. For these diseases, the main attractive study topic is the identification of the main reasons for these alterations

in brain synchronizations. Our experience from the motor imagery studies says that the shift of consciousness and concentration level significantly affects the captured synchronization timings which imposes a big challenge in recognizing the motor imagery activities. It may worth studying that the alterations in inter-regional synchronization timings in neurodegenerative diseases may be the reason for the observed synchronization alterations.

8.1.2. Common Spatial Patterns for Short-Lived EEG Signals

As the literature overview provided in the first chapter, the majority of BCI studies adopted the CSP as the most powerful signal processing method for motor imagery activity characterization. The short-lived activity-specific signal segments captured here enables satisfactory characterization of motor imagery activities. Using a sparse solutions for finding CSP filters from the captured short-lived signal segments and using sparse filters for motor imagery related feature extraction may provide brilliant activity recognition performances (Goksu, Ince, and Tewfik 2013).

8.1.3. Activity-Specific Timing Parameters for Multiple Channel Synchronizations

In this thesis, we captured the activity-specific timing parameters from bivariate synchronization patterns. In a brain connectivity-based study, the brain synchronization was analyzed by considering different spatial scales for healthy controls and schizophrenia patients and the major differences were obtained (Vergara et al. 2019). This study tells that not only pairwise interactions but also the multiple interactions is critical for functional network characterization. By using multivariate synchronization measures, the timing parameters for characteristic multivariate channel synchronizations can be obtained and used for accurate brain activity characterization which requires solving a 4 or more-dimensional parameter optimization problem (Shahsavari Baboukani et al. 2019; Jalili, Barzegaran, and Knyazeva 2014).

REFERENCES

Abásolo, D., R. Hornero, P. Espino, D. Álvarez, and J. Poza. 2006. "Entropy Analysis of the EEG Background Activity in Alzheimer's Disease Patients." *Physiological Measurement* 27 (3): 241–53. https://doi.org/10.1088/0967-3334/27/3/003.

Abiri, Reza, Soheil Borhani, Eric W. Sellers, Yang Jiang, and Xiaopeng Zhao. 2019. "A Comprehensive Review of EEG-Based Brain-Computer Interface Paradigms." *Journal of Neural Engineering* 16 (1): 11001. https://doi.org/10.1088/1741-2552/aaf12e.

Acir, Nurettin, and Cüneyt Güzeliş. 2004. "Automatic Spike Detection in EEG by a Two-Stage Procedure Based on Support Vector Machines." *Computers in Biology and Medicine* 34 (7): 561–75. https://doi.org/10.1016/j.compbiomed.2003.08.003.

Adeli, Hojjat, Samanwoy Ghosh-Dastidar, and Nahid Dadmehr. 2007. "A Wavelet-Chaos Methodology for Analysis of EEGs and EEG Subbands to Detect Seizure and Epilepsy." *IEEE Transactions on Biomedical Engineering* 54 (2): 205–11. https://doi.org/10.1109/TBME.2006.886855.

Adhikari, Avishek, Torfi Sigurdsson, Mihir A. Topiwala, and Joshua A. Gordon. 2010. "Cross-Correlation of Instantaneous Amplitudes of Field Potential Oscillations: A Straightforward Method to Estimate the Directionality and Lag between Brain Areas." *Journal of Neuroscience Methods* 191 (2): 191–200. https://doi.org/10.1016/j.jneumeth.2010.06.019.

Adhikari, Bhim M., Charles M. Epstein, and Mukesh Dhamala. 2018. "Enhanced Brain Network Activity in Complex Movement Rhythms: A Simultaneous Functional Magnetic Resonance Imaging and Electroencephalography Study." *Brain Connectivity* 8 (2): 68–81. https://doi.org/10.1089/brain.2017.0547.

Afshari, Saeedeh, and Mahdi Jalili. 2017. "Directed Functional Networks in Alzheimer's Disease: Disruption of Global and Local Connectivity Measures." *IEEE Journal of Biomedical and Health Informatics* 21 (4): 949–55. https://doi.org/10.1109/JBHI.2016.2578954.

Ahn, Minkyu, and Sung Chan Jun. 2015. “Performance Variation in Motor Imagery Brain-Computer Interface: A Brief Review.” *Journal of Neuroscience Methods* 243 (March): 103–10. https://doi.org/10.1016/j.jneumeth.2015.01.033.

Akaike, Hirotugu. 1969. “Fitting Autoregressive Models for Prediction.” *Annals of the Institute of Statistical Mathematics* 21 (1): 243–47. https://doi.org/10.1007/BF02532251.

Akin, M., and M. K. Kiymik. 2000. “Application of Periodogram and AR Spectral Analysis to EEG Signals.” *Journal of Medical Systems* 24 (4): 247–56. https://doi.org/10.1023/A:1005553931564.

Alais, David, Randolph Blake, and Sang Hun Lee. 1998. “Visual Features That Vary Together over Time Group Together over Space.” *Nature Neuroscience* 1 (2): 160–64. https://doi.org/10.1038/414.

Alanis-Espinosa, Myriam, and David Gutiérrez. 2020. “On the Assessment of Functional Connectivity in an Immersive Brain-Computer Interface During Motor Imagery.” *Frontiers in Psychology* 11 (July). https://doi.org/10.3389/fpsyg.2020.01301.

Alexander E. Hramov, Alexey A. Koronovskii, Valeri A. Makarov, Alexey N. Pavlov, and Evgenia Sitnikova. 2015. *Wavelets in Neuroscience. Springer Series in Synergetics*. Springer.

Allen, Elena A., Eswar Damaraju, Sergey M. Plis, Erik B. Erhardt, Tom Eichele, and Vince D. Calhoun. 2014. “Tracking Whole-Brain Connectivity Dynamics in the Resting State.” *Cerebral Cortex* 24 (3): 663–76. https://doi.org/10.1093/cercor/bhs352.

Allison, Brendan Z., and Christa Neuper. 2010. “Could Anyone Use a BCI?” In *Brain-Computer Interfaces*, 35–54. Springer. https://doi.org/10.1007/978-1-84996-272-8_3.

Altermann, M., and D. Kuhn. 1994. *Vergleich Der Bodensystematischen Einheiten Der Ehemaligen DDR Mit Denen Der Bundesrepublik Deutschland*. *Zeitschrift Fur Angewandte Geologie*. Vol. 40. Champaign, IL, USA: University of Illinois Press.

https://doi.org/10.1002/j.1538-7305.1948.tb01338.x.

Altunay, Semih, Ziya Telatar, and Osman Erogul. 2010. “Epileptic EEG Detection Using the Linear Prediction Error Energy.” *Expert Systems with Applications* 37 (8): 5661–65. https://doi.org/10.1016/j.eswa.2010.02.045.

Ambrosi, Pierfrancesco, Mauro Costagli, Ercan E. Kuruoglu, Laura Biagi, Guido Buonincontri, and Michela Tosetti. 2019. “Investigating Time-Varying Brain Connectivity with Functional Magnetic Resonance Imaging Using Sequential Monte Carlo.” *European Signal Processing Conference* 2019-Septe: 1–5. https://doi.org/10.23919/EUSIPCO.2019.8902503.

Anderson, Charles W., Erik A. Stolz, and Sanyogita Shamsunder. 1998. “Multivariate Autoregressive Models for Classification of Spontaneous Electroencephalographic Signals during Mental Tasks.” *IEEE Transactions on Biomedical Engineering* 45 (3): 277–86. https://doi.org/10.1109/10.661153.

Ang, Kai Keng, Zheng Yang Chin, Haihong Zhang, and Cuntai Guan. 2008. “Filter Bank Common Spatial Pattern (FBCSP) in Brain-Computer Interface.” In *Proceedings of the International Joint Conference on Neural Networks*, 2390–97. https://doi.org/10.1109/IJCNN.2008.4634130.

———. 2012. “Mutual Information-Based Selection of Optimal Spatial-Temporal Patterns for Single-Trial EEG-Based BCIs.” *Pattern Recognition* 45 (6): 2137–44. https://doi.org/10.1016/j.patcog.2011.04.018.

Arnhold, J., P. Grassberger, K. Lehnertz, and C. E. Elger. 1999. “A Robust Method for Detecting Interdependences: Application to Intracranially Recorded EEG.” *Physica D: Nonlinear Phenomena* 134 (4): 419–30. https://doi.org/10.1016/S0167-2789(99)00140-2.

Arnold, Matthias, Wolfgang H.R. Miltner, Herbert Witte, Reinhard Bauer, and Christoph Braun. 1998. “Adaptive AR Modeling of Nonstationary Time Series by Means of Kaiman Filtering.” *IEEE Transactions on Biomedical Engineering* 45 (5): 545–52. https://doi.org/10.1109/10.668739.

Arunkumar, A., R. K. Ramkumar, V. V. Venkatraman, Enas Abdulhay, Steven

Lawrence Fernandes, Seifedine Kadry, and Sophia Segal. 2017. “Classification of Focal and Non Focal EEG Using Entropies.” *Pattern Recognition Letters* 94 (July): 112–17. https://doi.org/10.1016/j.patrec.2017.05.007.

Ashok, Arun, Arun K. Bharathan, V. R. Soujya, and P. Nandakumar. 2013. “Tikhonov Regularized Spectrally Weighted Common Spatial Patterns.” In *2013 International Conference on Control Communication and Computing, ICCC 2013*, 315–18. IEEE Computer Society. https://doi.org/10.1109/ICCC.2013.6731671.

Asif, Anum, Muhammad Majid, and Syed Muhammad Anwar. 2019. “Human Stress Classification Using EEG Signals in Response to Music Tracks.” *Computers in Biology and Medicine* 107 (April): 182–96. https://doi.org/10.1016/j.compbiomed.2019.02.015.

Aşikgil, Bariş. 2011. “Information Complexity Criterion for Order Determination in Autoregressive Models.” *Hacettepe Journal of Mathematics and Statistics* 40 (4): 601–7.

Athanasiou, Alkinoos, Manousos A. Klados, Charis Styliadis, Nicolas Foroglou, Konstantinos Polyzoidis, and Panagiotis D. Bamidis. 2018. “Investigating the Role of Alpha and Beta Rhythms in Functional Motor Networks.” *Neuroscience* 378 (May): 54–70. https://doi.org/10.1016/j.neuroscience.2016.05.044.

Athif, Mohamed, and Hongliang Ren. 2019. “WaveCSP: A Robust Motor Imagery Classifier for Consumer EEG Devices.” *Australasian Physical and Engineering Sciences in Medicine* 42 (1): 159–68. https://doi.org/10.1007/s13246-019-00721-0.

Aviyente, Selin, Edward M. Bernat, Westley S. Evans, and Scott R. Sponheim. 2011. “A Phase Synchrony Measure for Quantifying Dynamic Functional Integration in the Brain.” *Human Brain Mapping* 32 (1): 80–93. https://doi.org/10.1002/hbm.21000.

Azab, Ahmed M., Lyudmila Mihaylova, Kai Keng Ang, and Mahnaz Arvaneh. 2019. “Weighted Transfer Learning for Improving Motor Imagery-Based Brain-Computer Interface.” *IEEE Transactions on Neural Systems and Rehabilitation Engineering* 27 (7): 1352–59. https://doi.org/10.1109/TNSRE.2019.2923315.

Babiloni, F., F. Cincotti, C. Babiloni, F. Carducci, D. Mattia, L. Astolfi, A. Basilisco, et al. 2005. “Estimation of the Cortical Functional Connectivity with the Multimodal Integration of High-Resolution EEG and FMRI Data by Directed Transfer Function.” *NeuroImage* 24 (1): 118–31. https://doi.org/10.1016/j.neuroimage.2004.09.036.

Bahraminasab, A., F. Ghasemi, A. Stefanovska, P. V.E. McClintock, and R. Friedrich. 2009. “Physics of Brain Dynamics: Fokker-Planck Analysis Reveals Changes in EEG δ-θ Interactions in Anæsthesia.” *New Journal of Physics* 11 (9). https://doi.org/10.1088/1367-2630/11/10/103051.

Bai, Lijuan, Tianyou Yu, and Yuanqing Li. 2015. “A Brain Computer Interface-Based Explorer.” *Journal of Neuroscience Methods* 244 (April): 2–7. https://doi.org/10.1016/j.jneumeth.2014.06.015.

Baker, Adam P., Matthew J. Brookes, Iead A. Rezek, Stephen M. Smith, Timothy Behrens, Penny J.Probert Smith, and Mark Woolrich. 2014. “Fast Transient Networks in Spontaneous Human Brain Activity.” *ELife* 2014 (3). https://doi.org/10.7554/eLife.01867.

Bakhshayesh, Hanieh, Sean P. Fitzgibbon, Azin S. Janani, Tyler S. Grummett, and Kenneth J. Pope. 2019a. “Detecting Connectivity in EEG: A Comparative Study of Data-Driven Effective Connectivity Measures.” *Computers in Biology and Medicine* 111: 103329. https://doi.org/10.1016/j.compbiomed.2019.103329.

———. 2019b. “Detecting Synchrony in EEG: A Comparative Study of Functional Connectivity Measures.” *Computers in Biology and Medicine* 105: 1–15. https://doi.org/10.1016/j.compbiomed.2018.12.005.

Bandt, Christoph, and Bernd Pompe. 2002. “Permutation Entropy: A Natural Complexity Measure for Time Series.” *Physical Review Letters* 88 (17): 4. https://doi.org/10.1103/PhysRevLett.88.174102.

Bandt, S. Kathleen, Pierre Besson, Ben Ridley, Francesca Pizzo, Romain Carron, Jean Regis, Fabrice Bartolomei, Jean Philippe Ranjeva, and Maxime Guye. 2019. “Connectivity Strength, Time Lag Structure and the Epilepsy Network in Resting-State FMRI.” *NeuroImage: Clinical* 24 (October): 102035.

https://doi.org/10.1016/j.nicl.2019.102035.

Baravalle, Roman, Natalí Guisande, Mauro Granado, Osvaldo A. Rosso, and Fernando Montani. 2019. "Characterization of Visuomotor/Imaginary Movements in EEG: An Information Theory and Complex Network Approach." *Frontiers in Physics* 7: 115. https://doi.org/10.3389/fphy.2019.00115.

Baravalle, Roman, Osvaldo A. Rosso, and Fernando Montani. 2018. "Rhythmic Activities of the Brain: Quantifying the High Complexity of Beta and Gamma Oscillations during Visuomotor Tasks." *Chaos* 28 (7). https://doi.org/10.1063/1.5025187.

Baravalle, Román, Osvaldo A. Rosso, and Fernando Montani. 2018. "Causal Shannon-Fisher Characterization of Motor/Imagery Movements in EEG." *Entropy* 20 (9). https://doi.org/10.3390/e20090660.

Başar, Erol. 2006. "The Theory of the Whole-Brain-Work." *International Journal of Psychophysiology* 60 (2): 133–38. https://doi.org/10.1016/j.ijpsycho.2005.12.007.

Başar, Erol, Canan Başar-Eroglu, Sirel Karakaş, and Martin Schürmann. 2001. "Gamma, Alpha, Delta, and Theta Oscillations Govern Cognitive Processes." *International Journal of Psychophysiology* 39 (2–3): 241–48. https://doi.org/10.1016/S0167-8760(00)00145-8.

Başar, Erol, Canan Başar-Eroğlu, Sirel Karakaş, and Martin Schürmann. 1999. "Are Cognitive Processes Manifested in Event-Related Gamma , Alpha , Theta and Delta OsciTheta Wavelengths Are between 4 – 8 Hertz and Have Been Found to Be Associated with Low Levels of Alertness as Well as Activities Associated with Cognitive Processing." *Neuroscience Letters* 259: 165–68.

Başar, Erol, Christina Schmiedt-Fehr, Adile Öniz, and Canan Başar-Eroğlu. 2008. "Brain Oscillations Evoked by the Face of a Loved Person." *Brain Research* 1214: 105–15. https://doi.org/10.1016/j.brainres.2008.03.042.

Bassett, Danielle S., Andreas Meyer-Lindenberg, Sophie Achard, Thomas Duke, and Edward Bullmore. 2006. "Adaptive Reconfiguration of Fractal Small-World Human Brain Functional Networks." *Proceedings of the National Academy of*

Sciences of the United States of America 103 (51): 19518–23. https://doi.org/10.1073/pnas.0606005103.

Bassett, Danielle Smith, and Ed Bullmore. 2006. "Small-World Brain Networks." *Neuroscientist* 12 (6): 512–23. https://doi.org/10.1177/1073858406293182.

Bastos, André M., and Jan Mathijs Schoffelen. 2016. "A Tutorial Review of Functional Connectivity Analysis Methods and Their Interpretational Pitfalls." *Frontiers in Systems Neuroscience* 9 (JAN2016): 175. https://doi.org/10.3389/fnsys.2015.00175.

Bastos, Andre M., Julien Vezoli, and Pascal Fries. 2015. "Communication through Coherence with Inter-Areal Delays." *Current Opinion in Neurobiology* 31: 173–80. https://doi.org/10.1016/j.conb.2014.11.001.

Batula, Alyssa M., Jesse A. Mark, Youngmoo E. Kim, and Hasan Ayaz. 2017. "Comparison of Brain Activation during Motor Imagery and Motor Movement Using FNIRS." *Computational Intelligence and Neuroscience* 2017. https://doi.org/10.1155/2017/5491296.

Bauer, Robert, Meike Fels, Mathias Vukelić, Ulf Ziemann, and Alireza Gharabaghi. 2015. "Bridging the Gap between Motor Imagery and Motor Execution with a Brain-Robot Interface." *NeuroImage* 108 (March): 319–27. https://doi.org/10.1016/j.neuroimage.2014.12.026.

Bayazit, Onur, Adile Öniz, Constanze Hahn, Onur Güntürkün, and Murat Özgören. 2009. "Dichotic Listening Revisited: Trial-by-Trial ERP Analyses Reveal Intra- and Interhemispheric Differences." *Neuropsychologia* 47 (2): 536–45. https://doi.org/10.1016/j.neuropsychologia.2008.10.002.

Benjamini, Yoav, and Yosef Hochberg. 1995. "Controlling the False Discovery Rate: A Practical and Powerful Approach to Multiple Testing." *Journal of the Royal Statistical Society: Series B (Methodological)* 57 (1): 289–300. https://doi.org/10.1111/j.2517-6161.1995.tb02031.x.

Bergen, R van. 1986. "A Discrete Mutual Information Estimator of Continuous Signals."

Berger, H. 1929. “Uber Das Elektroenkephalogramm Des Menschen. Arch. Pyschiatr. Nervenkr.” *Arch. Pyschiatr. Nervenkr* 87 (1): 527–70.

Billinger, Martin, Clemens Brunner, and Gernot R. Müller-Putz. 2013. “Single-Trial Connectivity Estimation for Classification of Motor Imagery Data.” *Journal of Neural Engineering* 10 (4). https://doi.org/10.1088/1741-2560/10/4/046006.

Blankertz, Benjamin, Klaus Robert Müller, Dean J. Krusienski, Gerwin Schalk, Jonathan R. Wolpaw, Alois Schlögl, Gert Pfurtscheller, José Del R. Millán, Michael Schröder, and Niels Birbaumer. 2006. “The BCI Competition III: Validating Alternative Approaches to Actual BCI Problems.” *IEEE Transactions on Neural Systems and Rehabilitation Engineering* 14 (2): 153–59. https://doi.org/10.1109/TNSRE.2006.875642.

Blankertz, Benjamin, Ryota Tomioka, Steven Lemm, Motoaki Kawanabe, and Klaus Robert Müller. 2008. “Optimizing Spatial Filters for Robust EEG Single-Trial Analysis.” *IEEE Signal Processing Magazine* 25 (1): 41–56. https://doi.org/10.1109/MSP.2008.4408441.

Boeijinga, P. H., and F. H. Lopes da Silva. 1989. “A New Method to Estimate Time Delays between EEG Signals Applied to Beta Activity of the Olfactory Cortical Areas.” *Electroencephalography and Clinical Neurophysiology* 73 (3): 198–205. https://doi.org/10.1016/0013-4694(89)90120-X.

Bola, Michał, Carolin Gall, and Bernhard A. Sabel. 2015. “Disturbed Temporal Dynamics of Brain Synchronization in Vision Loss.” *Cortex* 67: 134–46. https://doi.org/10.1016/j.cortex.2015.03.020.

Bowyer, Susan M. 2016. “Coherence a Measure of the Brain Networks: Past and Present.” *Neuropsychiatric Electrophysiology* 2 (1): 1–12. https://doi.org/10.1186/s40810-015-0015-7.

Breakspear, Michael. 2017. “Dynamic Models of Large-Scale Brain Activity.” *Nature Neuroscience* 20 (3): 340–52. https://doi.org/10.1038/nn.4497.

Breakspear, Michael, and Cornelis J. Stam. 2005. “Dynamics of a Neural System with a Multiscale Architecture.” *Philosophical Transactions of the Royal Society B:*

Biological Sciences 360 (1457): 1051–74. https://doi.org/10.1098/rstb.2005.1643.

Broersen, P. M.T., and H. E. Wensink. 1998. "Autoregressive Model Order Selection by a Finite Sample Estimator for the Kullback-Leibler Discrepancy." *IEEE Transactions on Signal Processing* 46 (7): 2058–61. https://doi.org/10.1109/78.700984.

Brunner, Clemens, Martin Billinger, Carmen Vidaurre, and Christa Neuper. 2011. "A Comparison of Univariate, Vector, Bilinear Autoregressive, and Band Power Features for Brain-Computer Interfaces." *Medical and Biological Engineering and Computing* 49 (11): 1337–46. https://doi.org/10.1007/s11517-011-0828-x.

Brunner, Clemens, Muhammad Naeem, and Gert Pfurtscheller. 2009. "Dimensionality Reduction and Channel Selection of Motor Imagery Electroencephalographic Data." *Computational Intelligence and Neuroscience* 2009. https://doi.org/10.1155/2009/537504.

Brunner, Clemens, Reinhold Scherer, Bernhard Graimann, Gernot Supp, and Gert Pfurtscheller. 2006. "Online Control of a Brain-Computer Interface Using Phase Synchronization." *IEEE Transactions on Biomedical Engineering* 53 (12): 2501–6. https://doi.org/10.1109/TBME.2006.881775.

Bu, Yeqiang, Shenyou Peng, Shiwei Wu, Yujie Wei, Gang Wang, Jiabin Liu, and Hongtao Wang. 2018. "Unconventional Deformation Behaviours of Nanoscaled High-Entropy Alloys." *Entropy* 20 (10): 750. https://doi.org/10.3390/e20100750.

Bufalari, S., D. Mattia, F. Babiloni, M. Mattiocco, M. G. Marciani, and F. Cincotti. 2006. "Autoregressive Spectral Analysis in Brain Computer Interface Context." In *Annual International Conference of the IEEE Engineering in Medicine and Biology - Proceedings*, 3736–39. https://doi.org/10.1109/IEMBS.2006.260238.

Bullmore, Ed, and Olaf Sporns. 2009. "Complex Brain Networks: Graph Theoretical Analysis of Structural and Functional Systems." *Nature Reviews Neuroscience*. https://doi.org/10.1038/nrn2575.

———. 2012. "The Economy of Brain Network Organization." *Nature Reviews Neuroscience* 13 (5): 336–49. https://doi.org/10.1038/nrn3214.

Bünau, Paul Von, Frank C. Meinecke, Franz C. Király, and Klaus Robert Müller. 2009. "Finding Stationary Subspaces in Multivariate Time Series." *Physical Review Letters* 103 (21): 214101. https://doi.org/10.1103/PhysRevLett.103.214101.

Burgess, Richard C. 2011. "Evaluation of Brain Connectivity: The Role of Magnetoencephalography." *Epilepsia* 52 (SUPPL. 4): 28–31. https://doi.org/10.1111/j.1528-1167.2011.03148.x.

Calhoun, Vince D., Kent A. Kiehl, and Godfrey D. Pearlson. 2008. "Modulation of Temporally Coherent Brain Networks Estimated Using ICA at Rest and during Cognitive Tasks." *Human Brain Mapping* 29 (7): 828–38. https://doi.org/10.1002/hbm.20581.

Canolty, Ryan T, Karunesh Ganguly, Steven W Kennerley, Charles F Cadieu, Kilian Koepsell, Jonathan D Wallis, and Jose M Carmena. 2010. "Oscillatory Phase Coupling Coordinates Anatomically Dispersed Functional Cell Assemblies." *Proceedings of the National Academy of Sciences of the United States of America* 107 (40): 17356–61. https://doi.org/10.1073/pnas.1008306107.

Carrillo-de-la-Peña, M. T., S. Galdo-Álvarez, and C. Lastra-Barreira. 2008. "Equivalent Is Not Equal: Primary Motor Cortex (MI) Activation during Motor Imagery and Execution of Sequential Movements." *Brain Research* 1226 (August): 134–43. https://doi.org/10.1016/j.brainres.2008.05.089.

Carvalhaes, Claudio, and J. Acacio De Barros. 2015. "The Surface Laplacian Technique in EEG: Theory and Methods." *International Journal of Psychophysiology* 97 (3): 174–88. https://doi.org/10.1016/j.ijpsycho.2015.04.023.

Caton, Richard. 1875. "Electrical Currents of the Brain." *The Journal of Nervous and Mental Disease* 2 (4): 610.

Cengiz, Bülent, and H. Evren Boran. 2016. "The Role of the Cerebellum in Motor Imagery." *Neuroscience Letters* 617 (March): 156–59. https://doi.org/10.1016/j.neulet.2016.01.045.

Chaudhary, Shalu, Sachin Taran, Varun Bajaj, and Siuly Siuly. 2020. "A Flexible Analytic Wavelet Transform Based Approach for Motor-Imagery Tasks

Classification in BCI Applications." *Computer Methods and Programs in Biomedicine* 187: 105325. https://doi.org/10.1016/j.cmpb.2020.105325.

Chaudhary, Ujwal, Niels Birbaumer, and Ander Ramos-Murguialday. 2016. "Brain-Computer Interfaces for Communication and Rehabilitation." *Nature Reviews Neurology*. https://doi.org/10.1038/nrneurol.2016.113.

Chen, Guanrong and Dong, Xiaoning. 1998. *From Chaos to Order Methodologies, Perspectives and Applications*. Vol. 24. World Scientific.

Chen, Gang, Daniel R. Glen, Ziad S. Saad, J. Paul Hamilton, Moriah E. Thomason, Ian H. Gotlib, and Robert W. Cox. 2011. "Vector Autoregression, Structural Equation Modeling, and Their Synthesis in Neuroimaging Data Analysis." *Computers in Biology and Medicine* 41 (12): 1142–55. https://doi.org/10.1016/j.compbiomed.2011.09.004.

Chen, Huafu, Qin Yang, Wei Liao, Qiyong Gong, and Shan Shen. 2009. "Evaluation of the Effective Connectivity of Supplementary Motor Areas during Motor Imagery Using Granger Causality Mapping." *NeuroImage* 47 (4): 1844–53. https://doi.org/10.1016/j.neuroimage.2009.06.026.

Chen, L. Leon, Radhika Madhavan, Benjamin I. Rapoport, and William S. Anderson. 2013. "Real-Time Brain Oscillation Detection and Phase-Locked Stimulation Using Autoregressive Spectral Estimation and Time-Series Forward Prediction." *IEEE Transactions on Biomedical Engineering* 60 (3): 753–62. https://doi.org/10.1109/TBME.2011.2109715.

Chestek, Cynthia A., Vikash Gilja, Christine H. Blabe, Brett L. Foster, Krishna V. Shenoy, Josef Parvizi, and Jaimie M. Henderson. 2013. "Hand Posture Classification Using Electrocorticography Signals in the Gamma Band over Human Sensorimotor Brain Areas." *Journal of Neural Engineering* 10 (2). https://doi.org/10.1088/1741-2560/10/2/026002.

Chung, Yoon Gi, Jae Hwan Kang, and Sung Phil Kim. 2012. "Correlation of Fronto-Central Phase Coupling with Sensorimotor Rhythm Modulation." *Neural Networks* 36: 46–50. https://doi.org/10.1016/j.neunet.2012.08.006.

Chung, Yoon Gi, Min Ki Kim, and Sung Phil Kim. 2011. “Inter-Channel Connectivity of Motor Imagery EEG Signals for a Noninvasive BCI Application.” In *Proceedings - International Workshop on Pattern Recognition in NeuroImaging, PRNI 2011*, 49–52. https://doi.org/10.1109/PRNI.2011.9.

Cohen, David. 1968. “Magnetoencephalography: Evidence of Magnetic Fields Produced by Alpha-Rhythm Currents.” *Science* 161 (3843): 784–86. https://doi.org/10.1126/science.161.3843.784.

Cohen, Michael X. 2015. “Effects of Time Lag and Frequency Matching on Phase-Based Connectivity.” *Journal of Neuroscience Methods* 250: 137–46. https://doi.org/10.1016/j.jneumeth.2014.09.005.

Costandi, Moheb. 2016. *Neuroplasticity*. MIt Press.

Coyle, Damien, Girijesh Prasad, and Thomas Martin McGinnity. 2005. “A Time-Series Prediction Approach for Feature Extraction in a Brain-Computer Interface.” *IEEE Transactions on Neural Systems and Rehabilitation Engineering* 13 (4): 461–67. https://doi.org/10.1109/TNSRE.2005.857690.

Curran, Eleanor A., and Maria J. Stokes. 2003. “Learning to Control Brain Activity: A Review of the Production and Control of EEG Components for Driving Brain-Computer Interface (BCI) Systems.” *Brain and Cognition*. Academic Press Inc. https://doi.org/10.1016/S0278-2626(03)00036-8.

Daly, Ian, Slawomir J. Nasuto, and Kevin Warwick. 2012. “Brain Computer Interface Control via Functional Connectivity Dynamics.” *Pattern Recognition* 45 (6): 2123–36. https://doi.org/10.1016/j.patcog.2011.04.034.

Dat, Tran Huy, and Cuntai Guan. 2007. “Feature Selection Based on Fisher Ratio and Mutual Information Analyses for Robust Brain Computer Interface.” In *ICASSP, IEEE International Conference on Acoustics, Speech and Signal Processing - Proceedings*, 1:I-337-I–340. https://doi.org/10.1109/ICASSP.2007.366685.

Dauwels, J., F. Vialatte, T. Musha, and A. Cichocki. 2010. “A Comparative Study of Synchrony Measures for the Early Diagnosis of Alzheimer’s Disease Based on EEG.” *NeuroImage* 49 (1): 668–93.

https://doi.org/10.1016/j.neuroimage.2009.06.056.

Dawson, Kim A. 2004. “Temporal Organization of the Brain: Neurocognitive Mechanisms and Clinical Implications.” *Brain and Cognition* 54 (1): 75–94. https://doi.org/10.1016/S0278-2626(03)00262-8.

Decety, Jean. 1996. “The Neurophysiological Basis of Motor Imagery.” *Behavioural Brain Research*. Elsevier B.V. https://doi.org/10.1016/0166-4328(95)00225-1.

Dechent, Peter, Klaus Dietmar Merboldt, and Jens Frahm. 2004. “Is the Human Primary Motor Cortex Involved in Motor Imagery?” *Cognitive Brain Research* 19 (2): 138–44. https://doi.org/10.1016/j.cogbrainres.2003.11.012.

Demuru, Matteo, and Matteo Fraschini. 2020. “EEG Fingerprinting: Subject-Specific Signature Based on the Aperiodic Component of Power Spectrum.” *Computers in Biology and Medicine* 120 (April): 103748. https://doi.org/10.1016/j.compbiomed.2020.103748.

Deng, Siyi, William Winter, Samuel Thorpe, and Ramesh Srinivasan. 2012. “Improved Surface Laplacian Estimates of Cortical Potential Using Realistic Models of Head Geometry.” *IEEE Transactions on Biomedical Engineering* 59 (11 PART1): 2979–85. https://doi.org/10.1109/TBME.2012.2183638.

Dimitriadis, S. I., N. A. Laskaris, and A. Tzelepi. 2013. “On the Quantization of Time-Varying Phase Synchrony Patterns into Distinct Functional Connectivity Microstates (FCμstates) in a Multi-Trial Visual ERP Paradigm.” *Brain Topography* 26 (3): 397–409. https://doi.org/10.1007/s10548-013-0276-z.

Dimitriadis, Stavros, Yu Sun, Nikolaos Laskaris, Nitish Thakor, and Anastasios Bezerianos. 2016. “Revealing Cross-Frequency Causal Interactions During a Mental Arithmetic Task Through Symbolic Transfer Entropy: A Novel Vector-Quantization Approach.” *IEEE Transactions on Neural Systems and Rehabilitation Engineering* 24 (10): 1017–28. https://doi.org/10.1109/TNSRE.2016.2516107.

Dodia, Shubham, Damodar Reddy Edla, Annushree Bablani, Dharavath Ramesh, and Venkatanareshbabu Kuppili. 2019. “An Efficient EEG Based Deceit Identification Test Using Wavelet Packet Transform and Linear Discriminant Analysis.” *Journal*

of Neuroscience Methods 314 (February): 31–40. https://doi.org/10.1016/j.jneumeth.2019.01.007.

Dornhege, Guido, Benjamin Blankertz, Gabriel Curio, and Klaus Robert Müller. 2004. "Boosting Bit Rates in Noninvasive EEG Single-Trial Classifications by Feature Combination and Multiclass Paradigms." *IEEE Transactions on Biomedical Engineering* 51 (6): 993–1002. https://doi.org/10.1109/TBME.2004.827088.

Dornhege, Guido, Benjamin Blankertz, Matthias Krauledat, Florian Losch, Gabriel Curio, and Klaus Robert Müller. 2006. "Combined Optimization of Spatial and Temporal Filters for Improving Brain-Computer Interfacing." *IEEE Transactions on Biomedical Engineering* 53 (11): 2274–81. https://doi.org/10.1109/TBME.2006.883649.

Dreyer, Alexander M., and Christoph S. Herrmann. 2015. "Frequency-Modulated Steady-State Visual Evoked Potentials: A New Stimulation Method for Brain-Computer Interfaces." *Journal of Neuroscience Methods* 241: 1–9. https://doi.org/10.1016/j.jneumeth.2014.12.004.

Duckrow, R. B., and A. M. Albano. 2003. "Comment on 'Performance of Different Synchronization Measures in Real Data: A Case Study on Electroencephalographic Signals.'" *Physical Review E - Statistical Physics, Plasmas, Fluids, and Related Interdisciplinary Topics* 67 (6): 3. https://doi.org/10.1103/PhysRevE.67.063901.

Duda, Richard O, and Peter E Hart. 2000. *Pattern Classification, Second Edition: 1(A Wiley-Interscience Publication)*. https://www.google.com/books?hl=tr&lr=&id=Br33IRC3PkQC&oi=fnd&pg=PR3&dq=duda+pattern+classification&ots=2xEXJrg7Ft&sig=kSQjlnThzarBKogXNUWCMLjq6YU.

Dyson, M., F. Sepulveda, and J. Q. Gan. 2010. "Localisation of Cognitive Tasks Used in EEG-Based BCIs." *Clinical Neurophysiology* 121 (9): 1481–93. https://doi.org/10.1016/j.clinph.2010.03.011.

Eagleman, David. 2019. *Incognito : Beynin Gizli Hayatı*. Domingo.

Ehrsson, H. Henrik, Stefan Geyer, and Eiichi Naito. 2003. "Imagery of Voluntary

Movement of Fingers, Toes, and Tongue Activates Corresponding Body-Part-Specific Motor Representations." *Journal of Neurophysiology* 90 (5): 3304–16. https://doi.org/10.1152/jn.01113.2002.

Emre Cek, M., Murat Ozgoren, and F. Acar Savaci. 2010. "Continuous Time Wavelet Entropy of Auditory Evoked Potentials." *Computers in Biology and Medicine* 40 (1): 90–96. https://doi.org/10.1016/j.compbiomed.2009.11.005.

Fadlallah, Bilal H. 2015. "Quantifying Cognitive Processes in the Human Brain Using Measures of Dependence." *Dissertation Abstracts International: Section B: The Sciences and Engineering*. University of Florida. http://ezproxy.leedsbeckett.ac.uk/login?url=http://search.ebscohost.com/login.aspx?direct=true&db=psyh&AN=2015-99020-004&site=ehost-live&scope=site.

Faes, Luca, Daniele Marinazzo, Giandomenico Nollo, and Alberto Porta. 2016. "An Information-Theoretic Framework to Map the Spatiotemporal Dynamics of the Scalp Electroencephalogram." *IEEE Transactions on Biomedical Engineering* 63 (12): 2488–96. https://doi.org/10.1109/TBME.2016.2569823.

Fang, Yonghui, Minyou Chen, and Xufei Zheng. 2015. "Extracting Features from Phase Space of EEG Signals in Brain-Computer Interfaces." *Neurocomputing* 151 (P3): 1477–85. https://doi.org/10.1016/j.neucom.2014.10.038.

Farwell, L. A., and E. Donchin. 1988. "Talking off the Top of Your Head: Toward a Mental Prosthesis Utilizing Event-Related Brain Potentials." *Electroencephalography and Clinical Neurophysiology* 70 (6): 510–23. https://doi.org/10.1016/0013-4694(88)90149-6.

Fasil, O. K., and R. Rajesh. 2019. "Time-Domain Exponential Energy for Epileptic EEG Signal Classification." *Neuroscience Letters* 694: 1–8. https://doi.org/10.1016/j.neulet.2018.10.062.

Feng, Jiankui, Erwei Yin, Jing Jin, Rami Saab, Ian Daly, Xingyu Wang, Dewen Hu, and Andrzej Cichocki. 2018. "Towards Correlation-Based Time Window Selection Method for Motor Imagery BCIs." *Neural Networks* 102: 87–95. https://doi.org/10.1016/j.neunet.2018.02.011.

Fingelkurts, Andrew A., Alexander A. Fingelkurts, and Seppo Kähkönen. 2005. "Functional Connectivity in the Brain - Is It an Elusive Concept?" *Neuroscience and Biobehavioral Reviews*. https://doi.org/10.1016/j.neubiorev.2004.10.009.

Firat Ince, Nuri, Sami Arica, and Ahmed Tewfik. 2006. "Classification of Single Trial Motor Imagery EEG Recordings with Subject Adapted Non-Dyadic Arbitrary Time-Frequency Tilings." *Journal of Neural Engineering* 3 (3): 235–44. https://doi.org/10.1088/1741-2560/3/3/006.

Fisher, R. A. 1936. "The Use of Multiple Measurements in Taxonomic Problems." *Annals of Eugenics* 7 (2): 179–88. https://doi.org/10.1111/j.1469-1809.1936.tb02137.x.

Fraschini, Matteo, Matteo Demuru, Alessandra Crobe, Francesco Marrosu, Cornelis J. Stam, and Arjan Hillebrand. 2016. "The Effect of Epoch Length on Estimated EEG Functional Connectivity and Brain Network Organisation." *Journal of Neural Engineering* 13 (3). https://doi.org/10.1088/1741-2560/13/3/036015.

Freiwald, Winrich A., Pedro Valdes, Jorge Bosch, Rolando Biscay, Juan Carlos Jimenez, Luis Manuel Rodriguez, Valia Rodriguez, Andreas K. Kreiter, and Wolf Singer. 1999. "Testing Non-Linearity and Directedness of Interactions between Neural Groups in the Macaque Inferotemporal Cortex." In *Journal of Neuroscience Methods*, 94:105–19. https://doi.org/10.1016/S0165-0270(99)00129-6.

Friedrich, Elisabeth V.C., Reinhold Scherer, and Christa Neuper. 2012. "The Effect of Distinct Mental Strategies on Classification Performance for Brain-Computer Interfaces." *International Journal of Psychophysiology* 84 (1): 86–94. https://doi.org/10.1016/j.ijpsycho.2012.01.014.

Fries, Pascal. 2005. "A Mechanism for Cognitive Dynamics: Neuronal Communication through Neuronal Coherence." *Trends in Cognitive Sciences* 9 (10): 474–80. https://doi.org/10.1016/j.tics.2005.08.011.

Friston, K. J., Katrin H. Preller, Chris Mathys, Hayriye Cagnan, Jakob Heinzle, Adeel Razi, and Peter Zeidman. 2019. "Dynamic Causal Modelling Revisited." *NeuroImage* 199 (4): 730–44. https://doi.org/10.1016/j.neuroimage.2017.02.045.

Friston, Karl J. 2000. “The Labile Brain. I. Neuronal Transients and Nonlinear Coupling.” *Philosophical Transactions of the Royal Society B: Biological Sciences* 355 (1394): 215–36. https://doi.org/10.1098/rstb.2000.0560.

Frye, Richard E., and Meng Hung Wu. 2011. “Multichannel Least-Squares Linear Regression Provides a Fast, Accurate, Unbiased and Robust Estimation of Granger Causality for Neurophysiological Data.” *Computers in Biology and Medicine* 41 (12): 1118–31. https://doi.org/10.1016/j.compbiomed.2011.04.012.

Gao, Lin, Jue Wang, and Longwei Chen. 2013. “Event-Related Desynchronization and Synchronization Quantification in Motor-Related EEG by Kolmogorov Entropy.” *Journal of Neural Engineering* 10 (3). https://doi.org/10.1088/1741-2560/10/3/036023.

Gao, Qing, Xujun Duan, and Huafu Chen. 2011. “Evaluation of Effective Connectivity of Motor Areas during Motor Imagery and Execution Using Conditional Granger Causality.” *NeuroImage* 54 (2): 1280–88. https://doi.org/10.1016/j.neuroimage.2010.08.071.

Gao, Yunyuan, Huixu Su, Rihui Li, and Yingchun Zhang. 2019. “Synchronous Analysis of Brain Regions Based on Multi-Scale Permutation Transfer Entropy.” *Computers in Biology and Medicine* 109: 272–79. https://doi.org/10.1016/j.compbiomed.2019.04.038.

Gao, Zhongke, Shan Li, Qing Cai, Weidong Dang, Yuxuan Yang, Chaoxu Mu, and Pan Hui. 2019. “Relative Wavelet Entropy Complex Network for Improving EEG-Based Fatigue Driving Classification.” *IEEE Transactions on Instrumentation and Measurement* 68 (7): 2491–97. https://doi.org/10.1109/TIM.2018.2865842.

GASTAUT, H. 1952. “[Electrocorticographic Study of the Reactivity of Rolandic Rhythm].” *Revue Neurologique* 87 (2): 176–82. http://www.ncbi.nlm.nih.gov/pubmed/13014777.

Gastaut, H, R Naquet, and Y Gastaut. 1965. “A Study of the Mu Rhythm in Subjects Lacking One or More Limbs.” In *Electroenceph Clin Neurophysiol*, 18:720–21. ELSEVIER SCI IRELAND LTD CUSTOMER RELATIONS MANAGER, BAY 15, SHANNON ….

Gaxiola-Tirado, Jorge Antonio, Rocio Salazar-Varas, and David Gutierrez. 2018. "Using the Partial Directed Coherence to Assess Functional Connectivity in Electroencephalography Data for Brain-Computer Interfaces." *IEEE Transactions on Cognitive and Developmental Systems* 10 (3): 776–83. https://doi.org/10.1109/TCDS.2017.2777180.

Gibson, Jerry. 2018. "Entropy Power, Autoregressive Models, and Mutual Information." *Entropy* 20 (10): 750.

Goksu, Fikri, Nuri F. Ince, and Ahmed H. Tewfik. 2013. "Greedy Solutions for the Construction of Sparse Spatial and Spatio-Spectral Filters in Brain Computer Interface Applications." *Neurocomputing* 108 (May): 69–78. https://doi.org/10.1016/j.neucom.2012.12.003.

Göksu, Hüseyin. 2018. "BCI Oriented EEG Analysis Using Log Energy Entropy of Wavelet Packets." *Biomedical Signal Processing and Control* 44 (July): 101–9. https://doi.org/10.1016/j.bspc.2018.04.002.

Goldberger, A. L., L. A. Amaral, L. Glass, J. M. Hausdorff, P. C. Ivanov, R. G. Mark, J. E. Mietus, G. B. Moody, C. K. Peng, and H. E. Stanley. 2000. "PhysioBank, PhysioToolkit, and PhysioNet: Components of a New Research Resource for Complex Physiologic Signals." *Circulation* 101 (23). https://doi.org/10.1161/01.cir.101.23.e215.

Goldhacker, Markus, Ana M. Tomé, Mark W. Greenlee, and Elmar W. Lang. 2018. "Frequency-Resolved Dynamic Functional Connectivity Reveals Scale-Stable Features of Connectivity-States." *Frontiers in Human Neuroscience* 12: 253. https://doi.org/10.3389/fnhum.2018.00253.

Golub, Gene H, and Michael A Saunders. 1970. "Linear Least Squares and Quadratic Programming." In *Integer and Nonlinear Programming*, 229–56. https://apps.dtic.mil/docs/citations/AD0700923.

Gómez-Herrero, Germán, Wei Wu, Kalle Rutanen, Miguel C. Soriano, Gordon Pipa, and Raul Vicente. 2015. "Assessing Coupling Dynamics from an Ensemble of Time Series." *Entropy* 17 (4): 1958–70. https://doi.org/10.3390/e17041958.

Gomez, Carlos, Jesus Poza, Javier Gomez-Pilar, Alejandro Bachiller, Celia Juan-Cruz, Miguel A. Tola-Arribas, Alicia Carreres, Monica Cano, and Roberto Hornero. 2016. “Analysis of Spontaneous EEG Activity in Alzheimer’s Disease Using Cross-Sample Entropy and Graph Theory.” In *Proceedings of the Annual International Conference of the IEEE Engineering in Medicine and Biology Society, EMBS*, 2016-Octob:2830–33. Institute of Electrical and Electronics Engineers Inc. https://doi.org/10.1109/EMBC.2016.7591319.

Gonuguntla, Venkateswarlu, Yubo Wang, and Kalyana C. Veluvolu. 2016. “Event-Related Functional Network Identification: Application to EEG Classification.” *IEEE Journal on Selected Topics in Signal Processing* 10 (7): 1284–94. https://doi.org/10.1109/JSTSP.2016.2602007.

Gosset, William Sealy. 1908. “Student.” *The Application of the’Law of Error’to the Work of the Brewery*, 3–6.

Gotman, Jean. 1983. “Measurement of Small Time Differences between EEG Channels: Method and Application to Epileptic Seizure Propagation.” *Electroencephalography and Clinical Neurophysiology* 56 (5): 501–14. https://doi.org/10.1016/0013-4694(83)90235-3.

Govindan, R. B., J. Raethjen, F. Kopper, J. C. Claussen, and G. Deuschl. 2005. “Estimation of Time Delay by Coherence Analysis.” *Physica A: Statistical Mechanics and Its Applications* 350 (2–4): 277–95. https://doi.org/10.1016/j.physa.2004.11.043.

Gowreesunker, B. Vikrham, Ahmed H. Tewfik, Vijay A. Tadipatri, Nuri F. Ince, James Ashe, and Giuseppe Pellizzer. 2009. “Overcoming Measurement Time Variability in Brain Machine Interface.” In *Proceedings of the 31st Annual International Conference of the IEEE Engineering in Medicine and Biology Society: Engineering the Future of Biomedicine, EMBC 2009*, 3134–37. IEEE Computer Society. https://doi.org/10.1109/IEMBS.2009.5332568.

Granger, C. W. J. 1969. “Investigating Causal Relations by Econometric Models and Cross-Spectral Methods.” *Econometrica* 37 (3): 424. https://doi.org/10.2307/1912791.

Greenblatt, R. E., M. E. Pflieger, and A. E. Ossadtchi. 2012. “Connectivity Measures Applied to Human Brain Electrophysiological Data.” *Journal of Neuroscience Methods*. https://doi.org/10.1016/j.jneumeth.2012.02.025.

Grosse-Wentrup, Moritz, and Martin Buss. 2008. “Multiclass Common Spatial Patterns and Information Theoretic Feature Extraction.” *IEEE Transactions on Biomedical Engineering* 55 (8): 1991–2000. https://doi.org/10.1109/TBME.2008.921154.

Grosse-Wentrup, Moritz, Bernhard Schölkopf, and Jeremy Hill. 2011. “Causal Influence of Gamma Oscillations on the Sensorimotor Rhythm.” *NeuroImage* 56 (2): 837–42. https://doi.org/10.1016/j.neuroimage.2010.04.265.

Gu, Lingyun, Zhenhua Yu, Tian Ma, Haixian Wang, Zhanli Li, and Hui Fan. 2020. “EEG-Based Classification of Lower Limb Motor Imagery with Brain Network Analysis.” *Neuroscience* 436 (April): 93–109. https://doi.org/10.1016/j.neuroscience.2020.04.006.

Güdücü, C., B. O. Olcay, L. Schäfer, M. Aziz, V. A. Schriever, M. Özgören, and T. Hummel. 2019. “Separating Normosmic and Anosmic Patients Based on Entropy Evaluation of Olfactory Event-Related Potentials.” *Brain Research* 1708 (April): 78–83. https://doi.org/10.1016/j.brainres.2018.12.012.

Guger, Christoph. 2018. “G.Tec Medical Engineering | Brain-Computer Interfaces and Neurotechnology.” 2018. https://www.gtec.at/.

Gupta, Anubha, Pushpendra Singh, and Mandar Karlekar. 2018. “A Novel Signal Modeling Approach for Classification of Seizure and Seizure-Free EEG Signals.” *IEEE Transactions on Neural Systems and Rehabilitation Engineering* 26 (5): 925–35. https://doi.org/10.1109/TNSRE.2018.2818123.

Gürkan, Güray, Aydin Akan, and Tülay Ö Seyhan. 2014. “Analysis of Brain Connectivity Changes after Propofol Injection by Generalized Partial Directed Coherence.” *Digital Signal Processing: A Review Journal* 25 (1): 156–63. https://doi.org/10.1016/j.dsp.2013.11.011.

Gutiérrez, David, and Rocio Salazar-Varas. 2012. “Using Eigenstructure Decompositions of Time-Varying Autoregressions in Common Spatial Patterns-

Based EEG Signal Classification." *Biomedical Signal Processing and Control* 7 (6): 622–31. https://doi.org/10.1016/j.bspc.2012.03.004.

Guyon, Isabelle. 1998. *Pattern Classification*. *Pattern Analysis and Applications*. Vol. 1. John Wiley & Sons. https://doi.org/10.1007/bf01237942.

Gysels, E., P. Renevey, and P. Celka. 2005. "SVM-Based Recursive Feature Elimination to Compare Phase Synchronization Computed from Broadband and Narrowband EEG Signals in Brain-Computer Interfaces." *Signal Processing* 85 (11): 2178–89. https://doi.org/10.1016/j.sigpro.2005.07.008.

Halder, S., D. Agorastos, R. Veit, E. M. Hammer, S. Lee, B. Varkuti, M. Bogdan, W. Rosenstiel, N. Birbaumer, and A. Kübler. 2011. "Neural Mechanisms of Brain-Computer Interface Control." *NeuroImage* 55 (4): 1779–90. https://doi.org/10.1016/j.neuroimage.2011.01.021.

Hamedi, Mahyar, Sh Hussain Salleh, Chee Ming Ting, S. Balqis Samdin, and Alias Mohd Noor. 2015. "Sensor Space Time-Varying Information Flow Analysis of Multiclass Motor Imagery through Kalman Smoother and Em Algorithm." In *2015 International Conference on BioSignal Analysis, Processing and Systems, ICBAPS 2015*, 118–22. Institute of Electrical and Electronics Engineers Inc. https://doi.org/10.1109/ICBAPS.2015.7292230.

Hanakawa, Takashi. 2016. "Organizing Motor Imageries." *Neuroscience Research*. Elsevier Ireland Ltd. https://doi.org/10.1016/j.neures.2015.11.003.

Handiru, Vikram Shenoy, and Vinod A. Prasad. 2016. "Optimized Bi-Objective EEG Channel Selection and Cross-Subject Generalization with Brain-Computer Interfaces." *IEEE Transactions on Human-Machine Systems* 46 (6): 777–86. https://doi.org/10.1109/THMS.2016.2573827.

Hansen, Enrique C.A., Demian Battaglia, Andreas Spiegler, Gustavo Deco, and Viktor K. Jirsa. 2015. "Functional Connectivity Dynamics: Modeling the Switching Behavior of the Resting State." *NeuroImage* 105 (January): 525–35. https://doi.org/10.1016/j.neuroimage.2014.11.001.

Hardwick, Robert M, Svenja Caspers, Simon B Eickhoff, and Stephan P Swinnen.

2018. “Neural Correlates of Action: Comparing Meta-Analyses of Imagery, Observation, and Execution.” *Neuroscience and Biobehavioral Reviews*. https://doi.org/10.1016/j.neubiorev.2018.08.003.

Hari, Riitta, and Lauri Parkkonen. 2015. “The Brain Timewise: How Timing Shapes and Supports Brain Function.” *Philosophical Transactions of the Royal Society B: Biological Sciences* 370 (1668). https://doi.org/10.1098/rstb.2014.0170.

Harrison, L., W. D. Penny, and K. Friston. 2003. “Multivariate Autoregressive Modeling of FMRI Time Series.” *NeuroImage* 19 (4): 1477–91. https://doi.org/10.1016/S1053-8119(03)00160-5.

Haykin, Simon. 1995. *Neural Networks: A Comprehensive Foundation*. *Control Engineering Practice*. Vol. 3. Macmillan. https://doi.org/10.1016/0967-0661(95)90080-2.

———. 2001. *Kalman Filtering and Neural Networks*. *Kalman Filtering and Neural Networks*. Vol. 47. John Wiley & Sons. https://doi.org/10.1002/0471221546.

Haykin, Simon, and Bernard Widrow. 2005. *Least-Mean-Square Adaptive Filters*. *Least-Mean-Square Adaptive Filters*. Vol. 31. John Wiley & Sons. https://doi.org/10.1002/0471461288.

He, Bin, Bryan Baxter, Bradley J. Edelman, Christopher C. Cline, and Wenjing W. Ye. 2015. “Noninvasive Brain-Computer Interfaces Based on Sensorimotor Rhythms.” *Proceedings of the IEEE* 103 (6): 907–25. https://doi.org/10.1109/JPROC.2015.2407272.

He, Fei, and Yuan Yang. 2021. “Nonlinear System Identification of Neural Systems from Neurophysiological Signals.” *Neuroscience*. https://doi.org/10.1016/j.neuroscience.2020.12.001.

Herff, Christian, Lorenz Diener, Miguel Angrick, Emily Mugler, Matthew C. Tate, Matthew A. Goldrick, Dean J. Krusienski, Marc W. Slutzky, and Tanja Schultz. 2019. “Generating Natural, Intelligible Speech From Brain Activity in Motor, Premotor, and Inferior Frontal Cortices.” *Frontiers in Neuroscience* 13 (November): 1267. https://doi.org/10.3389/fnins.2019.01267.

Hermanto, Beni Rio, Tati R. Mengko, Adi Indrayanto, and Ary S. Prihatmanto. 2013. "Brain Signal Reference Concept Using Cross Correlation Based for Brain Computer Interface." In *Proc. of 2013 3rd Int. Conf. on Instrumentation, Communications, Information Technol., and Biomedical Engineering: Science and Technol. for Improvement of Health, Safety, and Environ., ICICI-BME 2013*, 388–91. IEEE Computer Society. https://doi.org/10.1109/ICICI-BME.2013.6698531.

Hettiarachchi, Imali T., Thanh Thi Nguyen, and Saeid Nahavandi. 2016. "Multivariate Adaptive Autoregressive Modeling and Kalman Filtering for Motor Imagery BCI." In *Proceedings - 2015 IEEE International Conference on Systems, Man, and Cybernetics, SMC 2015*, 3164–68. https://doi.org/10.1109/SMC.2015.549.

Hétu, Sébastien, Mathieu Grégoire, Arnaud Saimpont, Michel Pierre Coll, Fanny Eugène, Pierre Emmanuel Michon, and Philip L. Jackson. 2013. "The Neural Network of Motor Imagery: An ALE Meta-Analysis." *Neuroscience and Biobehavioral Reviews*. Pergamon. https://doi.org/10.1016/j.neubiorev.2013.03.017.

Higashi, Hiroshi, and Toshihisa Tanaka. 2013. "Simultaneous Design of FIR Filter Banks and Spatial Patterns for EEG Signal Classification." *IEEE Transactions on Biomedical Engineering* 60 (4): 1100–1110. https://doi.org/10.1109/TBME.2012.2215960.

Hill, Peter D. 1985. "Kernel Estimation of a Distribution Function." *Communications in Statistics - Theory and Methods* 14 (3): 605–20. https://doi.org/10.1080/03610928508828937.

Hipólito, Inês, Maxwell J.D. Ramstead, Laura Convertino, Anjali Bhat, Karl Friston, and Thomas Parr. 2021. "Markov Blankets in the Brain." *Neuroscience and Biobehavioral Reviews* 125 (July 2020): 88–97. https://doi.org/10.1016/j.neubiorev.2021.02.003.

Hipp, Joerg F., Andreas K. Engel, and Markus Siegel. 2011. "Oscillatory Synchronization in Large-Scale Cortical Networks Predicts Perception." *Neuron* 69 (2): 387–96. https://doi.org/10.1016/j.neuron.2010.12.027.

Hipp, Joerg F., David J. Hawellek, Maurizio Corbetta, Markus Siegel, and Andreas K.

Engel. 2012. “Large-Scale Cortical Correlation Structure of Spontaneous Oscillatory Activity.” *Nature Neuroscience* 15 (6): 884–90. https://doi.org/10.1038/nn.3101.

Hjorth, Bo. 1970. “EEG Analysis Based on Time Domain Properties.” *Electroencephalography and Clinical Neurophysiology* 29 (3): 306–10. https://doi.org/10.1016/0013-4694(70)90143-4.

Höller, Yvonne, Jürgen Bergmann, Martin Kronbichler, Julia Sophia Crone, Elisabeth Verena Schmid, Aljoscha Thomschewski, Kevin Butz, Verena Schütze, Peter Höller, and Eugen Trinka. 2013. “Real Movement vs. Motor Imagery in Healthy Subjects.” *International Journal of Psychophysiology* 87 (1): 35–41. https://doi.org/10.1016/j.ijpsycho.2012.10.015.

Hou, Huirang, Biao Sun, and Qinghao Meng. 2019. “Slow Cortical Potential Signal Classification Using Concave–Convex Feature.” *Journal of Neuroscience Methods* 324. https://doi.org/10.1016/j.jneumeth.2019.05.012.

Hsu, Wei Yen. 2011. “EEG-Based Motor Imagery Classification Using Enhanced Active Segment Selection and Adaptive Classifier.” *Computers in Biology and Medicine* 41 (8): 633–39. https://doi.org/10.1016/j.compbiomed.2011.05.014.

Hsu, Wei Yen, Chou Ching Lin, Ming Shaung Ju, and Yung Nien Sun. 2007. “Wavelet-Based Fractal Features with Active Segment Selection: Application to Single-Trial EEG Data.” *Journal of Neuroscience Methods* 163 (1): 145–60. https://doi.org/10.1016/j.jneumeth.2007.02.004.

Hsu, Wei Yen, and Yung Nien Sun. 2009. “EEG-Based Motor Imagery Analysis Using Weighted Wavelet Transform Features.” *Journal of Neuroscience Methods* 176 (2): 310–18. https://doi.org/10.1016/j.jneumeth.2008.09.014.

Huan, Nai Jen, and Ramaswamy Palaniappan. 2004. “Neural Network Classification of Autoregressive Features from Electroencephalogram Signals for Brain-Computer Interface Design.” *Journal of Neural Engineering* 1 (3): 142–50. https://doi.org/10.1088/1741-2560/1/3/003.

Huang, Dengfeng, Aifeng Ren, Jing Shang, Qiao Lei, Yun Zhang, Zhongliang Yin, Jun

Li, Karen M. Von Deneen, and Liyu Huang. 2016. “Combining Partial Directed Coherence and Graph Theory to Analyse Effective Brain Networks of Different Mental Tasks.” *Frontiers in Human Neuroscience* 10 (MAY2016). https://doi.org/10.3389/fnhum.2016.00235.

Huang, Guang Bin, Lei Chen, and Chee Kheong Siew. 2006. “Universal Approximation Using Incremental Constructive Feedforward Networks with Random Hidden Nodes.” *IEEE Transactions on Neural Networks* 17 (4): 879–92. https://doi.org/10.1109/TNN.2006.875977.

Hutchison, R. Matthew, Thilo Womelsdorf, Elena A. Allen, Peter A. Bandettini, Vince D. Calhoun, Maurizio Corbetta, Stefania Della Penna, et al. 2013. “Dynamic Functional Connectivity: Promise, Issues, and Interpretations.” *NeuroImage* 80 (October): 360–78. https://doi.org/10.1016/j.neuroimage.2013.05.079.

Hyvärinen, A., and E. Oja. 2000. “Independent Component Analysis: Algorithms and Applications.” *Neural Networks* 13 (4–5): 411–30. https://doi.org/10.1016/S0893-6080(00)00026-5.

Ibáñez-Molina, Antonio J., Sergio Iglesias-Parro, María F. Soriano, and José I. Aznarte. 2015. “Multiscale Lempel-Ziv Complexity for EEG Measures.” *Clinical Neurophysiology* 126 (3): 541–48. https://doi.org/10.1016/j.clinph.2014.07.012.

Ibrahim Al-Omari, Amer. 2014. “Estimation of Entropy Using Random Sampling.” *Journal of Computational and Applied Mathematics* 261 (May): 95–102. https://doi.org/10.1016/j.cam.2013.10.047.

Ince, Nuri F., Fikri Goksu, Ahmed H. Tewfik, and Sami Arica. 2009. “Adapting Subject Specific Motor Imagery EEG Patterns in Space-Time-Frequency for a Brain Computer Interface.” *Biomedical Signal Processing and Control* 4 (3): 236–46. https://doi.org/10.1016/j.bspc.2009.03.005.

Ince, Nuri F., Ahmed H. Tewfik, and Sami Arica. 2007. “Extraction Subject-Specific Motor Imagery Time-Frequency Patterns for Single Trial EEG Classification.” *Computers in Biology and Medicine* 37 (4): 499–508. https://doi.org/10.1016/j.compbiomed.2006.08.014.

Jalili, Mahdi, Elham Barzegaran, and Maria G. Knyazeva. 2014. “Synchronization of EEG: Bivariate and Multivariate Measures.” *IEEE Transactions on Neural Systems and Rehabilitation Engineering* 22 (2): 212–21. https://doi.org/10.1109/TNSRE.2013.2289899.

Jeannerod, M., M. A. Arbib, G. Rizzolatti, and H. Sakata. 1995. “Grasping Objects: The Cortical Mechanisms of Visuomotor Transformation.” *Trends in Neurosciences* 18 (7): 314–20. https://doi.org/10.1016/0166-2236(95)93921-J.

Jeannerod, Marc. 2001. “Neural Simulation of Action: A Unifying Mechanism for Motor Cognition.” *NeuroImage* 14 (1 II): S103–9. https://doi.org/10.1006/nimg.2001.0832.

Jensen, Ole, and Ali Mazaheri. 2010. “Shaping Functional Architecture by Oscillatory Alpha Activity: Gating by Inhibition.” *Frontiers in Human Neuroscience* 4 (November): 186. https://doi.org/10.3389/fnhum.2010.00186.

Jeong, Jaeseung, John C. Gore, and Bradley S. Peterson. 2001. “Mutual Information Analysis of the EEG in Patients with Alzheimer’s Disease.” *Clinical Neurophysiology* 112 (5): 827–35. https://doi.org/10.1016/S1388-2457(01)00513-2.

Jeunet, Camille, Bernard Nkaoua, Sriram Subramanian, Martin Hachet, and Fabien Lotte. 2015. “Predicting Mental Imagery-Based BCI Performance from Personality, Cognitive Profile and Neurophysiological Patterns.” *PLoS ONE* 10 (12): e0143962. https://doi.org/10.1371/journal.pone.0143962.

Jian, Wenjuan, Minyou Chen, and Dennis J. McFarland. 2017. “EEG Based Zero-Phase Phase-Locking Value (PLV) and Effects of Spatial Filtering during Actual Movement.” *Brain Research Bulletin* 130: 156–64. https://doi.org/10.1016/j.brainresbull.2017.01.023.

Jiao, Yong, Yu Zhang, Xun Chen, Erwei Yin, Jing Jin, Xingyu Wang, and Andrzej Cichocki. 2019. “Sparse Group Representation Model for Motor Imagery EEG Classification.” *IEEE Journal of Biomedical and Health Informatics* 23 (2): 631–41. https://doi.org/10.1109/JBHI.2018.2832538.

Jin, Jing, Brendan Z. Allison, Xingyu Wang, and Christa Neuper. 2012. “A Combined Brain-Computer Interface Based on P300 Potentials and Motion-Onset Visual Evoked Potentials.” *Journal of Neuroscience Methods* 205 (2): 265–76. https://doi.org/10.1016/j.jneumeth.2012.01.004.

Jin, Jing, Yangyang Miao, Ian Daly, Cili Zuo, Dewen Hu, and Andrzej Cichocki. 2019. “Correlation-Based Channel Selection and Regularized Feature Optimization for MI-Based BCI.” *Neural Networks* 118 (October): 262–70. https://doi.org/10.1016/j.neunet.2019.07.008.

Jin, Seung Hyun, Yong Ju Kwon, Jin Su Jeong, Suk Won Kwon, and Dong Hoon Shin. 2006. “Increased Information Transmission during Scientific Hypothesis Generation: Mutual Information Analysis of Multichannel EEG.” *International Journal of Psychophysiology* 62 (2): 337–44. https://doi.org/10.1016/j.ijpsycho.2006.06.003.

Jin, Seung Hyun, Peter Lin, and Mark Hallett. 2010. “Linear and Nonlinear Information Flow Based on Time-Delayed Mutual Information Method and Its Application to Corticomuscular Interaction.” *Clinical Neurophysiology* 121 (3): 392–401. https://doi.org/10.1016/j.clinph.2009.09.033.

———. 2012. “Reorganization of Brain Functional Small-World Networks during Finger Movements.” *Human Brain Mapping* 33 (4): 861–72. https://doi.org/10.1002/hbm.21253.

Jin, Zhichao, Guoxu Zhou, Daqi Gao, and Yu Zhang. 2018. “EEG Classification Using Sparse Bayesian Extreme Learning Machine for Brain–Computer Interface.” *Neural Computing and Applications*, 2018. https://doi.org/10.1007/s00521-018-3735-3.

Jolliffe, I. T. 1986. “Principal Components in Regression Analysis.” In *Principal Component Analysis*, 129–55. Springer. https://doi.org/10.1007/978-1-4757-1904-8_8.

Jurcak, Valer, Daisuke Tsuzuki, and Ippeita Dan. 2007. “10/20, 10/10, and 10/5 Systems Revisited: Their Validity as Relative Head-Surface-Based Positioning Systems.” *NeuroImage* 34 (4): 1600–1611.

https://doi.org/10.1016/j.neuroimage.2006.09.024.

Kahana, Michael J. 2006. “The Cognitive Correlates of Human Brain Oscillations.” *Journal of Neuroscience*. https://doi.org/10.1523/JNEUROSCI.3737-05c.2006.

Kaminski, Maciej, Aneta Brzezicka, Jan Kaminski, and Katarzyna J. Blinowska. 2016. “Measures of Coupling between Neural Populations Based on Granger Causality Principle.” *Frontiers in Computational Neuroscience* 10 (OCT): 114. https://doi.org/10.3389/fncom.2016.00114.

Kang, Hyohyeong, Yunjun Nam, and Seungjin Choi. 2009. “Composite Common Spatial Pattern for Subject-to-Subject Transfer.” *IEEE Signal Processing Letters* 16 (8): 683–86. https://doi.org/10.1109/LSP.2009.2022557.

Kang, Jiannan, Huimin Chen, Xin Li, and Xiaoli Li. 2019. “EEG Entropy Analysis in Autistic Children.” *Journal of Clinical Neuroscience* 62: 199–206. https://doi.org/10.1016/j.jocn.2018.11.027.

Kang, Jun Su, Ukeob Park, V. Gonuguntla, K. C. Veluvolu, and Minho Lee. 2015. “Human Implicit Intent Recognition Based on the Phase Synchrony of EEG Signals.” *Pattern Recognition Letters* 66 (November): 144–52. https://doi.org/10.1016/j.patrec.2015.06.013.

Kannathal, N, Min Lim Choo, U. Rajendra Acharya, and P. K. Sadasivan. 2005. “Entropies for Detection of Epilepsy in EEG.” *Computer Methods and Programs in Biomedicine* 80 (3): 187–94. https://doi.org/10.1016/j.cmpb.2005.06.012.

Karakuş, Oktay. 2017. “Generalised Bayesian Model Selection Using Reversible Jump Markov Chain Monte Carlo.”

Karakus, Oktay, Ercan E. Kuruoglu, and Mustafa A. Altinkaya. 2015. “Estimation of the Nonlinearity Degree for Polynomial Autoregressiv Processes with RJMCMC.” In *2015 23rd European Signal Processing Conference, EUSIPCO 2015*, 953–57. https://doi.org/10.1109/EUSIPCO.2015.7362524.

Karamzadeh, Nader, Andrei Medvedev, Afrouz Azari, Amir Gandjbakhche, and Laleh Najafizadeh. 2013. “Capturing Dynamic Patterns of Task-Based Functional

Connectivity with EEG." *NeuroImage* 66 (February): 311–17. https://doi.org/10.1016/j.neuroimage.2012.10.032.

Kasess, Christian H., Christian Windischberger, Ross Cunnington, Rupert Lanzenberger, Lukas Pezawas, and Ewald Moser. 2008. "The Suppressive Influence of SMA on M1 in Motor Imagery Revealed by FMRI and Dynamic Causal Modeling." *NeuroImage* 40 (2): 828–37. https://doi.org/10.1016/j.neuroimage.2007.11.040.

Kee, Chea Yau, S. G. Ponnambalam, and Chu Kiong Loo. 2017. "Binary and Multi-Class Motor Imagery Using Renyi Entropy for Feature Extraction." *Neural Computing and Applications* 28 (8): 2051–62. https://doi.org/10.1007/s00521-016-2178-y.

Keirn, Zachary A., and Jorge I. Aunon. 1990. "A New Mode of Communication Between Man and His Surroundings." *IEEE Transactions on Biomedical Engineering* 37 (12): 1209–14. https://doi.org/10.1109/10.64464.

Kelso, J. A.Scott, Guillaume Dumas, and Emmanuelle Tognoli. 2013. "Outline of a General Theory of Behavior and Brain Coordination." *Neural Networks* 37: 120–31. https://doi.org/10.1016/j.neunet.2012.09.003.

Kendall, Maurice George. 1946. "The Advanced Theory of Statistics." *The Advanced Theory of Statistics.*, no. 2nd Ed.

Kendall, MG. 1938. "Rank Correlation." *Nature*. https://doi.org/10.2307/2280246.

Keshmiri, Soheil. 2020. "Entropy and the Brain: An Overview." *Entropy*. MDPI AG. https://doi.org/10.3390/E22090917.

Khalaf, Aya, Ervin Sejdic, and Murat Akcakaya. 2019. "Common Spatial Pattern and Wavelet Decomposition for Motor Imagery EEG- FTCD Brain-Computer Interface." *Journal of Neuroscience Methods* 320 (January): 98–106. https://doi.org/10.1016/j.jneumeth.2019.03.018.

Khanna, Preeya, and Jose M. Carmena. 2015. "Neural Oscillations: Beta Band Activity across Motor Networks." *Current Opinion in Neurobiology*.

https://doi.org/10.1016/j.conb.2014.11.010.

Kilintari, Marina, Shalini Narayana, Abbas Babajani-Feremi, Roozbeh Rezaie, and Andrew C. Papanicolaou. 2016. “Brain Activation Profiles during Kinesthetic and Visual Imagery: An FMRI Study.” *Brain Research* 1646 (September): 249–61. https://doi.org/10.1016/j.brainres.2016.06.009.

Kim, Youngjoo, Jiwoo Ryu, Ko Keun Kim, Clive C. Took, Danilo P. Mandic, and Cheolsoo Park. 2016. “Motor Imagery Classification Using Mu and Beta Rhythms of EEG with Strong Uncorrelating Transform Based Complex Common Spatial Patterns.” *Computational Intelligence and Neuroscience* 2016: 1. https://doi.org/10.1155/2016/1489692.

Kira, Kenji, and Larry A. Rendell. 1992. “A Practical Approach to Feature Selection.” In *Machine Learning Proceedings 1992*, 249–56. Elsevier. https://doi.org/10.1016/b978-1-55860-247-2.50037-1.

Kirschner, Aaron, Julia Wing Yan Kam, Todd C. Handy, and Lawrence M. Ward. 2012. “Differential Synchronization in Default and Task-Specific Networks of the Human Brain.” *Frontiers in Human Neuroscience* 6 (MAY 2012): 1–10. https://doi.org/10.3389/fnhum.2012.00139.

Klimesch, Wolfgang. 1996. “Memory Processes, Brain Oscillations and EEG Synchronization.” *International Journal of Psychophysiology* 24 (1–2): 61–100. https://doi.org/10.1016/S0167-8760(96)00057-8.

———. 2012. “Alpha-Band Oscillations, Attention, and Controlled Access to Stored Information.” *Trends in Cognitive Sciences*. https://doi.org/10.1016/j.tics.2012.10.007.

Klimesch, Wolfgang, Paul Sauseng, and Simon Hanslmayr. 2007. “EEG Alpha Oscillations: The Inhibition-Timing Hypothesis.” *Brain Research Reviews* 53 (1): 63–88. https://doi.org/10.1016/j.brainresrev.2006.06.003.

Koley, B., and D. Dey. 2012. “An Ensemble System for Automatic Sleep Stage Classification Using Single Channel EEG Signal.” *Computers in Biology and Medicine* 42 (12): 1186–95. https://doi.org/10.1016/j.compbiomed.2012.09.012.

Kornmüller, Alois Eduard. 1935. “Der Mechanismus Des Epileptischen Anfalles Auf Grund Bioelektrischer Untersuchungen Am Zentralnervensystem.” *Fortschr. d. Neurol. Psychiatry* 7: 391–400; 414–32.

Kozachenko, L. F., and N. N. Leonenko. 1987. “Sample Estimate of the Entropy of a Random Vector.” *Problems of Information Transmission* 23 (2): 95–101.

Kraeutner, Sarah, Alicia Gionfriddo, Timothy Bardouille, and Shaun Boe. 2014. “Motor Imagery-Based Brain Activity Parallels That of Motor Execution: Evidence from Magnetic Source Imaging of Cortical Oscillations.” *Brain Research* 1588: 81–91. https://doi.org/10.1016/j.brainres.2014.09.001.

Kraskov, Alexander, Harald Stögbauer, and Peter Grassberger. 2004. “Estimating Mutual Information.” *Physical Review E - Statistical Physics, Plasmas, Fluids, and Related Interdisciplinary Topics* 69 (6): 16. https://doi.org/10.1103/PhysRevE.69.066138.

Krusienski, Dean J., Dennis J. McFarland, and Jonathan R. Wolpaw. 2006. “An Evaluation of Autoregressive Spectral Estimation Model Order for Brain-Computer Interface Applications.” In *Annual International Conference of the IEEE Engineering in Medicine and Biology - Proceedings*, 1323–26. https://doi.org/10.1109/IEMBS.2006.259822.

———. 2012. “Value of Amplitude, Phase, and Coherence Features for a Sensorimotor Rhythm-Based Brain-Computer Interface.” *Brain Research Bulletin* 87 (1): 130–34. https://doi.org/10.1016/j.brainresbull.2011.09.019.

Ktonas, P. Y., and R. Mallart. 1991. “Estimation of Time Delay between EEG Signals for Epileptic Focus Localization: Statistical Error Considerations.” *Electroencephalography and Clinical Neurophysiology* 78 (2): 105–10. https://doi.org/10.1016/0013-4694(91)90109-H.

Kumar, Shiu, Alok Sharma, and Tatsuhiko Tsunoda. 2017. “An Improved Discriminative Filter Bank Selection Approach for Motor Imagery EEG Signal Classification Using Mutual Information.” *BMC Bioinformatics* 18 (December). https://doi.org/10.1186/s12859-017-1964-6.

Kuruoğlu, Ercan E. 2002. “Nonlinear Least Lp-Norm Filters for Nonlinear Autoregressive α-Stable Processes.” *Digital Signal Processing: A Review Journal* 12 (1): 119–42. https://doi.org/10.1006/dspr.2001.0416.

Labate, Domenico, Fabio La Foresta, Giuseppe Morabito, Isabella Palamara, and Francesco Carlo Morabito. 2013. “Entropic Measures of EEG Complexity in Alzheimer’s Disease through a Multivariate Multiscale Approach.” *IEEE Sensors Journal* 13 (9): 3284–92. https://doi.org/10.1109/JSEN.2013.2271735.

Lachaux, Jean Philippe, Antoine Lutz, David Rudrauf, Diego Cosmelli, Michel Le Van Quyen, Jacques Martinerie, and Francisco Varela. 2002. “Estimating the Time-Course of Coherence between Single-Trial Brain Signals: An Introduction to Wavelet Coherence.” *Neurophysiologie Clinique* 32 (3): 157–74. https://doi.org/10.1016/S0987-7053(02)00301-5.

Lachaux, Jean Philippe, Eugenio Rodriguez, Jacques Martinerie, and Francisco J. Varela. 1999. “Measuring Phase Synchrony in Brain Signals.” *Human Brain Mapping* 8 (4): 194–208. https://doi.org/10.1002/(SICI)1097-0193(1999)8:4<194::AID-HBM4>3.0.CO;2-C.

Lafleur, Karl, Kaitlin Cassady, Alexander Doud, Kaleb Shades, Eitan Rogin, and Bin He. 2013. “Quadcopter Control in Three-Dimensional Space Using a Noninvasive Motor Imagery-Based Brain-Computer Interface.” *Journal of Neural Engineering* 10 (4). https://doi.org/10.1088/1741-2560/10/4/046003.

Lang, E. W., A. M. Tomé, I. R. Keck, J. M. Górriz-Sáez, and C. G. Puntonet. 2012. “Brain Connectivity Analysis: A Short Survey.” *Computational Intelligence and Neuroscience*. https://doi.org/10.1155/2012/412512.

Lau-Zhu, Alex, Michael P.H. Lau, and Gráinne McLoughlin. 2019. “Mobile EEG in Research on Neurodevelopmental Disorders: Opportunities and Challenges.” *Developmental Cognitive Neuroscience*. Elsevier Ltd. https://doi.org/10.1016/j.dcn.2019.100635.

Lawhern, Vernon, W. David Hairston, Kaleb McDowell, Marissa Westerfield, and Kay Robbins. 2012. “Detection and Classification of Subject-Generated Artifacts in EEG Signals Using Autoregressive Models.” *Journal of Neuroscience Methods*

208 (2): 181–89. https://doi.org/10.1016/j.jneumeth.2012.05.017.

Lemm, Steven, Benjamin Blankertz, Gabriel Curio, and Klaus Robert Müller. 2005. "Spatio-Spectral Filters for Improving the Classification of Single Trial EEG." *IEEE Transactions on Biomedical Engineering* 52 (9): 1541–48. https://doi.org/10.1109/TBME.2005.851521.

Lemm, Steven, Christin Schäfer, and Gabriel Curio. 2004. "BCI Competition 2003 - Data Set III: Modeling of Sensorimotor μ Rhythms for Classification of Imaginary Hand Movements." *IEEE Transactions on Biomedical Engineering* 51 (6): 1077–80. https://doi.org/10.1109/TBME.2004.827076.

Lenartowicz, A., and R. A. Poldrack. 2010. "Brain Imaging." In *Encyclopedia of Behavioral Neuroscience*, 187–93. Chichester, UK: John Wiley & Sons, Ltd. https://doi.org/10.1016/B978-0-08-045396-5.00052-X.

Lerga, Jonatan, Nicoletta Saulig, and Vladimir Mozetič. 2017. "Algorithm Based on the Short-Term Rényi Entropy and IF Estimation for Noisy EEG Signals Analysis." *Computers in Biology and Medicine* 80: 1–13. https://doi.org/10.1016/j.compbiomed.2016.11.002.

Li, Gongfa, Du Jiang, Yanling Zhou, Guozhang Jiang, Jianyi Kong, and Gunasekaran Manogaran. 2019. "Human Lesion Detection Method Based on Image Information and Brain Signal." *IEEE Access* 7: 11533–42. https://doi.org/10.1109/ACCESS.2019.2891749.

Li, Gongfa, Jiahan Li, Zhaojie Ju, Ying Sun, and Jianyi Kong. 2019. "A Novel Feature Extraction Method for Machine Learning Based on Surface Electromyography from Healthy Brain." *Neural Computing and Applications* 31 (12): 9013–22. https://doi.org/10.1007/s00521-019-04147-3.

Li, Junhua, Yijun Wang, Liqing Zhang, Andrzej Cichocki, and Tzyy Ping Jung. 2016. "Decoding EEG in Cognitive Tasks With Time-Frequency and Connectivity Masks." *IEEE Transactions on Cognitive and Developmental Systems* 8 (4): 298–308. https://doi.org/10.1109/TCDS.2016.2555952.

Li, Peiyang, Xurui Wang, Fali Li, Rui Zhang, Teng Ma, Yueheng Peng, Xu Lei, et al.

2015. “Autoregressive Model in the Lp Norm Space for EEG Analysis.” *Journal of Neuroscience Methods* 240 (January): 170–78. https://doi.org/10.1016/j.jneumeth.2014.11.007.

Li, Peng, Ke Li, Chengyu Liu, Dingchang Zheng, Zong Ming Li, and Changchun Liu. 2016. “Detection of Coupling in Short Physiological Series by a Joint Distribution Entropy Method.” *IEEE Transactions on Biomedical Engineering* 63 (11): 2231–42. https://doi.org/10.1109/TBME.2016.2515543.

Li, Peng, Chengyu Liu, Ke Li, Dingchang Zheng, Changchun Liu, and Yinglong Hou. 2015. “Assessing the Complexity of Short-Term Heartbeat Interval Series by Distribution Entropy.” *Medical and Biological Engineering and Computing* 53 (1): 77–87. https://doi.org/10.1007/s11517-014-1216-0.

Li, Yang, Mengying Lei, Weigang Cui, Yuzhu Guo, and Hua Liang Wei. 2019. “A Parametric Time-Frequency Conditional Granger Causality Method Using Ultra-Regularized Orthogonal Least Squares and Multiwavelets for Dynamic Connectivity Analysis in EEGs.” *IEEE Transactions on Biomedical Engineering* 66 (12): 3509–25. https://doi.org/10.1109/TBME.2019.2906688.

Liang, Zhenhu, Yinghua Wang, Gaoxiang Ouyang, Logan J. Voss, Jamie W. Sleigh, and Xiaoli Li. 2013. “Permutation Auto-Mutual Information of Electroencephalogram in Anesthesia.” *Journal of Neural Engineering* 10 (2). https://doi.org/10.1088/1741-2560/10/2/026004.

Liang, Zhenhu, Yinghua Wang, Xue Sun, Duan Li, Logan J. Voss, Jamie W. Sleigh, Satoshi Hagihira, and Xiaoli Li. 2015. “EEG Entropy Measures in Anesthesia.” *Frontiers in Computational Neuroscience* 9 (JAN). https://doi.org/10.3389/fncom.2015.00016.

Liao, X., D. Yao, D. Wu, and C. Li. 2007. “Combining Spatial Filters for the Classification of Single-Trial EEG in a Finger Movement Task.” *IEEE Transactions on Biomedical Engineering* 54 (5): 821–31. https://doi.org/10.1109/TBME.2006.889206.

Lin, Aijing, Kang K. L. Liu, Ronny P. Bartsch, and Plamen Ch. Ivanov. 2020. “Dynamic Network Interactions among Distinct Brain Rhythms as a Hallmark of

Physiologic State and Function." *Communications Biology* 3 (1): 197. https://doi.org/10.1038/s42003-020-0878-4.

Liu, Weifeng, Puskal P. Pokharel, and Jose C. Principe. 2007. "Correntropy: Properties and Applications in Non-Gaussian Signal Processing." *IEEE Transactions on Signal Processing* 55 (11): 5286–98. https://doi.org/10.1109/TSP.2007.896065.

Llanos, Catalina, Manuel Rodriguez, Clara Rodriguez-Sabate, Ingrid Morales, and Magdalena Sabate. 2013. "Mu-Rhythm Changes during the Planning of Motor and Motor Imagery Actions." *Neuropsychologia* 51 (6): 1019–26. https://doi.org/10.1016/j.neuropsychologia.2013.02.008.

Loo, Chu Kiong, Andrews Samraj, and Gin Chong Lee. 2011. "Evaluation of Methods for Estimating Fractal Dimension in Motor Imagery-Based Brain Computer Interface." *Discrete Dynamics in Nature and Society* 2011. https://doi.org/10.1155/2011/724697.

Lotte, F., M. Congedo, A. Lécuyer, F. Lamarche, and B. Arnaldi. 2007. "A Review of Classification Algorithms for EEG-Based Brain-Computer Interfaces." *Journal of Neural Engineering*. https://doi.org/10.1088/1741-2560/4/2/R01.

Lotte, Fabien. 2008. "Study of Electroencephalographic Signal Processing and Classification Techniques towards the Use of Brain-Computer Interfaces in Virtual Reality Applications." *Thesis*. http://tel.archives-ouvertes.fr/tel-00356346/en/.

Lotte, Fabien, and Cuntai Guan. 2010. "Spatially Regularized Common Spatial Patterns for EEG Classification." In *Proceedings - International Conference on Pattern Recognition*, 3712–15. https://doi.org/10.1109/ICPR.2010.904.

———. 2011. "Regularizing Common Spatial Patterns to Improve BCI Designs: Unified Theory and New Algorithms." *IEEE Transactions on Biomedical Engineering* 58 (2): 355–62. https://doi.org/10.1109/TBME.2010.2082539.

Lotze, Martin, and Ulrike Halsband. 2006. "Motor Imagery." *Journal of Physiology Paris* 99 (4–6): 386–95. https://doi.org/10.1016/j.jphysparis.2006.03.012.

Lotze, Martin, Pedro Montoya, Michael Erb, Ernst Hülsmann, Herta Flor, Uwe Klose,

Niels Birbaumer, and Wolfgang Grodd. 1999. “Activation of Cortical and Cerebellar Motor Areas during Executed and Imagined Hand Movements: An FMRI Study.” *Journal of Cognitive Neuroscience* 11 (5): 491–501. https://doi.org/10.1162/089892999563553.

Lu, Chia Feng, Shin Teng, Chih I. Hung, Po Jung Tseng, Liang Ta Lin, Po Lei Lee, and Yu Te Wu. 2011. “Reorganization of Functional Connectivity during the Motor Task Using EEG Time-Frequency Cross Mutual Information Analysis.” *Clinical Neurophysiology* 122 (8): 1569–79. https://doi.org/10.1016/j.clinph.2011.01.050.

Lu, Haiping, Konstantinos N. Plataniotis, and Anastasios N. Venetsanopoulos. 2009. “Regularized Common Spatial Patterns with Generic Learning for EEG Signal Classification.” In *Proceedings of the 31st Annual International Conference of the IEEE Engineering in Medicine and Biology Society: Engineering the Future of Biomedicine, EMBC 2009*, 6599–6602. https://doi.org/10.1109/IEMBS.2009.5332554.

Luppino, G., and G. Rizzolatti. 2000. “The Organization of the Frontal Motor Cortex.” *News in Physiological Sciences* 15 (5): 219–24. https://doi.org/10.1152/physiologyonline.2000.15.5.219.

Ma, Xiangyu, Zhizheng Zhuo, Lijiang Wei, Zhe Ma, Zhaoxia Li, and Haiyun Li. 2020. “Altered Temporal Organization of Brief Spontaneous Brain Activities in Patients with Alzheimer’s Disease.” *Neuroscience* 425: 1–11. https://doi.org/10.1016/j.neuroscience.2019.11.025.

Ma, Zhiwei, and Nanyin Zhang. 2018. “Temporal Transitions of Spontaneous Brain Activity.” *ELife* 7 (2013): 1–23. https://doi.org/10.7554/eLife.33562.

Maars, Nicholaas J.I., and Fernando H. Lopes Da Silva. 1983. “Propagation of Seizure Activity in Kindled Dogs.” *Electroencephalography and Clinical Neurophysiology* 56 (2): 194–209. https://doi.org/10.1016/0013-4694(83)90074-3.

Madadi Asl, Mojtaba, Alireza Valizadeh, and Peter A. Tass. 2018. “Propagation Delays Determine Neuronal Activity and Synaptic Connectivity Patterns Emerging in Plastic Neuronal Networks.” *Chaos* 28 (10). https://doi.org/10.1063/1.5037309.

Makarov, Vladimir V., Maxim O. Zhuravlev, Anastasija E. Runnova, Pavel Protasov, Vladimir A. Maksimenko, Nikita S. Frolov, Alexander N. Pisarchik, and Alexander E. Hramov. 2018. “Betweenness Centrality in Multiplex Brain Network during Mental Task Evaluation.” *Physical Review E* 98 (6): 1–9. https://doi.org/10.1103/PhysRevE.98.062413.

Makeig, Scott, Stefan Debener, Julie Onton, and Arnaud Delorme. 2004. “Mining Event-Related Brain Dynamics.” *Trends in Cognitive Sciences* 8 (5): 204–10. https://doi.org/10.1016/j.tics.2004.03.008.

Malan, Nitesh Singh, and Shiru Sharma. 2019. “Feature Selection Using Regularized Neighbourhood Component Analysis to Enhance the Classification Performance of Motor Imagery Signals.” *Computers in Biology and Medicine* 107: 118–26. https://doi.org/10.1016/j.compbiomed.2019.02.009.

Mallat, Stephane. 2009. *A Wavelet Tour of Signal Processing*. *A Wavelet Tour of Signal Processing*. Elsevier Inc. https://doi.org/10.1016/B978-0-12-374370-1.X0001-8.

Mammone, Nadia, Cosimo Ieracitano, Hojjat Adeli, Alessia Bramanti, and Francesco C. Morabito. 2018. “Permutation Jaccard Distance-Based Hierarchical Clustering to Estimate EEG Network Density Modifications in MCI Subjects.” *IEEE Transactions on Neural Networks and Learning Systems* 29 (10): 5122–35. https://doi.org/10.1109/TNNLS.2018.2791644.

Manis, George, Md Aktaruzzaman, and Roberto Sassi. 2017. “Bubble Entropy: An Entropy Almost Free of Parameters.” *IEEE Transactions on Biomedical Engineering* 64 (11): 2711–18. https://doi.org/10.1109/TBME.2017.2664105.

Mariani, Andrea, Andrea Giorgetti, and Marco Chiani. 2015. “Model Order Selection Based on Information Theoretic Criteria: Design of the Penalty.” *IEEE Transactions on Signal Processing* 63 (11): 2779–89. https://doi.org/10.1109/TSP.2015.2414900.

Marinazzo, Daniele, Wei Liao, Huafu Chen, and Sebastiano Stramaglia. 2011. “Nonlinear Connectivity by Granger Causality.” *NeuroImage* 58 (2): 330–38. https://doi.org/10.1016/j.neuroimage.2010.01.099.

Martens, S. M., N. J. Hill, J. Farquhar, and B. Schölkopf. 2009. “Overlap and Refractory Effects in a Brain-Computer Interface Speller Based on the Visual P300 Event-Related Potential.” *Journal of Neural Engineering* 6 (2): 026003. https://doi.org/10.1088/1741-2560/6/2/026003.

Mashat, M. Ebrahim M., Chin Teng Lin, and DIngguo Zhang. 2019. “Effects of Task Complexity on Motor Imagery-Based Brain-Computer Interface.” *IEEE Transactions on Neural Systems and Rehabilitation Engineering* 27 (10): 2178–85. https://doi.org/10.1109/TNSRE.2019.2936987.

Mateo, J., A. Torres, M. A. García, C. Sánchez, and R. Cervigon. 2013. “Robust Volterra Filter Design for Enhancement of Electroencephalogram Signal Processing.” *Circuits, Systems, and Signal Processing* 32 (1): 233–53. https://doi.org/10.1007/s00034-012-9447-5.

Mateo, J., A. M. Torres, E. M. Sanchez-Morla, and J. L. Santos. 2015. “Eye Movement Artefact Suppression Using Volterra Filter for Electroencephalography Signals.” *Journal of Medical and Biological Engineering* 35 (3): 395–405. https://doi.org/10.1007/s40846-015-0036-5.

Matias, Fernanda S., Pedro V. Carelli, Claudio R. Mirasso, and Mauro Copelli. 2015. “Self-Organized near-Zero-Lag Synchronization Induced by Spike-Timing Dependent Plasticity in Cortical Populations.” *PLoS ONE* 10 (10): e0140504. https://doi.org/10.1371/journal.pone.0140504.

McDonough, Ian M., and Kaoru Nashiro. 2014. “Network Complexity as a Measure of Information Processing across Resting-State Networks: Evidence from the Human Connectome Project.” *Frontiers in Human Neuroscience* 8 (JUNE): 409. https://doi.org/10.3389/fnhum.2014.00409.

McFarland, Dennis J., Lynn M. McCane, Stephen V. David, and Jonathan R. Wolpaw. 1997. “Spatial Filter Selection for EEG-Based Communication.” *Electroencephalography and Clinical Neurophysiology* 103 (3): 386–94. https://doi.org/10.1016/S0013-4694(97)00022-2.

McFarland, Dennis J., and Jonathan R. Wolpaw. 2008. “Sensorimotor Rhythm-Based Brain-Computer Interface (BCI): Model Order Selection for Autoregressive

Spectral Analysis." *Journal of Neural Engineering* 5 (2): 155–62. https://doi.org/10.1088/1741-2560/5/2/006.

McMackin, Roisin, Peter Bede, Niall Pender, Orla Hardiman, and Bahman Nasseroleslami. 2019. "Neurophysiological Markers of Network Dysfunction in Neurodegenerative Diseases." *NeuroImage: Clinical*. https://doi.org/10.1016/j.nicl.2019.101706.

Melia, Umberto, Marc Guaita, Montserrat Vallverdú, Cristina Embid, Isabel Vilaseca, Manel Salamero, and Joan Santamaria. 2015. "Mutual Informationmeasuresapplied to EEG Signals for Sleepiness Characterization." *Medical Engineering and Physics* 37 (3): 297–308. https://doi.org/10.1016/j.medengphy.2015.01.002.

Melia, Umberto, Marc Guaita, Montserrat Vallverdú, Josep M Montserrat, Isabel Vilaseca, Manel Salamero, Carles Gaig, Pere Caminal, and Joan Santamaria. 2014. "Correntropy Measures to Detect Daytime Sleepiness from EEG Signals." *Physiological Measurement* 35 (10): 2067–83. https://doi.org/10.1088/0967-3334/35/10/2067.

Menicucci, Danilo, Francesco Di Gruttola, Valentina Cesari, Angelo Gemignani, Diego Manzoni, and Laura Sebastiani. 2020. "Task-Independent Electrophysiological Correlates of Motor Imagery Ability from Kinaesthetic and Visual Perspectives." *Neuroscience* 443: 176–87. https://doi.org/10.1016/j.neuroscience.2020.07.038.

Meunier, David, Renaud Lambiotte, and Edward T. Bullmore. 2010. "Modular and Hierarchically Modular Organization of Brain Networks." *Frontiers in Neuroscience* 4 (DEC): 200. https://doi.org/10.3389/fnins.2010.00200.

Micheloyannis, Sifis, Michael Vourkas, Manolis Bizas, Panagiotis Simos, and Cornelis J. Stam. 2003. "Changes in Linear and Nonlinear EEG Measures as a Function of Task Complexity: Evidence for Local and Distant Signal Synchronization." *Brain Topography* 15 (4): 239–47. https://doi.org/10.1023/A:1023962125598.

Mijalkov, Mite, Joana B. Pereira, and Giovanni Volpe. 2020. "Delayed Correlations Improve the Reconstruction of the Brain Connectome." *PLoS ONE* 15 (2): e0228334. https://doi.org/10.1371/journal.pone.0228334.

Milton, John, Ana Solodkin, Petr Hluštík, and Steven L. Small. 2007. “The Mind of Expert Motor Performance Is Cool and Focused.” *NeuroImage* 35 (2): 804–13. https://doi.org/10.1016/j.neuroimage.2007.01.003.

Miraglia, Francesca, Fabrizio Vecchio, and Paolo Maria Rossini. 2018. “Brain Electroencephalographic Segregation as a Biomarker of Learning.” *Neural Networks* 106: 168–74. https://doi.org/10.1016/j.neunet.2018.07.005.

Mishuhina, Vasilisa, and Xudong Jiang. 2021. “Complex Common Spatial Patterns on Time-Frequency Decomposed EEG for Brain-Computer Interface.” *Pattern Recognition* 115. https://doi.org/10.1016/j.patcog.2021.107918.

Mišić, Bratislav, and Olaf Sporns. 2016. “From Regions to Connections and Networks: New Bridges between Brain and Behavior.” *Current Opinion in Neurobiology*. https://doi.org/10.1016/j.conb.2016.05.003.

Mizuhara, Hiroaki, and Yoko Yamaguchi. 2007. “Human Cortical Circuits for Central Executive Function Emerge by Theta Phase Synchronization.” *NeuroImage* 36 (1): 232–44. https://doi.org/10.1016/j.neuroimage.2007.02.026.

Montalto, Alessandro, Luca Faes, and Daniele Marinazzo. 2014. “MuTE: A MATLAB Toolbox to Compare Established and Novel Estimators of the Multivariate Transfer Entropy.” *PLoS ONE* 9 (10): 1–13. https://doi.org/10.1371/journal.pone.0109462.

Mooij, Anne H., Birgit Frauscher, Mina Amiri, Willem M. Otte, and Jean Gotman. 2016. “Differentiating Epileptic from Non-Epileptic High Frequency Intracerebral EEG Signals with Measures of Wavelet Entropy.” *Clinical Neurophysiology* 127 (12): 3529–36. https://doi.org/10.1016/j.clinph.2016.09.011.

Morash, Valerie, Ou Bai, Stephen Furlani, Peter Lin, and Mark Hallett. 2008. “Classifying EEG Signals Preceding Right Hand, Left Hand, Tongue, and Right Foot Movements and Motor Imageries.” *Clinical Neurophysiology* 119 (11): 2570–78. https://doi.org/10.1016/j.clinph.2008.08.013.

Mottaz, Anais, Marco Solcà, Cécile Magnin, Tiffany Corbet, Armin Schnider, and Adrian G. Guggisberg. 2015. “Neurofeedback Training of Alpha-Band Coherence

Enhances Motor Performance." *Clinical Neurophysiology* 126 (9): 1754–60. https://doi.org/10.1016/j.clinph.2014.11.023.

Müller-Putz, Gernot R., Reinhold Scherer, Clemens Brunner, Robert Leeb, and Gert Pfurtscheller. 2007. "Better than Random: A Closer Look on BCI Results." *2007 1st COST Neuromath Workgroup Meeting, Rome, Italy* 10 (1): 95–96. http://infoscience.epfl.ch/record/164768.

Munzert, Jörn, Britta Lorey, and Karen Zentgraf. 2009a. "Cognitive Motor Processes: The Role of Motor Imagery in the Study of Motor Representations." *Brain Research Reviews* 60 (2): 306–26. https://doi.org/10.1016/j.brainresrev.2008.12.024.

———. 2009b. "Cognitive Motor Processes: The Role of Motor Imagery in the Study of Motor Representations." *Brain Research Reviews*. https://doi.org/10.1016/j.brainresrev.2008.12.024.

Muthukumaraswamy, Suresh D., and Blake W. Johnson. 2004. "Primary Motor Cortex Activation during Action Observation Revealed by Wavelet Analysis of the EEG." *Clinical Neurophysiology* 115 (8): 1760–66. https://doi.org/10.1016/j.clinph.2004.03.004.

Na, Sun Hee, Seung Hyun Jin, Soo Yong Kim, and Byung Joo Ham. 2002. "EEG in Schizophrenic Patients: Mutual Information Analysis." *Clinical Neurophysiology* 113 (12): 1954–60. https://doi.org/10.1016/S1388-2457(02)00197-9.

Nagel, Joachim H. 2003. "Biopotential Amplifiers." *Clinical Engineering* 2: 14-1-14–14. https://doi.org/10.1201/b18990-30.

Neuper, C., and G. Pfurtscheller. 2001. "Event-Related Dynamics of Cortical Rhythms: Frequency-Specific Features and Functional Correlates." *International Journal of Psychophysiology* 43 (1): 41–58. https://doi.org/10.1016/S0167-8760(01)00178-7.

Neuper, Christa, Reinhold Scherer, Miriam Reiner, and Gert Pfurtscheller. 2005. "Imagery of Motor Actions: Differential Effects of Kinesthetic and Visual-Motor Mode of Imagery in Single-Trial EEG." *Cognitive Brain Research* 25 (3): 668–77. https://doi.org/10.1016/j.cogbrainres.2005.08.014.

Neuper, Christa, Reinhold Scherer, Selina Wriessnegger, and Gert Pfurtscheller. 2009a. "Motor Imagery and Action Observation: Modulation of Sensorimotor Brain Rhythms during Mental Control of a Brain-Computer Interface." *Clinical Neurophysiology* 120 (2): 239–47. https://doi.org/10.1016/j.clinph.2008.11.015.

———. 2009b. "Motor Imagery and Action Observation: Modulation of Sensorimotor Brain Rhythms during Mental Control of a Brain-Computer Interface." *Clinical Neurophysiology* 120 (2): 239–47. https://doi.org/10.1016/j.clinph.2008.11.015.

Neuper, Christa, Michael Wörtz, and Gert Pfurtscheller. 2006. "Chapter 14 ERD/ERS Patterns Reflecting Sensorimotor Activation and Deactivation." *Progress in Brain Research*. Elsevier. https://doi.org/10.1016/S0079-6123(06)59014-4.

Nguyen-Ky, Tai, Peng Wen, Yan Li, and Mel Malan. 2012. "Measuring the Hypnotic Depth of Anaesthesia Based on the EEG Signal Using Combined Wavelet Transform, Eigenvector and Normalisation Techniques." *Computers in Biology and Medicine* 42 (6): 680–91. https://doi.org/10.1016/j.compbiomed.2012.03.004.

Nicolas-Alonso, Luis Fernando, and Jaime Gomez-Gil. 2012. "Brain Computer Interfaces, a Review." *Sensors* 12 (2): 1211–79. https://doi.org/10.3390/s120201211.

Nobukawa, Sou, Teruya Yamanishi, Shinya Kasakawa, Haruhiko Nishimura, Mitsuru Kikuchi, and Tetsuya Takahashi. 2020. "Classification Methods Based on Complexity and Synchronization of Electroencephalography Signals in Alzheimer's Disease." *Frontiers in Psychiatry* 11: 255. https://doi.org/10.3389/fpsyt.2020.00255.

Nobukawa, Sou, Teruya Yamanishi, Haruhiko Nishimura, Yuji Wada, Mitsuru Kikuchi, and Tetsuya Takahashi. 2019. "Atypical Temporal-Scale-Specific Fractal Changes in Alzheimer's Disease EEG and Their Relevance to Cognitive Decline." *Cognitive Neurodynamics* 13 (1): 1–11. https://doi.org/10.1007/s11571-018-9509-x.

Nolte, Guido, Ou Bai, Lewis Wheaton, Zoltan Mari, Sherry Vorbach, and Mark Hallett. 2004. "Identifying True Brain Interaction from EEG Data Using the Imaginary Part of Coherency." *Clinical Neurophysiology* 115 (10): 2292–2307.

https://doi.org/10.1016/j.clinph.2004.04.029.

Nyhof, Luke. 2014. “Biomedical Signal Filtering for Noisy Environments.” Deakin University.

O’Neill, George C., Prejaas Tewarie, Diego Vidaurre, Lucrezia Liuzzi, Mark W. Woolrich, and Matthew J. Brookes. 2018. “Dynamics of Large-Scale Electrophysiological Networks: A Technical Review.” *NeuroImage* 180 (May 2017): 559–76. https://doi.org/10.1016/j.neuroimage.2017.10.003.

Olcay, B. Orkan, and Bilge Karaçalı. 2019. “Evaluation of Synchronization Measures for Capturing the Lagged Synchronization between EEG Channels: A Cognitive Task Recognition Approach.” *Computers in Biology and Medicine* 114 (November): 103441. https://doi.org/10.1016/j.compbiomed.2019.103441.

Olcay, Bilal Orkan. 2014. “Analysis of Olfactory Evoked Potentials.” Izmir Institute of Technology. http://openaccess.iyte.edu.tr/handle/11147/4205.

Olcay, Bilal Orkan, Bilge Karacali, Murat Ozgoren, and Cagdas Guducu. 2017. “Entropik Kümeleme Kullanilarak Beyin Aktivitesi Karakteriz Asyonu.” In *2017 25th Signal Processing and Communications Applications Conference, SIU 2017*, 1–4. Institute of Electrical and Electronics Engineers (IEEE). https://doi.org/10.1109/SIU.2017.7960503.

Olejarczyk, Elzbieta, Laura Marzetti, Vittorio Pizzella, and Filippo Zappasodi. 2017. “Comparison of Connectivity Analyses for Resting State EEG Data.” *Journal of Neural Engineering* 14 (3). https://doi.org/10.1088/1741-2552/aa6401.

Oostendorp, Thom F., and Adriaan Van Oosterom. 1996. “Correction to ‘the Surface Laplacian of the Potential: Theory and Application.’” *IEEE Transactions on Biomedical Engineering* 43 (8): 866. https://doi.org/10.1109/TBME.1996.508550.

Orkan Olcay, B., Murat Özgören, and Bilge Karaçalı. 2021. “On the Characterization of Cognitive Tasks Using Activity-Specific Short-Lived Synchronization between Electroencephalography Channels.” *Neural Networks* 143 (November): 452–74. https://doi.org/10.1016/j.neunet.2021.06.022.

Özbek, Mehmet Erdal. 2009. “Representations of Musical Instrument Sounds for Classification and Separation.” http://acikerisim.deu.edu.tr:8080/xmlui/handle/20.500.12397/9223.

Özgören, Murat, Canan Başar-Eroğlu, and Erol Başar. 2005. “Beta Oscillations in Face Recognition.” *International Journal of Psychophysiology* 55 (1): 51–59. https://doi.org/10.1016/j.ijpsycho.2004.06.005.

Ozgoren, Murat, Onur Bayazit, Sibel Kocaaslan, Necati Gokmen, and Adile Oniz. 2010. “Brain Function Assessment in Different Conscious States.” In *Nonlinear Biomedical Physics*, 4:S6. Springer. https://doi.org/10.1186/1753-4631-4-S1-S6.

Padmasair, Y., K. SubbaRao, V. Malini, and C. Raghavendra Rao. 2010. “Linear Prediction Modelling for the Analysis of the Epileptic EEG.” In *ACE 2010 - 2010 International Conference on Advances in Computer Engineering*, 6–9. IEEE. https://doi.org/10.1109/ACE.2010.20.

Palmigiano, Agostina, Theo Geisel, Fred Wolf, and Demian Battaglia. 2017. “Flexible Information Routing by Transient Synchrony.” *Nature Neuroscience* 20 (7): 1014–22. https://doi.org/10.1038/nn.4569.

Palmini, Andre. 2006. “The Concept of the Epileptogenic Zone: A Modern Look at Penfield and Jasper’s Views on the Role of Interictal Spikes.” *Epileptic Disorders* 8 (SUPPL. 2): S10-5.

Palva, J. Matias, Sheng H. Wang, Satu Palva, Alexander Zhigalov, Simo Monto, Matthew J. Brookes, Jan Mathijs Schoffelen, and Karim Jerbi. 2018. “Ghost Interactions in MEG/EEG Source Space: A Note of Caution on Inter-Areal Coupling Measures.” *NeuroImage* 173: 632–43. https://doi.org/10.1016/j.neuroimage.2018.02.032.

Pampu, Nicolae C., Raul Vicente, Raul C. Muresan, Viola Priesemann, Felix Siebenhuhner, and Michael Wibral. 2013. “Transfer Entropy as a Tool for Reconstructing Interaction Delays in Neural Signals.” In *ISSCS 2013 - International Symposium on Signals, Circuits and Systems*. https://doi.org/10.1109/ISSCS.2013.6651210.

Pardey, J., S. Roberts, and L. Tarassenko. 1996. “A Review of Parametric Modelling Techniques for EEG Analysis.” *Medical Engineering and Physics*. https://doi.org/10.1016/1350-4533(95)00024-0.

Park, Chang hyun, Won Hyuk Chang, Minji Lee, Gyu Hyun Kwon, Laehyun Kim, Sung Tae Kim, and Yun Hee Kim. 2015. “Which Motor Cortical Region Best Predicts Imagined Movement?” *NeuroImage* 113 (June): 101–10. https://doi.org/10.1016/j.neuroimage.2015.03.033.

Park, Cheolsoo, Clive Cheong Took, and Danilo P. Mandic. 2014. “Augmented Complex Common Spatial Patterns for Classification of Noncircular EEG from Motor Imagery Tasks.” *IEEE Transactions on Neural Systems and Rehabilitation Engineering* 22 (1): 1–10. https://doi.org/10.1109/TNSRE.2013.2294903.

Park, Il, and José C. Príncipe. 2008. “Correntropy Based Granger Causality.” In *ICASSP, IEEE International Conference on Acoustics, Speech and Signal Processing - Proceedings*, 3605–8. https://doi.org/10.1109/ICASSP.2008.4518432.

Park, Sang Hoon, David Lee, and Sang Goog Lee. 2018. “Filter Bank Regularized Common Spatial Pattern Ensemble for Small Sample Motor Imagery Classification.” *IEEE Transactions on Neural Systems and Rehabilitation Engineering* 26 (2): 498–505. https://doi.org/10.1109/TNSRE.2017.2757519.

Patel, Mainak, and Badal Joshi. 2013. “Decoding Synchronized Oscillations within the Brain: Phase-Delayed Inhibition Provides a Robust Mechanism for Creating a Sharp Synchrony Filter.” *Journal of Theoretical Biology* 334 (October): 13–25. https://doi.org/10.1016/j.jtbi.2013.05.022.

Pereda, Ernesto, Rodrigo Quian Quiroga, and Joydeep Bhattacharya. 2005. “Nonlinear Multivariate Analysis of Neurophysiological Signals.” *Progress in Neurobiology*. https://doi.org/10.1016/j.pneurobio.2005.10.003.

Petrides, Michael. 1994. “Frontal Lobes and Behaviour.” *Current Opinion in Neurobiology* 4 (2): 207–11. https://doi.org/10.1016/0959-4388(94)90074-4.

Pfurtscheller, G., and A. Berghold. 1989. “Patterns of Cortical Activation during Planning of Voluntary Movement.” *Electroencephalography and Clinical*

Neurophysiology 72 (3): 250–58. https://doi.org/10.1016/0013-4694(89)90250-2.

Pfurtscheller, G., C. Brunner, A. Schlögl, and F. H. Lopes da Silva. 2006. "Mu Rhythm (de)Synchronization and EEG Single-Trial Classification of Different Motor Imagery Tasks." *NeuroImage* 31 (1): 153–59. https://doi.org/10.1016/j.neuroimage.2005.12.003.

Pfurtscheller, G., and F. H. Lopes Da Silva. 1999. "Event-Related EEG/MEG Synchronization and Desynchronization: Basic Principles." *Clinical Neurophysiology* 110 (11): 1842–57. https://doi.org/10.1016/S1388-2457(99)00141-8.

Pfurtscheller, G., C. Neuper, C. Brunner, and F. Lopes Da Silva. 2005. "Beta Rebound after Different Types of Motor Imagery in Man." *Neuroscience Letters* 378 (3): 156–59. https://doi.org/10.1016/j.neulet.2004.12.034.

Pfurtscheller, G., C. Neuper, C. Guger, W. Harkam, H. Ramoser, A. Schlögl, B. Obermaier, and M. Pregenzer. 2000. "Current Trends in Graz Brain-Computer Interface (BCI) Research." *IEEE Transactions on Rehabilitation Engineering* 8 (2): 216–19. https://doi.org/10.1109/86.847821.

Pfurtscheller, G., C. Neuper, A. Schlogl, and K. Lugger. 1998. "Separability of EEG Signals Recorded during Right and Left Motor Imagery Using Adaptive Autoregressive Parameters." *IEEE Transactions on Rehabilitation Engineering* 6 (3): 316–25. https://doi.org/10.1109/86.712230.

Pfurtscheller, G., R. Scherer, G. R. Müller-Putz, and F. H. Lopes Da Silva. 2008. "Short-Lived Brain State after Cued Motor Imagery in Naive Subjects." *European Journal of Neuroscience* 28 (7): 1419–26. https://doi.org/10.1111/j.1460-9568.2008.06441.x.

Pfurtscheller, G., and T. Solis-Escalante. 2009. "Could the Beta Rebound in the EEG Be Suitable to Realize a 'Brain Switch'?" *Clinical Neurophysiology* 120 (1): 24–29. https://doi.org/10.1016/j.clinph.2008.09.027.

Pfurtscheller, G, Ch Neuper, C Andrew, and G Edlinger. 1997. "Foot and Hand Area Mu Rhythms." In *International Journal of Psychophysiology*, 26:121–35. Elsevier.

https://doi.org/10.1016/S0167-8760(97)00760-5.

Pfurtscheller, Gert, and Christa Neuper. 1997. “Motor Imagery Activates Primary Sensorimotor Area in Humans.” *Neuroscience Letters* 239 (2–3): 65–68. https://doi.org/10.1016/S0304-3940(97)00889-6.

Pilgramm, Sebastian, Benjamin de Haas, Fabian Helm, Karen Zentgraf, Rudolf Stark, Jörn Munzert, and Britta Krüger. 2016. “Motor Imagery of Hand Actions: Decoding the Content of Motor Imagery from Brain Activity in Frontal and Parietal Motor Areas.” *Human Brain Mapping* 37 (1): 81–93. https://doi.org/10.1002/hbm.23015.

Pincus, Sieven M. 1991. “Approximate Entropy as a Measure of System Complexity.” *Proceedings of the National Academy of Sciences of the United States of America* 88 (6): 2297–2301. https://doi.org/10.1073/pnas.88.6.2297.

Pineda, Jaime A. 2005. “The Functional Significance of Mu Rhythms: Translating ‘Seeing’ and ‘Hearing’ into ‘Doing.’” *Brain Research Reviews*. Elsevier. https://doi.org/10.1016/j.brainresrev.2005.04.005.

Porro, Carlo A., Maria Pia Francescato, Valentina Cettolo, Mathew E. Diamond, Patrizia Baraldi, Chiava Zuiani, Massimo Bazzocchi, and Pietro E. Di Prampero. 1996. “Primary Motor and Sensory Cortex Activation during Motor Performance and Motor Imagery: A Functional Magnetic Resonance Imaging Study.” *Journal of Neuroscience* 16 (23): 7688–98. https://doi.org/10.1523/jneurosci.16-23-07688.1996.

Priestley, Maurice Bertram. 1988. “Non-Linear and Non-Stationary Time Series Analysis.” *London: Academic Press, 1988*.

Principe, J C. 2010. “Information Theoretic Learning: Rényi Entropy and Kernel Perspectives,” 515.

Pudil, P., J. Novovičová, and J. Kittler. 1994. “Floating Search Methods in Feature Selection.” *Pattern Recognition Letters* 15 (11): 1119–25. https://doi.org/10.1016/0167-8655(94)90127-9.

Rabinovich, Mikhail I, and M K Muezzinoglu. 2010. “Nonlinear Dynamics of the Brain: Emotion and Cognition.” *Physics-Uspekhi* 53 (4): 357–72. https://doi.org/10.3367/ufne.0180.201004b.0371.

Raghu, S., Natarajan Sriraam, Yasin Temel, Shyam Vasudeva Rao, Alangar Satyaranjandas Hegde, and Pieter L. Kubben. 2019. “Performance Evaluation of DWT Based Sigmoid Entropy in Time and Frequency Domains for Automated Detection of Epileptic Seizures Using SVM Classifier.” *Computers in Biology and Medicine* 110 (July): 127–43. https://doi.org/10.1016/j.compbiomed.2019.05.016.

Rahman, Md Mostafizur, and Shaikh Anowarul Fattah. 2020. “An Efficient Feature Extraction Scheme for Classification of Mental Tasks Based on Inter-Channel Correlation in Wavelet Domain Utilizing EEG Signal.” *Biomedical Signal Processing and Control* 61: 102033. https://doi.org/10.1016/j.bspc.2020.102033.

Ramadan, Rabie A., and Athanasios V. Vasilakos. 2017. “Brain Computer Interface: Control Signals Review.” *Neurocomputing* 223 (February): 26–44. https://doi.org/10.1016/j.neucom.2016.10.024.

Ramoser, Herbert, Johannes Müller-Gerking, and Gert Pfurtscheller. 2000. “Optimal Spatial Filtering of Single Trial EEG during Imagined Hand Movement.” *IEEE Transactions on Rehabilitation Engineering* 8 (4): 441–46. https://doi.org/10.1109/86.895946.

Rangaprakash, D. 2014. “Connectivity Analysis of Multichannel EEG Signals Using Recurrence Based Phase Synchronization Technique.” *Computers in Biology and Medicine* 46 (1): 11–21. https://doi.org/10.1016/j.compbiomed.2013.10.025.

Rao, Murali, Sohan Seth, Jianwu Xu, Yunmei Chen, Hemant Tagare, and José C. Príncipe. 2011. “A Test of Independence Based on a Generalized Correlation Function.” *Signal Processing* 91 (1): 15–27. https://doi.org/10.1016/j.sigpro.2010.06.002.

Rao, Stephen M., Andrew R. Mayer, and Deborah L. Harrington. 2001. “The Evolution of Brain Activation during Temporal Processing.” *Nature Neuroscience* 4 (3): 317–23. https://doi.org/10.1038/85191.

Rathee, Dheeraj, Hubert Cecotti, and Girijesh Prasad. 2017. “Single-Trial Effective Brain Connectivity Patterns Enhance Discriminability of Mental Imagery Tasks.” *Journal of Neural Engineering* 14 (5). https://doi.org/10.1088/1741-2552/aa785c.

Rathee, Dheeraj, Haider Raza, Girijesh Prasad, and Hubert Cecotti. 2017. “Current Source Density Estimation Enhances the Performance of Motor-Imagery-Related Brain–Computer Interface.” *IEEE Transactions on Neural Systems and Rehabilitation Engineering* 25 (12): 2461–71. https://doi.org/10.1109/TNSRE.2017.2726779.

Ravasz, Erzsébet, and Albert László Barabási. 2003. “Hierarchical Organization in Complex Networks.” *Physical Review E - Statistical Physics, Plasmas, Fluids, and Related Interdisciplinary Topics* 67 (2): 7. https://doi.org/10.1103/PhysRevE.67.026112.

Ren, Shen, Junhua Li, Fumihiko Taya, Joshua DeSouza, Nitish V. Thakor, and Anastasios Bezerianos. 2017. “Dynamic Functional Segregation and Integration in Human Brain Network during Complex Tasks.” *IEEE Transactions on Neural Systems and Rehabilitation Engineering* 25 (6): 547–56. https://doi.org/10.1109/TNSRE.2016.2597961.

Rezaie, Roozbeh, Panagiotis G. Simos, Jack M. Fletcher, Jenifer Juranek, Paul T. Cirino, Zhimin Li, Antony D. Passaro, and Andrew C. Papanicolaou. 2011. “The Timing and Strength of Regional Brain Activation Associated with Word Recognition in Children with Reading Difficulties.” *Frontiers in Human Neuroscience* 5 (MAY): 8. https://doi.org/10.3389/fnhum.2011.00045.

Richman, Joshua S., and J. Randall Moorman. 2000. “Physiological Time-Series Analysis Using Approximate and Sample Entropy.” *American Journal of Physiology - Heart and Circulatory Physiology* 278 (6 47-6). https://doi.org/10.1152/ajpheart.2000.278.6.h2039.

Rocca, D. La, P. Campisi, B. Vegso, P. Cserti, G. Kozmann, F. Babiloni, and F. De Vico Fallani. 2014. “Human Brain Distinctiveness Based on EEG Spectral Coherence Connectivity.” *IEEE Transactions on Biomedical Engineering* 61 (9): 2406–12. https://doi.org/10.1109/TBME.2014.2317881.

Roelfsema, Pieter R., Andreas K. Engel, Peter König, and Wolf Singer. 1997. "Visuomotor Integration Is Associated with Zero Time-Lag Synchronization among Cortical Areas." *Nature* 385 (6612): 157–61. https://doi.org/10.1038/385157a0.

Rosário, R. S., P. T. Cardoso, M. A. Muñoz, P. Montoya, and J. G.V. Miranda. 2015. "Motif-Synchronization: A New Method for Analysis of Dynamic Brain Networks with EEG." *Physica A: Statistical Mechanics and Its Applications* 439 (December): 7–19. https://doi.org/10.1016/j.physa.2015.07.018.

Rosso, O. A., M. T. Martin, A. Figliola, K. Keller, and A. Plastino. 2006. "EEG Analysis Using Wavelet-Based Information Tools." *Journal of Neuroscience Methods* 153 (2): 163–82. https://doi.org/10.1016/j.jneumeth.2005.10.009.

Rosso, Osvaldo A. 2007. "Entropy Changes in Brain Function." *International Journal of Psychophysiology* 64 (1): 75–80. https://doi.org/10.1016/j.ijpsycho.2006.07.010.

Rosso, Osvaldo A., Susana Blanco, Juliana Yordanova, Vasil Kolev, Alejandra Figliola, Martin Schürmann, and Erol Ba ar. 2001. "Wavelet Entropy: A New Tool for Analysis of Short Duration Brain Electrical Signals." *Journal of Neuroscience Methods* 105 (1): 65–75. https://doi.org/10.1016/S0165-0270(00)00356-3.

Royer, Audrey S., Alexander J. Doud, Minn L. Rose, and Bin He. 2010. "EEG Control of a Virtual Helicopter in 3-Dimensional Space Using Intelligent Control Strategies." *IEEE Transactions on Neural Systems and Rehabilitation Engineering* 18 (6): 581–89. https://doi.org/10.1109/TNSRE.2010.2077654.

Rubinov, Mikail, and Olaf Sporns. 2010. "Complex Network Measures of Brain Connectivity: Uses and Interpretations." *NeuroImage* 52 (3): 1059–69. https://doi.org/10.1016/j.neuroimage.2009.10.003.

Saha, Simanto, Khawza Iftekhar Uddin Ahmed, Raqibul Mostafa, Leontios Hadjileontiadis, and Ahsan Khandoker. 2018a. "Evidence of Variabilities in EEG Dynamics during Motor Imagery-Based Multiclass Brain-Computer Interface." *IEEE Transactions on Neural Systems and Rehabilitation Engineering* 26 (2): 371–82. https://doi.org/10.1109/TNSRE.2017.2778178.

———. 2018b. “Evidence of Variabilities in EEG Dynamics during Motor Imagery-Based Multiclass Brain-Computer Interface.” *IEEE Transactions on Neural Systems and Rehabilitation Engineering* 26 (2): 371–82. https://doi.org/10.1109/TNSRE.2017.2778178.

Sakkalis, V. 2011. “Review of Advanced Techniques for the Estimation of Brain Connectivity Measured with EEG/MEG.” *Computers in Biology and Medicine* 41 (12): 1110–17. https://doi.org/10.1016/j.compbiomed.2011.06.020.

Salyers, Jacob B., Yue Dong, and Yan Gai. 2019. “Continuous Wavelet Transform for Decoding Finger Movements From Single-Channel EEG.” *IEEE Transactions on Biomedical Engineering* 66 (6): 1588–97. https://doi.org/10.1109/TBME.2018.2876068.

Sanei, Saeid, and J. A. Chambers. 2013. *EEG Signal Processing*. *EEG Signal Processing*. John Wiley & Sons. https://doi.org/10.1002/9780470511923.

Santamaría, Ignacio, Puskal P. Pokharel, and Jose C. Principe. 2006. “Generalized Correlation Function: Definition, Properties, and Application to Blind Equalization.” *IEEE Transactions on Signal Processing* 54 (6 I): 2187–97. https://doi.org/10.1109/TSP.2006.872524.

Santamaria, Lorena, and Christopher James. 2019. “On the Existence of Phase-Synchronised States during Motor Imagery Tasks.” *Biomedical Signal Processing and Control* 54: 101630. https://doi.org/10.1016/j.bspc.2019.101630.

Santos Toural, Jorge Esteban, Arquímedes Montoya Pedrón, and Enrique Juan Marañón Reyes. 2021. “Classification among Healthy, Mild Cognitive Impairment and Alzheimer’s Disease Subjects Based on Wavelet Entropy and Relative Beta and Theta Power.” *Pattern Analysis and Applications* 24 (2): 413–22. https://doi.org/10.1007/s10044-020-00910-8.

Sargolzaei, Saman, Mercedes Cabrerizo, Mohammed Goryawala, Anas Salah Eddin, and Malek Adjouadi. 2015. “Scalp EEG Brain Functional Connectivity Networks in Pediatric Epilepsy.” *Computers in Biology and Medicine* 56 (January): 158–66. https://doi.org/10.1016/j.compbiomed.2014.10.018.

Sarmukadam, Kimaya, Vicki Bitsika, Christopher F. Sharpley, Mary M.E. McMillan, and Linda L. Agnew. 2020. “Comparing Different EEG Connectivity Methods in Young Males with ASD.” *Behavioural Brain Research* 383. https://doi.org/10.1016/j.bbr.2020.112482.

Sauseng, Paul, Wolfgang Klimesch, Manuel Schabus, and Michael Doppelmayr. 2005. “Fronto-Parietal EEG Coherence in Theta and Upper Alpha Reflect Central Executive Functions of Working Memory.” In *International Journal of Psychophysiology*, 57:97–103. https://doi.org/10.1016/j.ijpsycho.2005.03.018.

Schack, Baerbel, Sabine Weiss, and Peter Rappelsberger. 2003. “Cerebral Information Transfer during Word Processing: Where and When Does It Occur and How Fast Is It?” *Human Brain Mapping* 19 (1): 18–36. https://doi.org/10.1002/hbm.10104.

Schalk, Gerwin, Eric C. Leuthardt, Peter Brunner, Jeffrey G. Ojemann, Lester A. Gerhardt, and Jonathan R. Wolpaw. 2008. “Real-Time Detection of Event-Related Brain Activity.” *NeuroImage* 43 (2): 245–49. https://doi.org/10.1016/j.neuroimage.2008.07.037.

Schalk, Gerwin, Dennis J. McFarland, Thilo Hinterberger, Niels Birbaumer, and Jonathan R. Wolpaw. 2004. “BCI2000: A General-Purpose Brain-Computer Interface (BCI) System.” *IEEE Transactions on Biomedical Engineering* 51 (6): 1034–43. https://doi.org/10.1109/TBME.2004.827072.

Scheeringa, René, Marcel C.M. Bastiaansen, Karl Magnus Petersson, Robert Oostenveld, David G. Norris, and Peter Hagoort. 2008. “Frontal Theta EEG Activity Correlates Negatively with the Default Mode Network in Resting State.” *International Journal of Psychophysiology* 67 (3): 242–51. https://doi.org/10.1016/j.ijpsycho.2007.05.017.

Scheeringa, René, Karl Magnus Petersson, Robert Oostenveld, David G. Norris, Peter Hagoort, and Marcel C.M. Bastiaansen. 2009. “Trial-by-Trial Coupling between EEG and BOLD Identifies Networks Related to Alpha and Theta EEG Power Increases during Working Memory Maintenance.” *NeuroImage* 44 (3): 1224–38. https://doi.org/10.1016/j.neuroimage.2008.08.041.

Schloegl, A., K. Lugger, and G. Pfurtscheller. 1997. “Using Adaptive Autoregressive

Parameters for a Brain-Computer-Interface Experiment." *Annual International Conference of the IEEE Engineering in Medicine and Biology - Proceedings* 4: 1533–35. https://doi.org/10.1109/iembs.1997.757002.

Schlögl, Alois. 2000. *The Electroencephalogram and the Adaptive Autoregressive Model : Theory and Applications*. Shaker.

Schlögl, Alois, Felix Lee, Horst Bischof, and Gert Pfurtscheller. 2005. "Characterization of Four-Class Motor Imagery EEG Data for the BCI-Competition 2005." *Journal of Neural Engineering* 2 (4). https://doi.org/10.1088/1741-2560/2/4/L02.

Schreiber, Thomas. 2000. "Measuring Information Transfer." *Physical Review Letters* 85 (2): 461–64. https://doi.org/10.1103/PhysRevLett.85.461.

Shahsavari Baboukani, Payam, Ghasem Azemi, Boualem Boashash, Paul Colditz, and Amir Omidvarnia. 2019. "A Novel Multivariate Phase Synchrony Measure: Application to Multichannel Newborn EEG Analysis." *Digital Signal Processing: A Review Journal* 84 (January): 59–68. https://doi.org/10.1016/j.dsp.2018.08.019.

Shahverdiev, E. M., S. Sivaprakasam, and K. A. Shore. 2002. "Lag Synchronization in Time-Delayed Systems." *Physics Letters, Section A: General, Atomic and Solid State Physics* 292 (6): 320–24. https://doi.org/10.1016/S0375-9601(01)00824-6.

Sharma, Rajeev, Ram Bilas Pachori, and U. Rajendra Acharya. 2015. "Application of Entropy Measures on Intrinsic Mode Functions for the Automated Identification of Focal Electroencephalogram Signals." *Entropy* 17 (2): 669–91. https://doi.org/10.3390/e17020669.

Shenoy, Krishna V., and Jonathan C. Kao. 2021. "Measurement, Manipulation and Modeling of Brain-Wide Neural Population Dynamics." *Nature Communications*. https://doi.org/10.1038/s41467-020-20371-1.

Shine, James M., Eli J. Müller, Brandon Munn, Joana Cabral, Rosalyn J. Moran, and Michael Breakspear. 2021. "Computational Models Link Cellular Mechanisms of Neuromodulation to Large-Scale Neural Dynamics." *Nature Neuroscience*. https://doi.org/10.1038/s41593-021-00824-6.

Sideridis, Georgios, Panagiotis Simos, Andrew Papanicolaou, and Jack Fletcher. 2014. "Using Structural Equation Modeling to Assess Functional Connectivity in the Brain: Power and Sample Size Considerations." *Educational and Psychological Measurement* 74 (5): 733–58. https://doi.org/10.1177/0013164414525397.

Sirigu, A., J.-R. Duhamel, L. Cohen, B. Pillon, B. Dubois, and Y. Agid. 1996. "The Mental Representation of Hand Movements After Parietal Cortex Damage." *Science* 273 (5281): 1564–68. https://doi.org/10.1126/science.273.5281.1564.

Sitaram, Ranganatha, Andrea Caria, and Niels Birbaumer. 2009. "Hemodynamic Brain-Computer Interfaces for Communication and Rehabilitation." *Neural Networks* 22 (9): 1320–28. https://doi.org/10.1016/j.neunet.2009.05.009.

Siuly, Siuly, and Yan Li. 2012. "Improving the Separability of Motor Imagery EEG Signals Using a Cross Correlation-Based Least Square Support Vector Machine for Brain-Computer Interface." *IEEE Transactions on Neural Systems and Rehabilitation Engineering* 20 (4): 526–38. https://doi.org/10.1109/TNSRE.2012.2184838.

Skidmore, F., D. Korenkevych, Y. Liu, G. He, E. Bullmore, and Panos M. Pardalos. 2011. "Connectivity Brain Networks Based on Wavelet Correlation Analysis in Parkinson FMRI Data." *Neuroscience Letters* 499 (1): 47–51. https://doi.org/10.1016/j.neulet.2011.05.030.

Solis-Escalante, Teodoro, Gernot R. Müller-Putz, Gert Pfurtscheller, and Christa Neuper. 2012. "Cue-Induced Beta Rebound during Withholding of Overt and Covert Foot Movement." *Clinical Neurophysiology* 123 (6): 1182–90. https://doi.org/10.1016/j.clinph.2012.01.013.

Solodkin, Ana, Petr Hlustik, E. Elinor Chen, and Steven L. Small. 2004. "Fine Modulation in Network Activation during Motor Execution and Motor Imagery." *Cerebral Cortex* 14 (11): 1246–55. https://doi.org/10.1093/cercor/bhh086.

Solomon, Jack P., Sarah N. Kraeutner, Timothy Bardouille, and Shaun G. Boe. 2019. "Probing the Temporal Dynamics of Movement Inhibition in Motor Imagery." *Brain Research* 1720 (June): 146310. https://doi.org/10.1016/j.brainres.2019.146310.

Song, Le, and Julien Epps. 2007. “Classifying EEG for Brain-Computer Interface: Learning Optimal Filters for Dynamical System Features.” *Computational Intelligence and Neuroscience* 2007. https://doi.org/10.1155/2007/57180.

Spiegler, Andreas, Bernhard Graimann, and Gert Pfurtscheller. 2004. “Phase Coupling between Different Motor Areas during Tongue-Movement Imagery.” *Neuroscience Letters* 369 (1): 50–54. https://doi.org/10.1016/j.neulet.2004.07.054.

Sporns, O., G. Tononi, and G. M. Edelman. 2000. “Connectivity and Complexity: The Relationship between Neuroanatomy and Brain Dynamics.” *Neural Networks*. Elsevier Science Ltd. https://doi.org/10.1016/S0893-6080(00)00053-8.

Sporns, Olaf, Dante R. Chialvo, Marcus Kaiser, and Claus C. Hilgetag. 2004. “Organization, Development and Function of Complex Brain Networks.” *Trends in Cognitive Sciences* 8 (9): 418–25. https://doi.org/10.1016/j.tics.2004.07.008.

Srinivasan, Vairavan, Chikkannan Eswaran, and Natarajan Sriraam. 2007. “Approximate Entropy-Based Epileptic EEG Detection Using Artificial Neural Networks.” *IEEE Transactions on Information Technology in Biomedicine* 11 (3): 288–95. https://doi.org/10.1109/TITB.2006.884369.

Stam, C. J. 2005. “Nonlinear Dynamical Analysis of EEG and MEG: Review of an Emerging Field.” *Clinical Neurophysiology*. Elsevier. https://doi.org/10.1016/j.clinph.2005.06.011.

Stam, C. J., and B. W. Van Dijk. 2002. “Synchronization Likelihood: An Unbiased Measure of Generalized Synchronization in Multivariate Data Sets.” *Physica D: Nonlinear Phenomena* 163 (3–4): 236–51. https://doi.org/10.1016/S0167-2789(01)00386-4.

Stam, C. J., and E. C.W. van Straaten. 2012. “The Organization of Physiological Brain Networks.” *Clinical Neurophysiology*. https://doi.org/10.1016/j.clinph.2012.01.011.

Stam, Cornelis J., Michael Breakspear, Anne Marie Van Cappellen van Walsum, and Bob W. Van Dijk. 2003. “Nonlinear Synchronization in EEG and Whole-Head MEG Recordings of Healthy Subjects.” *Human Brain Mapping* 19 (2): 63–78.

https://doi.org/10.1002/hbm.10106.

Stam, Cornelis J., Guido Nolte, and Andreas Daffertshofer. 2007. “Phase Lag Index: Assessment of Functional Connectivity from Multi Channel EEG and MEG with Diminished Bias from Common Sources.” *Human Brain Mapping* 28 (11): 1178–93. https://doi.org/10.1002/hbm.20346.

Steen, Frederik Van de, Luca Faes, Esin Karahan, Jitkomut Songsiri, Pedro A. Valdes-Sosa, and Daniele Marinazzo. 2019. “Critical Comments on EEG Sensor Space Dynamical Connectivity Analysis.” *Brain Topography* 32 (4): 643–54. https://doi.org/10.1007/s10548-016-0538-7.

Stoica, Petre. 1997. *Introduction to Spectral Analysis*. Prentice hall.

Subasi, Abdulhamit. 2007. “Selection of Optimal AR Spectral Estimation Method for EEG Signals Using Cramer-Rao Bound.” *Computers in Biology and Medicine* 37 (2): 183–94. https://doi.org/10.1016/j.compbiomed.2005.12.001.

Sukel Kayt. 2019. “Neuroanatomy: The Basics | Dana Foundation.” 2019. https://www.dana.org/article/neuroanatomy-the-basics/.

Sun, Rui, Wan Wa Wong, Jing Wang, and Raymond Kai Yu Tong. 2017. “Changes in Electroencephalography Complexity Using a Brain Computer Interface-Motor Observation Training in Chronic Stroke Patients: A Fuzzy Approximate Entropy Analysis.” *Frontiers in Human Neuroscience* 11: 444. https://doi.org/10.3389/fnhum.2017.00444.

Sun, Yijun. 2007. “Iterative RELIEF for Feature Weighting: Algorithms, Theories, and Applications.” *IEEE Transactions on Pattern Analysis and Machine Intelligence* 29 (6): 1035–51. https://doi.org/10.1109/TPAMI.2007.1093.

Sun, Ying, Chao Xu, Gongfa Li, Wanfen Xu, Jianyi Kong, Du Jiang, Bo Tao, and Disi Chen. 2020. “Intelligent Human Computer Interaction Based on Non Redundant EMG Signal.” *Alexandria Engineering Journal* 59 (3): 1149–57. https://doi.org/10.1016/j.aej.2020.01.015.

Swiderski, Bartosz, Stanislaw Osowski, and Andrzej Rysz. 2005. “Lyapunov Exponent

of EEG Signal for Epileptic Seizure Characterization." In *Proceedings of the 2005 European Conference on Circuit Theory and Design*, 2:153–56. https://doi.org/10.1109/ECCTD.2005.1523016.

Tallgren, P., S. Vanhatalo, K. Kaila, and J. Voipio. 2005. "Evaluation of Commercially Available Electrodes and Gels for Recording of Slow EEG Potentials." *Clinical Neurophysiology* 116 (4): 799–806. https://doi.org/10.1016/j.clinph.2004.10.001.

Tarvainen, Mika P., Jaana K. Hiltunen, Perttu O. Ranta-Aho, and Pasi A. Karjalainen. 2004. "Estimation of Nonstationary EEG with Kalman Smoother Approach: An Application to Event-Related Synchronization (ERS)." *IEEE Transactions on Biomedical Engineering* 51 (3): 516–24. https://doi.org/10.1109/TBME.2003.821029.

Tass, P., M. G. Rosenblum, J. Weule, J. Kurths, A. Pikovsky, J. Volkmann, A. Schnitzler, and H. J. Freund. 1998. "Detection of n:M Phase Locking from Noisy Data: Application to Magnetoencephalography." In *Physical Review Letters*, 81:3291–94. World Scientific. https://doi.org/10.1103/PhysRevLett.81.3291.

Telesford, Qawi K., Sean L. Simpson, Jonathan H. Burdette, Satoru Hayasaka, and Paul J. Laurienti. 2011. "The Brain as a Complex System: Using Network Science as a Tool for Understanding the Brain." *Brain Connectivity* 1 (4): 295–308. https://doi.org/10.1089/brain.2011.0055.

Teplan, Michal. 2002. "Fundamentals of EEG Measurement." *Measurement Science Review* 2 (2): 1–11.

Thul, Alexander, Julia Lechinger, Johann Donis, Gabriele Michitsch, Gerald Pichler, Eberhard F. Kochs, Denis Jordan, Rüdiger Ilg, and Manuel Schabus. 2016. "EEG Entropy Measures Indicate Decrease of Cortical Information Processing in Disorders of Consciousness." *Clinical Neurophysiology* 127 (2): 1419–27. https://doi.org/10.1016/j.clinph.2015.07.039.

Thuraisingham, R. A. 2007. "A New Method Using Coherence to Obtain the Model Order in the Evaluation of Partial Directed Coherence." *Computers in Biology and Medicine* 37 (9): 1361–65. https://doi.org/10.1016/j.compbiomed.2006.12.004.

Tognoli, Emmanuelle, and J. A.Scott Kelso. 2009. “Brain Coordination Dynamics: True and False Faces of Phase Synchrony and Metastability.” *Progress in Neurobiology* 87 (1): 31–40. https://doi.org/10.1016/j.pneurobio.2008.09.014.

Tolić, Martina, and Franjo Jović. 2013. “Classification of Wavelet Transformed EEG Signals with Neural Network for Imagined Mental and Motor Tasks.” *Kinesiology* 45 (1): 130–38.

Troughton, Paul T., and Simon J. Godsill. 1998. “A Reversible Jump Sampler for Autoregressive Time Series.” In *ICASSP, IEEE International Conference on Acoustics, Speech and Signal Processing - Proceedings*, 4:2257–60. IEEE. https://doi.org/10.1109/ICASSP.1998.681598.

Tsuchimoto, Shohei, Shuka Shibusawa, Seitaro Iwama, Masaaki Hayashi, Kohei Okuyama, Nobuaki Mizuguchi, Kenji Kato, and Junichi Ushiba. 2021. “Use of Common Average Reference and Large-Laplacian Spatial-Filters Enhances EEG Signal-to-Noise Ratios in Intrinsic Sensorimotor Activity.” *Journal of Neuroscience Methods* 353 (December 2020): 109089. https://doi.org/10.1016/j.jneumeth.2021.109089.

Tzovara, Athina, Micah M. Murray, Gijs Plomp, Michael H. Herzog, Christoph M. Michel, and Marzia De Lucia. 2012. “Decoding Stimulus-Related Information from Single-Trial EEG Responses Based on Voltage Topographies.” *Pattern Recognition* 45 (6): 2109–22. https://doi.org/10.1016/j.patcog.2011.04.007.

Übeyli, Elif Derya. 2010. “Least Squares Support Vector Machine Employing Model-Based Methods Coefficients for Analysis of EEG Signals.” *Expert Systems with Applications* 37 (1): 233–39. https://doi.org/10.1016/j.eswa.2009.05.012.

Uhlhaas, Peter J., Gordon Pipa, Bruss Lima, Lucia Melloni, Sergio Neuenschwander, Danko Nikolić, and Wolf Singer. 2009. “Neural Synchrony in Cortical Networks: History, Concept and Current Status.” *Frontiers in Integrative Neuroscience* 3 (JUL): 1–19. https://doi.org/10.3389/neuro.07.017.2009.

Vapnik, Vladimir N. 2000. “The Nature of Statistical Learning Theory.” The Nature of Statistical Learning Theory. 2000. https://doi.org/10.1007/978-1-4757-3264-1.

Varela, Francisco, Jean Philippe Lachaux, Eugenio Rodriguez, and Jacques Martinerie. 2001. “The Brainweb: Phase Synchronization and Large-Scale Integration.” *Nature Reviews Neuroscience* 2 (4): 229–39. https://doi.org/10.1038/35067550.

Varsehi, Hesam, and S. Mohammad P. Firoozabadi. 2021. “An EEG Channel Selection Method for Motor Imagery Based Brain–Computer Interface and Neurofeedback Using Granger Causality.” *Neural Networks* 133: 193–206. https://doi.org/10.1016/j.neunet.2020.11.002.

Vasicek, Oldrich. 1976. “A Test for Normality Based on Sample Entropy.” *Journal of the Royal Statistical Society. Series B (Methodological)* 38 (1): 54–59. http://www.jstor.org/stable/2984828.

Vergara, Victor M., Eswar Damaraju, Jessica A. Turner, Godfrey Pearlson, Aysenil Belger, Daniel H. Mathalon, Steven G. Potkin, et al. 2019. “Altered Domain Functional Network Connectivity Strength and Randomness in Schizophrenia.” *Frontiers in Psychiatry* 10 (July): 1–11. https://doi.org/10.3389/fpsyt.2019.00499.

Vibert, Jean François, Khachayar Pakdaman, and Noureddine Azmy. 1994. “Interneural Delay Modification Synchronizes Biologically Plausible Neural Networks.” *Neural Networks* 7 (4): 589–607. https://doi.org/10.1016/0893-6080(94)90039-6.

Vicente, Raul, Leonardo L. Gollo, Claudio R. Mirasso, Ingo Fischer, and Gordon Pipa. 2008. “Dynamical Relaying Can Yield Zero Time Lag Neuronal Synchrony despite Long Conduction Delays.” *Proceedings of the National Academy of Sciences of the United States of America* 105 (44): 17157–62. https://doi.org/10.1073/pnas.0809353105.

Vicente, Raul, Michael Wibral, Michael Lindner, and Gordon Pipa. 2011. “Transfer Entropy-a Model-Free Measure of Effective Connectivity for the Neurosciences.” *Journal of Computational Neuroscience* 30 (1): 45–67. https://doi.org/10.1007/s10827-010-0262-3.

Vidaurre, Carmen, Nicole Krämer, Benjamin Blankertz, and Alois Schlögl. 2009. “Time Domain Parameters as a Feature for EEG-Based Brain-Computer Interfaces.” *Neural Networks* 22 (9): 1313–19. https://doi.org/10.1016/j.neunet.2009.07.020.

Vidaurre, Diego, Laurence T. Hunt, Andrew J. Quinn, Benjamin A.E. Hunt, Matthew J. Brookes, Anna C. Nobre, and Mark W. Woolrich. 2018. “Spontaneous Cortical Activity Transiently Organises into Frequency Specific Phase-Coupling Networks.” *Nature Communications* 9 (1). https://doi.org/10.1038/s41467-018-05316-z.

Vivot, Rocío Martínez, Carla Pallavicini, Federico Zamberlan, Daniel Vigo, and Enzo Tagliazucchi. 2020. “Meditation Increases the Entropy of Brain Oscillatory Activity.” *Neuroscience* 431: 40–51. https://doi.org/10.1016/j.neuroscience.2020.01.033.

Walden, A. T., and A. Contreras Cristan. 1998. “The Phase-Corrected Undecimated Discrete Wavelet Packet Transform and Its Application to Interpreting the Timing of Events.” *Proceedings of the Royal Society A: Mathematical, Physical and Engineering Sciences* 454 (1976): 2243–66. https://doi.org/10.1098/rspa.1998.0257.

Wang, Danny J.J., Kay Jann, Chang Fan, Yang Qiao, Yu Feng Zang, Hanbing Lu, and Yihong Yang. 2018a. “Correction: Neurophysiological Basis of Multi-Scale Entropy of Brain Complexity and Its Relationship With Functional Connectivity (Front. Neurosci,(2018), 12, 352, 10.3389/Fnins.2018.00352).” *Frontiers in Neuroscience* 12: 352. https://doi.org/10.3389/fnins.2018.00539.

———. 2018b. “Neurophysiological Basis of Multi-Scale Entropy of Brain Complexity and Its Relationship with Functional Connectivity.” *Frontiers in Neuroscience* 12 (MAY). https://doi.org/10.3389/fnins.2018.00352.

Wang, Haixian, and Wenming Zheng. 2008. “Local Temporal Common Spatial Patterns for Robust Single-Trial EEG Classification.” *IEEE Transactions on Neural Systems and Rehabilitation Engineering* 16 (2): 131–39. https://doi.org/10.1109/TNSRE.2007.914468.

Wang, Huifang E., Christian G. Bénar, Pascale P. Quilichini, Karl J. Friston, Viktor K. Jirsa, and Christophe Bernard. 2014. “A Systematic Framework for Functional Connectivity Measures.” *Frontiers in Neuroscience* 8 (DEC): 405. https://doi.org/10.3389/fnins.2014.00405.

Wang, Jie, Zuren Feng, Na Lu, and Jing Luo. 2018. “Toward Optimal Feature and Time Segment Selection by Divergence Method for EEG Signals Classification.” *Computers in Biology and Medicine* 97 (June): 161–70. https://doi.org/10.1016/j.compbiomed.2018.04.022.

Wang, Jie, Zuren Feng, Xiaodong Ren, Na Lu, Jing Luo, and Lei Sun. 2020. “Feature Subset and Time Segment Selection for the Classification of EEG Data Based Motor Imagery.” *Biomedical Signal Processing and Control* 61. https://doi.org/10.1016/j.bspc.2020.102026.

Wang, Yifeng, Xinju Huang, Xuezhi Yang, Qi Yang, Xinqi Wang, Georg Northoff, Yajing Pang, Chong Wang, Qian Cui, and Huafu Chen. 2019. “Low Frequency Phase-Locking of Brain Signals Contribute to Efficient Face Recognition.” *Neuroscience* 422: 172–83. https://doi.org/10.1016/j.neuroscience.2019.10.024.

Wang, Yijun, Bo Hong, Xiaorong Gao, and Shangkai Gao. 2006. “Phase Synchrony Measurement in Motor Cortex for Classifying Single-Trial EEG during Motor Imagery.” In *Annual International Conference of the IEEE Engineering in Medicine and Biology - Proceedings*, 75–78. https://doi.org/10.1109/IEMBS.2006.259673.

Wang, Yunhua, Patrick Berg, and Michael Scherg. 1999. “Common Spatial Subspace Decomposition Applied to Analysis of Brain Responses under Multiple Task Conditions: A Simulation Study.” *Clinical Neurophysiology* 110 (4): 604–14. https://doi.org/10.1016/S1388-2457(98)00056-X.

Wei, Qingguo, Yijun Wang, Xiaorong Gao, and Shangkai Gao. 2007. “Amplitude and Phase Coupling Measures for Feature Extraction in an EEG-Based Brain-Computer Interface.” *Journal of Neural Engineering* 4 (2): 120–29. https://doi.org/10.1088/1741-2560/4/2/012.

Wei, Wu, Gao Xiaorong, and Gao Shangkai. 2005. “One-versus-the-Rest (OVR) Algorithm: An Extension of Common Spatial Patterns (CSP) Algorithm to Multi-Class Case.” In *Annual International Conference of the IEEE Engineering in Medicine and Biology - Proceedings*, 7 VOLS:2387–90. IEEE. https://doi.org/10.1109/iembs.2005.1616947.

Wendling, Fabrice, Karim Ansari-Asl, Fabrice Bartolomei, and Lotfi Senhadji. 2009. "From EEG Signals to Brain Connectivity: A Model-Based Evaluation of Interdependence Measures." *Journal of Neuroscience Methods* 183 (1): 9–18. https://doi.org/10.1016/j.jneumeth.2009.04.021.

Wheaton, Lewis A., Guido Nolte, Stephan Bohlhalter, Esteban Fridman, and Mark Hallett. 2005. "Synchronization of Parietal and Premotor Areas during Preparation and Execution of Praxis Hand Movements." *Clinical Neurophysiology* 116 (6): 1382–90. https://doi.org/10.1016/j.clinph.2005.01.008.

Wibral, Michael, Nicolae Pampu, Viola Priesemann, Felix Siebenhühner, Hannes Seiwert, Michael Lindner, Joseph T Lizier, and Raul Vicente. 2013. "Measuring Information-Transfer Delays." *PLOS ONE* 8 (2): e55809. https://doi.org/10.1371/journal.pone.0055809.

Wibral, Michael, Benjamin Rahm, Maria Rieder, Michael Lindner, Raul Vicente, and Jochen Kaiser. 2011. "Transfer Entropy in Magnetoencephalographic Data: Quantifying Information Flow in Cortical and Cerebellar Networks." *Progress in Biophysics and Molecular Biology* 105 (1–2): 80–97. https://doi.org/10.1016/j.pbiomolbio.2010.11.006.

Wibral, Michael, Raul Vicente, and Michael Lindner. 2014. "Transfer Entropy in Neuroscience." In , 3–36. https://doi.org/10.1007/978-3-642-54474-3_1.

Wierzgała, Piotr, Dariusz Zapała, Grzegorz M. Wojcik, and Jolanta Masiak. 2018. "Most Popular Signal Processing Methods in Motor-Imagery BCI: A Review and Meta-Analysis." *Frontiers in Neuroinformatics* 12: 78. https://doi.org/10.3389/fninf.2018.00078.

Witham, Claire L., Minyan Wang, and Stuart N. Baker. 2007. "Cells in Somatosensory Areas Show Synchrony with Beta Oscillations in Monkey Motor Cortex." *European Journal of Neuroscience* 26 (9): 2677–86. https://doi.org/10.1111/j.1460-9568.2007.05890.x.

Wolpaw, Jonathan R., Niels Birbaumer, Dennis J. McFarland, Gert Pfurtscheller, and Theresa M. Vaughan. 2002. "Brain-Computer Interfaces for Communication and Control." *Clinical Neurophysiology* 113 (6): 767–91.

https://doi.org/10.1016/S1388-2457(02)00057-3.

Wu, Meng Hung, Richard E. Frye, and George Zouridakis. 2011. “A Comparison of Multivariate Causality Based Measures of Effective Connectivity.” *Computers in Biology and Medicine* 41 (12): 1132–41. https://doi.org/10.1016/j.compbiomed.2011.06.007.

Wu, Wei, Zhe Chen, Xiaorong Gao, Yuanqing Li, Emery N. Brown, and Shangkai Gao. 2015. “Probabilistic Common Spatial Patterns for Multichannel EEG Analysis.” *IEEE Transactions on Pattern Analysis and Machine Intelligence* 37 (3): 639–53. https://doi.org/10.1109/TPAMI.2014.2330598.

Wu, Wei, Xiaorong Gao, Bo Hong, and Shangkai Gao. 2008. “Classifying Single-Trial EEG during Motor Imagery by Iterative Spatio-Spectral Patterns Learning (ISSPL).” *IEEE Transactions on Biomedical Engineering* 55 (6): 1733–43. https://doi.org/10.1109/TBME.2008.919125.

Xie, Hua, Vince D. Calhoun, Javier Gonzalez-Castillo, Eswar Damaraju, Robyn Miller, Peter A. Bandettini, and Sunanda Mitra. 2018. “Whole-Brain Connectivity Dynamics Reflect Both Task-Specific and Individual-Specific Modulation: A Multitask Study.” *NeuroImage*. Academic Press Inc. https://doi.org/10.1016/j.neuroimage.2017.05.050.

Xu, L., H. Zhang, M. Hui, Z. Long, Z. Jin, Y. Liu, and L. Yao. 2014. “Motor Execution and Motor Imagery: A Comparison of Functional Connectivity Patterns Based on Graph Theory.” *Neuroscience* 261 (March): 184–94. https://doi.org/10.1016/j.neuroscience.2013.12.005.

Yates, Darran. 2012. “Neurodegenerative Disease: Neurodegenerative Networking.” *Nature Reviews Neuroscience* 13 (5): 288–89. https://doi.org/10.1038/nrn3248.

Yu, Tianyou, Yuanqing Li, Jinyi Long, and Zhenghui Gu. 2012. “Surfing the Internet with a BCI Mouse.” *Journal of Neural Engineering* 9 (3). https://doi.org/10.1088/1741-2560/9/3/036012.

Yuan, Han, and Bin He. 2014. “Brain-Computer Interfaces Using Sensorimotor Rhythms: Current State and Future Perspectives.” *IEEE Transactions on*

Biomedical Engineering. IEEE Computer Society. https://doi.org/10.1109/TBME.2014.2312397.

Zalesky, Andrew, Alex Fornito, Luca Cocchi, Leonardo L. Gollo, and Michael Breakspear. 2014. "Time-Resolved Resting-State Brain Networks." *Proceedings of the National Academy of Sciences of the United States of America* 111 (28): 10341–46. https://doi.org/10.1073/pnas.1400181111.

Zanon, Marco, Sara Borgomaneri, and Alessio Avenanti. 2018. "Action-Related Dynamic Changes in Inferior Frontal Cortex Effective Connectivity: A TMS/EEG Coregistration Study." *Cortex* 108 (November): 193–209. https://doi.org/10.1016/j.cortex.2018.08.004.

Zarjam, Pega, Julien Epps, Fang Chen, and Nigel H. Lovell. 2013. "Estimating Cognitive Workload Using Wavelet Entropy-Based Features during an Arithmetic Task." *Computers in Biology and Medicine* 43 (12): 2186–95. https://doi.org/10.1016/j.compbiomed.2013.08.021.

Zeng, Ke, Gaoxiang Ouyang, He Chen, Yue Gu, Xianzeng Liu, and Xiaoli Li. 2018. "Characterizing Dynamics of Absence Seizure EEG with Spatial-Temporal Permutation Entropy." *Neurocomputing* 275 (January): 577–85. https://doi.org/10.1016/j.neucom.2017.09.007.

Zhang, Hang, Lele Xu, Shuling Wang, Baoquan Xie, Jia Guo, Zhiying Long, and Li Yao. 2011. "Behavioral Improvements and Brain Functional Alterations by Motor Imagery Training." *Brain Research* 1407: 38–46. https://doi.org/10.1016/j.brainres.2011.06.038.

Zhang, Xu Sheng, Rob J. Roy, and Erik Weber Jensen. 2001. "EEG Complexity as a Measure of Depth of Anesthesia for Patients." *IEEE Transactions on Biomedical Engineering* 48 (12): 1424–33. https://doi.org/10.1109/10.966601.

Zhang, Yong, Bo Liu, Xiaomin Ji, and Dan Huang. 2017. "Classification of EEG Signals Based on Autoregressive Model and Wavelet Packet Decomposition." *Neural Processing Letters* 45 (2): 365–78. https://doi.org/10.1007/s11063-016-9530-1.

Zhang, Yu, Chang S. Nam, Guoxu Zhou, Jing Jin, Xingyu Wang, and Andrzej Cichocki. 2019. “Temporally Constrained Sparse Group Spatial Patterns for Motor Imagery BCI.” *IEEE Transactions on Cybernetics* 49 (9): 3322–32. https://doi.org/10.1109/TCYB.2018.2841847.

Zhang, Yu, Yu Wang, Guoxu Zhou, Jing Jin, Bei Wang, Xingyu Wang, and Andrzej Cichocki. 2018. “Multi-Kernel Extreme Learning Machine for EEG Classification in Brain-Computer Interfaces.” *Expert Systems with Applications* 96 (April): 302–10. https://doi.org/10.1016/j.eswa.2017.12.015.

Zhang, Yu, Guoxu Zhou, Jing Jin, Xingyu Wang, and Andrzej Cichocki. 2015. “Optimizing Spatial Patterns with Sparse Filter Bands for Motor-Imagery Based Brain-Computer Interface.” *Journal of Neuroscience Methods* 255 (November): 85–91. https://doi.org/10.1016/j.jneumeth.2015.08.004.

Zhou, Changsong, Lucia Zemanová, Gorka Zamora, Claus C. Hilgetag, and Jürgen Kurths. 2006. “Hierarchical Organization Unveiled by Functional Connectivity in Complex Brain Networks.” *Physical Review Letters* 97 (23): 3–6. https://doi.org/10.1103/PhysRevLett.97.238103.

Zhou, Zhongxing, and Baikun Wan. 2012. “Wavelet Packet-Based Independent Component Analysis for Feature Extraction from Motor Imagery EEG of Complex Movements.” *Clinical Neurophysiology* 123 (9): 1779–88. https://doi.org/10.1016/j.clinph.2012.02.071.

Ziaeemehr, Abolfazl, Mina Zarei, Alireza Valizadeh, and Claudio R. Mirasso. 2020. “Frequency-Dependent Organization of the Brain’s Functional Network through Delayed-Interactions.” *Neural Networks* 132: 155–65. https://doi.org/10.1016/j.neunet.2020.08.003.

Zink, Nicolas, Moritz Mückschel, and Christian Beste. 2020. “Resting-State EEG Dynamics Reveals Differences in Network Organization and Its Fluctuation between Frequency Bands.” *Neuroscience* 453: 43–56. https://doi.org/10.1016/j.neuroscience.2020.11.037.

Ziqiang, Zuo, and Sadasivan Puthusserypady. 2007. “Analysis of Schizophrenic EEG Synchrony Using Empirical Mode Decomposition.” In *2007 15th International*

Conference on Digital Signal Processing, DSP 2007, 131–34. https://doi.org/10.1109/ICDSP.2007.4288536.

VITA

Name & Surname: Bilal Orkan OLCAY

EDUCATION

2014-2021 Doctor of Philosophy in Electronics and Communication Engineering

Graduate School of Engineering and Sciences, İzmir Institute of Technology, İzmir, Turkey
Thesis Title: ON THE CHARACTERIZATION OF MOTOR IMAGERY FUNCTIONS BASED ON SYSTEMATIC TIMING ORGANIZATION OF THE HUMAN BRAIN
Supervisor: Prof. Dr. Bilge KARAÇALI

2011-2014 Master of Science in Electronics and Communication Engineering

Graduate School of Engineering and Sciences, İzmir Institute of Technology, İzmir, Turkey
Thesis Title: ANALYSIS OF OLFACTORY EVOKED POTENTIALS
Supervisor: Prof. Dr. Ferit Acar SAVACI

2006-2011 Bachelor of Science in Electrical and Electronics Engineering

Faculty of Engineering, Çukurova University, Adana, Turkey
Thesis Title: ARM-9 MICROCONTROLLER BASED MP-3 PLAYER APPLICATIONS
Supervisor: Assoc. Prof. Dr. Murat AKSOY

PUBLICATIONS (Journal Papers)

Olcay, B. O., Özgören, M., & Karaçalı, B. (2021). On the characterization of cognitive tasks using activity-specific short-lived synchronization between electroencephalography channels. *Neural Networks, 143,* 452-474.

Olcay, B. O., & Karaçalı, B. (2019). Evaluation of synchronization measures for capturing the lagged synchronization between EEG channels: A cognitive task recognition approach. *Computers in biology and medicine*, *114*, 103441.

Guducu, C., Olcay, B. O., Schäfer, L., Aziz, M., Schriever, V. A., Özgören, M., & Hummel, T. (2019). Separating normosmic and anosmic patients based on entropy evaluation of olfactory event-related potentials. *Brain research*, *1708*, 78-83.